Fibroblast Growth Factor 2 (FGF2) in cartilage injury and repair

Sumayya Nafisa Khan

A thesis submitted to the University of Oxford for the degree of

Doctor of Philosophy

Michaelmas 2018

The Kennedy Institute of Rheumatology

Nuffield Department of Orthopaedics, Rheumatology and

Musculoskeletal Sciences

St Edmund Hall

University of Oxford

Abstract

Fibroblast Growth Factors (FGFs) are important pleiotropic growth factors with a proven role in joint development and postnatal homeostasis. Previously our group has shown that FGF2 is released upon cartilage injury and *Fgf2* knockout (KO) mice develop accelerated osteoarthritis (OA), suggesting it is chondroprotective *in vivo*. Work from others has shown that the accelerated OA phenotype in the *Fgf2* KOs is phenocopied by deletion of *Fgfr3* but not *Fgfr1*, suggesting that the FGFR may determine FGF2's action in the joint.

In the work presented here, I investigate the role of FGF2 in promoting enhanced cartilage regeneration. I first explore the control and function of different FGF receptors (FGFRs) and ligands; then perform an *in vivo* model of focal cartilage injury in the *Fgf2* KO mouse.

FGFR3 mRNA expression levels were rapidly down-regulated by injury in an FGF2-dependent manner, but recovered after chondrocytes were isolated and cultured *in vitro*. I did not observe significant differences in intracellular signalling or expression of a panel of FGF-dependent genes using receptor selective mutant ligands. *In vivo*, *Fgf2* KO mice failed to repair focal cartilage defects compared with wild-type (WT) controls. Mesenchymal stem cells (MSCs) were activated by FGF2; leading to enhanced scratch assay closure and keeping cells in a more motile state but not in promoting cell adhesion to damaged tissue. FGF2 suppressed chondrogenesis of MSCs *in vitro*. Taken together, I identified a primary role for FGF2 in promoting intrinsic cartilage repair, which may be due to local activation of MSCs. These results provide mechanistic insights into how cartilage repairs and may have important clinical implications.

Acknowledgements

I thank my supervisor Professor Tonia Vincent for her continual support and guidance throughout my PhD.

I am grateful for the help of Dr Hayat Muhammad for the chondrogenesis and MSC experiments.

I also thank Dr Heba Ismail and Dr Anastasios Chanalaris for their technical teaching, valuable advice and friendship during my PhD study.

Statement of originality

I hereby confirm that all the experimental work presented in this thesis has been performed by me. Any collaboration, assistance, or relevant prior experimental findings by others has been fully acknowledged in the relevant sections, with standard referencing practices.

The work has been carried out at the Kennedy Institute of Rheumatology, University of Oxford. The Kennedy Trustees and subsequently the Arthritis Research UK Centre for OA Pathogenesis funded this work.

Copyright declaration

Table of content

List of figures

List of tables

Abbreviations

ACAN	Aggrecan
ADAMTS	A Disintegrin and Metalloproteinase with Thrombospondin motifs
AER	Apical Ectodermal Ridge
AKT	Protein kinase B
ARG-1	Arginase 1
BMP	Bone Morphogenic Protein
BSA	Bovine Serum Albumin
CAM	Cell Adhesion Molecule
CAS9	CRISPR Associated Protein 9
CHD	Cell adhesion molecule Homology Domain
COL2	Collagen type II
COMP	Cartilage Oligomeric Matrix Protein
CREB	Cyclic adenosine monophosphate Response Element-Binding protein
CRISPR	Clustered Regularly Interspaced Short Palindromic Repeats
CS	Chondroitin Sulfate
CTGF	Connective Tissue Growth Factor
Cux1	Cut-like homeobox 1
DAG	Diacylglycerol
DMEM	Dulbecco's Modified Eagle's Medium
DNA	Deoxyribonucleic Acid
DS	Dermatan Sulfate
DTT	Dithiothreitol
DUSP6	Dual-Specificity Phosphatase 6
ECL	Enhanced Chemiluminescence
ECM	Extracellular Matrix
EDTA	Ethylenediaminetetraacetic Acid
ELISA	Enzyme-Linked Immunosorbent Assay
eNOS	Endothelial Nitric Oxide Synthase
ErbB	Human Epidermal Growth Factor Receptor
ERG	Erythroblast transformation-specific Related Gene
ERK	Extracellularly Regulated Kinase
ETS	E26 Transformation-Specific
ETV	E26 transformation-specific, Translocation Variant
FACS	Fluorescence-Activated Cell Sorting
FBS	Foetal Bovine Serum
FGF	Fibroblast Growth Factor
FGFR	Fibroblast Growth Factor Receptor
FGFRi	Fibroblast Growth Factor Receptor inhibitor
FOXO1	Forkhead box protein O1
FRS2α	Fibroblast growth factor Receptor Substrate 2 alpha
GAB1	Growth factor receptor bound 2, Associated Binding protein 1
GAG	Glycosaminoglycan
GDF	Growth and Differentiation Factor
GFP	Green Fluorescent Protein
GRB2	Growth factor Receptor Bound 2
h	hour(s)
HA	Hyaluronan

HAS1	Hyaluronan Synthase 1
HEPES	4-(2-hydroxyethyl)-1-piperazineethanesulfonic acid
HRP	Horseradish Peroxidase
HS	Heparan Sulfate
HSPG	Heparan Sulfate Proteoglycan
IG	Immunoglobulin
IGF-1	Insulin-like Growth Factor
Ihh	Indian-hedgehog
IL-1	Interleukin-1
INHBA	Inhibin, Beta A
ITS	Insulin-Transferrin-Selenium
JAK	Janus Kinase
JNK	c-Jun N-terminal Kinase
KO	Knock Out
KS	Keratin Sulfate
LDH	Lactate Dehydrogenase
MAPK	Mitogen Activated Protein Kinase
MCP	Metacarpophalangeal
MEK	Mitogen activated protein kinase kinase
min	minute(s)
MKP3	Mitogen activated protein Kinase, Phosphatase 3
MMP	Matrix Metalloproteinase
MRI	Magnetic Resonance Imaging
mRNA	messenger Ribonucleic Acid
MSC	Mesenchymal Stem Cells
MT-MMP	Membrane Type -Matrix Metalloproteinase
MTOR	Mammalian Target Of Rapamycin kinase
mTORC1	mammalian Target Of Rapamycin Complex 1
N-cadherin	Neural cadherin
N-CAM	Neural Cell Adhesion Molecule
NFκB	Nuclear Factor Kappa-light-chain-enhancer of activated B cells
NGF	Nerve Growth Factor
ns	non-significant
OA	Osteoarthritis
OP-1/BMP-7	Osteogenic Protein 1/ Bone Morphogenetic Protein-7
p-AKT	phosphorylated protein kinase B
PBS	Phosphate-Buffered Saline
PCM	Pericellular Matrix
PCR	Polymerase Chain Reaction
PDGF	Platelet Derived Growth Factor
PDPN	Podoplanin
p-ERK	phosphorylated Extracellular signal-Regulated Kinase
PI3K	Phosphatidylinositide 3-Kinase
PIP_2	phosphatidylinositol (4, 5)-biphosphate
PIP_3	phosphatidylinositol (3, 4, 5)-triphosphate
PKCδ	Protein Kinase C Delta
PLC	Phospholipase C
PMA	Phorbol 12-Myristate 13-Acetate
PPARγ	Peroxisome Proliferator Activated Receptor Gamma
PRELP	Proline/arginine-rich end leucine-rich repeat protein
PTGS2	Prostaglandin-Endoperoxide Synthase 2

PTHrP	Parathyroid Hormone-related Peptide
PVDF	Polyvinylidenefluoride
RAF	Proto-oncogene serine/threonine-protein kinase
RAS	Rat sarcoma
RGE	Relative Gene Expression
RHEB	Ras Homolog Enriched in Brain
RIPA	Radioimmunoprecipitation Assay
RTKs	Receptor Tyrosine Kinases
RUNX	Runt-related transcription factor
S.D.	Standard Deviation
SDS	Sodium Dodecyl Sulfate
SDS-PAGE	Sodium Dodecyl Sulfate–Polyacrylamide Gel Electrophoresis
SEF	Similar Expression to FGF
SF	Serum- Free
siRNA	small inhibitory Ribonucleic Acid
SOS	Son Of Sevenless
SOX	Sex-determining region Y-box 9
SPRY	Sprouty
Src	Proto-oncogene tyrosine-protein kinase
STAT	Signal Transducer and Activator of Transcription
TAK-1	Transforming growth factor β–Activated Kinase 1
TBST	Tris-Buffered Saline with Tween 20
TGFβ	Transforming Growth Factor Beta
TGFβi	Transforming Growth Factor Beta inhibitor
TIMP	Tissue Inhibitor of Matrix Metalloproteinase
TNFRSF12A	Tumour Necrosis Factor Receptor Superfamily member 12A
TSC2	Tuberous Sclerosis Complex 2
TSG-6	Tumour necrosis factor α-inducible gene 6
Wnt	Wingless-type integration site protein
WT	Wild-Type

1 Introduction

1.1 Structure of the knee joint

The knee joint (Figure 1.1) is one of the largest, most complicated synovial joints of the human body. It is an important load-bearing joint in humans and is commonly affected by osteoarthritis (OA). The knee is composed of 3 bones, the femur, tibia and patella. The bones are connected to each other by tough fibrous connective tissue called ligaments, which help stabilise the joint. The cruciate ligaments join the femur and tibia together at the middle of the knee joint. These ligaments are most commonly injured and subsequently lead to the development of OA.

Tendons are also fibrous connective tissue; however, they connect bone to muscles. The series of connections of ligaments, tendons, muscles and bones, allows for the movement of the joint. As muscles contract, they pull on the tendons to cause extension or flexion of the knee.

The joint is surrounded by a capsule made of a fibrous outer layer and a thin inner layer. The inner layer is termed the synovial membrane/synovium and secretes synovial fluid, which fills the synovial space. The synovial fluid acts as a lubricant for the articulating surfaces of the joint.

Within the knee there are many small fluid-filled sacs called bursae. They are also lined by a synovial membrane and are filled with synovial fluid. Bursae act as a cushion between bones and tendons and/or muscles around a joint.

The long bones are composed of a dense, hard outer later; the cortical bone and the inner trabecular bone. The trabecular bone consists of a meshwork of bony bars (trabeculae) with

many interconnecting spaces, thus making it less dense than cortical bone. The spaces within the trabecular bone contain bone marrow, which contains haematopoietic cells including mesenchymal stem cells (MSCs), adipose cells, and stromal cells.

Near the distal ends of the long bones are the growth plates where the bones continue to grow from until skeletal maturity is reached. The ends of the long bones are covered in articular cartilage, which provides the smooth surface for articulation and acts as a shock absorber during compression of the joint upon walking/running. The other cartilaginous structures in the knee joint are the menisci. These lie between the femoral and tibial cartilages and are c-shaped discs. They further act as “shock-absorbers” of the joint and also protect the ends of the femur and tibia from rubbing on each other. The lateral ends of the menisci are fused with the synovial membrane.

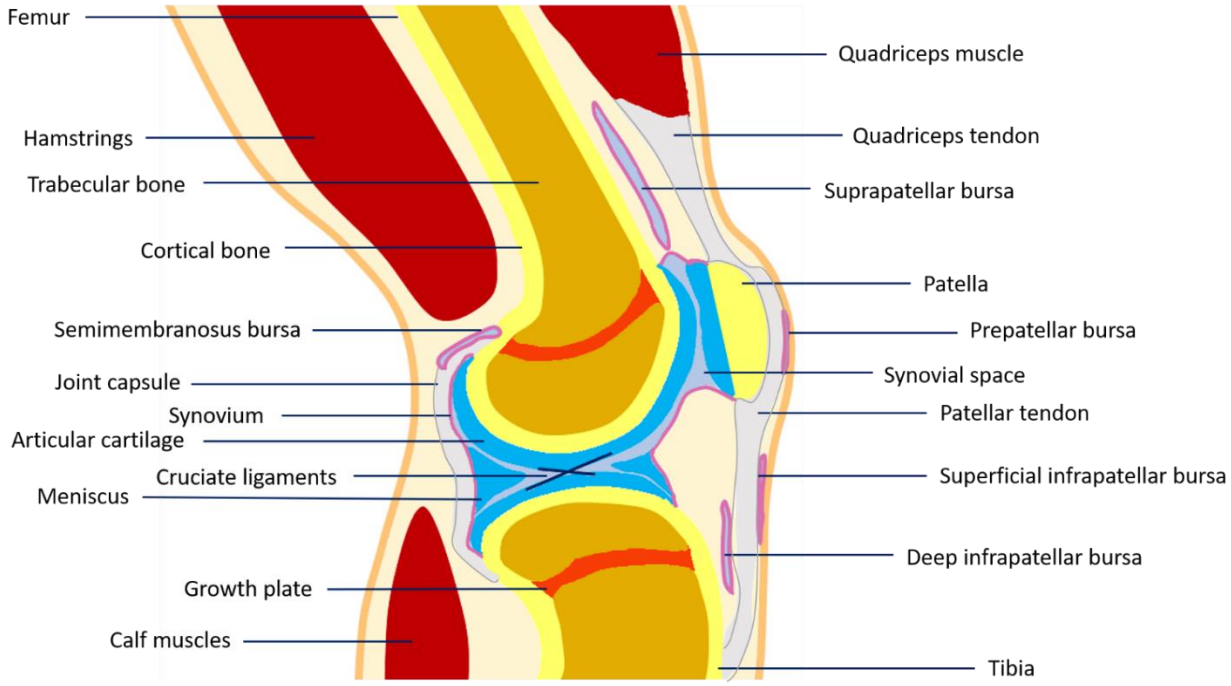

Figure 1.1: Anatomy of the knee joint

The knee joint is one of the largest synovial joints of the human body. The bones of the knee joint include the femur, tibia and patella (yellow). Ligaments are tough fibrous connective tissue that connect bone to bone. The cruciate ligaments (dark blue lines) join the femur and tibia together at the middle of the knee joint. Muscles (deep red) are attached to bones by tendons, which are also composed of fibrous connective tissue. The patella is partly held in place by the quadriceps tendon at the top of the patella, and the patellar tendon, which connects the patella to the tibia (grey). The joint is surrounded by a capsule made of a fibrous outer layer and a thin inner layer; the synovium (pink). The synovium secretes synovial fluid which fills the synovial space (light blue). Within the knee there are many small fluid-filled sacs called bursae, which are also lined by a synovial membrane and are filled with synovial fluid. The long bones are composed of a dense, hard outer later; the cortical bone (bright yellow) and the inner trabecular bone (dark yellow). Near the distal ends of the long bones are the growth plates (bright red) where the long bones continue to grow from until skeletal maturity is reached. The ends of the long bones are covered in cartilage (bright blue). The other cartilaginous structures in the knee joint are the menisci (bright blue triangles) which lie between the femoral and tibial cartilages with the lateral ends of the menisci being fused with the synovial membrane.

1.2 Cartilage: the tissue

There are 3 main types of cartilage found in the human body; elastic, hyaline and fibrocartilage. They vary in their relative composition and so serve different functions. Elastic cartilage is found in the ear and epiglottis, is composed mainly of elastin fibres and therefore functions to withstand repeated bending. Fibrocartilage is less cellular, more fibrous and inflexible; it is found in menisci, intervertebral discs and the pubic symphysis. Hyaline cartilage is the most prevalent type of cartilage; it is found in the larynx, trachea, bronchi, on the ventral ends of ribs and on the articulating surfaces of bones. This thesis focuses on the hyaline cartilage found in articulating joints.

1.3 The development of long bone (endochondral ossification)

Long bones form by endochondral ossification i.e. from a cartilaginous template. The first stage of chondrogenesis is the condensation of mesenchymal cells in the regions of the embryo destined to become bone. This allows for the initiation of cell-cell contacts which triggers cell differentiation. Two adhesion molecules; neural cadherin (N-cadherin) (Oberlender and Tuan, 1994, Neilson and Friesel, 1995) and neural cell adhesion molecule (N-CAM) (Widelitz *et al*., 1993) are known to be involved in this step. The fibroblastic pre-chondrogenic mesenchymal cells differentiate and take on a more rounded morphology of chondrocytes. This process is controlled by a number of transcription factors such as runt-related transcription factor 1 (RUNX1), and Sex-Determining region Y-box (SOX)5, 6 and 9 (Cole, 2011), of which SOX9 is considered the master regulator of chondrogenesis (Bi *et al*., 1999). A number of growth factors including fibroblast growth factors (FGFs) and transforming growth factor beta (TGFβ) family members are also involved in this process (DeLise *et al*., 2000). The chondrocytes then begin producing the extracellular matrix (ECM)

components of cartilage (described later), thus laying down a cartilaginous template for bone formation. A primary ossification centre develops in the centre of the diaphysis due to vascularisation in this region. Here the chondrocytes undergo proliferation, maturation and hypertrophy, processes regulated by parathyroid hormone-related peptide (PTHrP) and Indian-hedgehog (Ihh) (Vortkamp *et al*., 1996). Osteoblasts then migrate into the cartilage from the blood vessels and begin mineralising the ECM to form bone. This process radiates outward with the formation of the cartilaginous growth plates at the distal ends of the long bones that separate the epiphyses from the diaphysis. A secondary ossification site then forms in the centre of the epiphysis. The hypertrophic chondrocytes of the growth plates eventually cease proliferation and are replaced with bone; hence the growth plate thins and eventually fuses with the bone. At this point bone growth stops.

1.4 Intramembranous bone formation

Flat bones of the skeletal system that comprise the cranium and medial clavicles are formed by a process known as intramembranous ossification. In this process intramembranous bone forms from a mesenchymal condensation that directly gives rise to bone, without the need for an intermediate cartilaginous stage as in endochondral ossification. After condensation of mesenchyme, ossification centres are formed by direct bone matrix deposition-forming plates, which expand during development but do not fuse at the junction with neighbouring bones. The junctions between calvarial bones; the sutures, are responsible for regulating the expansive growth of the skull in concert with the brain. Here, osteogenic mesenchymal cells differentiate into osteoprogenitor cells and then into osteoblasts that express type I collagen, bone sialoprotein, and osteocalcin, and synthesize bone matrix along the bone margins. (Ornitz and Marie, 2002).

1.5 Joint formation

Joint formation occurs separately from the development of bone. In the region of the embryo destined to become the joint, mesenchymal stem cells condense and become closely associated; this region is known as the interzone. It gives rise to the synovial lining, menisci, ligaments and articular cartilage. The interzone is composed of 3 layers, the middle of which is termed the intermediate zone, the outer zones eventually form the articular cartilage (Ito and Kida, 2000). Cavitation occurs within the interzone, which leads to the formation of the synovial space; then joint morphogenesis occurs, where the joint-specific tissues form and the distal and proximal ends of the joints form their reciprocal shapes. (Pacifici *et al*., 2005).

Holder (1977) first demonstrated the importance of the interzone for the development of the joint structures by microsurgically removing it at the site of the elbow and showing that the humerus, ulna and radius developed normally but were fused together. The cells of the interzone have been shown to express regulatory molecules including TGFβ superfamily members: Growth and differentiation factors (GDF) 5 and 6 (Storm and Kingsley, 1996, Settle *et al*., 2003), Wingless-type integration site protein (Wnt)-4, 14, and 16 (Guo *et al*., 2004, Hartmann and Tabin, 2001); Bone morphogenic protein (BMP) antagonists Chordin (Francis-West *et al*., 1999) and Noggin (Brunet *et al*., 1998); FGF2, 4 and 13 (Kavanagh *et al*., 2006) and transcription factors Cut-like homeobox 1 (Cux1) (Lizarraga *et al*., 2002) and Erythroblast transformation-specific related gene (ERG). The importance of these molecules is clear from ablation experiments which generally lead to the absence of a joint/ joint deformities (Pacifici *et al*., 2005), however their precise function remains unclear.

There is good evidence that cavitation involves changes in the ECM, hyaluronan (HA) synthesis, and mechanical stimuli (Pitsillides and Ashhurst, 2008). Ito and Kida (2000) observed changes in the collagen fibril formation between the intermediate cells of the interzone and those destined to become the articular cartilage in developing rat knees. Craig *et al* (1990) showed hyaluronan to be present in the intermediate interzone just prior to cavitation and remained present as the joint continued to form. HA synthases and uridine diphosphoglucose dehydrogenase (an enzyme that produces the HA precursor subunit uridine diphosphate glucuronate) were also shown to be strongly expressed in cells immediately adjacent to forming cavities (Pitsillides *et al*., 1995). Furthermore, Dowthwaite *et al* (1998) showed treatment with exogenous HA hexasaccharides (which block HA interactions with cell surface receptors) caused inhibition of cavitation of developing chick joints. Many models of joint immobilisation have been shown to result in the fusion of opposing skeletal elements and the absence of a joint cavity (reviewed in Lamb *et al*., 2003). Kavanagh *et al* (2006) further showed that immobilisation of the chick joint reduced FGF2 expression in the cells that would normally border the joint cavity (but did not affect expression of FGF4 or GDF5). As FGF2 is known to induce HA synthesis, it can be speculated that immobilisation prevents cavitation because of a reduction in FGF2 in the cells of the interzone.

1.6 Articular cartilage composition and structure

Articular cartilage is the avascular, aneural connective tissue of diarthroidial joints that provides cushioning of the joint on loading and a smooth lubricated surface for articulation. Cartilage is composed of only one main cell type; the chondrocyte and a dense extracellular matrix (ECM).

Articular cartilage has a highly organised structure, typically divided into 4 zones based on the morphology of the chondrocytes and the arrangement of collagen fibres (depicted in Figure 1.2). The calcified zone lies directly above the subchondral bone; it contains hypertrophic chondrocytes and radially oriented collagen fibres. The end of the calcified zone is marked by the tidemark. Above this is the deep zone; it contains collagen fibres that are organised parallel to the articular surface. Here the hypertrophic chondrocytes are arranged into columns. The middle zone (also called the transitional zone) contains obliquely oriented collagen fibres with chondrocytes that are less organised. The superficial zone contains chondrocytes that appear more flattened with collagen fibres that are parallel to the articular surface.

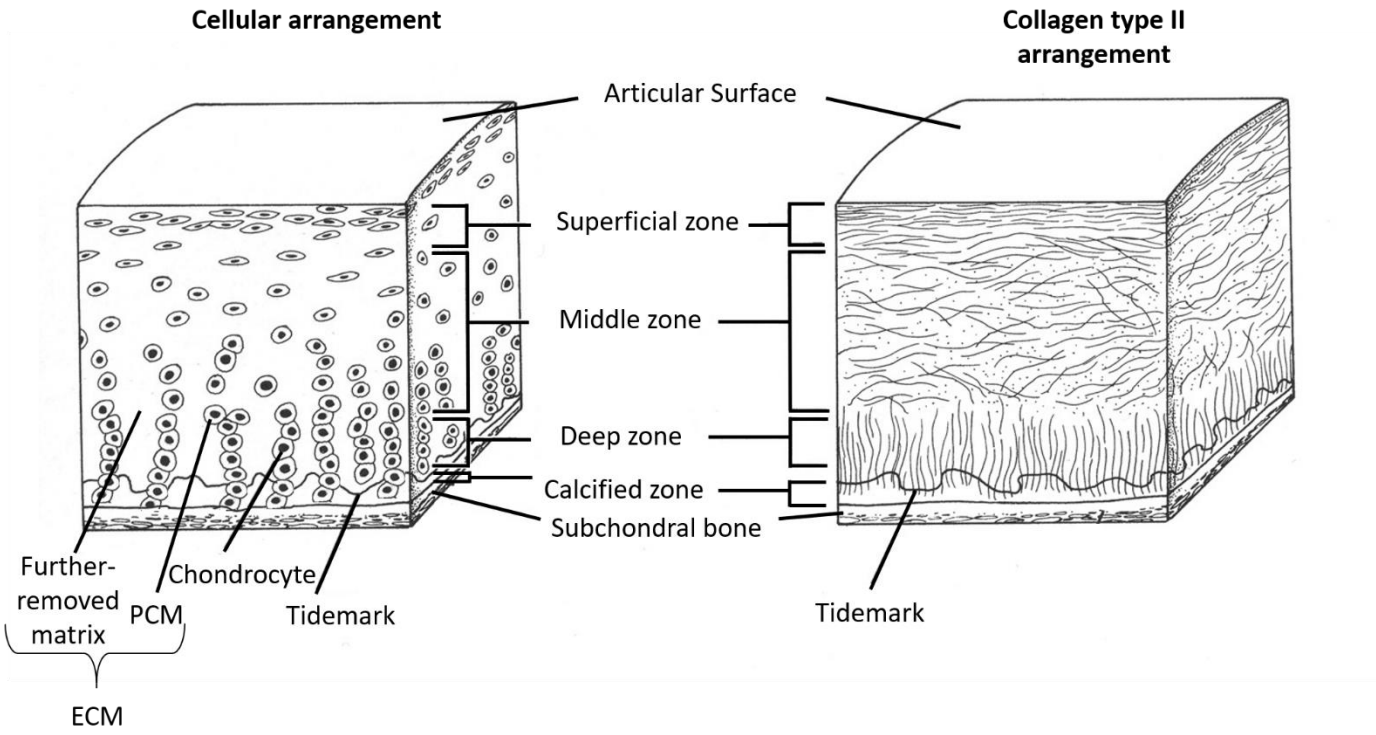

Figure 1.2: Diagram of the structure of articular cartilage
Articular cartilage is composed of one cell type the chondrocyte and its extracellular matrix (ECM). The ECM includes the pericellular matrix (PCM) which immediately surrounds the cells and the further removed matrix which is located further from the cells. Articular cartilage can be divided into 4 main regions, where the arrangement and morphology of the chondrocytes changes as does the arrangement of the collagen fibrils. The articular surface is smooth and lubricated to provide less friction during articulation. Immediately below this is the superficial zone, where chondrocytes appear flattened and collagen fibres lie parallel to the articular surface. Below this is the mid zone, where chondrocytes take on a more rounded morphology and are disorganised. Here the collagen fibres are obliquely orientated. In the deep zone chondrocytes appear hypertrophic and are arranged in columns with the collagen fibres organised perpendicular to the articular surface. The tidemark separates the deep zone from the calcified zone. The calcified cartilage lies immediately above the subchondral bone and also contains hypertrophic columnar chondrocytes. Image sourced and modified from Jazrawi *et al* (2011).

1.6.1. The chondrocyte

The chondrocytes occupy <5 % of the total volume of cartilage, and rely on the passive diffusion of nutrients, oxygen and waste products. Thus, chondrocytes reside in a hypoxic environment and so have an anaerobic metabolism. The main role of the chondrocyte in adult cartilage is the maintenance of the ECM by the slow turnover of its components. Chondrocytes are exquisitely mechano-sensitive, responding to mechanical stimuli, to influence normal mechanoadaptive matrix homoeostasis (Vincent and Wann, 2018).

1.6.2. The extracellular matrix

The ECM is highly hydrated and composed mainly of collagens that account for 60 % of the dry weight of cartilage and proteoglycans that account for 20 % of the dry weight of cartilage. Type II collagen gives cartilage its tensile properties and helps to stabilise the matrix. The proteoglycan aggrecan, is highly negatively charged, thus draws in sodium and water molecules to provide cartilage with its osmotic properties that subsequently enable it to resist compressive forces.

The ECM can be divided into 2 regions, the pericellular matrix (PCM) which immediately surrounds the chondrocytes and the further removed matrix.

1.6.2.1 Collagen

Collagens are a family of proteins that contain the repeating tripeptide motif Gly-Pro-X or Gly-X-Hyp; where X can be any other amino acid. 3 α-helical chains associate into a triple stranded helix. These helices are arranged into fibrils which are stabilised by covalent cross-links. These fibrils then aggregate into large bundles to form the collagen fibres which can be seen by light microscopy.

The most abundant type of collagen found in articular cartilage is type II collagen. Other collagens present in articular cartilage at reasonable abundance are types VI, IX, X and XI. Types IX and XI are present within the type II fibres in small quantities. Type X collagen is expressed by hypertrophic chondrocytes that lie within the calcified cartilage zone. Type VI collagen is located within the pericellular matrix.

1.6.2.2 Proteoglycans

Proteoglycans are proteins with attached glycosaminoglycan (GAG) chains such as chondroitin sulfate (CS), heparan sulfate (HS), keratan sulfate (KS) or dermatan sulfate (DS). The major proteoglycan in articular cartilage is aggrecan which is bound to hyaluronan, an interaction facilitated by link protein. Each aggrecan core protein has 3 globular domains and a rich region of CS and KS GAGs. The GAGs are negatively charged and therefore repel to maintain the expanded shape of cartilage.

Less abundant proteoglycans found in cartilage include biglycan (Fisher *et al*., 1989), fibromodulin (Antonsson *et al*., 1991), decorin (Krusius and Ruoslahti, 1986), proline/arginine-rich end leucine-rich repeat protein (PRELP) (Heinegård *et al*., 1986), chondroadherin (Neame *et al*., 1994), syndecan and perlecan. They have various functions; decorin and fibromodulin interact with collagen type II fibrils to aid in their assembly and orientation (Vogel and Trotter, 1987, Roughley and Lee, 1994); biglycan is located in the pericellular matrix (Bianco *et al*., 1990) and is thought to be involved in the network assembly of collagen type VI (Roughley and Lee, 1994); PRELP and chondroadherin bind to integrins on the cell surface to facilitate adhesion of chondrocytes to matrix proteins (Camper *et al*., 1997); whereas the syndecans are involved in ligand binding and signal

transduction at the cell surface (Beauvais and Rapraeger, 2004, Melrose *et al*., 2006). The role of perlecan is discussed in more detail below.

1.6.2.3 The pericellular matrix

The PCM is the part of the ECM that immediately surrounds the chondrocyte. It is seen histologically as a translucent zone around individual chondrocytes. The PCM is devoid of the type II collagen fibrils found in the further-removed matrix but contains collagen type VI (Poole *et al*., 1988). It also contains other non-collagenous proteins such as biglycan, decorin (Kavanagh and Ashhurst, 1999), fibronectin, hyaluronan (Poole *et al*., 1991), fibrillin (Keene *et al*., 1997), laminin (Dürr *et al*., 1996) and perlecan (Melrose *et al*., 2006, Vincent *et al*., 2007).

Perlecan consists of a core protein with 3 long chains of GAGs attached. The GAGs can be CS but are mainly HS (hence its other name; heparan sulfate proteoglycan 2). It interacts with a number of proteins including fibronectin (Hopf *et al*., 1999), PRELP (Bengtsson *et al*., 2002) and collagen type VI (Battaglia *et al*., 1992), and so may function to help stabilize cells within the ECM. The HS side chains of perlecan have also been shown to bind to various growth factors, sequestering them in the PCM and possibly contributing to cell surface growth factor signalling. These include connective tissue growth factor (CTGF) (Nishida *et al*., 2003, Tang *et al*., 2018), and FGF2 (Whitelock *et al*., 1996, Chong *et al*., 2013, Vincent *et al*., 2007).

1.6.2.4 Other non-collagenous, non-proteoglycan proteins

The ECM also contains a number of other non-collagenous proteins such as cartilage oligomeric matrix protein (COMP), anchorin and fibronectin. They can interact with collagen type II and proteoglycans and can be found on the cell surface, so function to help organise

and maintain the structure of cartilage and facilitate interactions between the chondrocyte and ECM (Burton-Wurster *et al*., 1997, Heinegård, 2009).

1.7 Matrix turnover in normal joints

In normal healthy articular cartilage, most of the constituents of the ECM are constantly being turned over, with the exception of the fibrillar collagens. Collagen type II has a purported half-life *in vivo* of over 100 years (Heinemeier *et al*., 2016). There is a homeostatic balance between ECM synthesis (anabolism) and breakdown (catabolism) which is mediated by a number of factors; including matrix metalloproteinases (MMPs), tissue inhibitors of MMPs (TIMPs), cartilage loading and various growth factors.

1.7.1 Matrix metalloproteinases

MMPs are a family of zinc-dependent proteolytic enzymes, of which there are 23 members. They are initially synthesized as inactive zymogens. The pro-peptide domain contains a conserved cysteine residue that interacts with the zinc ion in the active site, preventing binding of the substrate. This pro-peptide domain must be cleaved in order to activate the enzyme (Van Wart and Birkedal-Hansen, 1990). MMPs degrade all types of ECM proteins including collagen and proteoglycans. They can be divided into 4 main functional groups based on their substrates and domain structures; collagenases, gelatinases, stromelysins, and membrane type enzymes (MT-MMPs).

Collagenases include MMP-1, -8, and -13. They mainly cleave fibrillar collagens into characteristic 3/4 and 1/4 fragments. Gelatinases include MMP-2 and -9; their substrates include collagens type VI and XI, laminin and aggrecan. MMP-2 can also cleave collagen type II (Nagase *et al*., 2006). Stromelysins such as MMP-3 have a broad specificity with substrates

including proteoglycans, laminin and fibronectin (Matrisian, 1990). MT-MMPs are activated intracellularly and the active forms are located on the cell membrane. They include MMP-14, -15, -16, -24 and -25 and can activate proMMP-2. MMP-14 can also cleave collagen type II (Nagase *et al*., 2006).

1.7.2 Tissue inhibitors of metalloproteinases

Matrix metalloproteinases are inhibited by specific endogenous tissue inhibitors of matrix metalloproteinases (TIMPs) of which there are 4 family members (TIMPs 1-4). TIMP-1 inhibits MMP-3 (Brew *et al*., 2000). TIMP-2 and -3 inhibit MT-MMPs (Butler *et al*., 1997). TIMP-3 also binds strongly to other ECM protein (Pavloff *et al*., 1992) and is a strong inhibitor of a disintegrin and metalloproteinase with thrombospondin motifs (ADAMTS)-4 and -5 (Kashiwagi *et al*., 2001). TIMP-4 has been shown to be involved in the regulation of MMP-2 (Bigg *et al*., 1997).

1.7.3 Homeostatic mechanical load

Mechanical loading is an important factor for the homeostasis of cartilage. This is exemplified by the fact that cartilage undergoes disuse atrophy in patients with spinal cord injury (Vanwanseele *et al*., 2003). Immobilisation of the joint leads to alterations in the ECM; Palmoski *et al* (1979) showed rapid loss of proteoglycan content in the immobilised knee joints of canines, which was restored upon resumption of weight-bearing activities. The ECM is thought of as a mechanotransducer, whereas the chondrocyte is thought of as the mechanosensor (Vincent and Wann, 2018). Mechanical loading creates mechanical, electrical, and physicochemical signals to direct the synthesis and degradation of cartilage. Upon compression or cutting, the PCM has been shown to release heparan sulfate-bound molecules such as FGF2 (Vincent *et al*., 2007) and CTGF in complex with latent TGFβ (Tang *et*

al., 2018) which can then go on to bind to their cognate receptors and elicit signalling events in the chondrocytes. Cellular mechanosensors include cell-surface integrins (Ross *et al*., 2013), stretch and cation-sensitive ion channels (including sodium, potassium and calcium channels) (Lee *et al*., 2014, O'Conor *et al*., 2014, Mobasheri *et al*., 2010) and the primary cilium (Wann *et al*., 2012). Matrix proteins such as aggrecan, type II collagen (Korver *et al*., 1992), MMPs (Blain *et al*., 2001) and TIMPs (Vincent *et al*., 2004) have all been shown to be regulated in response to loading cartilage explants and chondrocytes *in vitro*. However, the regulation of these proteins is affected by the frequency and magnitude of the load applied (Ragan *et al*., 1999, Sauerland *et al*., 2003, Guilak *et al*., 1994). Excessive or injurious loading can lead to joint diseases such as osteoarthritis.

1.8 Cartilage injury

A crude way to damage cartilage is to cut the tissue from the intact articular surface (known as explantation). In porcine tissue, cartilage is cut from the metacarpophalangeal joint using a surgical scalpel. In murine tissue, the femoral head cartilage is removed by shearing through the growth plate of young mice (referred to as “hip explantation”). Work from our lab shows that in addition to release of PCM HS-bound growth factors, inflammatory signalling is activated when cartilage is injured through explantation by either method described above. This signalling includes activation of all 3 mitogen-activated protein kinases (MAPK); extracellularly regulated kinase (ERK); c-Jun N-terminal kinase (JNK); and p38 kinase, and also activates NFκB and Src signalling (Watt *et al*., 2013, Ismail *et al*., 2017, Chong *et al*., 2013). The activation of ERK was found to be mainly mediated by FGF2 release from the PCM (Vincent *et al*., 2002). Ismail *et al* (2017) recently showed that the activation of the MAPKs and NFκB were mediated by the activation of Transforming Growth Factor β–

Activated Kinase 1 (TAK-1). Inflammatory signalling drives injury response genes such as MMPs, cytokines, chemokines and Nerve growth factor (NGF) (Gruber *et al*., 2004, Chong *et al*., 2013, Driscoll *et al*., 2016). Additionally, the activation of JNK-2 has been shown to control the activity of aggrecanases (the key pathogenic matrix-degrading enzymes in osteoarthritis; see next section) *in vivo* (Ismail *et al*., 2016). Mechanical injury is the most important risk factor in the development of osteoarthritis. Understanding the molecular response of cartilage to injury is likely to be valuable in unravelling osteoarthritis pathogenesis.

1.9 Osteoarthritis

Osteoarthritis (OA) is the most common form of arthritis affecting most people over the age of 65. It is a degenerative disease of the diarthroidial joints characterized by cartilage degradation, intra-articular inflammation, synovitis and changes in the underlying bone including osteophyte formation. To begin with, surface fibrillations appear in the cartilage. As the disease progresses, these develop into fissures into the deep zone of cartilage through to the osteochondral junction, where vascular elements begin to penetrate the bone from the underlying bone marrow. This vascularisation may be accompanied by nerve development, causing pain in the joint (Walsh *et al*., 2010). The cartilage ECM components including proteoglycans and collagen start to degrade, a process mediated by aggrecanases and MMPs. New bone develops around the vascular elements as in endochondral bone formation and can lead to the development of osteophytes (Suri and Walsh, 2012). Chondrocytes appear more hypertrophic and are sometimes surrounded by intense metachromatic staining indicating increased proteoglycan formation, suggesting attempted repair of the damaged cartilage.

The degradation of aggrecan is thought to occur in the earlier stages of OA prior to collagen type II degradation. Initially MMPs that cleave aggrecan between Asn^{341}-Phe^{342} were thought to be the main aggrecan-degrading enzymes, however when bovine articular cartilage was treated with Interleukin-1 (IL-1; an inflammatory cytokine that stimulates cartilage breakdown), aggrecan cleavage occurred between Glu^{373}-Ala^{374} of the interglobular domain (Sandy *et al*., 1991). Sandy *et al* (1992) also showed that the synovial fluid of OA patients contained a majority of aggrecan fragments that were cleaved at this new site. This cleavage was not blocked by TIMP-1 or -2 or synthetic MMP inhibitors (Hughes *et al*., 1998), providing further evidence that MMPs were not involved in this disease-related "aggrecanase" activity. Aggrecanase 1 (also known as ADAMTS-4- a disintegrin and metalloproteinase with thrombospondin motifs) (Tortorella *et al*., 1999) and aggrecanase 2 (also known as ADAMTS-5) (Abbaszade *et al*., 1999) were later identified as the enzymes that cleave aggrecan at the Glu^{373}-Ala^{374} site. Since then at least 4 other cleavage sites have been identified for these aggrecanases in the chondroitin sulfate-rich CS-2 region of bovine aggrecan at $GELE^{1480}$-GRGD, $KEEE^{1667}$-GLGS, $TAQE^{1771}$-AGEG, and $VSQE^{1871}$-LGQR (Nagase and Kashiwagi, 2003) (Figure 1.3). ADAMTS-1 has also been shown to have aggrecanase activity but at the Glu^{1871}-Leu^{1872} bond within the chondroitin sulfate attachment domain of aggrecan (Kuno *et al*., 2000). More recent work has shown that deletion of ADAMTS-5 but not ADAMTS-1 (Vincent, unpublished data) or ADAMTS-4 (Glasson *et al*., 2004) in mice, significantly protects against surgically induced OA (Glasson *et al*., 2005) and inflammatory arthritis (Stanton *et al*., 2005). However in human OA, there is controversy as to whether both ADAMTS-5 and ADAMTS-4 mediate cartilage degradation (Song *et al*., 2007).

It has been suggested that the presence of aggrecan protects collagen from degradation, so in OA, collagen degradation usually occurs after proteoglycan loss (Troeberg and Nagase, 2012). The main collagenase in OA is thought to be MMP-13. Its expression is increased in human tissue (Reboul *et al*., 1996) and MMP-13 KO mice are protected from developing surgically-induced OA (Little *et al*., 2009), whereas constitutively active MMP-13 induces spontaneous cartilage degradation of the type seen in OA (Neuhold *et al*., 2001).

Further data have shown that when OA is induced in mice by surgical destabilisation of the joint, inflammatory genes including aggrecanases and MMPs are induced in a highly mechanosensitive manner (Burleigh *et al*., 2012). The absence of *Fgf2* accelerated disease, increased aggrecanase gene expression and enhanced inflammation in the joint (Sawaji *et al*., 2008, Chia *et al*., 2009). FGF2-mediated chondroprotection could be exploitable.

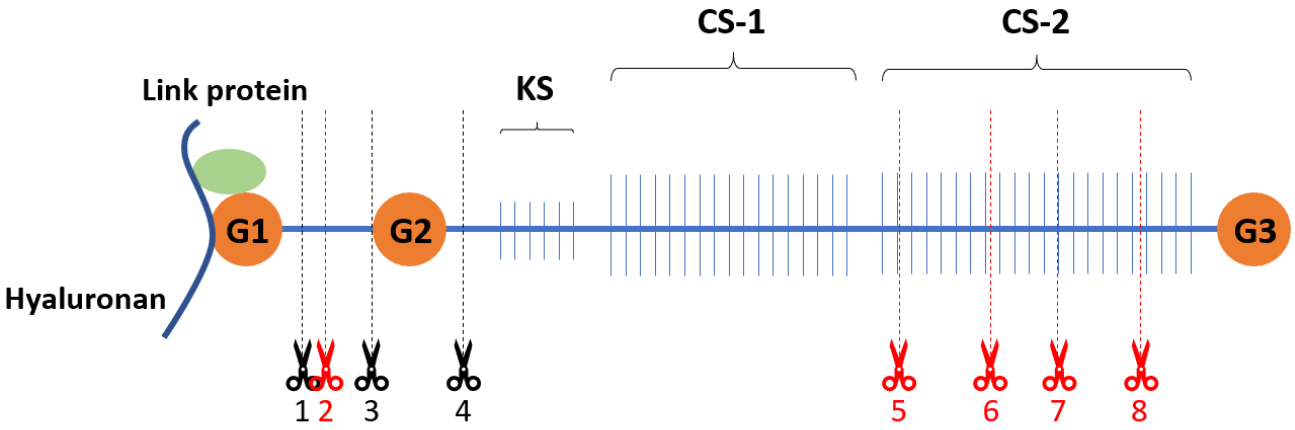

	Cleavage site
1	IPEN$^{341-342}$FFGV (IPES$^{341-342}$FFGV)
2	TEGE$^{373-374}$ARGS
3	TSED$^{441-442}$LVVQ
4	CFRG$^{666-667}$ISAV (CFRG$^{666-667}$VSAA)
5	SELE$^{1545-1546}$GRGT (GELE$^{1480-1481}$GRGD)
6	KEEE$^{1714-1715}$GLGS (KEEE$^{1667-1668}$GLGS)
7	TAQE$^{1819-1820}$AGEG (TAQE$^{1771-1772}$AGEG)
8	ISQE$^{1919-1920}$LGQR (IVQE$^{1871-1872}$LGQR)

Figure 1.3: Aggrecan structure and cleavage sites
Aggrecan is the major proteoglycan in articular cartilage. It is bound to hyaluronan via an interaction facilitated by link protein (green oval). Each aggrecan core protein has 3 globular domains and a rich region of chondroitin sulfate (CS) and keratan sulfate (KS) glycosaminoglycans. The diagram shows sites cleaved by matrix metalloproteinases in black and aggrecanases in red. The table shows the human protein sequence at the respective cleavage sites with those in parentheses representing the equivalent bovine sequences. Figure sourced and adapted from Nagase and Kashiwagi (2003).

1.10 Cartilage repair/regeneration

Up until recently, OA was believed to be a disease of wear and tear with no capacity for regeneration of the cartilaginous surface. However, with the advancement of new technologies, evidence of cartilage repair has been seen arthroscopically (Nakamura *et al*., 2008) and by MRI (Intema *et al*., 2011); although the mechanisms by which it repairs still need to be elucidated.

Repair may also be dependent on the size/type of damage. Superficial defects (those that do not cross the osteochondral junction) do not repair, whereas full-thickness defects (those that breach the osteochondral junction and expose the underlying bone marrow) do repair (Dell'Accio and Vincent, 2010). Shapiro *et al* (1993) characterised the morphological repair sequence of full-thickness cartilage defects in rabbits. Firstly, a fibrin clot formed to fill the defects and persisted for a few days. Then spindle-shaped mesenchymal cells appeared in the superficial and deep layers of the clot and eventually merged into one layer. Chondroid cells formed in the deeper layer, with bone formation underneath, while the chondrocytes in the immediate adjacent cartilage died. Within a few weeks, hypertrophic chondrocytes were seen in the deeper layers, and proteoglycan staining increased. Eventually the osteochondral junction reformed, as did the tidemark. The authors also provided some evidence that the repair tissue was derived from the bone marrow by using thymidine pulse chase experiments in which labelling was first seen in the bone marrow underlying the defect and then in the repair tissue but not in the adjacent cartilage. Anraku *et al* (2009) also showed a similar repair sequence in rat cartilage defects. The authors also characterised the reparative tissue via immunohistochemistry and *in situ* hybridization which showed similarity with that of embryonic joint development.

Eltawil *et al* (2009) created a full-thickness cartilage defect in a murine model and showed repair to be strain- and age-dependent. Young-adult DBA/1 mice consistently fully repaired the defect to the point that it could not be distinguished from the adjacent cartilage, whereas age matched C57BL/6 mice, or older DBA/1 mice attempted to repair the tissue but did not completely regenerate it. Roelofs *et al* (2017) further went on to use this model for a lineage tracing experiment and provided some evidence that mesenchymal stem cells that repair the chondral defect are also derived from the synovium.

As the repair process may be akin to the developmental process, molecules that facilitate chondrogenesis may be important for repair.

1.11 The FGF family of ligands

Fibroblast growth factors (FGFs) are a family of 22 proteins that are ubiquitously expressed and so are involved in a number of different processes around the body. In embryonic development, they maintain cells in their progenitor state, mediate their growth, differentiation, survival and patterning. In adult tissues, they mediate metabolic functions, tissue repair or regeneration. (Ornitz and Itoh, 2015). The FGFs can be divided into 2 groups, those that are secreted and signal to receptor tyrosine kinases (RTKs) and those that are intracellular and serve as cofactors for voltage-gated sodium channels and other molecules (FGF11, FGF12, FGF13, and FGF14) (Goldfarb, 2005). The secreted FGFs can be further divided into 2 groups, those that act in an autocrine/paracrine manner (the canonical FGFs) and those that act in an endocrine manner. Their ability to act in this way is regulated by their affinity for heparan sulfate (HS). The canonical FGFs (FGF2, FGF3, FGF4, FGF5, FGF6, FGF7, FGF8, FGF9, FGF10, FGF16, FGF17, FGF18, FGF20, and FGF22) have a high affinity for HS and so limits their diffusion across the ECM. The HS also acts as a co-factor for their

signalling to FGFRs (Rapraeger *et al*., 1991). The endocrine FGFs (FGF15/19, FGF21 and FGF23), on the other hand, have a low affinity for HS and use Klotho as a co-factor (Goetz *et al*., 2007, Potthoff *et al*., 2012). Here, I will focus on the roles of canonical FGFs in skeletal development and cartilage repair/regeneration.

1.12 The FGF-receptor family

Fibroblast Growth Factor Receptors (FGFRs) are classical tyrosine kinase receptors that are activated upon receptor dimerization. There are 4 types of signalling Fibroblast Growth Factor Receptors (FGFR1-4), each with two split intracellular kinase domains, a transmembrane domain and 3 immunoglobulin-like domains (Ig I, Ig II and Ig III). The first half of Ig III is encoded by an invariant exon (Ig IIIa), while the second half is alternatively spliced to form IIIb or IIIc isoforms. (***Figure 1.4***). Alternative splicing is mostly tissue specific, with epithelial cells predominantly expressing IIIb isoforms and mesenchymal cells predominantly expressing IIIc isoforms. This alternative splicing only occurs for *FGFR1-3* genes and produces FGFR isoforms with unique ligand binding properties (Ornitz *et al*., 1996; Zang *et al*., 2006). Activation through ligand binding mediates a number of different downstream signalling events through a cascade of protein phosphorylation.

There is also another FGFR (FGFR5 or FGFRL1) that was first found in human articular cartilage. However it does not contain an intracellular tyrosine kinase domain and therefore cannot elicit an intracellular signal (Wiedemann and Trueb, 2000). Hence it is thought to act as a decoy receptor (Trueb, 2011).

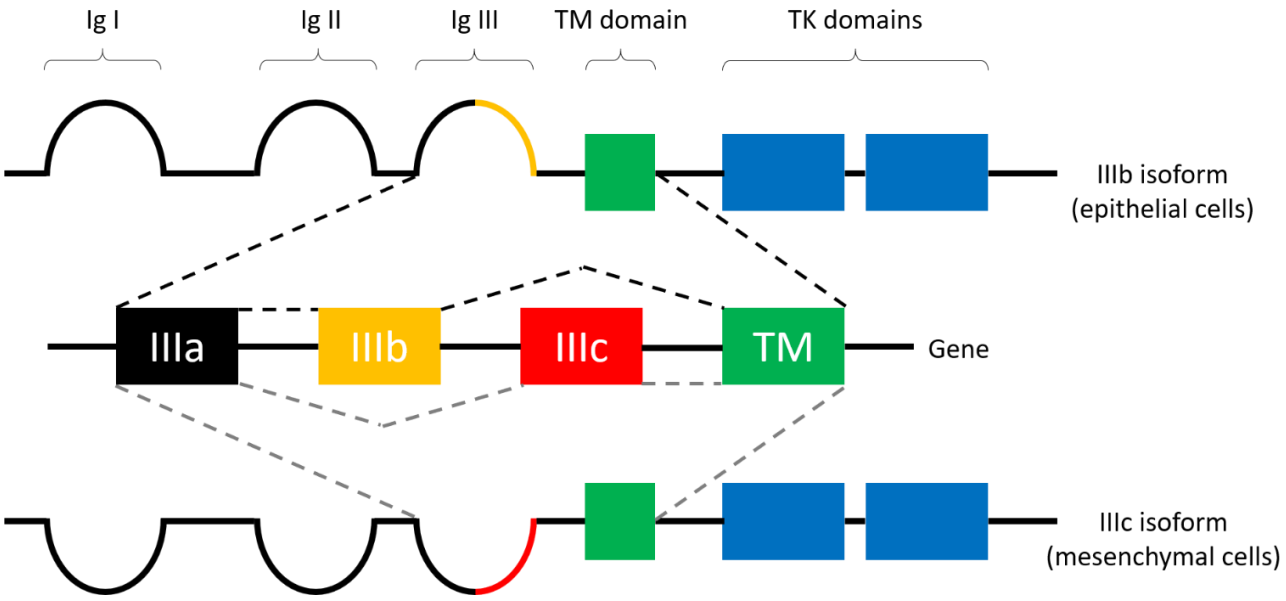

Figure 1.4: FGFR structure and splice variation
FGFR protein structure consists of 3 immunoglobulin-like domains (Ig I, Ig II and Ig III) a transmembrane (TM) domain and 2 split intracellular tyrosine kinase (TK) domains. The Ig III domain is encoded from 2 parts. The first half of Ig III is encoded by an invariant exon (IIIa), which is spliced to either exon IIIb or IIIc. IIIb or IIIc exons are spliced to the exon that encodes the transmembrane domain. Alternative splicing of either the IIIb or IIIc exons depends on the tissue type, with epithelial tissue predominately expressing the IIIb isoforms and mesenchymal cells predominantly expressing the IIIc isoforms. Dotted lines indicate splicing. Image adapted from Naski and Ornitz (1998).

1.13 FGF mediated signalling

HS interacts with FGFs and their receptors acting as a co-factor for their biological activity (Rapraeger *et al*., 1991, Yayon *et al*., 1991, Ornitz and Leder, 1992). The FGFs bind to their receptors between the 2nd and 3rd Ig like domain (Plotnikov *et al*., 1999) and HS binds to the HS binding sites of FGFs and the 3rd Ig like domain of FGFRs (Plotnikov *et al*., 2000). Based on the crystallographic structure HS is thought to promote the formation of a 1:1:1 FGF:FGFR:HS complex that leads to conformation changes that stabilise a symmetrical 2:2:2 dimer, which is biologically active (Schlessinger *et al*., 2000). Though this model is widely accepted, a 2:2:1 crystallographic structure has also been found for FGF1 in complex with FGFR2 (Pellegrini *et al*., 2000). Ornitz *et al* (1992) provided evidence that the length of HS is

important for the biological activity of FGF:FGFR complex, with octasaccharides being the minimum length required, with dose-dependent increase until dodecasaccharide length and a plateau in activity thereafter. This may provide a reason for the difference in the complex structure as decasaccharides can traverse both ligands within the dimer complex, while octasaccharides cannot.

Once receptor dimerization occurs, conformational change of FGFR structure leads to activation of the intracellular tyrosine kinase domains and transphosphorylation on 7 tyrosine residues. These phosphorylated tyrosines function as docking sites for adaptor proteins, which can also undergo phosphorylation to become activated and lead to the activation of multiple signal transduction pathways (Figure 1.5).The 4 main signalling pathways induced by FGFR activation are, Phospholipase C (PLC), Janus kinase/signal transducer and activator of transcription (JAK/STAT), mitogen-activated protein kinase (MAPK) and phosphatidylinositol-3-kinase/ Protein kinase B (PI3K/AKT) (Ellman *et al*., 2013, Carter *et al*., 2015). Activation of these pathways leads to regulation of target genes to mediate cellular processes.

Fibroblast growth factor receptor substrate 2α (FRS2α) is a key adaptor protein constitutively associated with the juxtamembrane region of FGFR and is phosphorylated by activated FGFR kinase. Phosphorylated FRS2α then recruits adaptor protein Growth factor receptor bound 2 (GRB2), which recruits the guanine nucleotide exchange factor Son of sevenless (SOS). The recruited SOS activates the Rat sarcoma (RAS) GTPase, which then activates proto-oncogene serine/threonine-protein kinase (RAF) which goes on to activate mitogen activated protein kinase kinase (MEK). MEK then phosphorylates MAPKs such as extracellularly regulated kinase1/2 (ERK1/2), which activate members of the E26

transformation-specific (ETS) transcription factor family such as ETS translocation variant 4 and 5 (ETV4 and ETV5) and expression of negative regulators of the FGF signalling pathways such as Sprouty (SPRY), Similar expression to FGF (SEF), and Dual-specificity phosphatase 6 (DUSP6) (Kouhara *et al*., 1997, Turner and Grose, 2010, Brent and Tabin, 2004).

GRB2 also recruits the adaptor protein GRB2 associated binding protein 1 (GAB1), which activates Phosphoinositide 3-kinase (PI3K) (Lamothe *et al*., 2004). PI3K then phosphorylates the enzyme AKT, which has a number of activities including phosphorylation of the Tuberous sclerosis complex 2 (TSC2), which leads to the activation of the Ras homolog enriched in brain (RHEB) GTPase, a potent activator of the protein kinase activity of mammalian target of rapamycin complex 1 (mTORC1). Activated AKT also leads to the phosphorylation of the pro-apoptotic transcription factor, Forkhead box protein O1 (FOXO1), causing it to exit the nucleus and promote cell survival (Manning and Cantley, 2007, Ornitz and Itoh, 2015).

The activated FGFR kinase also recruits and activates the enzyme phospholipase C gamma (PLCγ). PLCγ hydrolyses phosphatidylinositol (4, 5)-biphosphate (PIP_2) to phosphatidylinositol (3, 4, 5)-triphosphate (PIP_3) and diacylglycerol (DAG). PIP_3 induces calcium ion release from intracellular stores and the activation of downstream signalling pathways, while DAG activates the enzyme protein kinase C (PKC). PKC phosphorylates RAF, reinforcing the MAPK pathway (Turner and Grose, 2010).

JAKs are also activated by phosphorylated FGFRs. JAKs then phosphorylate and activate STATs particularly STAT1, 3 and 5, which are translocated to the nucleus and act as transcription factors (Su *et al*., 1997, Hart *et al*., 2000, Ornitz and Itoh, 2015).

The negative regulation of FGFR signalling is only partly understood. MAPK/ERK attenuation is the most studied. As mentioned above, ERK signalling leads to the transcription of some of the negative regulators of FGF signalling including *DUSP6* and MAPK phosphatases such as MAPK phosphatase 3 (*MKP3*), *SPRY* and *SEF*. SPRY and SEF proteins modulate receptor signalling at several points in the signal transduction cascade. SPRY proteins compete for GRB2 binding and so prevent SOS mediated RAS activation and activation of the PI3K-AKT pathway. Also, SPRY directly binds to RAF, blocking subsequent MAPK signalling (Lao et al., 2006). Transmembrane SEF can directly bind to FGFRs and so effects receptor phosphorylation, while cytoplasmic SEF can block nuclear translocation of phosphorylated ERK1/2 by binding to activated MEK, to inhibit dissociation of the MEK–MAPK complex (Torii *et al*., 2004, Kovalenko *et al*., 2006). MKP3 dephosphorylates ERK1/2 to attenuate MAPK signalling. DUSP6 directly dephosphorylates MAPK (ERK1/2) on phosphotyrosine and phosphothreonine residues. Moreover ERK1/2 have been shown to inhibit the recruitment of GRB2 by phosphorylating FRS2α (Ekerot *et al*., 2008, Turner and Grose, 2010, Ornitz and Itoh, 2015).Following activation of FGFRs by FGF ligands, the FGFRs are internalised and either degraded by the proteasome or recycled back to the cell membrane. This process is partly controlled by CBL-mediated monoubiquitylation. CBL is an E3 ubiquitin ligase that exists in a complex with GRB2 and is recruited to phosphorylated FRS2α, forming a ternary complex that is ubiquitinated and degraded. In addition, recruitment of phosphorylated CBL:GRB2 complex also attenuates FGFR signalling by competing with GRB2:SOS for binding to the direct GRB2-binding sites on phosphorylated FRS2α (Wong *et al*., 2002, Turner and Grose, 2010, Ornitz and Itoh, 2015).

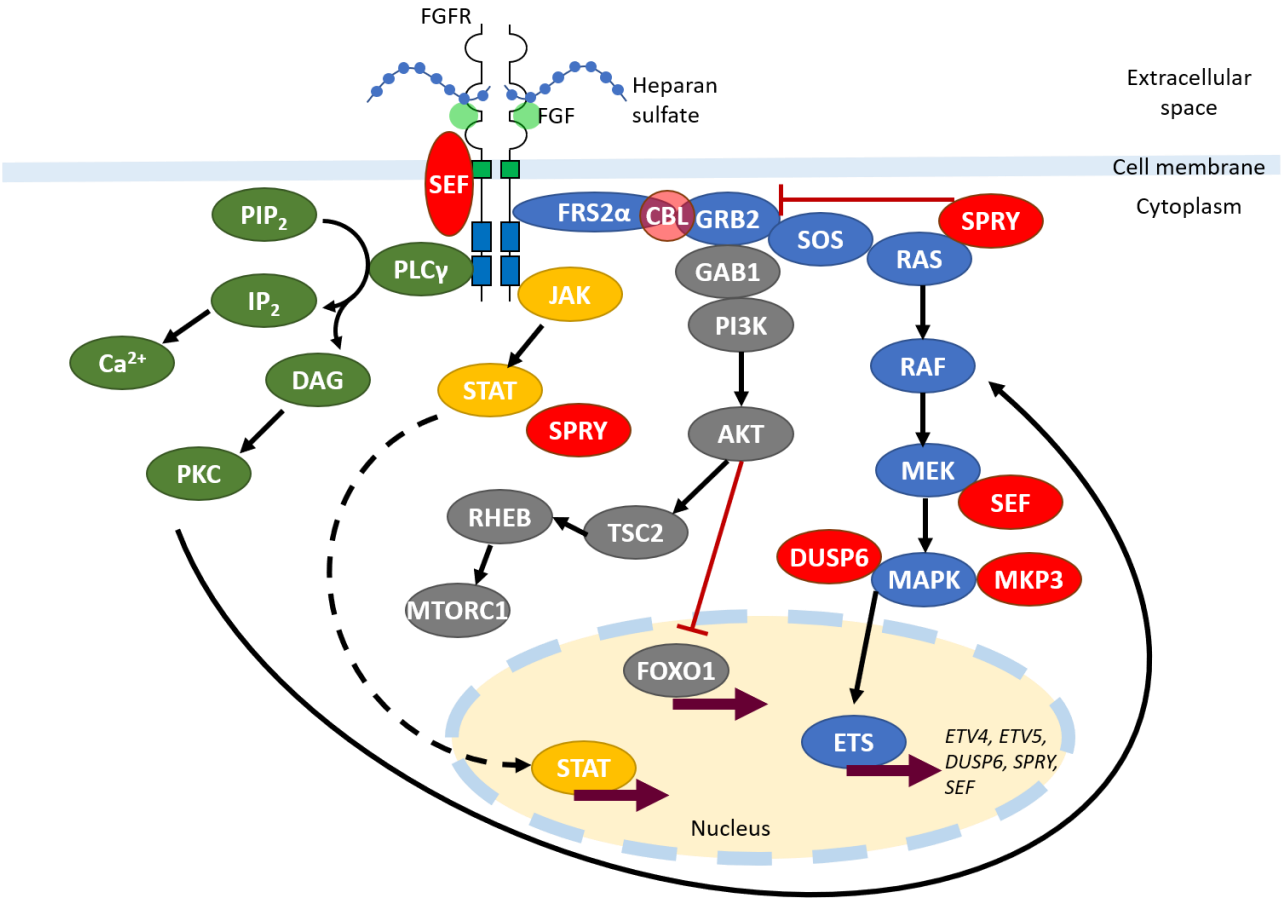

Figure 1.5: FGFR signalling pathways

Binding of FGFs and the co-factor heparan sulfate changes the conformation of FGFRs, allowing receptor dimerization and activation of the intracellular tyrosine kinase domains. This leads to transphosphorylation on tyrosine residues of FGFRs, which function as docking sites for adaptor proteins and activation of 4 main signalling pathways. Mitogen-activated protein kinase (MAPK) pathway (in blue): FGFR kinase phosphorylates FRS2α (a key adaptor protein that is constitutively associated with the juxtamembrane region of FGFR), which then recruits adaptor protein GRB2. GRB2 recruits SOS, a guanine nucleotide exchange factor, which activates RAS GTPase. RAS activates RAF protein kinase, which phosphorylates MEK. MEK then phosphorylates MAPKs such as extracellularly regulated kinase1/2, which activate members of the E26 transformation-specific (ETS) transcription factor family such as ETV4, 5 and expression of negative regulators of the FGF signalling pathways such as *SPRY*, *SEF*, and *DUSP6*. Phosphatidylinositol-3-kinase/ Protein kinase B (PI3K/AKT) pathway (in grey): GRB2 also recruits the adaptor protein GAB1 which activates PI3K. PI3K phosphorylates the enzyme AKT. AKT phosphorylates TSC2 and leads to activation of RHEB GTPase, a potent activator of mTORC1. Activated AKT also phosphorylates the pro-apoptotic transcription factor FOXO1, causing it to exit the nucleus and promote cell survival. The Phospholipase C (PLCγ) pathway (in green): activated FGFR kinase recruits and activates the enzyme PLCγ which hydrolyses PIP_2 to PIP_3 and DAG. PIP_3 induces calcium ion release from intracellular stores and the activation of downstream signalling pathways, while DAG activates the enzyme PKC (protein kinase C). PKC phosphorylates RAF reinforcing the MAPK pathway. The Janus kinase/signal transducer and activator of transcription (JAK/STAT)

pathway (in yellow): activated FGFRs phosphorylate JAKs which then phosphorylate and activate STATs. STATs can then translocate to the nucleus and act as transcription factors.

The negative regulation of FGFR signalling (in red). MAPK signalling leads to the transcription of some of the negative regulators of FGF signalling. SPRY proteins compete for GRB2 binding and so prevent SOS mediated RAS activation and activation of the PI3K-AKT pathway. Also, SPRY directly binds to RAF, blocking subsequent MAPK signalling. Cytoplasmic SEF binds to activated MEK to inhibit dissociation of the MEK–MAPK complex and thus block nuclear translocation of phosphorylated MAPKs. Transmembrane SEF directly binds to FGFRs and so effects receptor phosphorylation. MKP3 dephosphorylates the MAPKs ERK1/2 and DUSP6 directly dephosphorylates MAPKs. CBL (an E3 ubiquitin ligase) is recruited to GRB2 bound to phosphorylated FRS2α, forming a ternary complex that results in ubiquitination of FGFR and FRS2α and thus FGFR internalisation and either degradation by the proteasome or recycling back to the cell membrane.

Image modified from Turner and Grose (2010) and Ornitz and Itoh (2015).

1.14 FGF in endochondral ossification

FGFs and FGFRs are expressed throughout the development of the skeleton in a time- and space-dependent manner. At the precondensation stage, distal limb-bub mesenchyme express FGFR1 and FGFR2 (Figure 1.6A) (Orr-Urtreger *et al*., 1991, Sheeba *et al*., 2010), which respond to FGF4 and FGF8 produced by the apical ectodermal ridge (AER; a specialized thickening of epithelium at the tip of the growing limb) and are responsible for proximo-distal outgrowth. During condensation, FGFR2 expression is increased and overlaps with SOX9 expression. Cells in the periphery, which eventually become the periosteum and perichondrium express both FGFR1 and FGFR2 (Delezoide *et al*., 1998, Ohbayashi *et al*., 2002). When the mesenchyme differentiates into chondrocytes, FGFR3 expression is increased (Delezoide *et al*., 1998, Peters *et al*., 1993) along with SOX9 and collagen type II. (Figure 1.6B). FGF9 and FGF18 are expressed in adjacent mesenchyme and later in development are found in the perichondrium and periosteum (Ohbayashi *et al*., 2002, Liu *et al*., 2002). As chondrocytes become hypertrophic, FGFR3 expression is decreased, and FGFR1 expression increases (Figure 1.6C) (Peters *et al*., 1992, Jacob *et al*., 2006). As development continues, FGFR1 and FGFR2 are expressed in osteoblasts (Figure 1.6D) (Ohbayashi *et al*., 2002, Jacob *et al*., 2006), whereas FGFR3 is found in chondroprogenitor cells in the growth plate (Figure 1.6E) (Peters *et al*., 1993). Postnatally FGFR1 and FGFR3 are expressed in articular chondrocytes (Figure 1.6F) (Yan *et al*., 2011, Weng *et al*., 2012).

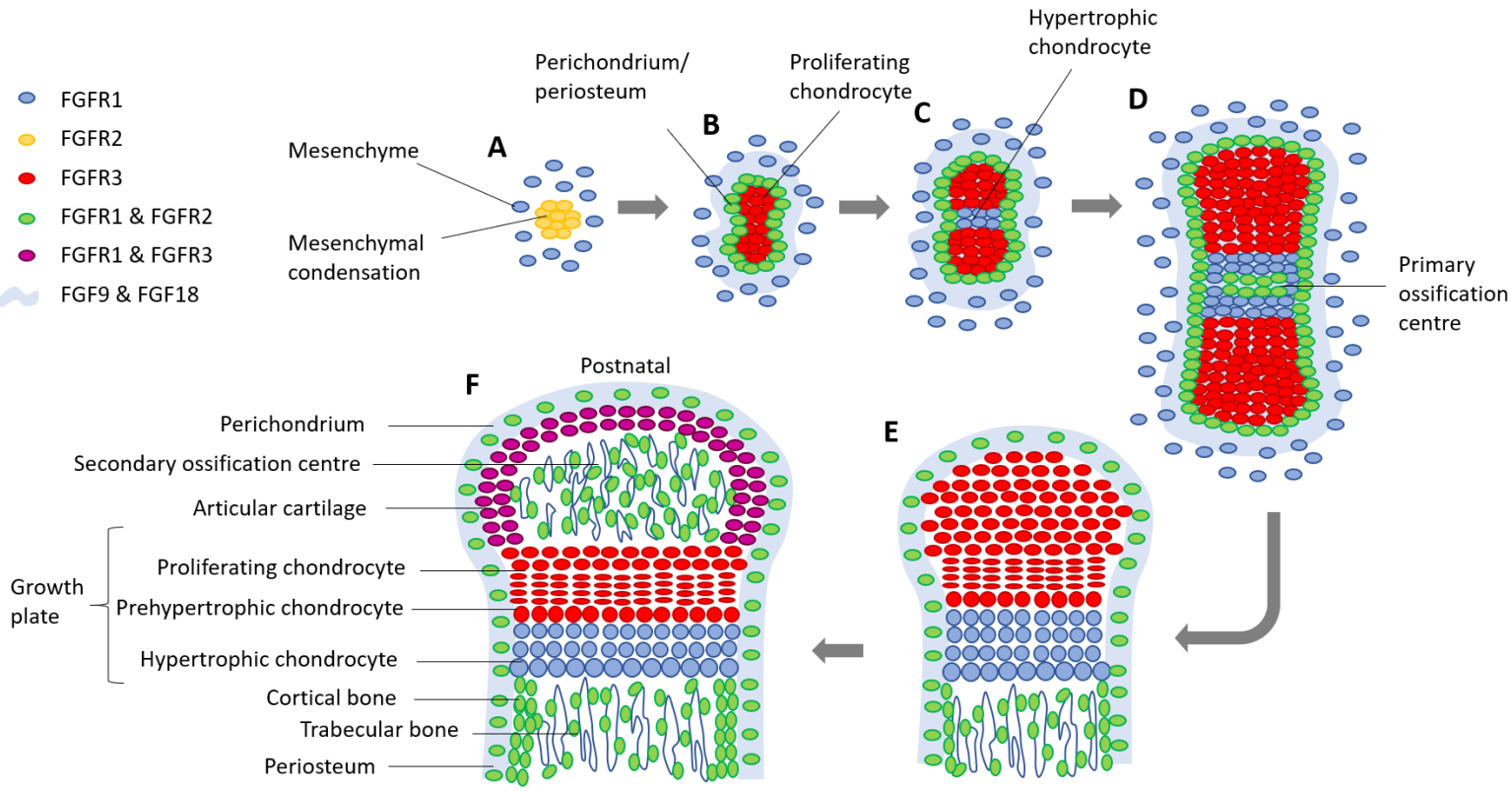

Figure 1.6: FGFs and FGFRs in endochondral ossification

FGFs and FGFRs are expressed during skeletal development in a time- and space-dependent manner. (A) Endochondral ossification begins with the condensation of mesenchymal cells in the regions of the embryo destined to become bone. As cells condense, FGFR2 expression is increased and cell differentiation occurs. (B) When the mesenchyme differentiates into chondrocytes, FGFR3 expression is increased. The chondrocytes begin producing the extracellular matrix components of cartilage, thus laying down a cartilaginous template for bone formation. Cells in the periphery, which eventually become the periosteum and perichondrium express both FGFR1 and FGFR2 while FGF9 and FGF18 are expressed in the adjacent mesenchyme. (C) The chondrocytes in the middle of the diaphysis become hypertrophic as FGFR3 expression decreases and FGFR1 expression increases. (D) A primary ossification centre develops in the centre of the diaphysis due to vascularisation in this region. Here the chondrocytes undergo proliferation, maturation and hypertrophy. Osteoblasts then migrate into the cartilage from the blood vessels and begin mineralising the ECM to form bone. As development continues FGFR1 and FGFR2 are expressed in osteoblasts. (E) This process radiates outward with the formation of the cartilaginous growth plates at the distal ends of the long bones that separate the epiphyses from the diaphysis. (F) A secondary ossification site then forms in the centre of the epiphysis. Postnatally FGFR1 and FGFR3 are expressed in the articular cartilage that lines the top of the epiphysis. Figure sourced and adapted from Ornitz and Marie (2015).

1.15 FGF in membranous bone formation

FGF2 and 9 have been shown to be expressed throughout the calvarial mesenchyme, underlying dura mater and developing bones (Kim *et al*., 1998, Rice *et al*., 2000). However, FGF2 expression is much higher in the sutural mesenchyme between the osteogenic fronts (Rice *et al*., 2000). FGF20 expression is detected in sutural mesenchyme (Hajihosseini and Heath, 2002) and FGF18 is expressed in osteogenic mesenchyme and differentiating osteoblasts (Ohbayashi *et al*., 2002). There is also increased FGF2 staining associated with osteoblast differentiation during sutural fusion (Mehrara *et al*., 1998).

FGFR1-3 are all expressed during intramembranous ossification of the skull (Delezoide *et al*., 1998). FGFR1 is expressed in mesenchyme and later in osteoblasts; FGFR2 is expressed at sites of ossification in differentiating osteoblasts and FGFR3 is detected at low levels in sutural osteogenic fronts at late stages of development (Ornitz and Marie, 2002).

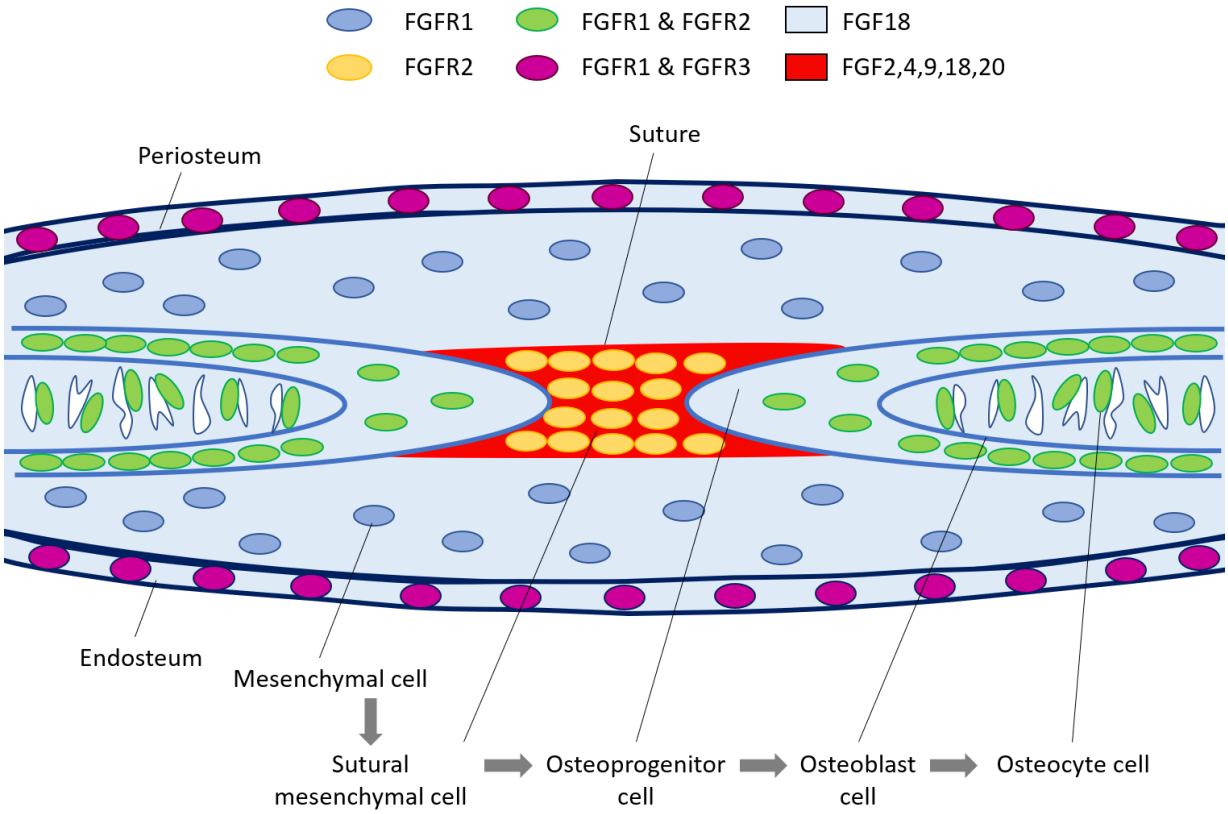

Figure 1.7: FGFs and FGFRs in intramembranous ossification
During intramembranous ossification expression of FGFs and FGFRs is temporally and spatially regulated. As with endochondral ossification, mesenchymal cells that express FGFR1 condense and begin to express FGFR2. However instead of forming a cartilaginous template, these mesenchymal cells progressively differentiate into osteoblasts, to form a mineralized matrix within ossification centres. In calvarial bones, the ossification centres expand during development but do not fuse at the junction with other cranial bones to allow for skull expansion during growth. This junction is termed a “suture”. The suture is where FGF2, FGF4, FGF9, FGF18 and FGF20 are expressed. FGF18 is also detected in calvarial mesenchymal cells. Proliferation of mesenchymal cells is followed by differentiation into osteoprogenitor cells which express FGFR1 and FGFR2. Osteoprogenitor cells differentiate into pre-osteoblasts and then into bone matrix-forming mature osteoblasts, which are found along the developing bone trabeculae. FGF18 is also expressed in osteogenic mesenchyme and in differentiated osteoblasts on the endosteal and periosteal surface of cranial bones. FGFR1 and FGFR3 are also expressed in the endosteum and periosteum. At the end of the bone formation period, osteoblasts die by apoptosis or become embedded in the matrix as osteocytes, which then eventually also undergo apoptosis. Figure sourced and adapted from Ornitz and Marie (2002).

1.16 Functional importance of FGF signalling through KO models and human genetic perturbation

The importance of FGF signalling in skeletal development was first highlighted with the discovery that a point mutation in the transmembrane domain of FGFR3 causes Achondroplasia; the most common form of dwarfism (Shiang *et al*., 1994). Since then many gain-of-function mutations in FGFR1-3 have been associated with skeletal dysplasias (Ornitz and Itoh, 2015).

Mutations associated with short-limb dwarfism of Hypochondroplasia, Achondroplasia and Thanatophoric dysplasia, activate FGFR3 by increasing degrees, reflecting the increase in severity of the phenotype (Naski *et al*., 1996). The G380R mutation in the transmembrane domain of FGFR3 activates the receptor in a ligand-dependent manner, whereas the R248C mutation in the extracellular domain or the K650E mutation in the intracellular domain of Thanatophoric dysplasia type I or type II, activates FGFR3 in a ligand-independent manner (Ornitz and Itoh, 2015). The gain-of-function in FGFR3 results in decreased chondrocyte proliferation, impaired hypertrophic differentiation (Legeai-Mallet *et al*., 2004), and increased apoptosis (Legeai-Mallet *et al*., 1998) of growth plate chondrocytes (Naski *et al*., 1998).

Craniosynostoses (syndromes that are characterised by premature fusion of the cranial sutures) are mainly due to gain-of-function mutations in FGFR2 but can also be due to mutations in FGFR1 and FGFR3 (Naski and Ornitz, 1998). Several of the mutations in FGFR1 and 2, that result in Apert syndrome, Crouzon syndrome, Pfeiffer syndrome and Jackson-Weiss syndrome lead to stabilisation of intermolecular disulfide bonds, causing ligand-independent dimerization and constitutive signalling (Neilson and Friesel, 1995, Galvin *et al*.,

1996, Robertson *et al*., 1998), while others can prolong the duration of the receptor signalling (Anderson *et al*., 1998, Ibrahimi *et al*., 2001) or alter ligand binding specificity (Yu *et al*., 2000, Hajihosseini *et al*., 2001). Analysis of fused cranial sutures in human craniosynostoses showed that increased bone formation at the sites of primary ossification was due to increased osteoblast maturation (De Pollack *et al*., 1996, Lomri *et al*., 1998).

Knocking out *Fgfr1* (Deng *et al*., 1994) or *Fgfr2* (Xu *et al*., 1998) in mice is embryonically lethal, reflecting their utmost importance in development. *Fgfr3* null mice, do not show any obvious developmental defects prenatally, but do show disruptions in endochondral ossification postnatally. These mice exhibit tail distortions, elongation of the vertebral bodies and develop scoliosis/kyphosis and bowed femurs. They have a tall stature due to expanded proliferating and hypertrophic chondrocyte zones of the growth plate, which persists into adulthood (Deng *et al*., 1996, Colvin *et* al., 1996). This highlights the importance of FGFR3 negatively regulating endochondral ossification.

KO models of FGF ligands have shown no obvious skeletal developmental defects except that of FGF8, 9 and 18 (indicating some redundancy of the other FGF ligands). FGF9 and 18 have stage-specific effects on chondrogenesis. At early stages of development of the proximal elements, there is a decrease in chondrocyte proliferation and a delayed initiation in chondrocyte hypertrophy in the *Fgf9*$^{-/-}$ mice (Hung *et al*., 2007). Decrease in chondrocyte proliferation of the more distal skeletal elements is also seen in *Fgf18*$^{-/-}$ mice (Liu *et al*., 2007). This is consistent with these ligands signalling through FGFR3 on immature chondrocytes to have a promitogenic effect (Iwata *et al*., 2000). At later stages of development both *Fgf9*$^{-/-}$ and *Fgf18*$^{-/-}$ mice show an expanded zone of hypertrophic chondrocytes in the growth plate with increased Ihh, Ptc and Pth1R expression; which

phenocopy with the *Fgfr3*$^{-/-}$ mice and therefore provide further evidence for FGFR3 signalling to negatively regulate chondrocyte proliferation and differentiation in the growth plate (Hung *et al*., 2007, Ohbayashi *et al*., 2002, Liu *et al*., 2002). *Fgf18*$^{-/-}$ mice but not *Fgfr3*$^{-/-}$ mice also show delayed ossification and decreases in osteogenic markers, with defects in osteoblast proliferation and differentiation; including delayed cranial suture closure; suggesting FGF18 signalling through other FGFRs is important in bone development (Ohbayashi *et al*., 2002, Liu *et al*., 2002, Liu *et al*., 2007).

Table 1: OA related phenotypes of mice that lack FGFs or FGFRs

Gene	Conditional/ whole body KO	OA related phenotype	Reference
Fgf2	Whole body (all isoforms)	Reduced bone mass, decreased trabecular bone volume by 4.5 months of age	(Montero *et al*., 2000)
		Accelerated spontaneous OA (by 6 months of age) Accelerated OA with DMM	(Chia *et al*., 2009)
	High molecular weight isoform	Increased bone mineral density Increased trabecular bone volume Increased cortical bone thickness Decreased cortical porosity (by 2 months of age)	(Homer-Bouthiette *et al*., 2014)
Fgf8	Conditional KO in AER (*Msx2-cre*)	Reduction in limb-bud size, hypoplasia or aplasia of specific skeletal elements	(Moon and Capecchi, 2000, Lewandoski *et al*., 2000)
Fgf9	Whole body	Rhizomelia (disproportionate shortening of the proximal skeletal elements).	(Hung *et al*., 2007)
Fgf10	Whole body	Abolished limb bud initiation	(Min *et al*., 1998, Sekine *et al*., 1999)
Fgf18	Whole body	Smaller skeletal size Increased curvature of radius and tibia Delayed ossification	(Ohbayashi *et al*., 2002, Liu *et al*., 2002)
Fgfr1	Conditional KO in adult articular chondrocytes (*Col2a1-creER*)	Delayed progression of articular cartilage degradation/OA following DMM surgery	(Weng *et al*., 2012)
Fgfr2	KO of IgIII domain	Failure of limb bud induction	(Xu *et al*., 1998)
	Conditional KO in chondrocyte and osteoblast lineages (*Dermo1-cre*)	Skeletal dwarfism in early postnatal development. Reduced bone density, reduced trabecular bone volume by (3 weeks of age) Non-ossified gap in dorsal midline of cervical and thoracic vertebrae and absences of spinous processes. Failure of cavitation of some tarsal joints. Reduced periosteal thickness.	(Yu *et al*., 2003)
Fgfr3	Whole body	Tail distortions (by P3) Elongation of vertebral bodies Scoliosis/kyphosis (by P7) Bowed femurs (by 2/3 months) Tall stature (by 3 months) Osteopenia/ defective trabecular bone mineralisation (by 4 months) Increased spontaneous cartilage degradation by 4 months.	(Colvin *et al*., 1996, Deng *et al*., 1996, Valverde-Franco *et al*., 2004, Valverde-Franco *et al*., 2006)
	Conditional KO in adult chondrocytes (*Col2a1-creER*)	Increased progression of articular cartilage degradation/OA following DMM surgery (within 1-month post-surgery)	(Tang *et al*., 2016)

1.17 FGF2

Fibroblast growth factor 2 (also known as basic FGF due to its overall basic composition of amino acids and high isoelectric point), was the first FGF to be identified and purified from extracts of the bovine pituitary; where it stimulated the growth of murine fibroblasts at low concentrations (Armelin, 1973, Gospodarowicz, 1975, Lemmon and Bradshaw, 1983). This original FGF2 was found to be an 18 kDa protein, however since its discovery, higher molecular weight isoforms of 22, 23, 24, and 34 kDa have also been found, though they remain localised to the nuclear compartment (Florkiewicz *et al*., 1991, Bugler *et al*., 1991, Arnaud *et al*., 1999). The low molecular weight isoform (18 kDa) is found primarily in the cytoplasm and is the only isoform exported from the cell (Davis *et al*., 1997). The low molecular weight isoform binds to all mesenchymal FGFRs (Ornitz *et al*., 1996).

Fgf2$^{-/-}$ mice (which do not have any functional FGF2 isoform) do not have any obvious developmental defects despite its ubiquitous expression in WT tissues (Hébert *et al*., 1990). *Fgf2*$^{-/-}$ mice are all viable, fertile and have a normal lifespan, however they exhibit; decreased vascular smooth muscle contractility and therefore low blood pressure (Zhou *et al*., 1998); reduced cortical neuron density (Ortega *et al*., 1998); and defects in response to cardiac (Virag *et al*., 2007), or cutaneous (Ortega *et al*., 1998) injury. Later in adulthood, *Fgf2*$^{-/-}$ mice also have reduced bone mineral density (Montero *et al*., 2000).

1.18 FGF2 in cartilage

In articular cartilage, FGF2 is found in the pericellular matrix (PCM) bound to the heparan sulfate proteoglycan; perlecan (Vincent *et al*., 2007, Chia *et al*., 2009). Upon injury or mechanical loading, it is released from this pericellular pool to act on its receptor/s to mediate cellular responses (Vincent *et al*., 2002, Vincent *et al*., 2007).

There is some controversy as to FGF2's role in cartilage. It has been shown to have anti-anabolic effects in human tissue in *in vitro* culture by inhibiting the effects of two anabolic factors normally produced in cartilage; insulin-like growth factor (IGF-1) and osteogenic protein 1 (OP-1) (Loeser *et al*., 2005). Li *et al* (2012) also showed FGF2 to cause proteoglycan loss (in a dose-dependent manner) when added to the culture medium of human knee cartilage explants. Furthermore, FGF2 stimulation of cultured human chondrocytes induced the expression of *MMP-13*; the major collagenase in cartilage (Im *et al*., 2007). These results suggest that FGF2 is pro-catabolic.

In contrast, our group found that FGF2 had anti-catabolic effects; suppressing IL-1-induced expression of the major aggrecanases *ADAMTS-4* and *ADAMTS-5* in human articular cartilage explants (Sawaji *et al*., 2008). Moreover, we have provided evidence for FGF2 being chondroprotective *in vivo*, as *Fgf2*$^{-/-}$ mice develop accelerated spontaneous OA with joint changes by 6 months of age. These mice also have accelerated OA with joint destabilisation, which can be prevented with FGF2 injection. *ADAMTS5* mRNA levels in the joints of these *Fgf2*$^{-/-}$ mice were also superinduced. (Chia *et al*., 2009). These results suggest a protective role for FGF2 in cartilage.

In light of the evidence presented in these papers, it becomes difficult to say for certain whether FGF2 is beneficial to cartilage or not. The reason for this is that the chondrocytes tested in these experiments were all from varying sources; human, mouse, porcine; human cartilage was from knees and ankles; and chondrocytes tested were in cell suspension, monolayer and explants. Therefore, there are multiple factors that differ in these experiments, which could account for the difference in the cell/tissue behaviour.

One theory to explain these opposing effects of FGF2 is that it mediates different effects depending on which receptor it is acting through. Knockout studies in mice have provided support for this theory. Valverde-Franco *et al* (2006) showed *Fgfr3*$^{-/-}$ mice develop accelerated spontaneous OA, with joint changes visible at 4 months of age. Tang *et al* (2016) also showed that mice in which *Fgfr3* is conditionally knocked out in adult mouse cartilage, have worse disease when OA is surgically induced by destabilising the medial meniscus. *Fgfr1* conditional knockout mice on the other hand, are protected from spontaneous and surgically-induced OA (Weng *et al*., 2012). These studies thus suggest FGF2 acts through FGFR1 to mediate catabolic effects and mediates chondroprotective effects through FGFR3. Therefore, the relative ratios of these receptors may determine the cellular response to FGF2.

Yan *et al* (2011) have already shown that *FGFR3* mRNA expression in osteoarthritic cartilage is down-regulated. They also showed that FGF2 can act through FGFR1 to down-regulate *FGFR3* in human articular chondrocytes (in monolayer). As one prominent effect of explantation of cartilage is a rapid release of FGF2, this may lead to a shift in the balance of FGFRs in favour of FGFR1. This is likely to have consequences upon the *in vitro* responsiveness of the tissue and thus explain the predominant pro-catabolic phenotype of explanted cartilage.

1.19 Aims and objectives

The main aims of this project are to investigate whether:

1. the regulation of FGFR balance may direct FGF2's effects by comparing the expression of *FGFR*s in porcine and murine cartilage in response to injury.
2. specific FGFR ligation drives different FGF-mediated signalling by using selective ligands.
3. FGF2 promotes intrinsic repair of cartilage by using an *in vivo* repair model.
4. FGF2's chondroprotective response is directed at the MSC rather than the chondrocyte by using migration assays and chondrogenesis assays.

2 Materials and Methods

2.1 Reagents and Chemicals

2.1.1 General reagents

Materials were purchased from the following sources: Trizma base, sodium chloride, sodium pyrophosphate, beta-glycerophosphate, Np40/IGEPAL sodium dodecyl sulfate (SDS), sodium vanadate, sodium deoxycholate, ammonium persulfate, Tris-HCl, tetramethyl-ethylenediamine, Tween 20, glycine, Bromophenol-2, bovine serum albumin (BSA), ethylenediaminetetraacetic acid (EDTA) and deoxycholic acid from Sigma-Aldrich Company Ltd (Dorset, UK); glycerol, methanol, ethanol, from VWR International (Leicestershire, UK).

2.1.2 Table of recombinant proteins and inhibitors used in tissue culture

Table 2: Table of recombinant proteins and inhibitors used in tissue culture

Proteins/inhibitors	**Specificity**	**Source**
FGFRi SB402451	All FGFRs	Gift from GSK
TGFβi SB431542	ALK4 and ALK5 inhibitor R&D systems	R&D systems, Minneapolis, USA
Heparan sulfate	Porcine glycosaminoglycan	Isolated in-house
FGF2	FGFR1 and FGFR3	Peprotech EC Ltd. London, UK
FGF18	Predominantly FGFR3, but also FGFR1	Peprotech EC Ltd. London, UK
FGF2-V2 (with 50 mM DTT)	FGFR1	ProCore, Israel.
FGF18-V1 (with 50 mM DTT)	FGFR3	ProCore, Israel.

2.1.3 Table of antibodies used for Western blotting

Table 3: Table of antibodies used for Western blotting

Antibody specificity	Type	Source	Dilution
Phospho-Akt (Ser473)	Rabbit monoclonal	Cell Signalling #4060	1:1000 5% milk/TBST
Phospho-Akt Substrate (RXXS*/T*)	Rabbit monoclonal	Cell signalling #9614	1:1000 5% milk/TBST
(T-ERK) ERK 1 Antibody (K-23)	rabbit polyclonal	Santa Cruz, sc-94	1:1000 5% milk/TBST
Anti-alpha Tubulin antibody [DM1A]	monoclonal mouse	Abcam ab7291	1:10,000 5% BSA/TBST
Phospho-p44/42 MAPK (Erk1/2) (Thr202/Tyr204)	Rabbit monoclonal	Cell Signalling #4370	1:1000 5% milk/TBST
p-MTOR Ser2448	rabbit polyclonal	Cell signalling #2971	1:1000 5% BSA/TBST
p-P70 S6 Kinase Thr389 (108D2)	Rabbit monoclonal	Cell Signalling #9234	1:1000 5% BSA/TBST
Phospho-Akt (Thr308) (244F9)	Rabbit monoclonal	Cell Signalling #4056	1:1000 5% BSA/TBST
β-Actin (D6A8)	Rabbit monoclonal	Cell Signalling 8457	1:1000 5% BSA/TBST
Polyclonal Swine Anti-Rabbit Immunoglobulins HRP	Swine polyclonal	Dako P0217	1:1000 5% milk/TBST
Rabbit Anti-mouse Immunoglobulins HRP	Rabbit polyclonal	Dako P0260	1:1000 5% milk/TBST

2.2 Tissue culture

Dulbecco's modified Eagle's medium (DMEM) with 4.5 g/l of glucose and L-glutamine (Lonza, Verviers, Belgium) was always supplemented with 100 U/ml Penicillin and 100 U/ml Streptomycin (Lonza, Verviers, Belgium), 2 µg/ml Amphotericin B (Sigma-Aldrich, Dorset, England) and 25 mM 4-(2-hydroxyethyl)-1-piperazineethanesulfonic acid (HEPES) solution

(Lonza, Verviers, Belgium). Serum containing DMEM had 10 % FBS (heat-inactivated; Gibco, Massachusetts, USA) added. Trypsin-EDTA was from Lonza (Verviers, Belgium).

All cell culture plastics were purchased from Beckton-Dickinson (Oxford, UK).

All experiments were carried out inside a class II laminar flow cabinet to maintain sterility of all tissues cultured.

2.3 Porcine cartilage explantation

Trotters from 3-6-month-old pigs were obtained from an abattoir (Cheale Meats Limited, Essex, UK) within 12 h of slaughter. Before use, trotters were soaked in 1 % virkon solution (Rely+On disinfectant Technologies, Suffolk, UK) for at least 20 min for disinfection. A 22-blade scalpel was used to skin the trotter and remove the 1st and 5th digits. Using a 10A-blade scalpel, the metacarpophalangeal (MCP) joint was opened carefully in a biological safety cabinet, (or for hypoxic experiments in an Invivo2 400 Hypoxia Workstation (Ruskinn Technology, Ltd, Bridgend, Wales) set at 1% O_2). The articular surface was washed with 10 ml PBS 3 times, to remove any synovial fluid. Cartilage was then dissected from the articular surfaces using a 15-blade scalpel (all scalpels were sterile and from Swann Morton, Sheffield, UK).

For 0 h time-points, explants were directly placed in a 7 ml bijou that was embedded in dry ice. For all other time-points, explants were placed in 7 ml bijous containing 3 ml serum-free or 10 % serum containing DMEM and cultured in a humidified incubator at 37 °C, 20 % O_2 (or for hypoxic experiments left in the hypoxic workstation at 37 °C, 1 % O_2). After the appropriate time, media was aspirated, and explants stored in RNA Later at -20 °C.

2.4 Porcine chondrocyte isolation

Porcine MCP cartilage explants were dissected into a 50 ml Falcon tube containing a 20 ml solution of 10 % FBS DMEM with 1 mg/ml collagenase A (Roche Pharmaceuticals, Hertfordshire, U.K.). Cartilage was left to digest overnight (~16 h), with shaking (180 RPM) at 37 °C. The digest was passed through a 70 µm cell strainer and centrifuged at 1500 RPM for 5 min. The cell pellet was resuspended in 20 ml serum-free DMEM and centrifuged at 1500 RMP for 5 min, 3 times.

Cells were counted and plated at $2x10^6$ cells/well of a 6-well plate in 2 ml 10 % FBS DMEM for gene expression experiments, or $1x10^6$ cells/well of a 12-well plate in 1 ml 10 % FBS DMEM for protein analysis experiments. Cells were left to adhere to the bottom of the plate overnight.

For digested samples, an aliquot of $2x10^6$ cells was taken before plating, then pelleted and lysed in 1 ml TRIzol (Ambion, UK).

2.5 Porcine MCP joint injections

Trotters were skinned, the 1st and 5th digits removed and incubated in a humidified environment at 37 °C for 2 h to equilibrate, before being injected. MCP joints were injected using a 25 G needle with either 1 ml 250 nM FGFRi SB402451, TGFβi SB431542 or 0.00125 % DMSO (vehicle control) on both sides of the joint; 1 ml 40 ng/ml FGF2, FGF18 or PBS, on both sides of the joint, or left non-injected. Trotters were then incubated at 37 °C, 5 % CO_2 for 1 h prior to explantation.

2.6 Synovium explantation

All possible synovium was explanted from the injected porcine MCP joint as soon as the joint was opened and placed directly into a bijou on dry ice. Samples were homogenised in 1 ml TRIzol (Ambion, UK).

2.7 Mouse hip explantation

Mice aged 5-6 weeks were euthanised in a CO_2 chamber and death confirmed by cervical dislocation. Mice were skinned from the midriff downwards; the leg was extended and the thigh muscle cut to the point of the femoral artery to expose the hip joint. Ligaments were cut to expose the femoral head; sterile forceps were used to squeeze the sides of the femoral head to release the articular cartilage from the bone.

For 0 h time-points, hips were placed directly in an Eppendorf tube and snap frozen in liquid nitrogen. For all other time-points, hips were placed directly into a well of a 96-well round bottom plate containing 100 µL of serum-free DMEM and cultured in an incubator at 37 °C, 5 % CO_2. At the required time, hips were removed from the media, placed in an Eppendorf tube containing 100 µL RNA Later and frozen at -80 °C.

2.8 RNA extraction

2.8.1 porcine chondrocytes in monolayer

Cell samples were lysed in 1 ml TRIzol (Ambion, UK), transferred to 1 ml Eppendorf tubes and either frozen at -80 °C or RNA extraction was continued. Samples were placed in an orbital mixer for 5 min at room temperature to disrupt nucleosome links. 200 µl 1-Bromo-3-chloropropane (Sigma-Aldrich, Dorset, England) was added, samples vortexed and left for 5

min at room temperature before centrifuging at 13,000 RPM for 10 min at 4 °C to phase separate.

500 µl of the RNA phase was added to equal volumes of 70 % ethanol and either stored overnight or immediately run through the Qiagen (Hilden, Germany) RNeasy Kit. 700 µL of the sample was added to an RNeasy Mini spin column placed in a 2 ml collection tube. Samples were centrifuged at 10,000 RMP for 15 s, the supernatant discarded and the process repeated until all the sample was run. 350 µl Buffer RW1 was added to each spin column, centrifuged at 10,000 RMP for 15 s. 80 µl DNase1/RDD mix was added to each column, and left to digest at room temperature for 15 min, prior to a further wash with Buffer RW1. 500 µl Buffer RPE was added to each spin column, centrifuged for 15 s at 10,000 RMP. 500 µl Buffer RPE was added to each spin column, centrifuged for 2 min at 10,000 RMP before placing the spin column in a new 2 ml collection tube and centrifuged for 1 min at 13,000 RMP to dry the membrane. Spin columns were placed in 1.5 ml collection Eppendorfs, 50 µl RNase free water was added directly to the column membranes and left for 2 min before centrifuging at 10,000 RPM for 3 min to elute the RNA.

The purity and concentration of the RNA was determined by measuring the absorbance at 230 nm, 260 nm and 280 nm using a NanoDrop spectrophotometer (Thermo Scientific, Wilmington, USA).

2.8.2 porcine explants

Explants were defrosted and homogenised in 3 ml TRIzol with a Polytron PT 1600E bench top homogeniser in 15-30 s bursts for no more than 2 min (while on ice). Samples were centrifuged at 4500 RMP, 4 °C for 10 min. 2 ml of the supernatant was aliquoted into 1 ml tubes and the extraction continued as for cell samples.

2.8.3 murine hips

4 mice hips were pooled per point. Hips were homogenised by cutting using a 15-blade scalpel in 150 µL RLT buffer containing 1 % β-mercaptoethanol. 295 µL of RNase free water was added to the homogenate. 5 µL Proteinase K (Qiagen, Hilden, Germany) was added per sample and the digestion carried out at 55 °C, 80 RPM for 10 min. Samples were centrifuged for 3 min at 10,000 RPM at room temperature. The supernatant was added to 225 µL of 100 % ethanol and then added to a Qiagen (Hilden, Germany) RNeasy MinElute Spin column. Samples were centrifuged at 10,000 RPM for 15 s. 350 µl buffer RW1 was added per column, centrifuged at 10,000 RPM for 15 s to wash the RNA. 80 µl of DNase1 solution was added directly to the membranes and left at room temperature for 15 min to digest. 350 µl buffer RW1 was added per column, centrifuged at 10,000 RPM for 15 s. 500 µl buffer RPE was added per column, centrifuged at 10,000 RPM for 15 s. 500 µl 80 % ethanol was added per column, centrifuged at 10,000 RPM for 2 min to wash. Columns were placed in new 2 ml collection tubes, centrifuged for 5 min at 13,000 RPM to dry the membranes. Columns were then placed in a new 1.5 ml collection tube, 14 µl RNase free water was added directly to the centre of the membrane and incubated at room temp for 10 min. Columns were finally centrifuged for 1 min at 13,000 RPM to elute the RNA.

1 µL of the RNA was added to 1 µL RNase free water and the purity and concentration of the RNA determined by measuring the absorbance at 230 nm, 260 nm and 280 nm using a NanoDrop spectrophotometer (Thermo Scientific, Wilmington, USA).

2.8.4 chondrogenic discs

Molecular grinding resin (G-Biosciences, Missouri, USA) was resuspended in TRIzol as per manufacturers instruction. A wide bore pipette tip was used to transfer chondrogenic discs

to new Eppendorf tubes. 50 µL of resin was added to each disc and homogenised using a disposable pestle. TRIzol from the corresponding discs was added to the homogenised disc/resin and samples centrifuged at 13,000 RPM, 4 °C for 5 min, to pellet the resin. Supernatant was transferred to a new Eppendorf tube and RNA extraction continued as for cells in monolayer. Samples were eluted in 20 µl RNase free water.

The purity and concentration of the RNA was determined by measuring the absorbance at 230 nm, 260 nm and 280 nm using a NanoDrop spectrophotometer (Thermo Scientific, Wilmington, USA).

2.9 Reverse transcription

RNA was reverse transcribed to cDNA in a 20 µl reaction using a High Capacity reverse transcription cDNA kit (Applied Biosystems, Paisley, U.K). Briefly, 100 ng RNA (for murine hips and chondrogenic discs) or 500 ng RNA (for chondrocytes) was added to RNase free water to a total volume of 13.2 µL. A master mix solution was made containing 1X buffer, 1X random primers, dNTP mix 10 mM, 50 U/µL Reverse transcriptase and 20 U/µL RNase inhibitor. 6.8 µL of the master mix was added to each RNA sample and briefly centrifuged to bring down the sample and remove any air bubbles. Samples were run in a bench top thermocycler at the following settings; 25 °C for 10 minutes, 37 °C for 2 h, 85 °C for 5 minutes and 4 °C until samples were removed. Samples were stored at -20 °C until required.

2.10 qPCR

2.10.1 for porcine explants and isolated primary articular chondrocytes

cDNA was diluted 1 in 5. A 10 µl reaction was carried out using 2.5 ng cDNA in a total volume of 4 µl with RNase free water; 5 µl 2X Fast SYBR Green PCR Master Mix (Applied

Biosystems/Life Technologies, Foster City, CA, USA) and 0.5 µl 10 mM specific forward and reverse primers. Samples were run in a 384 well plate in triplicate. The PCR reaction was carried out using the ViiA™ 7 Real-Time PCR System (Applied Biosystems) under the following conditions; 1X stage I: 95 °C for 20 s; 40X stage 2: 95 °C for 1 s; 60 °C for 20 s; 1X stage 3 (melt curve): 95 °C 15 s, 60 °C for 1 min, 95 °C for 15 s. Relative gene expression was calculated using the ΔΔCt method with *18S* as the control gene. (*18S* was deemed to be a good housekeeping gene as the Ct values between samples were consistent and within 0.5 of each other).

Receptor ratios were calculated by the following equation: 2^-(Ct value of FGFR1- Ct value of FGFR2 or FGFR3) for each individual sample.

2.10.2 for murine hips

30 µL RNase free water was added to the cDNA. 50 µL 2X TaqMan universal PCR master mix (Applied Biosystems/Life Technologies, Foster City, CA, USA) was added per sample and run on a TaqMan custom card. The PCR reaction was carried out using the ViiA™ 7 Real-Time PCR System (Applied Biosystems) under the following conditions; 1X stage I: 50 °C for 2 min, 95 °C for 10 min; 40X stage 2: 95 °C for 15 s; 60 °C for 1 min. Relative gene expression was calculated using the ΔΔCt method with *18S* as the control gene.

2.10.3 for chondrogenic discs

cDNA was diluted 1 in 5. A 10 µl reaction was carried out using 1 ng cDNA in a total volume of 3 µl with RNase free water; 5 µl 2X TaqMan universal PCR master mix and 0.5 µl 20X TaqMan primers. Samples were run in a 384 well plate in duplicate. The PCR reaction was carried out using the ViiA™ 7 Real-Time PCR System (Applied Biosystems) under the

following conditions; 1X stage I: 95 °C for 20 s; 40X stage 2: 95 °C for 1 s; 60 °C for 20 s. Relative gene expression was calculated using the ΔΔCt method with β2M as the control gene.

2.11 Primers

2.11.1 SYBR green

Porcine specific primers were designed and tested in house prior to use. Briefly; USCS Genome browser was used to examine all gene variants to find the most conserved exons between all variants. Ensembl 2015 was used to identify the sequence of the most conserved exons. NCBI primer-BLAST was used to generate appropriate primer pairs. Primers were run using USC-In Silico PCR to check specificity. 1-3 primer pairs for each gene were then run on a standard curve qPCR reaction to test the efficiency of the primers. PCR products were then run on a 2.5 % agarose gel to make sure only one product was amplified and that it was of the correct length.

Table 4: Optimised SYBR Green primers

PRIMER	**Forward Sequence (5'-3')**	**Reverse Sequence (5'-3')**
18S	TGCAGAATCCTCGCCAATACA	AGTCGCTCCAAGTCTTCACG
FGFR1	GAGGCTACAAGGTCCGTTATG	ATGCTGCCATACTCGTTCTC
FGFR2	GCCTCTATGCTTGTACCGCT	GTGTCGTCCTCGTCATCTCC
FGFR3	TGGAGCCTGGTCATGGA	TGCTGGATGCTGCCAAA
NGF	CACTGGAACTCGTATTGTACCACAA	GCCTGCTTGCCGTCCAT
PDPN	ACCCGTGAAGAGCCCTAT	GCTTCCTACAGTAAACACATCCT
TSG6	GCGAAAGATGGGATGCTTATTG	ATTTGGGAAGCCTGGAGATTTA
ARG1	GCTTTGCTGATGTCCCTAATG	CTGGTCCTTCCGTTCTTCTT

2.11.2 TaqMan

Table 5: TaqMan primers for murine hip explants

PRIMER	
Fgfr1	Mm00438930_m1
Fgfr2	Mm00438941_m1
Fgfr3	Mm00433294_m1
Fgfr4	Mm01341852_m1
Fgf2	Mm00433287_m1
Fgf18	Mm00433286_m1
Ngf	Mm00443039_m1
Inhba	Mm00434339_m1
Tnfrsf12a	Mm00489103_m1
Arg1	Mm00475988_m1
Timp1	Mm00441818_m1
Has1	Mm03048195_m1
Tsg6	Mm00493736_m1
Ptgs2	Mm00478374_m1
18S	Hs99999901_s1

Table 6: TaqMan primers for chondrogenic discs

PRIMER	
18S	Hs99999901_s1
FGFR1	Hs00241111_m1
FGFR2	Hs01552918_m1
FGFR3	Hs00179829_m1
FGFR4	Hs01106910_g1
COL1A1	Hs00164004_m1
COL2A1	Hs00264051_m1
COL10A1	Hs00166657_m1
AGRCN	Hs00153936_m1
TGFβR3	Hs00234257_m1
SOX9	Hs00165814_m1
COMP	Hs00164359_m1
RUNX2	Hs01047973_m1

2.12 Western blotting

Cells were lysed in 200 µl radioimmunoprecipitation assay (RIPA) buffer consisting of 100 mM Trizma base (pH 7.4), 300 mM sodium chloride, 20 mM sodium pyro-phosphate, 2 mM EDTA, 50 mM beta-glycerophosphate, 1 % (w/v) deoxycholic acid, 0.2 % SDS and 2 % (v/v) Np40/IGEPAL with freshly supplemented 0.2 mM sodium orthovanadate (New England

Biolabs, Hitchin, UK) 1 µM DTT (Enzo life sciences, Exeter, UK), protease inhibitors (Roche, distributed by Sigma-Aldrich, Dorset, UK) and 1 µg/ml Microcystin-LR (Enzo life sciences, Exeter, UK) for 30 minutes. Lysates were centrifuged at 13,000 RPM for 15 min at 4 °C. 180 µl of the supernatant was collected and stored at -20 °C. 10 µl 5X sample buffer was added to 40 µl of the supernatant/lysate, samples were boiled for 2 min, sonicated for 10 min, then boiled again for 5 min before centrifuging for 5 min at 13,000 RPM (to pellet any cell debris). 45 µl of the lysate was then resolved by sodium dodecyl sulfate–polyacrylamide gel electrophoresis (SDS-PAGE) on a 10 % acrylamide gel or precast NuPAGE 4-12 % Bis-Tris gradient polyacrylamide mini gels (1.5 mm thickness) (Novex, San Diego, USA) and then transferred to polyvinylidenefluoride (PVDF) membranes. Gels were stained with Coomassie blue; membranes were Ponceau stained and destained in TBST to check the efficiency of the transfer before blocking membranes in 5 % milk/TBST. Membranes were incubated with antibodies against proteins of interest. Secondary antibodies were HRP-conjugated and bands were visualised by enhanced chemiluminescence (ECL) (Amersham, Little Chalfont, UK). The luminescence of protein bands was then exposed onto a blue X-ray film (Fuji film Super RX, Fuji Film, Bedford, UK) in a dark room and processed in a developer.

2.13 Phospho-array

The Human Phospho-kinase Array kit (R&D systems, Minneapolis, USA) was used as per manufacturer's instructions. Primary porcine articular chondrocytes were isolated as mentioned previously and plated at $2x10^6$ cells/well in a 6 well dish and left to adhere to the dish for 24 h. Cells were serum starved for 24 h prior to stimulation with FGF2 or FGF18 20 ng/ml for 20 min. Media was aspirated and cells washed in 0.5 ml 1X PBS, then frozen at -20 °C. Cells were lysed in 300 µL lysis buffer 6, scraped using a cell scraper, transferred to an

Eppendorf tube and pipetted up and down. Samples were rotated at 4 °C for 30 min. Membranes were blocked in 1 ml Array Buffer 1 for 1 h at room temperature. Cell lysates were centrifuged at 13,000 RPM for 5 min at 4 °C. The supernatant was collected into 2 ml Eppendorf tubes. 1700 µl assay buffer 1 was added to each lysate. Blocking buffer was removed from the membranes and replaced with 1 ml lysate and incubated overnight at 4 °C with rocking. Membranes A and B were washed together in 20 ml 1X wash buffer for 10 min on a rocking platform, 3 times. Membranes were incubated with a cocktail of corresponding detection antibodies for 2 h at room temperature with rocking. Membranes A and B were washed together in 20 ml 1X wash buffer for 10 min on a rocking platform, 3 times. Membranes were incubated with streptavidin-HRP (1:2000) for 30 min at room temperature with rocking then washed in 20 ml 1X wash buffer for 10 min on a rocking platform, 3 times. Chemi-reagent 1 and 2 were mixed in equal volumes, 1 ml was added to each membrane and incubated for 1 min. Excess Chemi-reagent was removed and membranes were exposed to X-ray film for 1-10 min. Fixed films were scanned into a computer and the integrated density of each dot was calculated using Image J. The relative change in integrated density of 20-min dots compared to 0-min dots were calculated in Microsoft Excel and represented as a heat map.

2.14 *In vivo* scarification

Animal husbandry: animals were house in approved animal care facilities, in individually ventilated cages, with 3-6 animals per cage, with a 12 h light/dark cycle, at an ambient temperature of 21 °C. The mice were fed a standard mouse chow and water ad libitum.

All procedures were approved by the local ethics committee and the UK Home Office and carried out by licenced personnel.

Constitutive *Fgf2*$^{-/-}$ C57BL/6 mice were backcrossed onto the DBA/1 strain for 10 generations.

Mice were anaesthetized by inhalation of Isoflurane (4 % induction and 1.5–2 % maintenance) in 1 L/min oxygen. All animals received a subcutaneous injection of Vetergesic (Alstoe Animal Health Ltd) prior to surgery. The right leg was shaved and the skin cleaned with iodine. All surgery was performed under a dissection microscope using sterile tools. A 15-blade scalpel was used to create an incision in the skin along the medial side of the patella and forceps used to separate the skin from the muscle. A microsurgical scalpel was used to create an incision medially and proximally to the insertion of the patellar tendon and extended proximally to the attachment of the quadriceps muscle. The patella was dislocated laterally and the joint fully flexed to expose the patellar groove. A longitudinal full-thickness cartilage defect was made in the patellar groove using a 25 G needle. The patellar dislocation was then reduced. A 6.0 coated vicryl suture with a round-bodied needle was used to suture the patella back into place. The skin was then sutured with a 5.0 Ethilon suture with a reverse cutting needle. The mice were fully mobile within 5 min following withdrawal of Isoflurane.

Mice were culled 8 weeks post-surgery, 3 histological sections taken from defined anatomical locations; one where the growth plate (GP) is just visible as 4 distinct points, one where the points of the growth plate begin to touch and one from the middle section of that region. The repair tissue was scored blind, by two independent assessors using a modified Pineda score (as shown in **Error! Reference source not found.**), where a score of 1 equates to poor repair and 14 equates to complete repair for each section.

Table 7: Modified Pineda scoring criteria

Scoring criteria	**Score**
Filling of defect (%)	
125	3
100	4
75	3
50	2
25	1
0	0
Reconstitution of osteochondral junction	
Yes	2
Almost	1
Not closed	0
Matrix staining	
Normal	4
Reduced	3
Significantly reduced	2
Faint	1
No stain	0
Cell morphology	
Normal	4
Mostly hyaline and fibrocartilage	3
Mostly fibrocartilage	2
Some fibrocartilage but mostly non-chondrocytic cells	1
Non-chondrocytic cells only	0

First, the mean of the summed score for each section was calculated for the 2 assessors. Then the median of the 3 sections was used as the final repair score for each mouse.

2.15 Histology

Operated knees were skinned, removed from the body of the mouse, and the muscle trimmed prior to fixation in formalin for no less than 24 h. Tissues were processed and embedded by the histology department at the Kennedy Institute of Rheumatology. Tissue processing was carried out in the Tissue Tek VIP (Sakura, Alphen aan den Rijn, Netherlands) automated machine set to the following run: formal saline for 1 h 30 min at 40 °C, 70 %

ethanol for 1 h 30 min at 40 °C, 5 times 100 % ethanol for 1 h 30 min at 40 °C, 3 times Xylene for 1 h 30 min at 40 °C, 4 times paraffin for 1 h 30 min at 63 °C. Knees were embedded in paraffin wax with a 90 ° flexion, and the femur was perpendicular to the front of the block.

The knees were then trimmed to the landmark point at which the growth plate was visible as 4 distinct points. The joint was then serially sectioned at 5 µm intervals until the point at which the 4 points of the growth plate merged. 2 sections were collected per slide. 3 slides were taken from the defined region (one in the middle and one from either end), baked at 60 °C overnight and dewaxed.

Staining was carried out by the histology department at the Kennedy Institute of Rheumatology in an automated staining machine using the following protocol; 20 s in water, 30 s in Harris haematoxylin, 1 min wash in water, 20 s in acid alcohol (70 % ethanol plus 10 ml hydrochloric acid per litre), 1 min wash in water, 1 min in blueing water (600 ml water plus 1.6 ml ammonia), 6 min in fast green, 15 s in 1 % acetic acid, 1 min wash in water, 2 min in safranin-O, 1 min wash in water, 1 min in ethanol 3 times, 1 min in Xylene 3 times and mounted in DPX.

Slides were imaged using an Olympus BX61 microscope.

2.16 Mesenchymal stem cell isolation

MSCs were either purchased from Lonza (human) or isolated from the epididymal fat pad of 4 to 6-week-old WT, *Fgf2*$^{-/-}$ or green fluorescent protein (GFP)-labelled mice by differential adhesion to plastic. Briefly; epididymal fat pads were digested in 4 mg/ml collagenase A for 45 min with shaking at 120 RPM, 37 °C. The digest was filtered through a 70 µm cell strainer into a falcon tube and centrifuged at 1200 RPM for 10 min to pellet the cells. Cells were re-

suspended in mouse MSC growth medium (α-MEM+Glutamax (Gibco, Massachusetts, USA), 20 % FBS, 1 % Pen/strep) and cultured on 10 cm Petri-dishes overnight. Medium was aspirated and the plate washed with 10 ml PBS to remove non-adherent cells. Cells were cultured in growth medium until 90 % confluency, with replacement of medium every 2 days.

MSC markers were confirmed by FACS analysis and cells were tested for their ability to undergo tri-lineage differentiation (adipogenesis, osteogenesis and chondrogenesis).

2.17 Chondrogenesis disc assay

DMEM was supplemented with 1X ITS (Corning, Wiesbaden, Germany), 100 µg/ml sodium pyruvate, 25 µg/ml ascorbate-2-phosphate, 40 µg/m L-proline, 1X L-glutamine 100 nM dexamethasone (Sigma, Dorset, U.K.).

Human Lonza MSCs were expanded, cells were trypsinised, counted and resuspended to 5×10^6 cells/ml in supplemented DMEM. 100 µL of cell suspension was added per well to the 6.5 mm insert of a 12 well transwell plate with 0.4 µm pores (Costar/Corning, Wiesbaden, Germany). The plate was centrifuged at 200 g for 5 min to help sediment cells on the membrane. 600 µL of supplemented DMEM was added to the bottom chamber of each well. The plate was incubated at 37 °C, 5 % CO_2 overnight for cell discs to form. The medium was carefully aspirated and replaced (as a negative control), or with that containing 10 ng/µL TGFβ3 (R&D systems, Minneapolis, USA) as a positive control or that containing TGFβ3 and 20 ng/ml FGF2. The plate was incubated at 37 °C, 5 % CO_2 for 21 days with media replacement every other day.

Discs were either stored in TRIzol at -80 °C for RNA extraction or processed for histology (as in Materials and Methods: 2.15).

2.18 Adhesion assay

4 mm cartilage explants were taken from the distal part of porcine MCP joints (using a biopsy punch and scalpel), washed in PBS and placed in a well of a 24 well plate containing 100 µl serum-free α-MEM with either the cut (basal surface) or uninjured (articular surface) facing up.

Murine GFP MSCs were trypsinised, counted and resuspended to $2X10^5$ cells/ml; 10 µl of cell suspension was added to the top of each explant and cultured in an incubator at 37 °C, 5 % CO_2, for various times up to 24 h. Explants without cells added (no cells) were used as a negative control, to assess autofluorescence. Explants were washed twice by pipetting 200 µl PBS directly onto the explant to remove non-adhered cells; fixed for 24 h in 400 µl formalin; washed twice in 400 µl PBS and then stored in 400 µl PBS prior to imaging.

Just before imaging, the bottom of the explant was blotted on tissue to remove any excess PBS and placed on a glass slide. Images were taken using an Olympus BX61 microscope under the GFP channel with a 10X objective.

2.19 Scratch assays

MSCs were cultured in monolayer until 70-80 % confluency. Cells were serum starved for 4 h. A 10 µl pipette tip was used to create a scratch in the middle of each well. Medium was aspirated to remove any floating cells and replaced with fresh serum-free medium (control) or that containing 250 nM FGFRi or 20 ng/ml FGF2. Cells were immediately imaged (0 hrs) and placed in an incubator at 37 °C, 5 % CO_2 for 36 h, then imaged again. The images were

compiled. Image J software was used to calculate the area of each gap by drawing around it. The formula: 100- ((36 h area/ 0 h area)X100) was used to calculate the percentage of the gap closed.

Time-lapsed images of the scratch were carried out in an incubator at 37 °C, 5 % CO_2 on either a JuLi stage microscope, or an ibidi holographic phase microscope (HoloMonitor M4) with images taken every 20 min for 24 h or 36 h respectively. Image J software was used to calculate the area of each gap by drawing around it. The formula: 100- ((X h area/ 0 h area)X100) was used to calculate the percentage of the gap closed for hourly images until the gap was completely closed.

2.20 Statistical analysis

All statistical analysis was performed using Prism 7 programme (GraphPad Software Inc., USA). Significance was reported as not significant (ns) when p-value >0.05, significant (*) when p-value ≤0.05, very significant (**) when p ≤0.01, highly significant (***) when p-value ≤0.001 and extremely significant (****) when p-value ≤0.0001.

3 Modulation of expression of FGFRs in response to injury and FGF stimulation

3.1 Introduction

Our group has previously shown that upon cartilage injury FGF2 is released from the pericellular matrix to induce the phosphorylation of ERK. This occurs upon explantation (cutting the tissue from an intact joint surface), or re-cutting tissue that has been rested *in vitro* for 24 hours (Vincent *et al*., 2002). To induce this response, FGF2 must first bind to its cognate receptor. FGF2 is known to bind to all FGF receptors (FGFR1, FGFR2, FGFR3, and FGFR4) (Ornitz *et al*., 1996) although FGFR1 and FGFR3 are the most abundant in articular chondrocytes (Yan *et al*., 2011). These receptors have been shown to mediate opposing effects in the joint *in vivo.* Knocking out *Fgfr1* in articular cartilage prevented mice from developing spontaneously- or surgically-induced osteoarthritis (Weng *et al*., 2012). Whereas knocking out *Fgfr3* in articular cartilage enhanced the progression of surgically-induced osteoarthritis (Tang *et al*., 2016). Therefore, to better understand the role of FGF2 in cartilage injury, the relative abundance of these FGFRs and how they change during injury is important to study.

Porcine tissue has been widely used in *in vitro* cartilage studies. It is easily obtainable and has many similarities to human tissue including cartilage composition, thickness, and weight-bearing capabilities. Thus, in this chapter, I investigate the effects of cartilage injury on *FGFR* expression at an mRNA level in porcine articular cartilage explants and in a murine hip explantation model comparing wild-type and *Fgf2*$^{-/-}$ mice. I also assess how FGF2 and selective FGF ligands effect this *FGFR* expression in isolated porcine chondrocytes.

3.2 Regulation of *FGFRs* upon porcine cartilage explantation

Cartilage was explanted from porcine metacarpophalangeal (MCP) joints directly onto dry ice (0 h) to find out the basal expression of *FGFR*s in the tissue. Further explants were taken and cultured in serum-free media for 24 or 48 hours to investigate how the receptor expression changed in response to injury. RNA was extracted, reverse transcribed and gene expression for the *FGFR*s assessed by qPCR. Samples were normalised to *18S* and expressed relative to 0 h explants. The ratio of *FGFR1:FGFR3* was calculated from the Ct values of each receptor for the individual time-points.

Figure 3.1A shows that *FGFR1* expression remained relatively constant 24 hours after explantation, then dropped to approximately 50 % of its initial expression. *FGFR3* expression on the other hand, reduced by 75 % of its original expression by 24 hours and remained low at 48 hours (Figure 3.1B). Consequently, the *FGFR1:FGFR3* ratios shifted from approximately equal levels of *FGFR1* and *FGFR3* (0 h) to 4-fold more *FGFR1* compared to *FGFR3* at 24 hours post explantation. At 48 hours post explantation, this ratio decreased slightly to 3-fold higher *FGFR1*, due to the decrease in *FGFR1* at this point (Figure 3.1C and A).

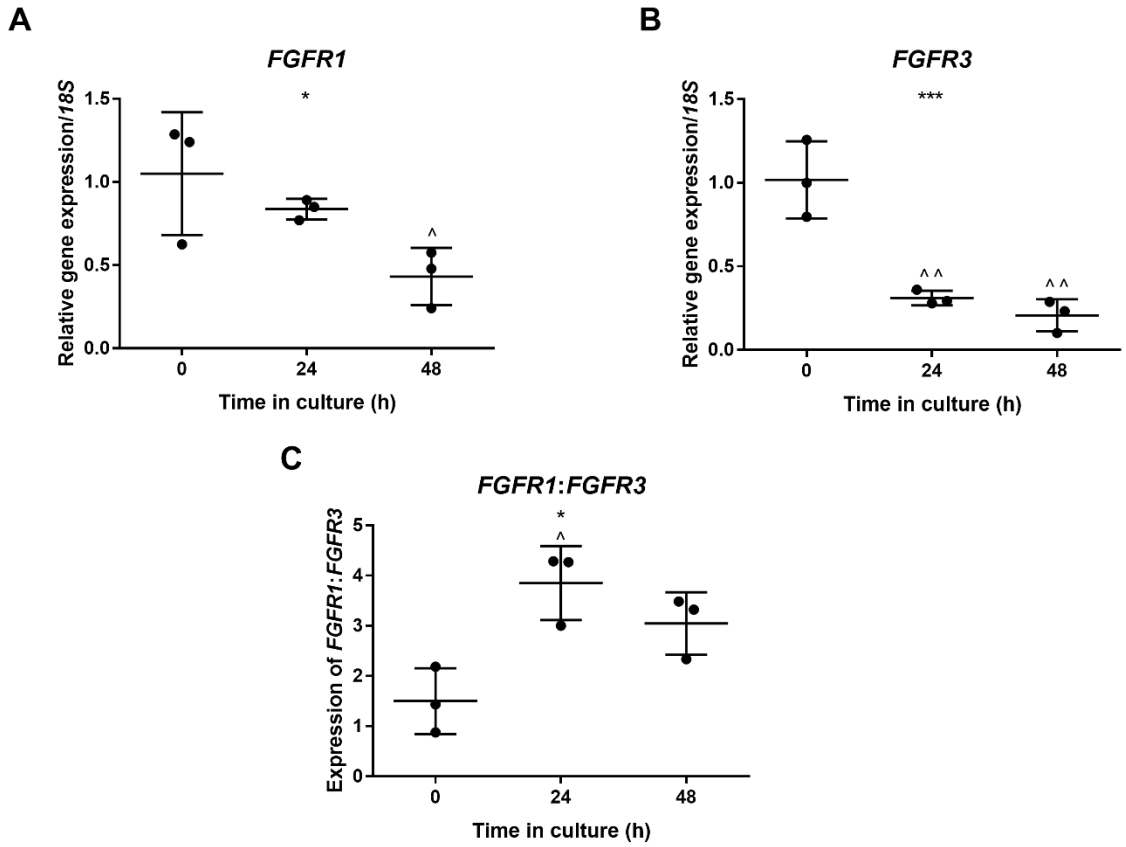

Figure 3.1: Regulation of *FGFR* ratios upon explantation of porcine cartilage

Cartilage was explanted from porcine MCP joints directly onto dry ice (0 h); or into serum-free DMEM and cultured for various times (24 h, 48 h). RNA was extracted, reverse transcribed and gene expression for *FGFR1* and *FGFR3* assessed by qPCR. All samples were normalised to *18S* and expressed relative to 0 h explants. **A**, *FGFR1*. **B**, *FGFR3*. **C**, relative expression of *FGFR1* as a ratio of *FGFR3* expression. Graphs show mean +/- S.D; one-way ANOVA *p<0.05, ***p<0.001; with Tukey post hoc test ^p<0.05, ^^p<0.01, compared against “0 h”; n=3 biological replicates.

3.3 Regulation of *FGFRs* upon explantation of porcine cartilage in hypoxia

The natural environment of articular cartilage is hypoxic due to its avascular nature and thickness. Work from our centre had previously identified *FGFR3* as a hypoxia-inducible gene (Lafont *et al*., 2008). Therefore, I investigated whether the regulation of *FGFR*s upon explantation was due to exposing the tissue to a normoxic environment (20 % O_2). In these experiments, the explantation experiment was repeated in a hypoxic workstation set at 1 % O_2. All media were equilibrated to the hypoxic environment overnight before the experiment was undertaken.

Figure 3.2 shows the regulation of *FGFR*s upon explantation in hypoxia was the same as that of the normoxic experiments. *FGFR1* still decreased to 50 % of its initial expression at 48 hours (Figure 3.2A), *FGFR3* decreased to 25 % of its initial expression by 48 hours (Figure 3.2B), and the *FGFR1:FGFR3* ratio shifted to 4-fold more *FGFR1* than *FGFR3* at 24 hours (Figure 3.2C) and then decreased to 3-fold at 48 hours post explantation.

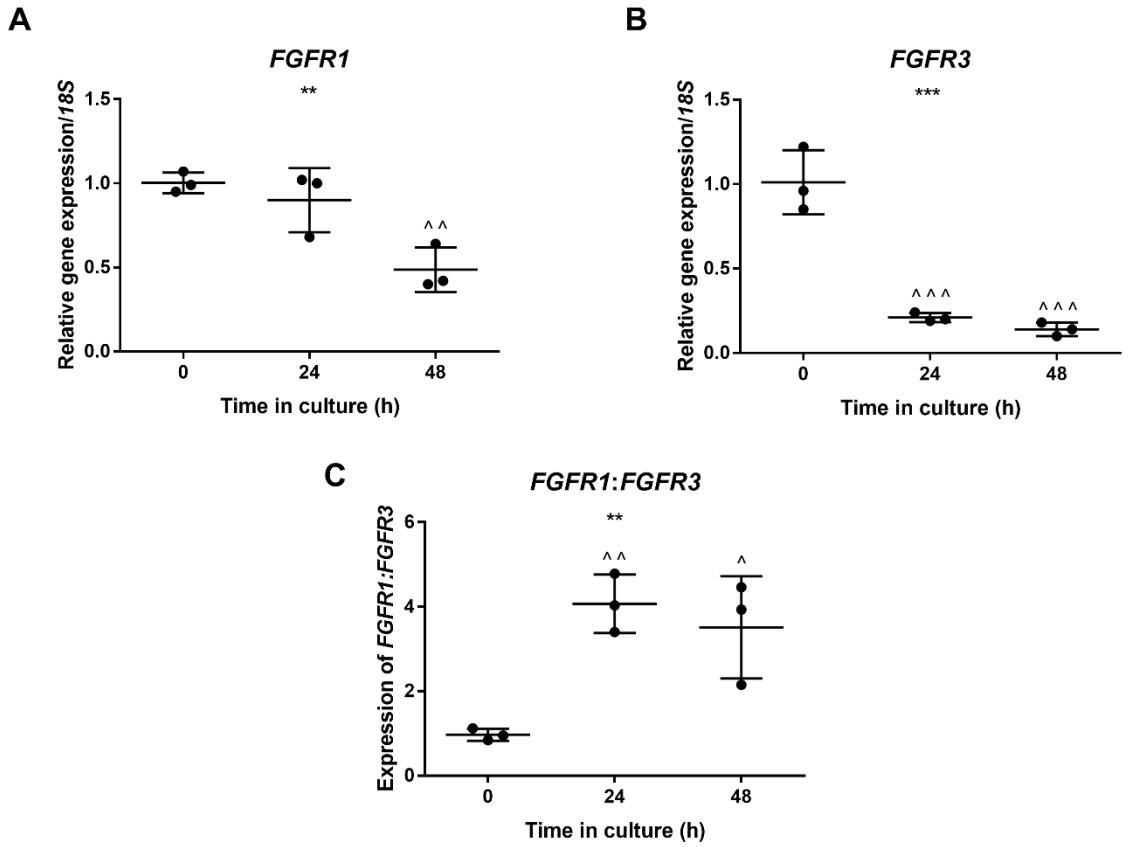

Figure 3.2: Hypoxia does not affect *FGFR* expression changes upon porcine cartilage explantation

In a hypoxic chamber (1 % O_2) cartilage was explanted from porcine MCP joints directly onto dry ice (0 h); or into serum-free DMEM and cultured for various times (24 h, 48 h). RNA was extracted from cartilage explants, reverse transcribed and gene expression for *FGFR1* and *FGFR3* assessed by qPCR. All samples were normalised to *18S* and expressed relative to 0 h explants. **A**, *FGFR1*. **B**, *FGFR3*. **C**, relative expression of *FGFR1* as a ratio of *FGFR3* expression. Graphs show mean +/- S.D; one-way ANOVA **p<0.01 ***p<0.001; with Tukey post hoc test ^p<0.05; ^^p<0.01 ^^^p<0.001 compared against “0 h”. n=3 biological replicates.

3.4 *FGFR* regulation upon explantation of porcine cartilage during an earlier time course

To investigate the initial effects of injury on *FGFR* gene expression, earlier time-points (of 2, 4, 6, 8 and 12 hours) were added to the explantation time course. I also examined the expression of *FGFR2* as it has been shown to be expressed at detectable levels in human articular chondrocytes (Yan *et al*., 2011). The expression of *FGFR4* could not be determined as suitable porcine primers could not be validated due to the incomplete annotation of the porcine genome. However, FGFR4 expression levels are very low in human articular chondrocytes (Yan *et al*., 2011), so the following analysis was performed for *FGFR1*, *FGFR2* and *FGFR3* only.

Figure 3.3 shows the abundance of the *FGFR*s at time-point 0 in porcine cartilage. A lower ΔCt value indicates higher abundance, therefore the abundance of *FGFR*s in porcine cartilage was *FGFR1*>*FGFR3*>*FGFR2*.

Figure 3.4A shows *FGFR1* expression remained constant for the first 12 hours after explantation; decreased by 50 % of its original expression after 24 hours, then decreased further to 25 % of 0-hour expression by 48 hours. This therefore suggests a decrease in *FGFR1* may have been a secondary response to injury (as the effect was not immediate). The overall the decrease in *FGFR1* expression fits the trend seen in Figure 3.1 and Figure 3.2, although these results differ in that decrease in expression occurs earlier at (24 hours compared to 48 hours in the previous experiments).

FGFR2 levels remained relatively constant throughout the time course (Figure 3.4B) and therefore the expression ratio of *FGFR1:FGFR2* also remained relatively constant at 9-fold

higher *FGFR1* than *FGFR2* (Figure 3.4E). This receptor ratio decreased at 24 hours, due to the decrease in *FGFR1* at this time-point, however it remained statistically insignificant due to the spread of the data.

FGFR3 expression increased slightly (0.4 fold) 2 hours after explantation, then decreased steadily over the next 46 hours (Figure 3.4C) by over 75 % of its original expression. A statistically significant reduction was apparent by 6 hours. This led to a steady shift in the *FGFR1:FGFR3* ratio from 2.5-fold higher *FGFR1* expression levels at 0 hours to approximately 6-fold higher *FGFR1* compared to *FGFR3*, over the time course (Figure 3.4D). Again, this response fits the trend seen in the previous experiments (Figure 3.1C and Figure 3.2C) however the fold change was greater by 48 h. Though this may be due to the initial receptor ratios being higher than the previous experiments (2.5-fold higher *FGFR1* compared to 1.5-fold higher *FGFR1* respectively). Nonetheless these results suggest that the initial injury was driving a rapid change in *FGFR3* regulation with a slower, perhaps secondary *FGFR1* response.

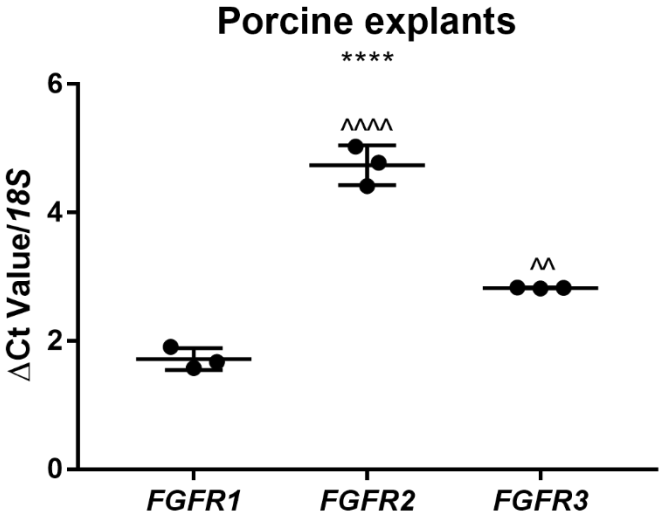

Figure 3.3: Abundance of *FGFR*s in porcine explants

Cartilage was explanted from porcine MCP joints directly onto dry ice, RNA was extracted, reverse transcribed and gene expression for *FGFR1*, *FGFR2* and *FGFR3* assessed by qPCR. All samples were normalised to *18S* to obtain ΔCt values. Graphs show mean +/- S.D; one-way ANOVA ****p<0.0001; with Tukey post hoc test ^^p>0.01, ^^^^p>0.0001 compared against "*FGFR1*". n=3 biological replicates.

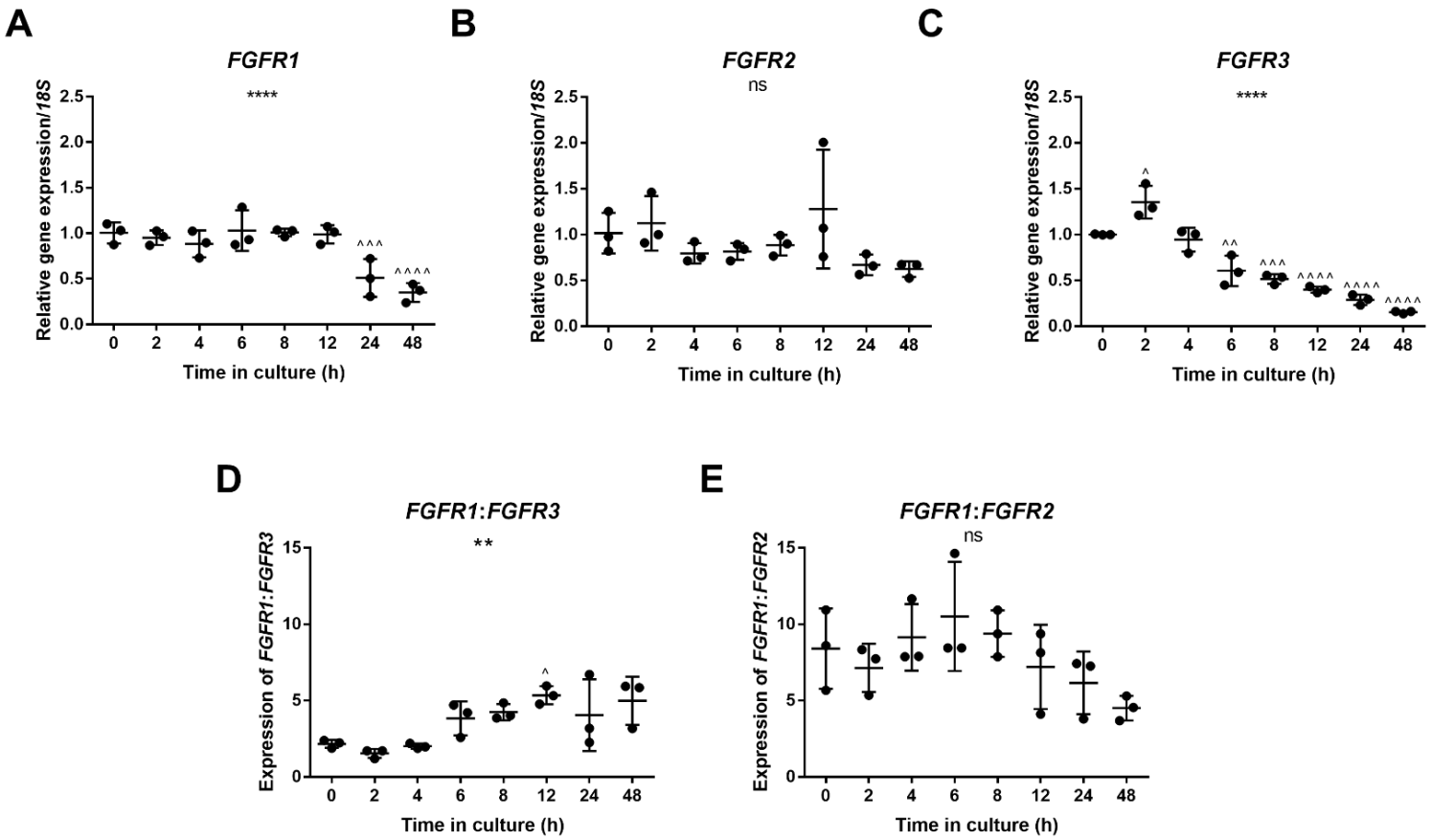

Figure 3.4: *FGFR* regulation upon porcine cartilage explantation during an early time course
Cartilage was explanted from porcine MCP joints directly onto dry ice (0 h); or into serum-free DMEM and cultured for various times (2, 4, 6, 8, 12, 24, or 48 h). RNA was extracted, reverse transcribed and gene expression for *FGFR1*, *FGFR2* and *FGFR3* assessed by qPCR. All samples were normalised to *18S* and expressed relative to 0 h explants. **A**, *FGFR1*. **B**, *FGFR2*. **C**, *FGFR3*. **D**, relative expression of *FGFR1* as a ratio of *FGFR3* expression. **E**, relative expression of *FGFR1* as a ratio of *FGFR2* expression. Graphs show mean +/- S.D; one-way ANOVA ns=non-significant, **p<0.01, ****p<0.0001; with Tukey post hoc test ^p>0.05, ^^p>0.01, ^^^p>0.001, ^^^^p>0.0001 compared against "0 h". n=3 biological replicates.

3.5 Regulation of FGF2-dependent genes upon porcine cartilage explantation

Our group has previously shown that FGF2 contributes to the regulation of a number of cartilage injury response genes (Chong *et al*., 2013). I next looked at how the expression of some of these FGF-dependent genes; *arginase 1* (*ARG1*), *Tumour Necrosis Factor α-stimulated gene-6* (*TSG6*) and *nerve growth factor* (*NGF*) (Driscoll *et al*., 2016), changed across the explantation time course, with a view to seeing whether the pattern of gene regulation related to the changes in *FGFR* expression.

Figure 3.5A shows *ARG1* expression increased steadily, peaking at 24-hours and was still 120-fold higher than initial expression at 48 hours. Conversely, *NGF* and *TSG6* expression increased rapidly within the first 4 hours and return to basal levels by 24 hours (Figure 3.5B and C).

These data suggest that FGF2-dependent genes have different patterns of regulation after explantation that could be dependent on FGFR expression levels. This will be explored further in section 3.10 (Regulation of Fgfrs and FGF-dependent genes upon murine hip explantation).

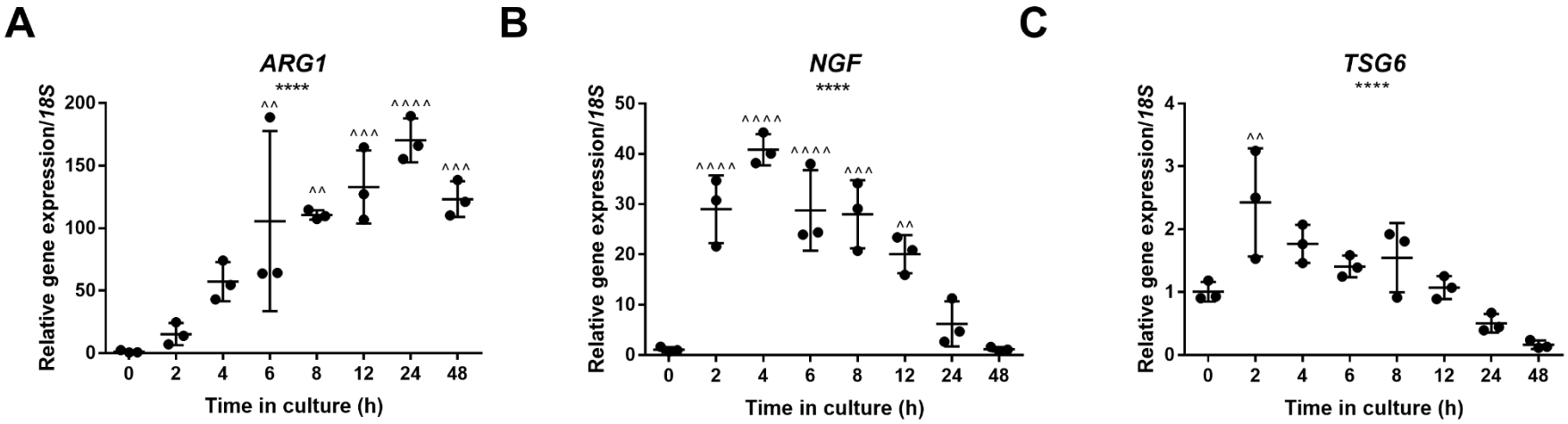

Figure 3.5: Regulation of FGF2-dependent genes upon porcine cartilage explantation

Cartilage was explanted from porcine MCP joints directly onto dry ice (0 h); or into serum-free DMEM and cultured for various times (2, 4, 6, 8, 12, 24, or 48 h). RNA was extracted, reverse transcribed and gene expression for *ARG1*, *NGF* and *TSG6* assessed by qPCR. All samples were normalised to *18S* and expressed relative to 0 h explants. **A**, *ARG1*. **B**, *NGF* **C**, *TSG6*. Graphs show mean +/- S.D; one-way ANOVA****p<0.0001; with Tukey post hoc test ^p>0.05, ^^p>0.01, ^^^p>0.001, ^^^^p>0.0001 compared against "0 h". n=3 biological replicates.

3.6 FGF ligand injection into porcine MCP joints does not regulate *FGFR*s

Explantation causes activation of several intracellular pathways in addition to those activated by FGF2 release (Gruber *et al*., 2004, Watt *et al*., 2013). To see whether *FGFR* expression was directly FGF2-dependent, I injected the porcine MCP joint space with FGF2; incubated the trotters for 24 hours prior to explantation onto dry ice and compared expression of *FGFR*s by qPCR. Also, to attempt to see if the responses seen were mediated through specific FGFRs, I injected the porcine MCP joint with FGF18, as it has been shown to have a higher selectivity for FGFR3 over FGFR1, while FGF2 has been shown to have higher selectivity of FGFR1 over FGFR3. (Zhang *et al*., 2006, Ellsworth *et al*., 2002, Ornitz *et al*., 1996). Porcine MCP joints were also injected with PBS; the vehicle control and non-injected trotters were used as a final control group to make sure the injection itself was not driving a response.

There was no significant change in the expression of either *FGFR1* or *FGFR3* (Figure 3.6A and B) after injection of FGF2 or FGF18, therefore the ratio of *FGFR1:FGFR3* remained equal (Figure 3.6C). This apparent non-responsiveness could have been due to a number of reasons; the FGF ligands used may have been at too low a concentration to see an effect, because of the relatively high volume of distribution in the joint; FGF ligands could have lost their bioavailability by binding to the synovium/synovial fluid; the intact articular surface could have prevented diffusion into the cartilage as it is a relatively impermeable layer; or the regulation of *FGFR*s upon injury requires FGF2 in combination with other injury-induced pathway activators.

To test if FGFs were able to activate the (more accessible) synovium, the experiment was repeated with FGF2 injections and synovial explants were taken as well as cartilage explants

4 hours after injection. This time-point was chosen as it was when an induction of *NGF* and *TSG-6* expression upon explantation could be seen (Figure 3.5). All explants were tested for *FGFR* regulation in addition to the other known FGF-dependent genes.

I first looked at the abundance of *FGFR*s in porcine synovium of the control samples, to see if it was likely that the FGF2 would bind and mediate downstream effects. Figure 3.7 shows the abundance of *FGFR*s to be *FGFR1>>FGFR2>FGFR3*. Therefore, there was potential for FGF2 to bind to the FGFR1 ligand as it had a similar ΔCt value to that seen in cartilage (Figure 3.3).

The only significant change in *FGFR* expression was a 30 % reduction in *FGFR1* in the synovium, following PBS or FGF2 injection (Figure 3.8A synovium); indicating that this was merely an effect of the injection itself. The *FGFR1:FGFR2* expression change also reached significance for the FGF2 injected trotter compared to control, but this was a marginal effect from 4-fold to 6-fold higher *FGFR1* expression than *FGFR2* expression (Figure 3.8E cartilage).

There was no change of FGF-dependent genes; *ARG1*, *NGF* and *TSG6* in either the cartilage or the synovium (Figure 3.9).

As there was no distinct change in the expression of the genes tested, these experiments suggested that there was an issue with activity or bioavailability of the ligands following injection. The issue of activity of the recombinant proteins was ruled out when ligands were later tested on isolated chondrocytes and robust FGF-dependent responses were seen. Therefore, the issue of concentration of the ligands or impenetrability of intact cartilage remain as untested possibilities for why strong significant responses were not seen.

Additionally, I was unable to rule out the possibility that FGF2 only affects *FGFR* expression when in combination with other signals induced by injury.

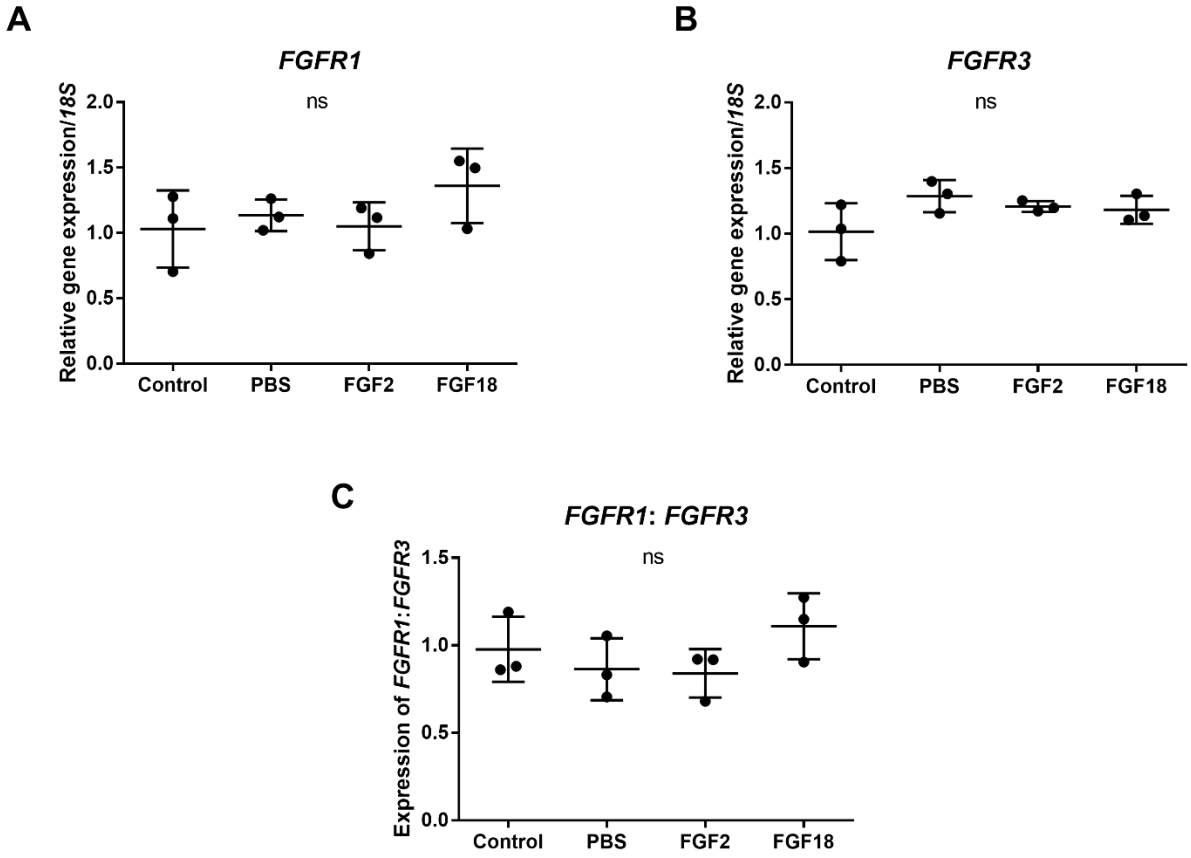

Figure 3.6: FGF ligand injection into the intact porcine joint does not regulate *FGFR*s

Porcine MCP joints were injected with 2 ml serum-free DMEM containing 40 ng/ml FGF2; FGF18 or PBS or left non-injected (control) and incubated at 37 °C, 5 % CO_2, for 24 h before explanting directly onto dry ice. Explants were homogenised and RNA extracted, reverse transcribed and gene expression for *FGFR1* and *FGFR3* assessed by qPCR. All samples were normalised to *18S* and expressed relative to control samples. **A**, *FGFR1*. **B**, *FGFR3*. **C**, relative expression of *FGFR1* as a ratio of *FGFR3* expression. Graphs show mean +/- S.D; one-way ANOVA with Tukey post hoc test compared against "control" samples; all analysis non-significant (ns). n=3 biological replicates.

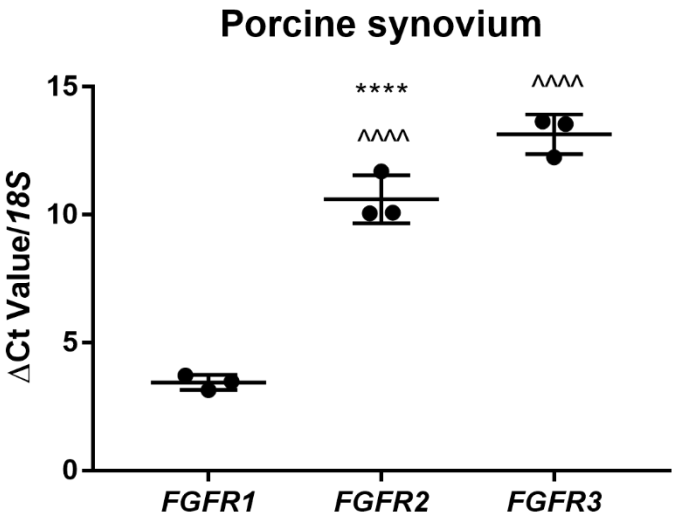

Figure 3.7: Abundance of *FGFR*s in porcine synovium

Porcine trotters were incubated at 37 °C, 5 % CO_2 for 4 h. Synovium was dissected directly onto dry ice, RNA extracted, reverse transcribed and gene expression for *FGFR*s assessed by qPCR. All samples were normalised to *18S* to obtain ΔCt values. Graphs show mean +/- S.D; one-way ANOVA, ****p<0.0001, with Tukey post hoc test ^^^^p<0.0001 compared to "*FGFR1*". n=3 biological replicates.

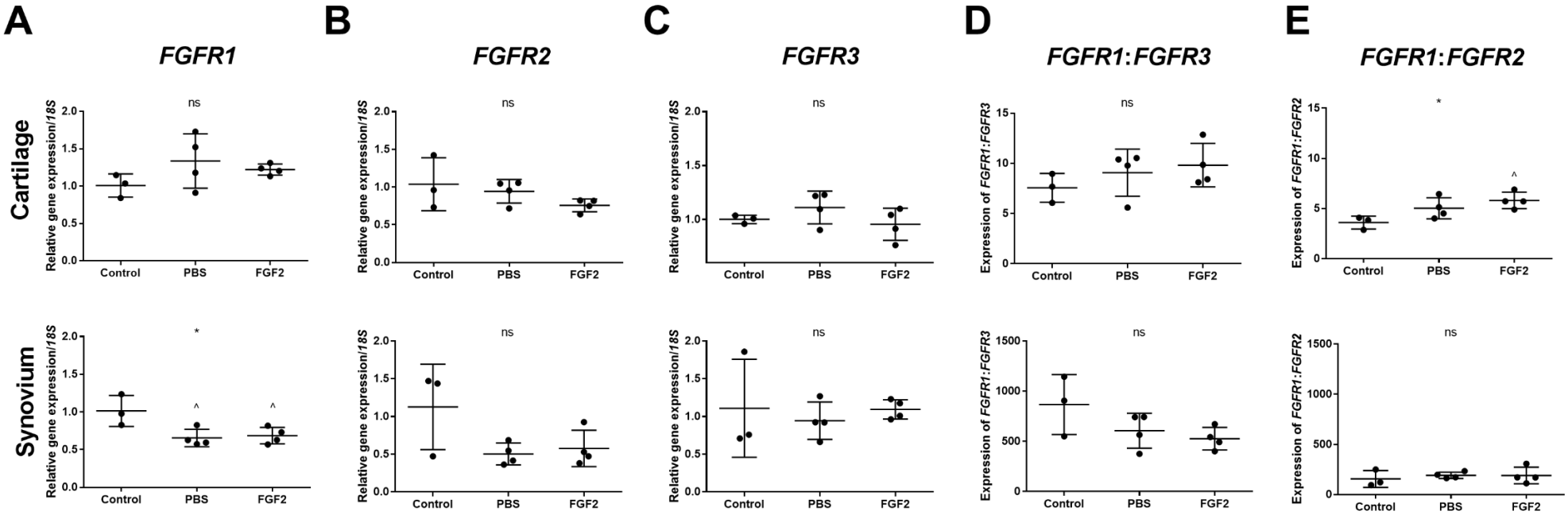

Figure 3.8: *FGFR* expression in cartilage and synovium after injecting FGF2 into the porcine MCP joint

Porcine MCP joints were injected with 2 ml serum-free DMEM containing 40 ng/ml FGF2 or PBS or left non-injected (Control) and incubated at 37 °C, 5 % CO_2 for 4 h. Synovium was dissected directly onto dry ice, then the cartilage was explanted onto dry ice. Explants were homogenised and RNA extracted, reverse transcribed and gene expression for *FGFR*s assessed by qPCR. **A**, *FGFR1*. **B**, *FGFR2*. **C**, *FGFR3*. **D**, relative expression of *FGFR1* as a ratio of *FGFR3* expression. **E**, relative expression of *FGFR1* as a ratio of *FGFR2* expression. All samples were normalised to *18S* and expressed relative to control samples. Graphs show mean +/- S.D; one-way ANOVA ns=non-significant, *p<0.05, with Tukey post hoc test ^p<0.05 compared to "control". Control n=3 biological replicates, PBS and FGF2 n=4 biological replicates.

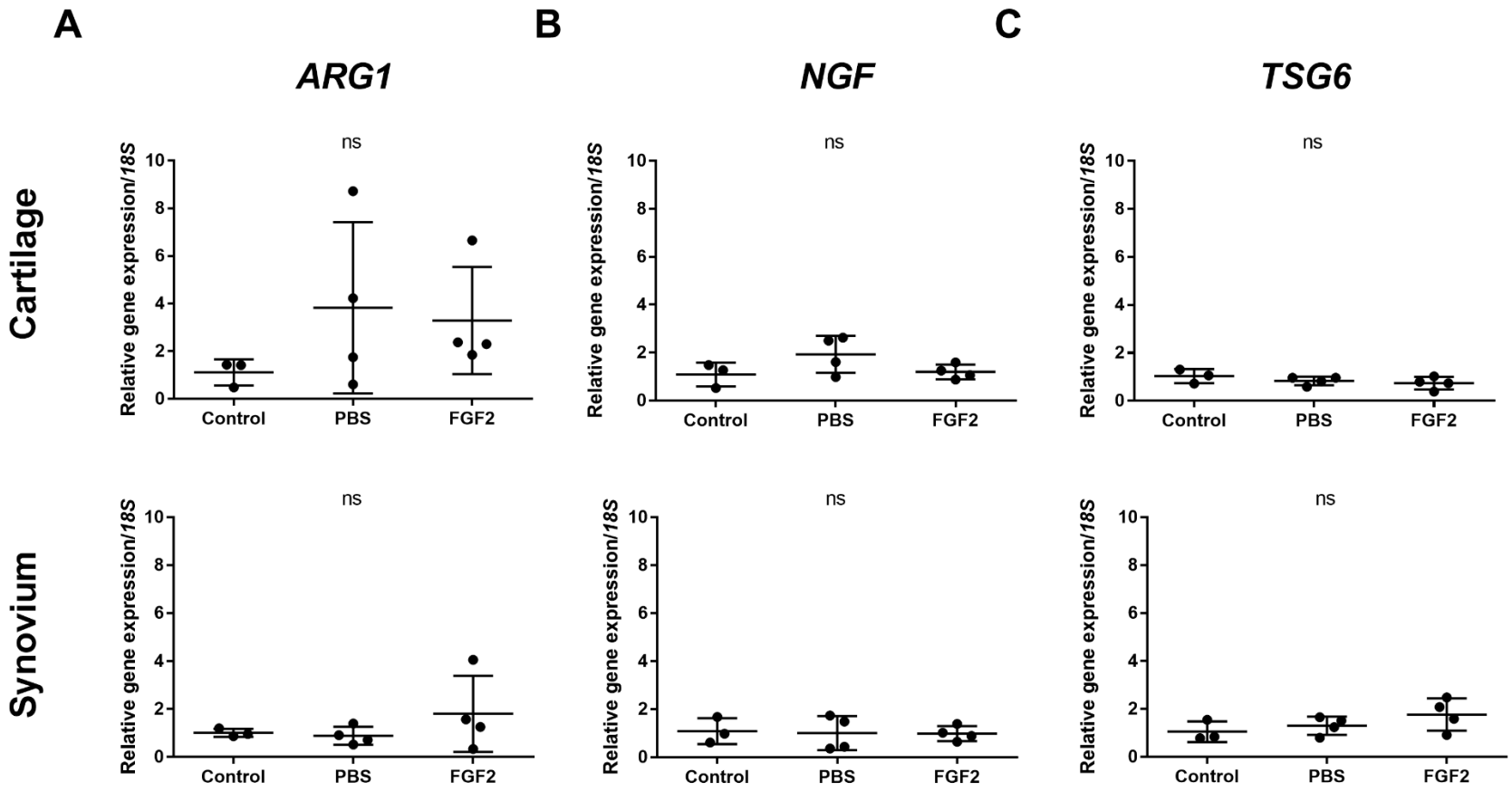

Figure 3.9: FGF-dependent gene expression is not regulated in cartilage or synovium, by injecting FGF2 into the porcine MCP joint

Porcine MCP joints were injected with 2 ml serum-free DMEM containing 40 ng/ml FGF2 or PBS or left non-injected (control) and incubated at 37 °C, 5 % CO_2 for 4 h. Synovium was dissected directly onto dry ice, then cartilage was explanted onto dry ice. Explants were homogenised and RNA extracted, reverse transcribed and gene expression for FGF2 dependent genes assessed by qPCR. **A**, *ARG1*. **B**, *NGF*. **C**, *TSG6*. All samples were normalised to *18S* and expressed relative to control samples. Graphs show mean +/- S.D; all results were non-significant; one-way ANOVA with Tukey post hoc test against "control". Control n=3 biological replicates, PBS and FGF2 n=4 biological replicates.

3.7 Blocking FGFR signalling inhibits the suppression of *FGFR3* and induction of FGF-dependent genes upon porcine cartilage explantation

Injecting FGF ligands into the joint proved ineffective at demonstrating a direct regulation of *FGFR* expression by FGF2. Therefore, a different approach was employed to demonstrate the dependence of FGF2. Trotters were injected with FGFRi SB402451 (an inhibitor that binds to the tyrosine kinase domain of all FGFRs) and incubated for 1 hour prior to explantation into media containing the FGFRi and cultured for 24 hours. Control trotters were injected with DMSO; a vehicle control. Figure 3.10 shows the gene expression of *FGFR*s.

Figure 3.10A confirmed the 50 % reduction in *FGFR1* upon explantation, consistent with previous experiments. This downregulation occurred even in the presence of the FGFR inhibitor. This therefore suggested that the response was not FGF-dependent, and so something else activated upon injury is probably driving this downregulation.

The expression of *FGFR2* remained the same 24 hours after explantation, regardless of the presence of FGFR inhibitor (Figure 3.10B). Consequently, the receptor ratio of *FGFR1:FGFR2*, shifted slightly, due to the decrease in *FGFR1*, but this occurred regardless of the presence of the FGFRi (Figure 3.10E).

Figure 3.10C shows that *FGFR3* decreased by 75 % of its initial expression 24 hours after explantation. This decrease was prevented by the presence of the FGFRi. Accordingly, the shift in the *FGFR1:FGFR3* ratio to favour *FGFR1* upon explantation is also prevented by the presence of the FGFRi (Figure 3.10D).

Therefore, these results show that the downregulation of *FGFR3* but not *FGFR1* upon explantation, was FGFR signalling dependent.

The regulation of FGF-dependent genes upon explantation was also tested in the presence of the FGFRi at 4 hours post explantation as this is when they were initially seen to increase after direct explantation in Figure 3.5. The expression of *Podoplanin* (*PDPN*) was investigated as it too was shown to be regulated upon injury in an FGF2-dependent manner (Chong *et al*., 2013).

TSG-6 and *PDPN* induction upon explantation was completely prevented in the presence of FGFRi (Figure 3.11C and D) as expected.

ARG1 and *NGF* expression were still increased upon explantation in the presence of the FGFRi, although the response was slightly reduced (Figure 3.11A and B). *ARG1* expression increased 50-fold after explantation in control samples; whereas in the presence of FGFRi this was only 10-fold increased (Figure 3.11A). *NGF* expression increased 11-fold after explantation in control samples; whereas in the presence of FGFRi this was 9-fold (Figure 3.11B). These results therefore suggest partial FGF2 dependence of the regulation of *ARG1* and *NGF* expression upon explantation.

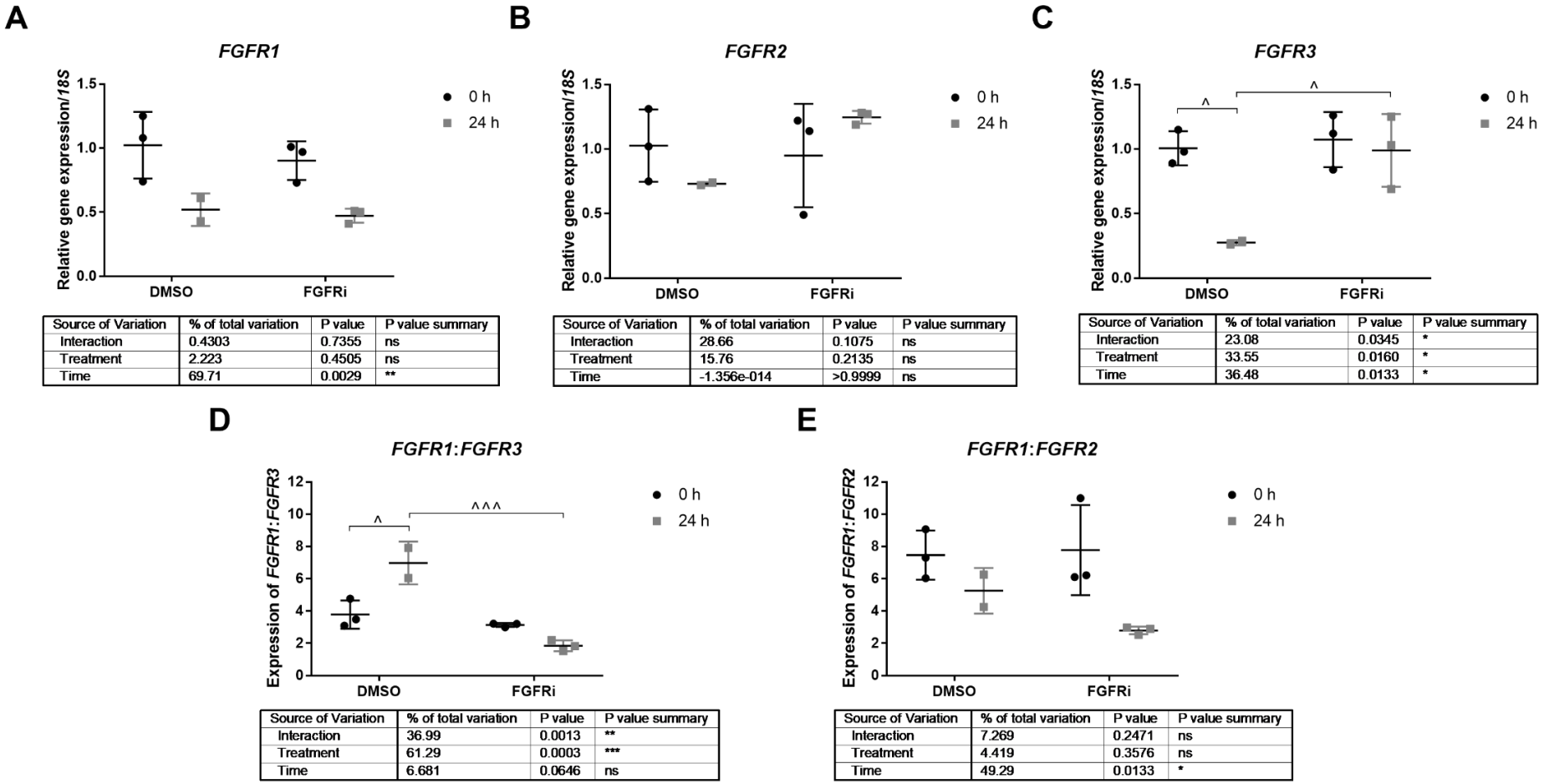

Source of Variation	% of total variation	P value	P value summary
Interaction	0.4303	0.7355	ns
Treatment	2.223	0.4505	ns
Time	69.71	0.0029	**

Source of Variation	% of total variation	P value	P value summary
Interaction	28.66	0.1075	ns
Treatment	15.76	0.2135	ns
Time	-1.356e-014	>0.9999	ns

Source of Variation	% of total variation	P value	P value summary
Interaction	23.08	0.0345	*
Treatment	33.55	0.0160	*
Time	36.48	0.0133	*

Source of Variation	% of total variation	P value	P value summary
Interaction	36.99	0.0013	**
Treatment	61.29	0.0003	***
Time	6.681	0.0646	ns

Source of Variation	% of total variation	P value	P value summary
Interaction	7.269	0.2471	ns
Treatment	4.419	0.3576	ns
Time	49.29	0.0133	*

Figure 3.10: Blocking FGFR signalling inhibits the suppression of *FGFR3* upon porcine cartilage explantation

Porcine MCP joints were injected with 2 ml FGFRi-SB402451 250 nM (FGFRi) or vehicle control (DMSO) and incubated at 37 °C, 5 % CO_2 for 1 h. Cartilage was explanted directly onto dry ice for 0 h time-points or into 3 ml of serum-free DMEM containing FGFRi or vehicle control for 24 h. Explants were homogenised, RNA extracted, reverse transcribed and gene expression for *FGFR* genes assessed by qPCR. **A**, *FGFR1*. **B**, *FGFR2*. **C**, *FGFR3*. **D**, relative expression of *FGFR1* as a ratio of *FGFR3* expression. **E**, relative expression of *FGFR1* as a ratio of *FGFR2* expression. All samples were normalised to *18S* and expressed relative to DMSO 0 h controls. Graphs show mean +/- S.D; Two-way ANOVA (tabulated results ns=non-significant, *p<0.05, **p<0.01, ***p<0.001) with Sidak post hoc test ^p<0.05, ^^^p<0.001. n=3 biological replicates.

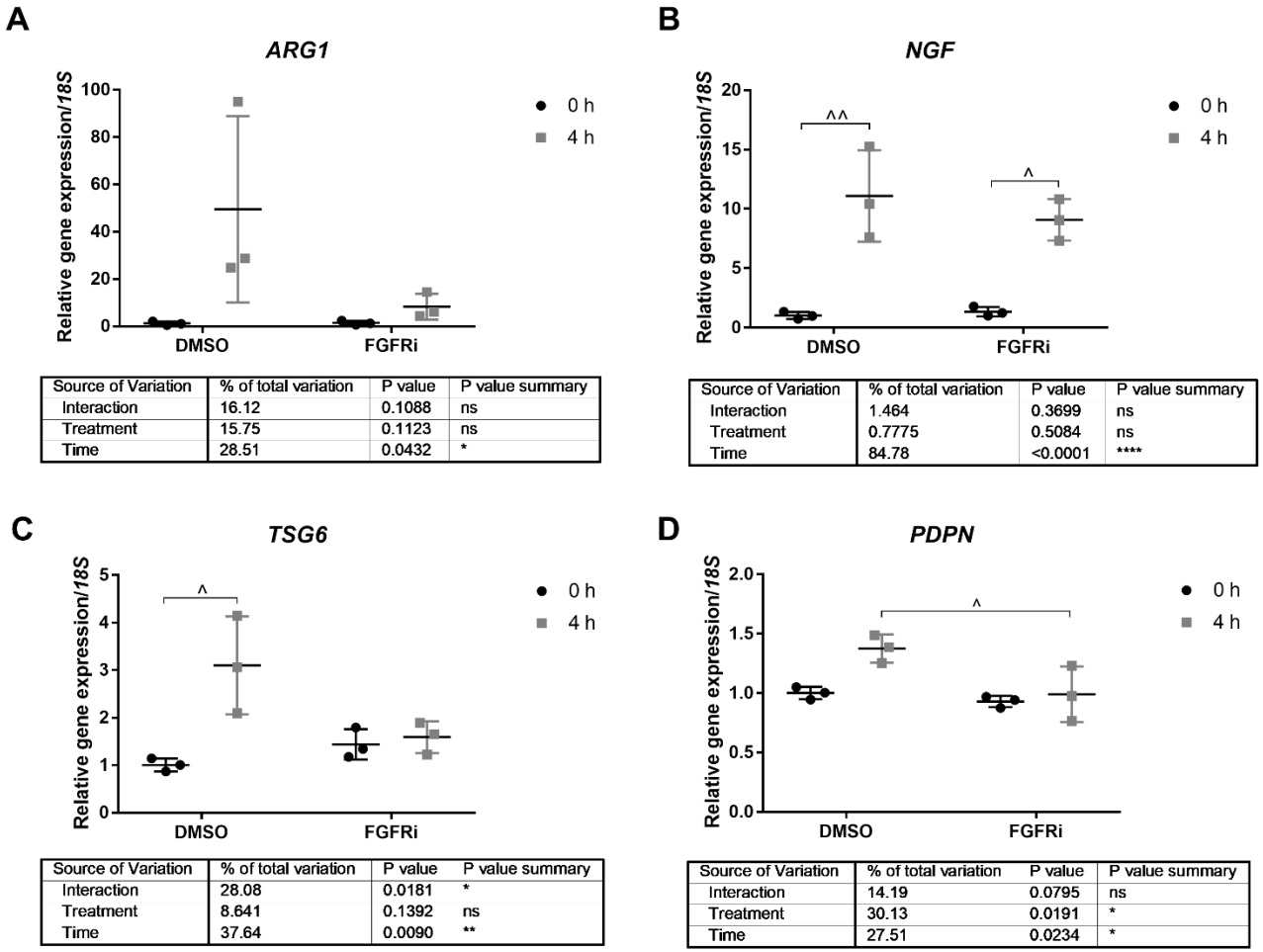

Source of Variation	% of total variation	P value	P value summary
Interaction	16.12	0.1088	ns
Treatment	15.75	0.1123	ns
Time	28.51	0.0432	*

Source of Variation	% of total variation	P value	P value summary
Interaction	1.464	0.3699	ns
Treatment	0.7775	0.5084	ns
Time	84.78	<0.0001	****

Source of Variation	% of total variation	P value	P value summary
Interaction	28.08	0.0181	*
Treatment	8.641	0.1392	ns
Time	37.64	0.0090	**

Source of Variation	% of total variation	P value	P value summary
Interaction	14.19	0.0795	ns
Treatment	30.13	0.0191	*
Time	27.51	0.0234	*

Figure 3.11: Blocking FGFR signalling suppresses the induction of FGF-dependent genes upon porcine cartilage explantation

Porcine MCP joints were injected with 2 ml FGFRi-SB402451 250 nM (FGFRi) or vehicle control (DMSO) and incubated at 37 °C, 5 % CO_2 for 1 h. Cartilage was explanted directly onto dry ice for 0 h time-points or into 3 ml of serum-free DMEM containing FGFRi or vehicle control for 4 h. Explants were homogenised, RNA extracted, reverse transcribed and gene expression for FGF-dependent genes assessed by qPCR. **A**, *ARG1*. **B**, *NGF*. **C**, *TSG6*. **D**, *PDPN*. All samples were normalised to *18S* and expressed relative to DMSO 0 h controls. Graphs show mean +/- S.D; Two-way ANOVA (tabulated results ns=non-significant, *p<0.05, **p<0.01, ****p<0.0001) with Sidak post hoc test ^p<0.05, ^^p<0.01. n=3 biological replicates.

3.8 *FGFR* expression changes by isolating and culturing porcine primary articular chondrocytes

Injecting FGF2 ligands into the porcine MCP joint caused no regulation of *FGFR*s. This may have been due to the reduced bioavailability of the ligand for the FGFRs i.e. intact cartilage may have been impenetrable, or the concentration of ligand needed to be higher. Therefore, another approach was needed to show a direct effect of FGF2. Considering these issues, I next worked with isolated primary articular chondrocytes. This is because the issue of penetrability is removed as most of the extracellular matrix is removed by enzymatic digestion. Also, the FGFRs (which are found on the cell membrane) are better exposed to the FGF ligands for the same reason. However, to obtain isolated cells, the cartilage must first be explanted, thereby disrupting *FGFR* ratios as shown in Figure 3.4. Therefore, I investigated how *FGFR* expression varied during the whole experimental procedure from dissection to cell isolation and culture.

Cartilage was explanted directly onto dry ice as a control (cartilage 0 h), or into media containing 1 mg/ml collagenase A to digest the ECM overnight. Cells were washed and some cells taken (isolated cells) to see how cell isolation affected the *FGFR*s. The rest of the cells were plated and left overnight to adhere to the culture plastic (cultured cells) before RNA was extracted, reverse transcribed and analysed via qPCR.

Figure 3.12A shows that *FGFR1* expression did not change in chondrocytes when cells were isolated but reduced non-significantly by 50 % when cells had been cultured overnight. *FGFR3* expression on the other hand, decreased by 75 % when cells were isolated, but remained down-regulated when cells had been cultured (Figure 3.12B). Consequently, the ratio of *FGFR1:FGFR3* shifted to 7-fold higher *FGFR1* when cells were isolated; due to the

decrease in *FGFR3*, and then shifted to 3-fold higher *FGFR1* when cells were cultured; because of the decrease in *FGFR1* (Figure 3.12C).

As the *FGFR1:FGFR3* ratio was starting to equalise once cells had adhered to the culture dish, I investigated if it would continue to do so with further time in culture. Considering that *FGFR3* had been shown to be induced by hypoxia (Lafont *et al*., 2008), cells were also cultured in the hypoxic workstation (set at 1 % O_2) to see if it would enhance the expression of *FGFR3* at a faster rate. The media contained 10 % FBS and was not refreshed throughout the culture period.

Figure 3.13A shows that *FGFR1* expression remained relatively constant throughout the culture period and was not affected by hypoxia. *FGFR3* expression on the other hand, did continue to increase with time in culture for the first 72 hours, then started to decrease. This decrease may have been due to additional cell stress as the culture media was not changed throughout the time course. The rate of increase was enhanced by culturing in hypoxia for the first 48 hours, however after this time, expression of *FGFR3* dropped below that of the normoxic (20 % O_2) condition (Figure 3.13B). Due to the changes in *FGFR3* expression, the *FGFR1:FGFR3* ratio began to decrease in the first 48 hours in culture, and then appeared to stabilise at around 0.5-fold, especially in normoxia (Figure 3.13C).

To carry out stimulation experiments with FGF ligands, roughly equal levels of FGFR1 and FGFR3 were desirable (to mimic the expression in intact articular cartilage). Therefore, a time between 24 and 48 hours (in the normoxic state) was identified as an ideal culture period (Figure 3.13C).

As FBS contains growth factors including FGF2, cells needed to be serum starved prior to a stimulation with FGF ligands. This step was also important to synchronise cells in the cell cycle and reset any endogenous signalling events. Therefore, I assessed how serum starving cells over 48 hours affected *FGFR* expression and also examined the effect of hypoxia.

Cells were isolated as before, plated and left to adhere to the culture plastic with media containing 10 % FBS, in a normoxic incubator. Then the medium was replaced with serum-free medium that had been equilibrated overnight in either the normoxic or hypoxic incubator. Cells were cultured for various times as shown.

Figure 3.14A shows that *FGFR1* expression remained relatively constant throughout the culture period, regardless of hypoxia. The *FGFR3* levels increased steadily, over the 48-hour time period (Figure 3.14B), regardless of hypoxia. Consequently, the *FGFR1:FGFR3* ratios shifted from 3-fold higher *FGFR1* to 1.5-fold higher *FGFR1* than *FGFR3* over the first 24 hours in normoxia, then remained relatively constant after this time-point (Figure 3.14C).

From these results it was decided that once cells were digested, they should be plated and left to adhere to the culture plate for 24 hours in the presence of 10 % FBS (for the *FGFR1:FGFR3* to equalise); then cells should be serum starved for 24 hours prior to stimulation with FGF ligands.

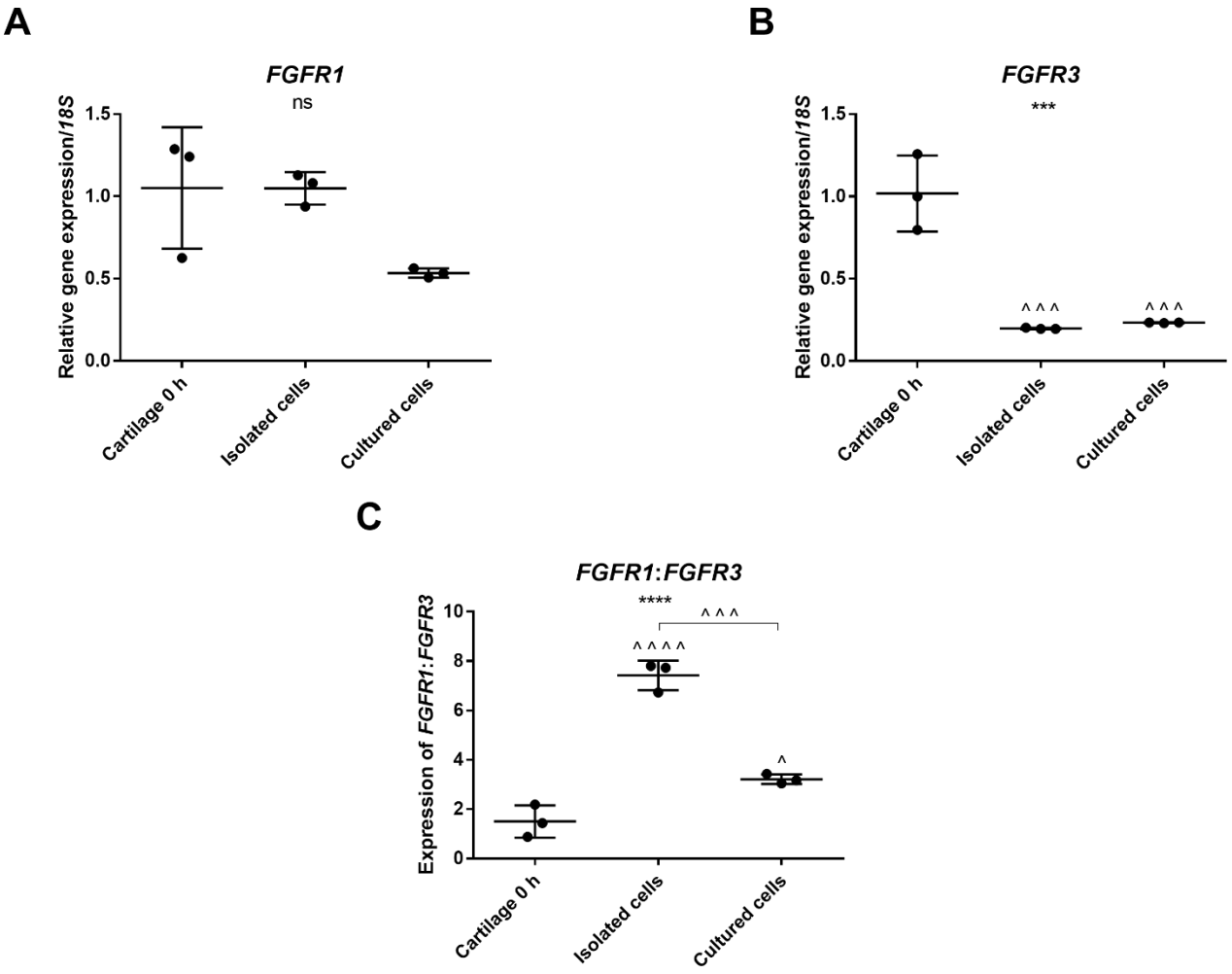

Figure 3.12: Regulation of *FGFR*s by experimental procedure

Cartilage was explanted from porcine MCP joints directly onto dry ice (Cartilage 0 h) or digested in 1 mg/ml collagenase/10 % FBS DMEM overnight (isolated cells). Isolated cells were plated at $2x10^6$ cells/well and left to adhere to the culture dish overnight (cultured cells). RNA was extracted, reverse transcribed and gene expression for *FGFR1* and *FGFR3* assessed by qPCR. All samples were normalised to *18S* and expressed relative to cartilage explants. **A**, *FGFR1*. **B**, *FGFR3*. **C**, relative expression of *FGFR1* as a ratio of *FGFR3* expression. Graphs show mean +/- S.D; one-way ANOVA ns=non-significant ***p<0.001 ****p<0.0001; with Tukey post hoc test ^p<0.05, ^^^p<0.001, ^^^^p<0.0001 compared to "Cartilage 0 h". n=3 biological replicates.

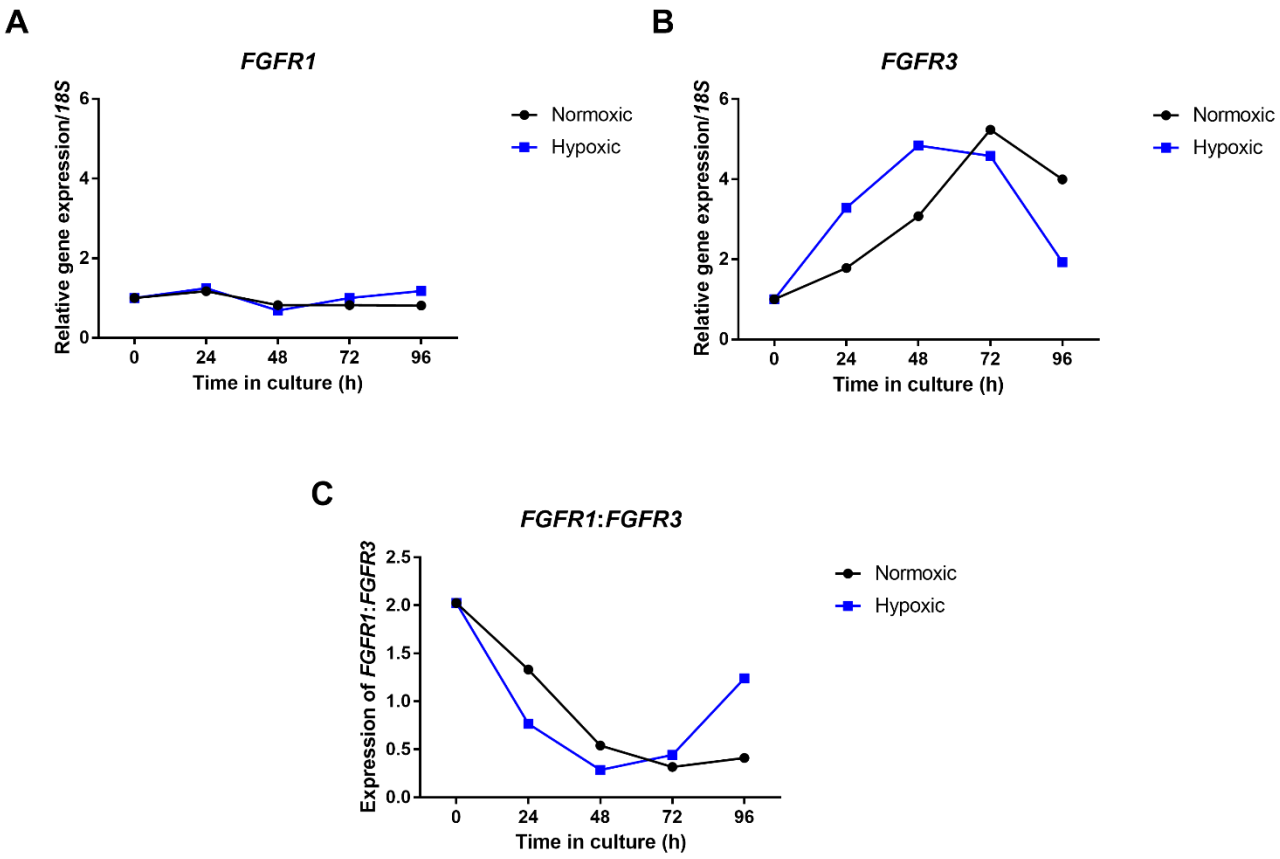

Figure 3.13: *FGFR3* levels continue to increase with time in culture, regardless of hypoxia

Primary porcine articular chondrocytes were plated at 2×10^6 cells/well in 10 % FBS DMEM and left overnight at 37 °C, 5 % CO_2 to adhere to the culture dish. Cell medium was replaced and cells lysed in TRIzol for 0 h time-points or were incubated at 37 °C, 20 % O_2 (Normoxia) or 1 % O_2 (Hypoxia). Cells were cultured for 24, 48, 72, or 96 h before being lysed. RNA was extracted, reverse transcribed and gene expression for *FGFR1* and *FGFR3* assessed by qPCR. All samples were normalised to *18S* and expressed relative to 0 h samples. **A**, *FGFR1*. **B**, *FGFR3*. **C**, relative expression of *FGFR1* as a ratio of *FGFR3* expression. (n=1)

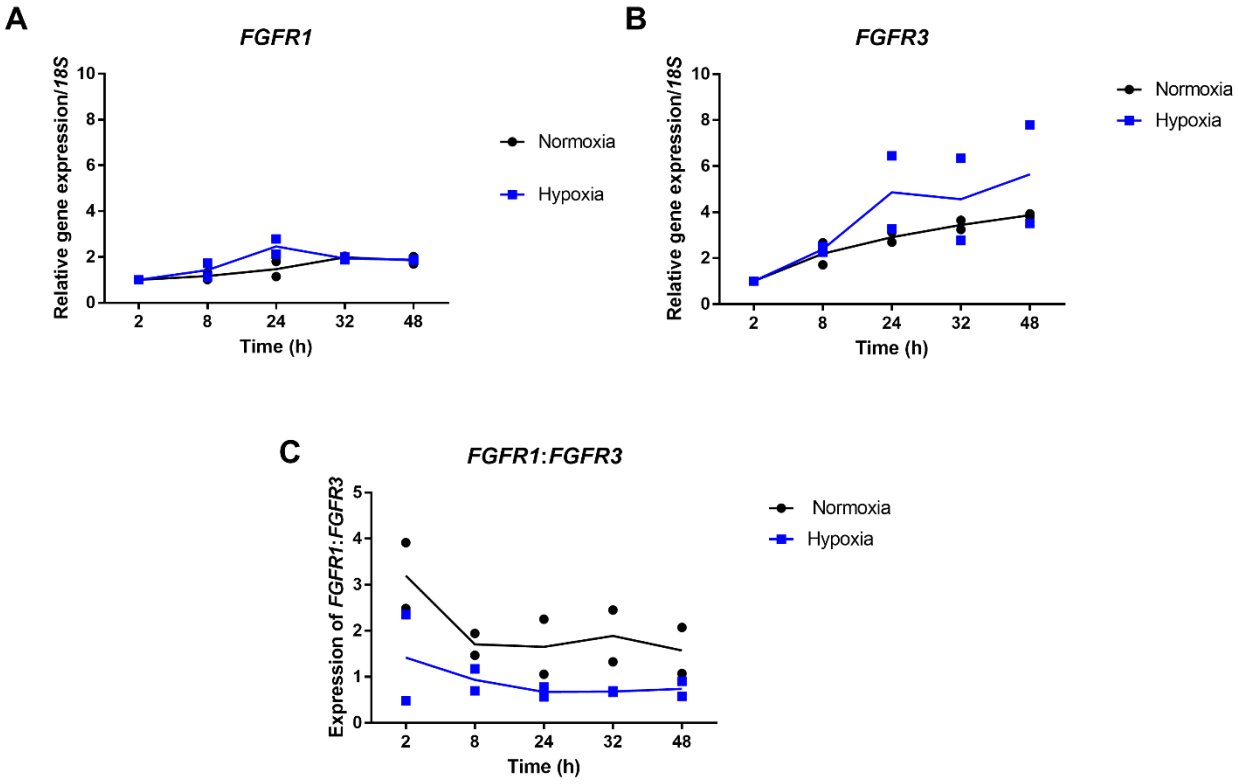

Figure 3.14: Serum starving keeps *FGFR* ratios constant after 24 h, regardless of culture conditions

Primary porcine articular chondrocytes were plated at 2×10^6 cells/well in 10 % FBS DMEM and left overnight at 37 °C, 5 % CO_2 to adhere to the culture dish. The media was replaced with serum-free media that had been equilibrated at 37 °C in either hypoxic (1 % O_2) or normoxic (20 % O_2) conditions overnight. Cells were cultured for various times before being lysed in TRIzol. RNA was extracted, reverse transcribed and gene expression for *FGFR1* and *FGFR3* assessed by qPCR. All samples were normalised to *18S* and expressed relative to 0 h samples. **A**, *FGFR1*. **B**, *FGFR3*. **C**, relative expression of *FGFR1* as a ratio of *FGFR3* expression. Graphs show mean. (n=2 biological replicates).

3.9 Regulation of *FGFR*s and FGF-dependent genes with selective FGF ligand stimulation in isolated porcine chondrocytes

To investigate a direct effect of FGF2 on *FGFR* expression, primary articular chondrocytes were stimulated with 20 ng/ml FGF2, with and without FGFRi. To attempt to find out which receptor FGF2 was acting through to mediate its effects, I also stimulated cells with FGF2-V2; an FGFR1 selective ligand, FGF18-V1; an FGFR3 selective ligand, and FGF18 (a pan receptor ligand with a relatively higher selectivity for FGFR3). Unstimulated cells were used as a control to see how gene expression varied across the culture period.

At the appropriate time-point, the medium was removed and cells lysed in TRIzol. RNA was extracted, reverse transcribed and analysed via qPCR. The *FGFR* genes were analysed in conjunction with known FGF-dependent genes. All samples were normalised to their respective 0-hour time-point.

Figure 3.15 shows the analysis of the abundance of the *FGFR*s in unstimulated cells at time-point 0. *FGFR1* and *FGFR3* had very similar ΔCt values suggesting an equal abundance. *FGFR2* showed a slightly higher ΔCt value indicating a lower abundance than *FGFR1* and *FGFR3*.

Figure 3.16A shows that *FGFR1* expression remained constant throughout the culture period. When stimulated with FGF2, chondrocytes modestly increased *FGFR1* expression from 4 hours after stimulation to 24 hours, where it reached a peak of 3-fold expression compared to 0 hours. At 48 hours post stimulation, the expression began to decrease again (Figure 3.16B). This response was completely prevented in the presence of the FGFRi (Figure 3.16C). In fact, in the presence of FGFRi, *FGFR1* expression decreased 12-hours post

stimulation to almost undetectable levels at 24-hours, but then increased back to normal levels of expression at 48-hours. This decrease in the presence of FGFRi suggested endogenous levels of an FGF ligand were probably acting to keep *FGFR1* expression at a constant level in control cells.

Stimulation with FGF2-V2 (Figure 3.16D) and FGF18 (Figure 3.16E) showed a similar regulation of *FGFR1* expression to that of FGF2. Stimulation with FGF18-V1 did not show any change in the regulation of *FGFR1* except at 48-hours, where it was slightly upregulated 1.5-fold (Figure 3.16F). These results therefore suggest that upregulation of *FGFR1* by FGF2 is likely to be mediated through FGFR1 activation and FGF18 is also acting through FGFR1.

Figure 3.17A shows that *FGFR2* expression remained relatively constant throughout the culture period. Upon FGF2 stimulation, expression of *FGFR2* decreased over the first 8 hours to 50 % of its initial expression and remained low until the 48-hour time-point where it returned to basal expression (Figure 3.17B). This response was completely prevented in the presence of the FGFRi (Figure 3.17C).

Stimulation with FGF2-V2 (the FGFR1 selective ligand), showed *FGFR2* expression remained relatively constant for the first 8 hours then began to increase thereafter, but only reached statistical significance at the 48-hour time-point where the expression was approximately 2.3-fold higher than 0 hour (Figure 3.17D). Stimulation with FGF18 (Figure 3.17E) showed a similar regulation of *FGFR2* expression to that of FGF2 stimulation. Stimulation with FGF18-V1 showed no change in the expression of *FGFR2* (Figure 3.17F).

Figure 3.18A shows that *FGFR3* expression remained relatively constant throughout the culture period. Upon FGF2 stimulation, the expression of *FGFR3* decreased over the first 8

hours to almost undetectable levels and then began to increase to return to basal levels by 48-hours (Figure 3.18B). In the presence of FGFRi this effect was completely abolished (Figure 3.18C).

Stimulation with FGF2-V2 also decreased expression of *FGFR3* over the first 8 hours, though this was to only 50 % of the 0-hour expression. *FGFR3* expression then began to increase after this point and by 48 hours, there was 3-fold higher expression compared to 0-hour (Figure 3.18D). FGF18 stimulation changed the expression of *FGFR3* in a similar way to FGF2 (Figure 3.18E). FGF18-V1 did not change the expression of *FGFR3* (Figure 3.18F).

The *FGFR1:FGFR2* ratios stayed the same in unstimulated cells, with around 5-fold higher *FGFR1* expression (Figure 3.19A). With stimulation with FGF2, FGF18 and FGF2-V2 the receptor ratios shifted in favour of *FGFR1* expression over *FGFR2* expression; with a peak change of around 25 to 30-fold higher *FGFR1* expression than *FGFR2* expression (Figure 3.19B, D and E). These changes were mainly driven by the changes in *FGFR1* as the shape of the graphs is similar to that of the *FGFR1* expression graphs (Figure 3.16B, D and E). In the presence of the FGFRi, the response of FGF2 was prevented but the receptor ratio shifted to around equal levels at 12-24 hours, due to the decrease in *FGFR1* at these times (Figure 3.19C and Figure 3.16C). Stimulation with FGF18-V1 did not change *FGFR1 to FGFR2* ratios (Figure 3.19F).

Figure 3.20A shows that *FGFR1:FGFR3* ratios stayed the same in unstimulated cells, with around equal levels of expression. With stimulation with FGF2, FGF18 and FGF2-V2 the receptor ratios shifted in favour of *FGFR1* expression over *FGFR3* expression; with a peak at 15 to 25-fold higher *FGFR1* expression than *FGFR3* expression at 8 hours (Figure 3.20B, D and E). These changes were mainly driven by changes in *FGFR3* as the shape of the graphs is

similar to that of the inverse *FGFR3* expression (Figure 3.18B, D and E). In the presence of the FGFRi, the response of FGF2 was largely prevented but the receptor ratio shifted to favour *FGFR3* expression at 12-24 hours, due to the decrease in *FGFR1* at these times (Figure 3.20C and Figure 3.16C). Stimulation with FGF18-V1 did not change *FGFR1* to *FGFR3* ratios (Figure 3.20F).

If one looks at the overall changes of *FGFR* expression, FGF18 stimulation caused a very similar response to FGF2 stimulation; FGF2-V2 stimulation also drove a similar response to FGF2 stimulation but at a dampened level; and FGF18-V1 stimulation does not cause any change in *FGFR* expression.

As a positive control, I also included some known FGF2-dependent genes in the analysis. When stimulated with FGF2, *ARG1* expression increased from 2 hours to peak at 12 hours by 20-fold and then decreased after this time-point (Figure 3.21B). This response was prevented by the FGFRi (Figure 3.21C). Stimulation with FGF18 also caused an increase in *ARG1* expression, though at a much lower level, with a peak of 5-fold increase at 24 hours (Figure 3.21E). Stimulation with selective ligands (FGF2-V2 and FGF18-V1) did not change *ARG1* expression (Figure 3.21D and F).

Figure 3.22 shows that *NGF* expression is fairly variable throughout the culture period but this is not greatly altered by stimulation with FGF ligands.

Figure 3.23A shows that *TSG-6* expression varied 2-fold during the culture period in isolated chondrocytes. With FGF2 stimulation, *TSG-6* expression increased to a peak of 6-fold expression at 6 hours post stimulation and then began to steadily decrease (Figure 3.23B). The presence of the FGFRi did suppress the induction by FGF2, however the overall levels of

TSG-6 expression were still slightly higher than that of unstimulated cells (Figure 3.23C). Simulation with FGF2-V2 did not affect *TSG-6* expression from that of unstimulated cells (Figure 3.23D). FGF18 stimulation caused a similar increase in *TSG-6* expression as FGF2 but to a lower level (maximum 4-fold increase at 8 hours) (Figure 3.23E). With FGF18-V1 stimulation, *TSG-6* expression did not vary throughout the culture period (Figure 3.23F).

These results therefore confirm that FGF2 directly induces the expression of *ARG1* and *TSG-6* in keeping with previous work from the group (Chong *et al*., 2013).

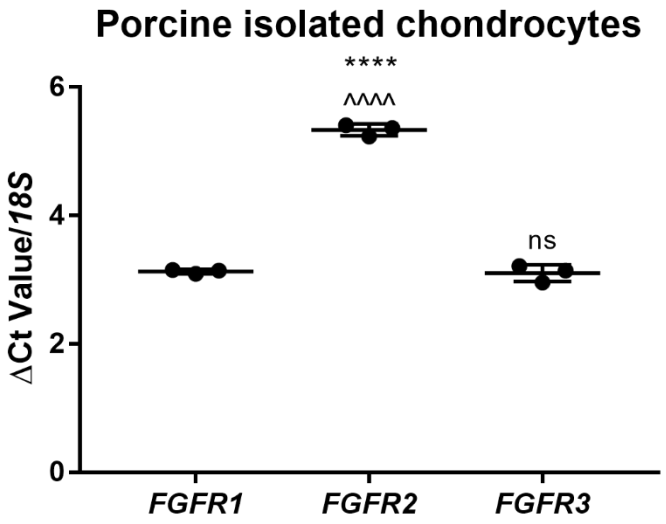

Figure 3.15: Abundance of *FGFR*s in isolated porcine chondrocytes

Primary articular chondrocytes were isolated separately from 3 trotters. Cells were plated at 2×10^6 cells/well in 10 % FBS DMEM and left for 24 h at 37 °C, 5 % CO_2 to adhere to the culture dish. Cells were serum starved for 24 h. Cells were lysed in TRIzol. RNA was extracted, reverse transcribed and gene expression for *FGFR*s assessed by qPCR. All samples were normalised to *18S* to obtain ΔCt values. Graphs show mean +/- S.D; one-way ANOVA; **p<0.01, with Tukey post hoc test ns=non-significant ^^p<0.01, compared to "*FGFR1*". n=3 biological replicates.

FGFR1

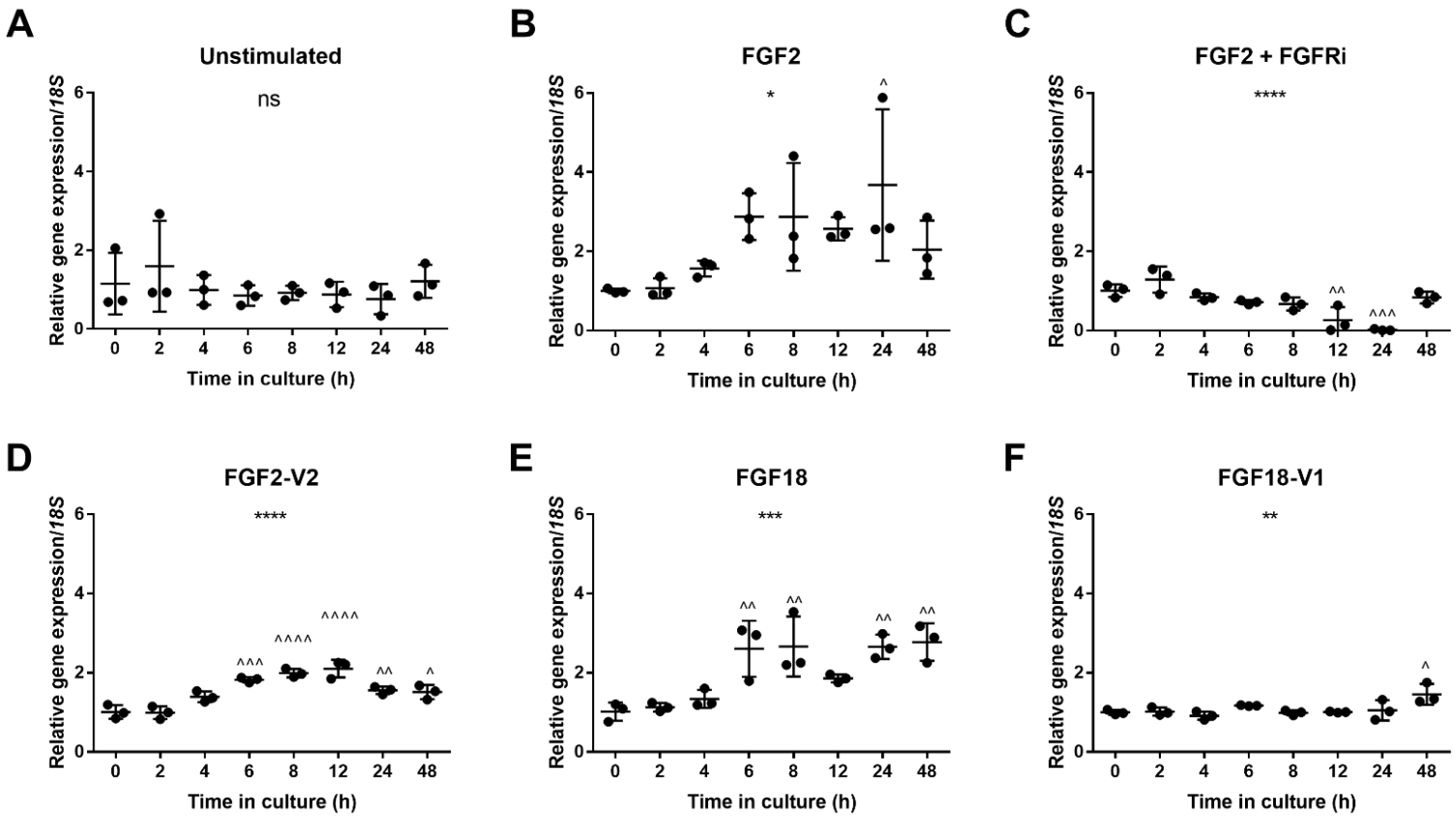

Figure 3.16: *FGFR1* expression is upregulated to a similar extent by FGF2, FGF18 and FGF2-V2 in isolated porcine chondrocytes
Primary articular chondrocytes were isolated separately from 3 trotters. Cells were plated at 2×10^6 cells/well in 10 % FBS DMEM and left for 24 h at 37 °C, 5 % CO_2 to adhere to the culture dish. Cells were serum starved for 24 h. Media was then changed to that containing 250 nM FGFRi SB402451 and incubated for 30 min for the FGF2 + FGFRi experiment only. Cells were stimulated with 20 ng/ml FGF ligands or serum-free media (unstimulated cells). Cells were cultured for various times before being lysed in TRIzol. RNA was extracted, reverse transcribed and gene expression for *FGFR1* assessed by qPCR. All samples were normalised to *18S* and expressed relative to 0 h samples. **A**, Unstimulated cells. **B**, FGF2 stimulated cells. **C,** FGF2 +FGFRi stimulated cells, **D**, FGF2-V2 stimulated cells (FGFR1 specific). **E**, FGF18 stimulated cells, **F**, FGF18-V1 stimulated cells (FGFR3 specific). Graphs show mean +/- S.D; one-way ANOVA; ns= non-significant, *p<0.05, **p<0.01, ***p<0.001, ****p<0.0001 with Tukey post hoc test ^p<0.05, ^^p<0.01, ^^^p<0.001, ^^^^p<0.0001 compared to "0 h". n=3 biological replicates.

FGFR2

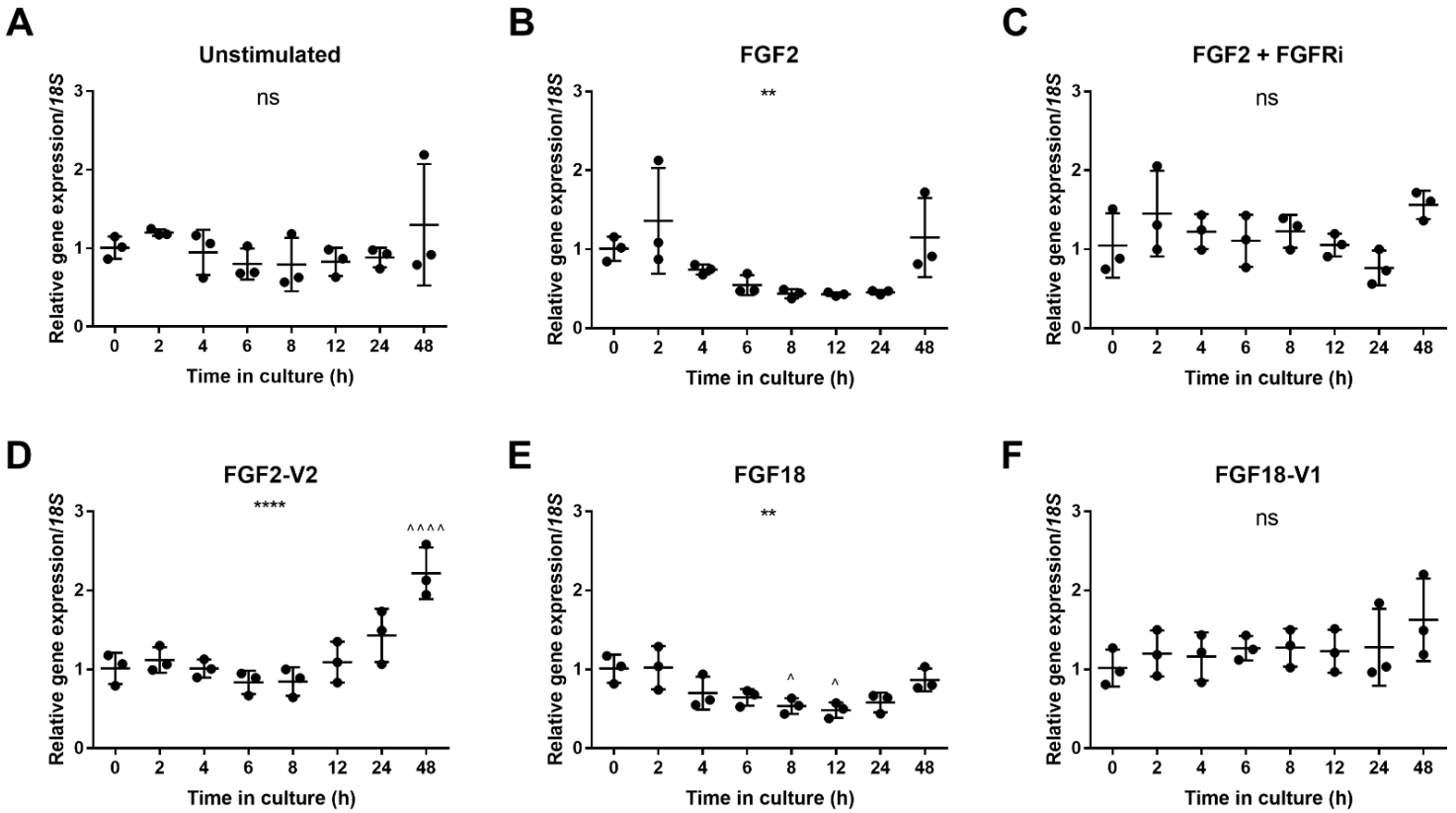

Figure 3.17: *FGFR2* expression is down-regulated to a similar extent by FGF2 and FGF18 in isolated porcine chondrocytes
Primary articular chondrocytes were isolated separately from 3 trotters. Cells were plated at 2×10^6 cells/well in 10 % FBS DMEM and left for 24 h at 37 °C, 5 % CO_2 to adhere to the culture dish. Cells were serum starved for 24 h. Media was then changed to that containing 250 nM FGFRi SB402451 and incubated for 30 min for the FGF2 + FGFRi experiment only. Cells were stimulated with 20 ng/ml FGF ligands or serum-free media (unstimulated cells). Cells were cultured for various times before being lysed in TRIzol. RNA was extracted, reverse transcribed and gene expression for *FGFR2* assessed by qPCR. All samples were normalised to *18S* and expressed relative to 0 h samples. **A**, Unstimulated cells. **B**, FGF2 stimulated cells. **C,** FGF2 +FGFRi stimulated cells, **D**, FGF2-V2 stimulated cells (FGFR1 specific). **E**, FGF18 stimulated cells, **F**, FGF18-V1 stimulated cells (FGFR3 specific). Graphs show mean +/- S.D; one-way ANOVA; ns= non-significant, **p<0.01, ****p<0.0001 with Tukey post hoc test ^p<0.05, ^^^^p<0.0001 compared to "0 h". n=3 biological replicates.

FGFR3

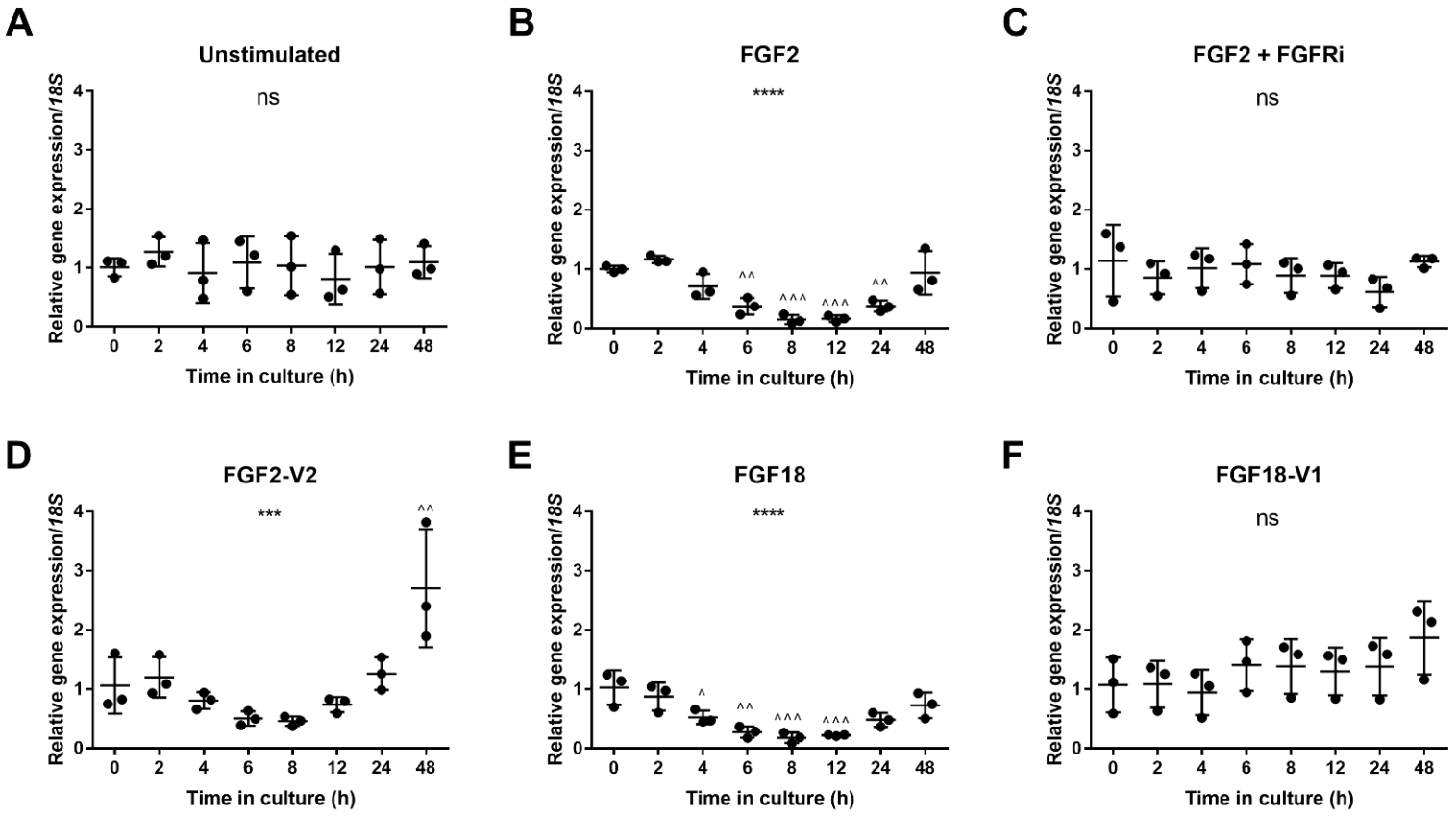

Figure 3.18: *FGFR3* expression is down-regulated to a similar extent by FGF2, FGF18 and FGF2-V2 in isolated porcine chondrocytes

Primary articular chondrocytes were isolated separately from 3 trotters. Cells were plated at 2×10^6 cells/well in 10 % FBS DMEM and left for 24 h at 37 °C, 5 % CO_2 to adhere to the culture dish. Cells were serum starved for 24 h. Media was then changed to that containing 250 nM FGFRi SB402451 and incubated for 30 min for the FGF2 + FGFRi experiment only. Cells were stimulated with 20 ng/ml FGF ligands or serum-free media (unstimulated cells). Cells were cultured for various times before being lysed in TRIzol. RNA was extracted, reverse transcribed and gene expression for *FGFR3* assessed by qPCR. All samples were normalised to *18S* and expressed relative to 0 h samples. **A**, Unstimulated cells. **B**, FGF2 stimulated cells. **C,** FGF2 +FGFRi stimulated cells, **D**, FGF2-V2 stimulated cells (FGFR1 specific). **E**, FGF18 stimulated cells, **F**, FGF18-V1 stimulated cells (FGFR3 specific). Graphs show mean +/- S.D; one-way ANOVA; ns= non-significant, ***p<0.001, ****p<0.0001 with Tukey post hoc test ^p<0.05, ^^p<0.01, ^^^p<0.001 compared to "0 h". n=3 biological replicates.

FGFR1:*FGFR2*

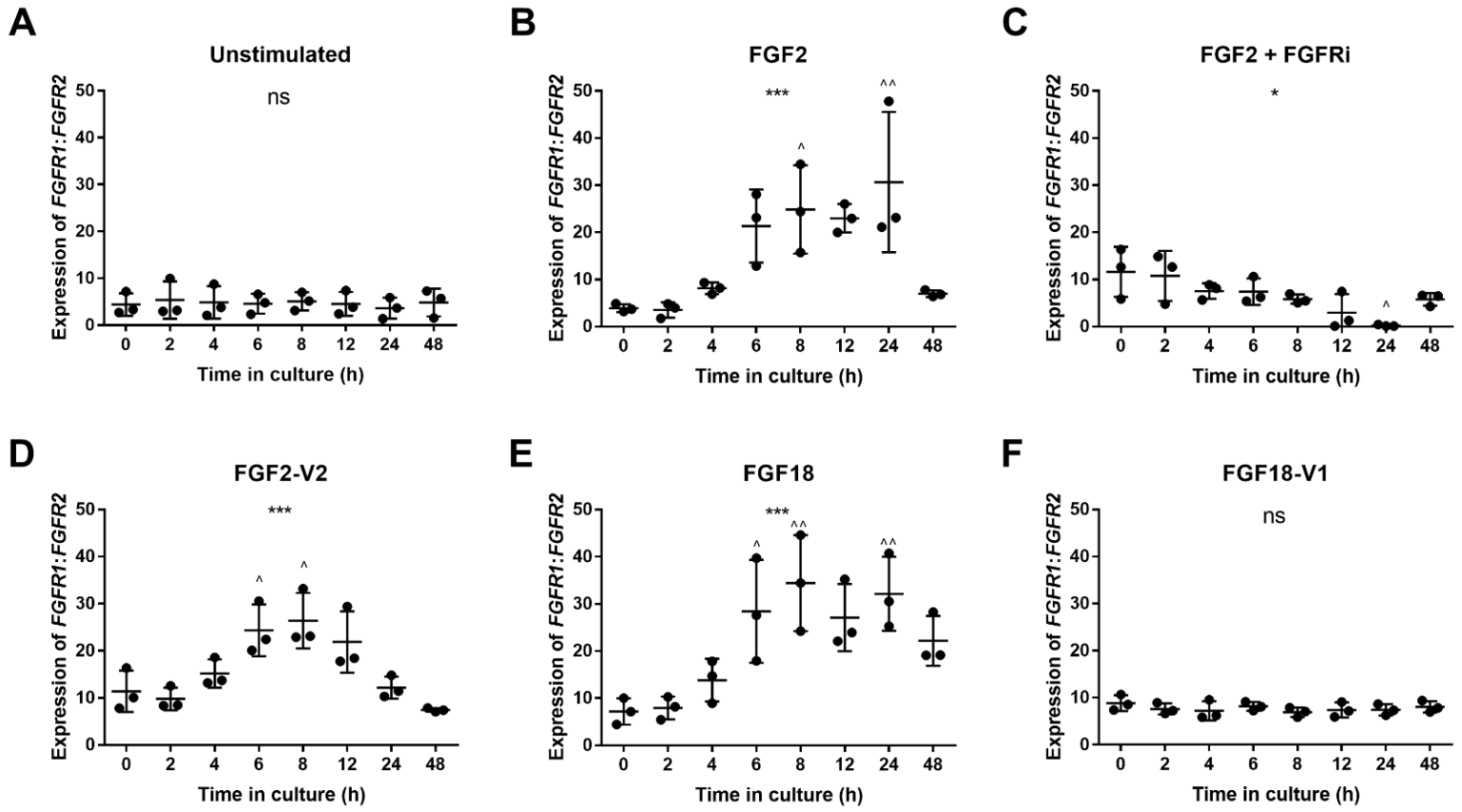

Figure 3.19: *FGFR* ratios shift to favour *FGFR1* expression over *FGFR2* expression, to a similar extent by FGF2, FGF18 and FGF2-V2 in isolated porcine chondrocytes
Primary articular chondrocytes were isolated separately from 3 trotters. Cells were plated at 2×10^6 cells/well in 10 % FBS DMEM and left for 24 h at 37 °C, 5 % CO_2 to adhere to the culture dish. Cells were serum starved for 24 h. Media was then changed to that containing 250 nM FGFRi SB402451 and incubated for 30 min for the FGF2 + FGFRi experiment only. Cells were stimulated with 20 ng/ml FGF ligands or serum-free media (unstimulated cells). Cells were cultured for various times before being lysed in TRIzol. RNA was extracted, reverse transcribed and gene expression for *FGFR1* and *FGFR2* assessed by qPCR. The relative expression of *FGFR1* was expressed as a ratio of *FGFR2* expression. **A**, Unstimulated cells. **B**, FGF2 stimulated cells. **C,** FGF2 +FGFRi stimulated cells, **D**, FGF2-V2 stimulated cells (FGFR1 specific). **E**, FGF18 stimulated cells, **F**, FGF18-V1 stimulated cells (FGFR3 specific). Graphs show mean +/- S.D; one-way ANOVA; ns= non-significant, *p<0.05, ***p<0.001, with Tukey post hoc test ^p<0.05, ^^p<0.01, compared to "0 h". n=3 biological replicates.

FGFR1:*FGFR3*

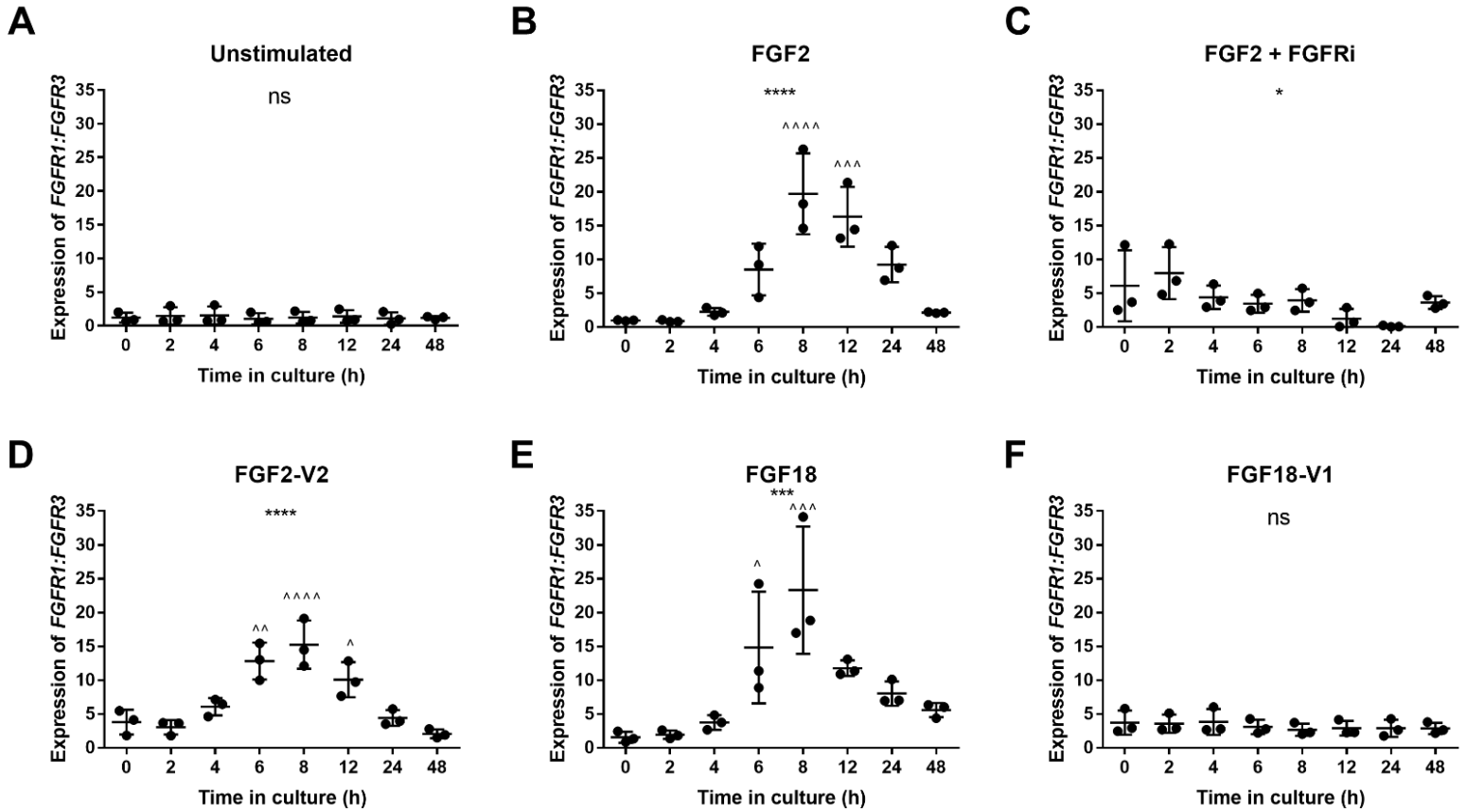

Figure 3.20: *FGFR* ratios shift to favour *FGFR1* expression over *FGFR3* expression, to a similar extent by FGF2, FGF18 and FGF2-V2 in isolated porcine chondrocytes
Primary articular chondrocytes were isolated separately from 3 trotters. Cells were plated at 2×10^6 cells/well in 10 % FBS DMEM and left for 24 h at 37 °C, 5 % CO_2 to adhere to the culture dish. Cells were serum starved for 24 h. Media was then changed to that containing 250 nM FGFRi SB402451 and incubated for 30 min for the FGF2 + FGFRi experiment only. Cells were stimulated with 20 ng/ml FGF ligands or serum-free media (unstimulated cells). Cells were cultured for various times before being lysed in TRIzol. RNA was extracted, reverse transcribed and gene expression for *FGFR1* and *FGFR3* assessed by qPCR. The relative expression of *FGFR1* was expressed as a ratio of *FGFR3* expression. **A**, Unstimulated cells. **B**, FGF2 stimulated cells. **C,** FGF2 +FGFRi stimulated cells, **D**, FGF2-V2 stimulated cells (FGFR1 specific). **E**, FGF18 stimulated cells, **F**, FGF18-V1 stimulated cells (FGFR3 specific). Graphs show mean +/- S.D; one-way ANOVA; ns= non-significant, *p<0.05, ***p<0.001, ****p<0.0001, with Tukey post hoc test ^p<0.05, ^^p<0.01, ^^^p<0.001, ^^^^p<0.0001 compared to "0 h". n=3 biological replicates.

ARG1

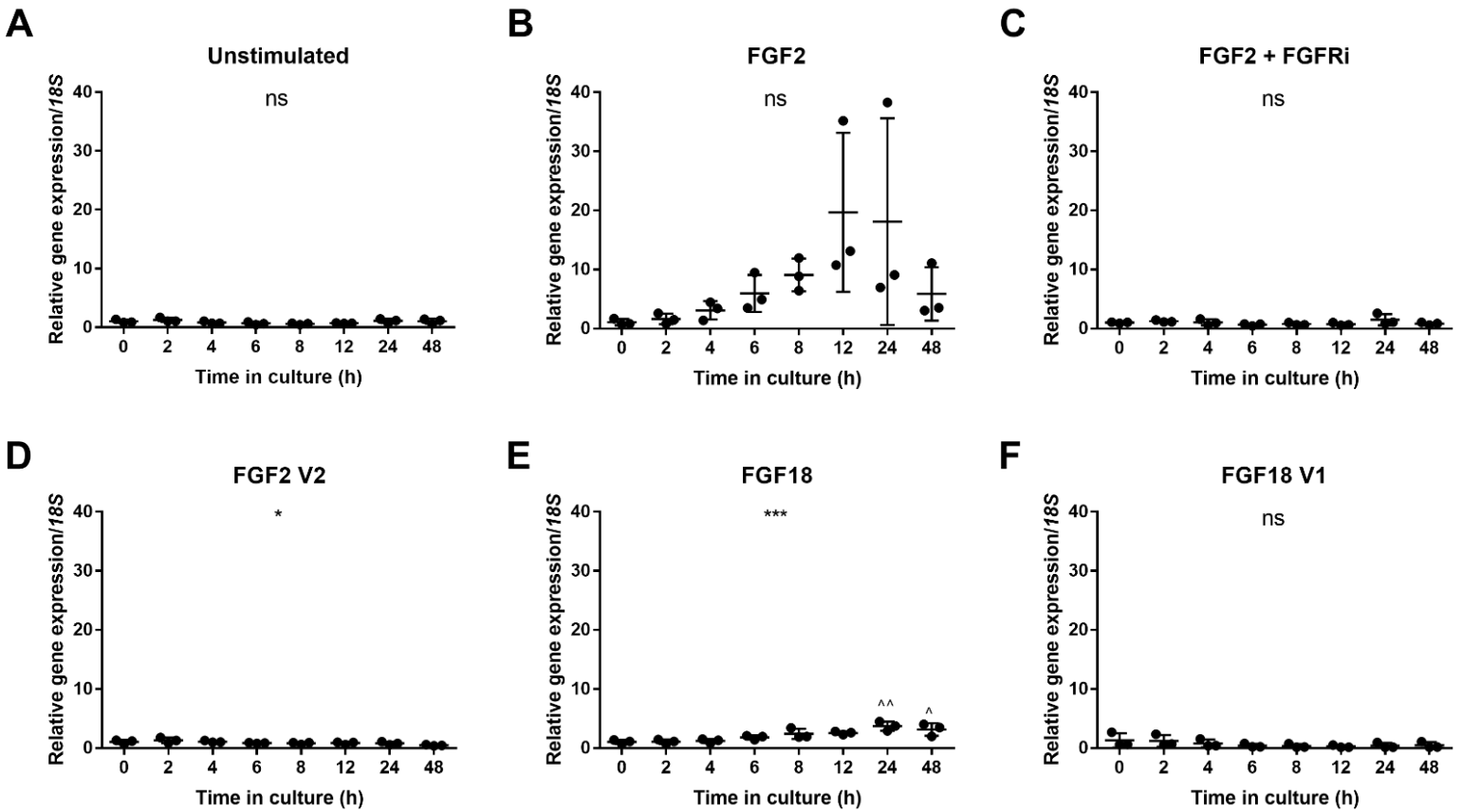

Figure 3.21: *ARG1* is regulated marginally by FGF2 and FGF18 in isolated porcine chondrocytes

Primary articular chondrocytes were isolated separately from 3 trotters. Cells were plated at 2×10^6 cells/well in 10 % FBS DMEM and left for 24 h at 37 °C, 5 % CO_2 to adhere to the culture dish. Cells were serum starved for 24 h. Media was then changed to that containing 250 nM FGFRi SB402451 and incubated for 30 min for the FGF2 + FGFRi experiment only. Cells were stimulated with 20 ng/ml FGF ligands or serum-free media (unstimulated cells). Cells were cultured for various times before being lysed in TRIzol. RNA was extracted, reverse transcribed and gene expression for *ARG1* assessed by qPCR. All samples were normalised to *18S* and expressed relative to 0 h samples. **A**, Unstimulated cells. **B**, FGF2 stimulated cells. **C,** FGF2 +FGFRi stimulated cells, **D**, FGF2-V2 stimulated cells (FGFR1 specific). **E**, FGF18 stimulated cells, **F**, FGF18-V1 stimulated cells (FGFR3 specific). Graphs show mean +/- S.D; one-way ANOVA; ns= non-significant, *p<0.05, ***p<0.001, with Tukey post hoc test ^p<0.05, ^^p<0.01, compared to "0 h". n=3 biological replicates.

NGF

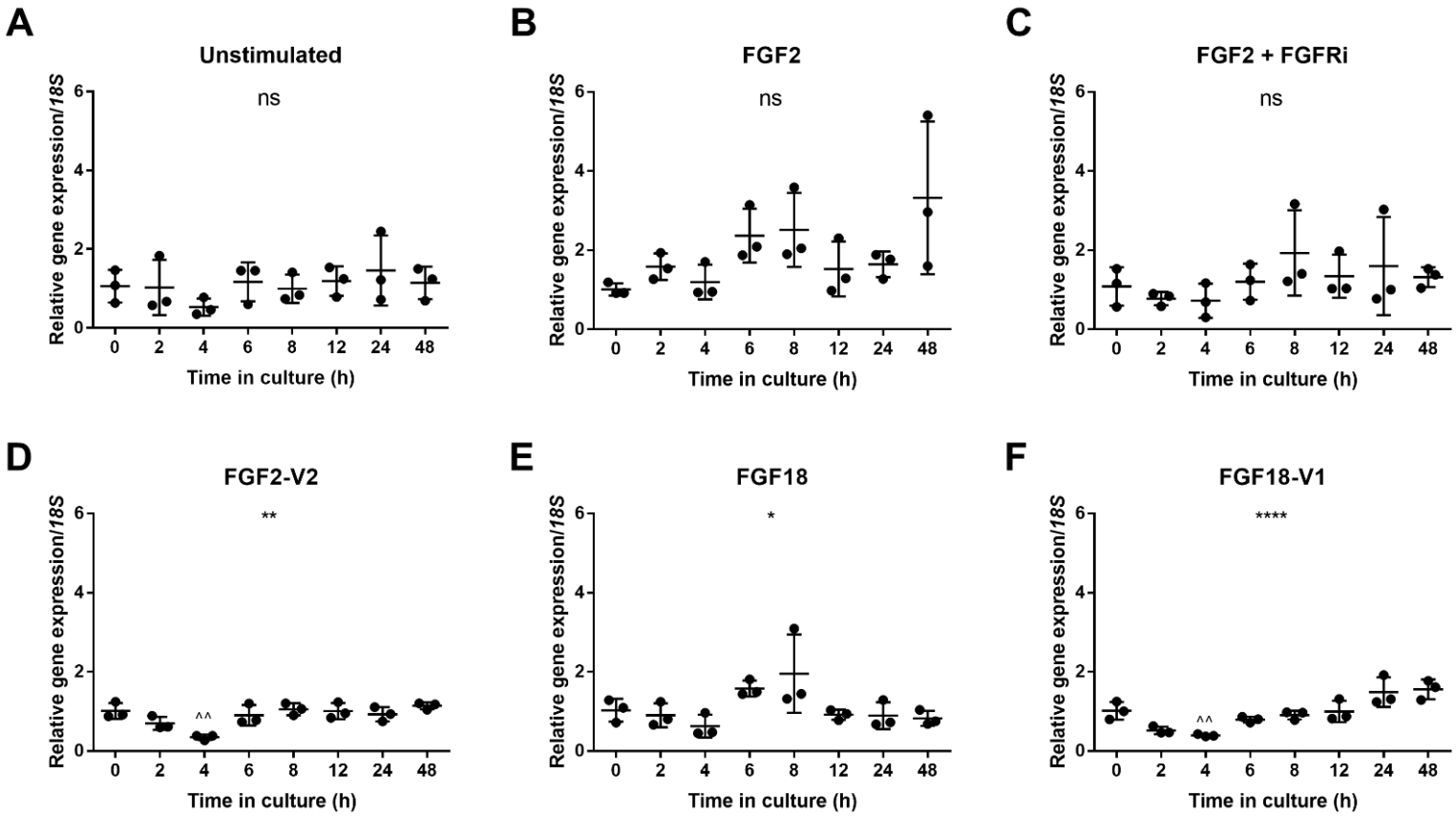

Figure 3.22: *NGF* expression is not changed by FGF stimulation in isolated porcine chondrocytes

Primary articular chondrocytes were isolated separately from 3 trotters. Cells were plated at 2×10^6 cells/well in 10 % FBS DMEM and left for 24 h at 37 °C, 5 % CO_2 to adhere to the culture dish. Cells were serum starved for 24 h. Media was then changed to that containing 250 nM FGFRi SB402451 and incubated for 30 min for the FGF2 + FGFRi experiment only. Cells were stimulated with 20 ng/ml FGF ligands or serum-free media (unstimulated cells). Cells were cultured for various times before being lysed in TRIzol. RNA was extracted, reverse transcribed and gene expression for *NGF* assessed by qPCR. All samples were normalised to *18S* and expressed relative to 0 h samples. **A**, Unstimulated cells. **B**, FGF2 stimulated cells. **C,** FGF2 +FGFRi stimulated cells, **D**, FGF2-V2 stimulated cells (FGFR1 specific). **E**, FGF18 stimulated cells, **F**, FGF18-V1 stimulated cells (FGFR3 specific). Graphs show mean +/- S.D; one-way ANOVA; ns= non-significant, *p<0.05, **p<0.01, ****p<0.0001, with Tukey post hoc test ^^p<0.01, compared to "0 h". n=3 biological replicates.

TSG6

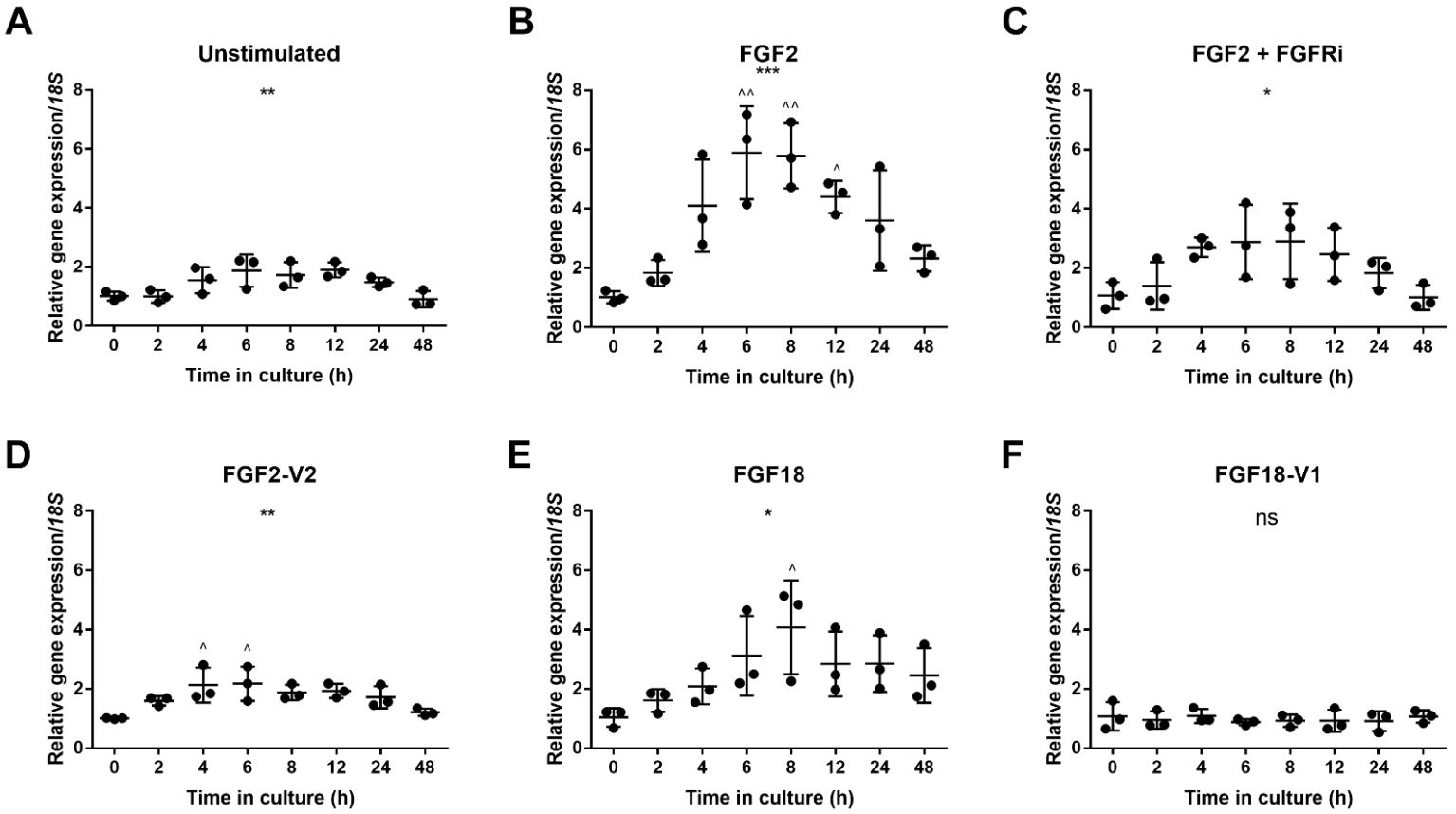

Figure 3.23: *TSG-6* is regulated by FGF2 and marginally by FGF18 in isolated porcine chondrocytes

Primary articular chondrocytes were isolated separately from 3 trotters. Cells were plated at 2×10^6 cells/well in 10 % FBS DMEM and left for 24 h at 37 °C, 5 % CO_2 to adhere to the culture dish. Cells were serum starved for 24 h. Media was then changed to that containing 250 nM FGFRi SB402451 and incubated for 30 min for the FGF2 + FGFRi experiment only. Cells were stimulated with 20 ng/ml FGF ligands or serum-free media (unstimulated cells). Cells were cultured for various times before being lysed in TRIzol. RNA was extracted, reverse transcribed and gene expression for *TSG6* assessed by qPCR. All samples were normalised to *18S* and expressed relative to 0 h samples. **A**, Unstimulated cells. **B**, FGF2 stimulated cells. **C,** FGF2 +FGFRi stimulated cells, **D**, FGF2-V2 stimulated cells (FGFR1 specific). **E**, FGF18 stimulated cells, **F**, FGF18-V1 stimulated cells (FGFR3 specific). Graphs show mean +/- S.D; one-way ANOVA; ns= non-significant, *p<0.05, **p<0.01, ***p<0.001, with Tukey post hoc test ^p<0.05, ^^p<0.01 compared to "0 h". n=3 biological replicates.

3.10 Regulation of *Fgfr*s and FGF-dependent genes upon murine hip explantation

Our group has previously shown that FGF2 is released upon cartilage injury (Vincent *et al*., 2002). It was likely therefore that the FGFR-dependent change in *FGFR* ratios was due to FGF2. To test this, I used a murine hip injury model to compare the response of wild-type (WT) C57BL/6 tissue to that of FGF2-deficient tissue (*Fgf2*$^{-/-}$). The *Fgf2*$^{-/-}$ mice were constitutive whole-body knockouts. Mice aged 5-6 weeks were euthanised, femoral head cartilage was explanted (as described in Methods section 2.7) directly into liquid nitrogen (0 h) or into serum-free medium and cultured in an incubator at 37 °C, 5 % CO_2, for 2 to 48 hours. 4 hips were pooled per point, RNA was extracted, reverse transcribed and gene expression analysed via qPCR on pre-designed microfluidic cards. All genes were normalised to *18s* and expressed relative to their respective 0 h time-point.

Figure 3.24 shows the abundance of the *Fgfr*s at 0 h. In WT tissue there was no significant difference in the ΔCt values of *Fgfr1* and *Fgfr3*, indicating equal abundance. ΔCt values for *Fgfr2* were slightly higher than those of *Fgfr1* and *Fgfr3*, indicating a slightly lower abundance. ΔCt values of *Fgfr4* were significantly higher, suggesting a much lower abundance than the other *Fgfr*s. Therefore, the abundance of *Fgfr*s in WT tissue was *Fgfr1=Fgfr3>Fgfr2>>Fgfr4* (Figure 3.24A). In *Fgf2*$^{-/-}$ tissue, ratios were similar to WT tissue, although the *Fgfr3* ΔCt values were slightly lower than those of *Fgfr1*. Therefore, the abundance of *Fgfr*s in *Fgf2*$^{-/-}$ tissue was *Fgfr3≥Fgfr1>Fgfr2>>Fgfr4*. (Figure 3.24B).

Figure 3.25A shows *Fgfr1* expression was significantly upregulated 6 hours post explantation, though the fold change was marginal at 1.75-fold. *Fgfr1* expression then reduced back to basal levels by 12 hours. This response occurred independently of the

genotype. Therefore, the change of *Fgfr1* expression upon explantation was not FGF2-dependent.

Fgfr2 expression in WT tissue decreased upon explantation, though this was not statistically significant until 8-12 hours (Figure 3.25B). 12-hour expression was 25 % that of 0-hour. 24 hours post explantation *Fgfr2* expression returned to basal levels. In the *Fgf2*$^{-/-}$ tissue, expression of *Fgfr2* did not change over time and there was a statistically significant difference between genotypes at the 12-hour time-point. These results therefore suggest that the moderate decrease in *Fgfr2* expression upon explantation is FGF2-dependent.

In WT tissue there was a bi-phasic change in *Fgfr3* expression over time with peak expression at 4 and 24 h (Figure 3.25C). Changes in *Fgfr3* expression in *Fgf2*$^{-/-}$ tissue was not statistically different from wild-type tissue, however in *Fgf2*$^{-/-}$ tissue, *Fgfr3* expression did not increase in the first 4 hours post explantation.

Unlike the other *Fgfr*s, *Fgfr4* expression did not significantly change over the culture period, though there was a lot of variation across samples (Figure 3.25D). This was probably due to extremely low expression levels of this receptor in the tissue (Figure 3.24).

To see how the *Fgfr*s changed in relation to each other, *Fgfr* ratios were calculated from the raw Ct values of each receptor for the individual time-points (i.e. not normalised to the 0 h time-points) for both genotypes. There was 4 times more *Fgfr1* expression than *Fgfr2* expression in both WT and *Fgf2*$^{-/-}$ hips at 0 h (Figure 3.26A). This *Fgfr1:Fgfr2* ratio changed upon WT murine hip explantation to favour *Fgfr1* expression, with a peak at 12 hours post explantation of approximately 14-fold higher *Fgfr1* expression. By 24 hours post explantation the *Fgfr1:Fgfr2* expression decreased to basal levels. This change in *Fgfr1:Fgfr2*

was largely due to the decrease in *Fgfr2* (Figure 3.25B). The *Fgfr1:Fgfr2* ratio also increased in the *Fgf2*$^{-/-}$ tissue; it reached a peak of 11-fold higher *Fgfr1* at 6 hours post explantation then decreased back to basal levels by 24 hours post explantation. This effect was mainly due to the changes in *Fgfr1* expression (Figure 3.25A). As a result of these changes in *Fgfr1:Fgfr2* expression, there was a statistically significant difference between WT and *Fgf2*$^{-/-}$ tissue at 12 hours post explantation, as WT tissue had 11-fold higher *Fgfr1* and *Fgf2*$^{-/-}$ tissue had basal levels (4-fold higher FGFR1).

Figure 3.26B shows that the *Fgfr1:Fgfr3* ratio in WT tissue was approximately equal at 0-hour. In *Fgf2*$^{-/-}$ tissue there was half as much *Fgfr1* compared to *Fgfr3*, however these differences between the tissues remained statistically insignificant. In both tissue types, the *Fgfr1:Fgfr3* expression shifted to favour *Fgfr1* expression upon explantation over the first 6 hours and returned to basal levels by 12 hours post explantation, though this was statistically insignificant for the *Fgf2*$^{-/-}$ tissue. The peak increase at 6 hours was significantly different between the genotypes, being higher in WT tissue compared with *Fgf2*$^{-/-}$ tissue. These changes in *Fgfr1:Fgfr3* were mainly due to the increase in *Fgfr1* expression in both tissue types (Figure 3.25A).

Unsurprisingly, the *Fgfr1:Fgfr4* expression was not significantly altered following murine hip explantation and was not different between genotypes (Figure 3.26C).

Chong *et al* (2013) described FGF2-dependent gene changes in the murine injury assay by looking at how the changes in gene expression varied between WT and *Fgf2*$^{-/-}$ tissue. However only the difference between 0 and 4 hours was tested. I therefore looked at how the expression of these known FGF2-dependent genes (*Tsg6, Tumour Necrosis Factor Receptor Superfamily member 12A (Tnfrsf12a), Hyaluronan Synthase 1 (Has1), Inhibin beta A*

(Inhba), Timp1, Prostaglandin-Endoperoxide Synthase 2 (Ptgs2), Arg1 and *Ngf*) changed between the tissues in a more extensive time course, to see if they correlated with the changes in *Fgfr* expression.

I found that there were 3 distinct patterns of induction of these genes upon murine explantation. The response was either early, late or biphasic. The early response genes were; *Tsg6*, *Tnfrsf12a* and *Has1* (Figure 3.27). These genes had a peak induction at 4 hours post explantation which was significantly reduced in the *Fgf2*$^{-/-}$ tissue. The induction of *Ngf* was also early, (peaking at 6 hours post explantation) however this induction was not FGF2-dependent (Figure 3.28). *Arg1* was the only late response gene, with a peak induction at 24-hours post explantation, which was significantly dampened in the *Fgf2*$^{-/-}$ tissue (Figure 3.29). The biphasic response genes were; *Inhba*, *Timp1* and *Ptgs2* (Figure 3.30). The first peak of induction occurred either at 4 or 6 hours post explantation and the second peak occurred at 24 hours post explantation. In the *Fgf2*$^{-/-}$ tissue, the first peak of induction was significantly reduced but there was no secondary peak. This therefore suggested the secondary peak of induction was entirely dependent on FGF2, or something it induced during the injury response. Thus, I also looked at how the expression of *Fgf*s changed during this explantation to better understand this biphasic response.

Fgf18 expression showed a similar FGF2 dependent bi-phasic response as that seen for the other genes (with peak induction at 4 and 24-hours post explantation. (Figure 3.31A).

WT tissue showed a peak 15-fold induction of *Fgf2* 4 hours post explantation and a secondary 5-fold peak at 24 hours (Figure 3.31B). No change in the expression of *Fgf2* could be detected for *Fgf2*$^{-/-}$ tissue as the transcript was no longer functional. Therefore the induction of *Fgf2* may just be a response to injury, or release of FGF2 upon injury could be

driving further production of FGF2 in a positive feedback loop and therefore driving the secondary induction of FGF2-dependent genes; though further experiments would be needed to test these theories.

Taken together these results show the upregulation of FGF2-dependent genes is to some extent regulated with differing patterns of expression; therefore, it is unlikely that their regulation is dependent on the altering ratios of *Fgfr*s during the explantation time course.

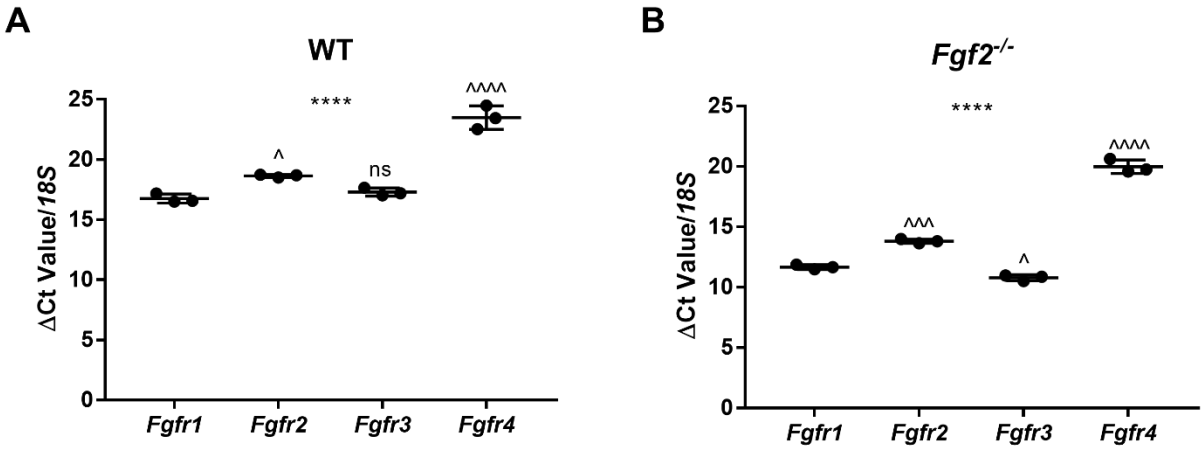

Figure 3.24: Abundance of *Fgfr*s in murine hips

Hips were explanted from WT or *Fgf2*$^{-/-}$ mice aged 5 to 6 weeks and snap frozen in liquid nitrogen. 4 hips were pooled per point, RNA was extracted, reverse transcribed and gene expression of *Fgfr*s assessed by qPCR on predesigned microfluidic cards. All samples were normalised to *18S* to obtain ΔCt values. Graphs show mean +/- S.D; One-way ANOVA ****p>0.0001 with Tukey post hoc test ns= non-significant, ^p<0.05, ^^^p>0.001, ^^^^p>0.0001 compared to "*Fgfr1*". n=3 biological replicates.

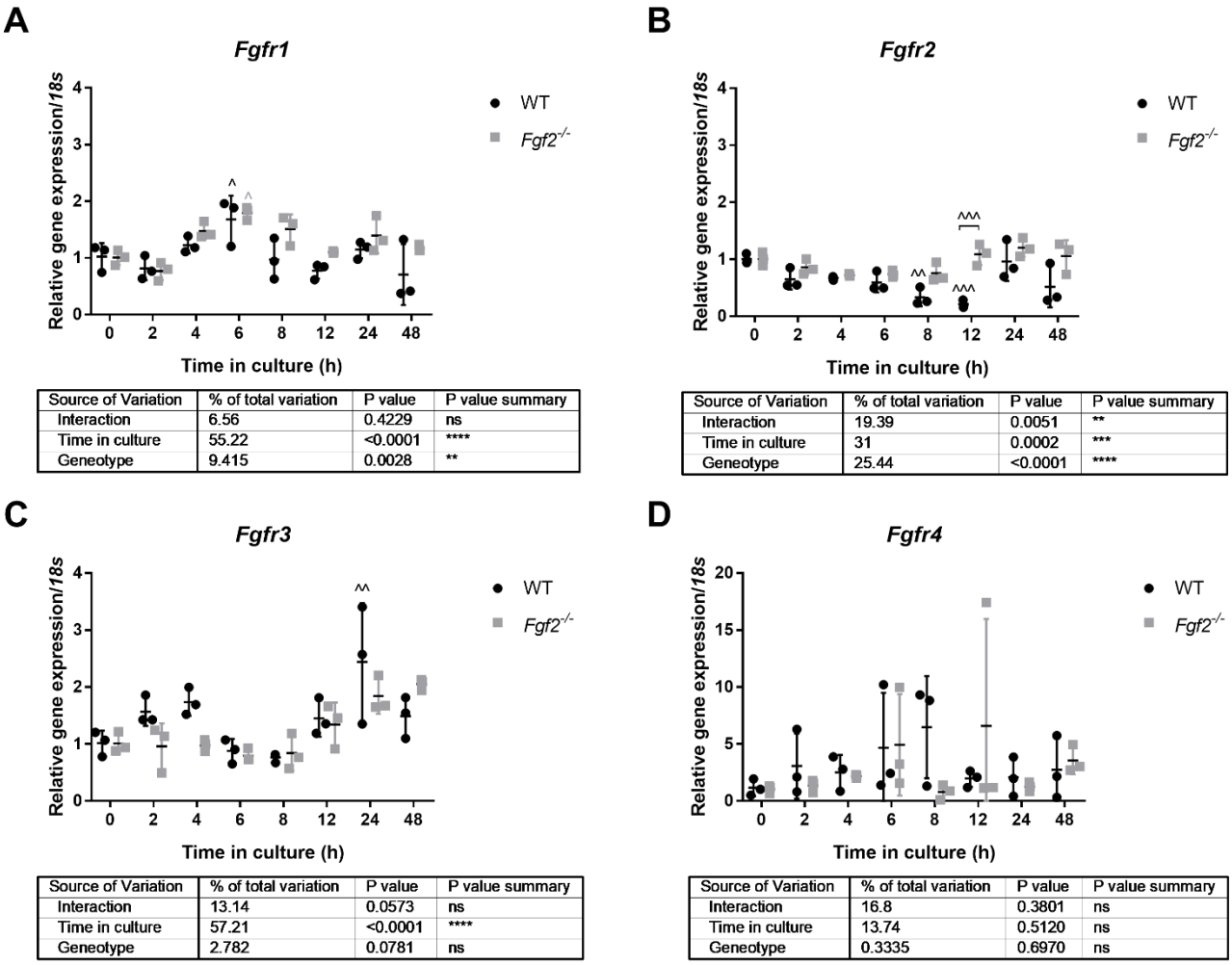

Source of Variation	% of total variation	P value	P value summary
Interaction	6.56	0.4229	ns
Time in culture	55.22	<0.0001	****
Geneotype	9.415	0.0028	**

Source of Variation	% of total variation	P value	P value summary
Interaction	19.39	0.0051	**
Time in culture	31	0.0002	***
Geneotype	25.44	<0.0001	****

Source of Variation	% of total variation	P value	P value summary
Interaction	13.14	0.0573	ns
Time in culture	57.21	<0.0001	****
Geneotype	2.782	0.0781	ns

Source of Variation	% of total variation	P value	P value summary
Interaction	16.8	0.3801	ns
Time in culture	13.74	0.5120	ns
Geneotype	0.3335	0.6970	ns

Figure 3.25: Regulation of *Fgfrs* upon murine hip explantation

Hips were explanted from WT or *Fgf2*$^{-/-}$ mice aged 5-6 weeks, snap frozen in liquid nitrogen (0 h) or cultured in serum-free media for 2-48 h at 37 °C, 5 % CO_2. 4 hips were pooled per point, RNA was extracted, reverse transcribed and gene expression of *Fgfr*s assessed by qPCR on predesigned microfluidic cards. All samples were normalised to *18s* and expressed relative to 0 h samples. **A**, *Fgfr1*. **B**, *Fgfr2*. **C**, *Fgfr3*. **D**, *Fgfr4*. Graphs show mean +/- S.D; Two-way ANOVA (tabulated results ns=non-significant, *p<0.05, **p<0.01, ***p<0.001, ****p>0.0001) with Tukey post hoc test ^p<0.05, ^^p<0.01, ^^^p>0.001, compared to “0 h”. n=3 biological replicates.

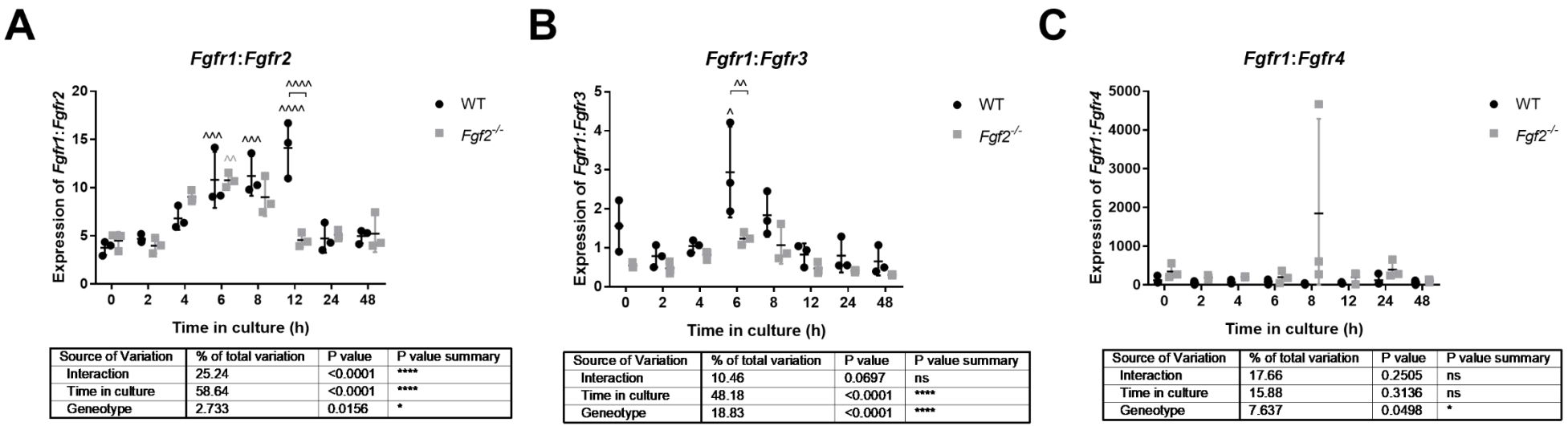

Source of Variation	% of total variation	P value	P value summary
Interaction	25.24	<0.0001	****
Time in culture	58.64	<0.0001	****
Geneotype	2.733	0.0156	*

Source of Variation	% of total variation	P value	P value summary
Interaction	10.46	0.0697	ns
Time in culture	48.18	<0.0001	****
Geneotype	18.83	<0.0001	****

Source of Variation	% of total variation	P value	P value summary
Interaction	17.66	0.2505	ns
Time in culture	15.88	0.3136	ns
Geneotype	7.637	0.0498	*

Figure 3.26: Regulation of *Fgfr* ratios upon murine hip explantation

Hips were explanted from WT or *Fgf2*$^{-/-}$ mice aged 5-6 weeks, snap frozen in liquid nitrogen (0 h) or cultured in serum-free media for 2-48 h at 37 °C, 5 % CO_2. 4 hips were pooled per point, RNA was extracted, reverse transcribed and gene expression of *Fgfr*s assessed by qPCR on predesigned microfluidic cards. -The relative expression of *Fgfr1* was expressed as a ratio of *Fgfr2/3/4* expression **A**, relative expression of *Fgfr1* as a ratio of *Fgfr2* expression. **B**, relative expression of *Fgfr1* as a ratio of *Fgfr3* expression. **C**, relative expression of *Fgfr1* as a ratio of *Fgfr4* expression. Graphs show mean +/- S.D; Two-way ANOVA (tabulated results ns=non-significant, *p<0.05, ****p>0.0001) with Tukey post hoc test ^p<0.05, ^^p<0.01, ^^^p>0.001, ^^^^p>0.0001, compared to “0 h”. n=3 biological replicates.

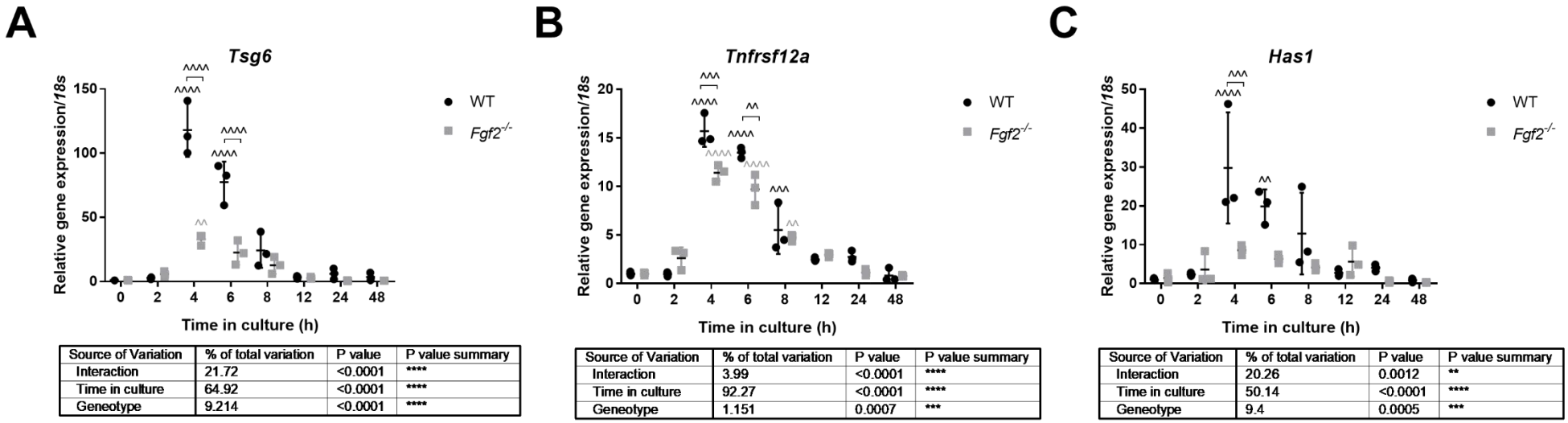

Source of Variation	% of total variation	P value	P value summary
Interaction	21.72	<0.0001	****
Time in culture	64.92	<0.0001	****
Geneotype	9.214	<0.0001	****

Source of Variation	% of total variation	P value	P value summary
Interaction	3.99	<0.0001	****
Time in culture	92.27	<0.0001	****
Geneotype	1.151	0.0007	***

Source of Variation	% of total variation	P value	P value summary
Interaction	20.26	0.0012	**
Time in culture	50.14	<0.0001	****
Geneotype	9.4	0.0005	***

Figure 3.27: FGF2 partially regulates the early induction of genes upon murine hip explantation

Hips were explanted from WT or *Fgf2*$^{-/-}$ mice aged 5-6 weeks, snap frozen in liquid nitrogen (0 h) or cultured in serum-free media for 2-48 h at 37 °C, 5 % CO_2. 4 hips were pooled per point, RNA was extracted, reverse transcribed and expression of FGF-dependant genes assessed by qPCR on predesigned microfluidic cards. All samples were normalised to *18*s and expressed relative to 0 h samples. **A**, *Tsg6*. **B**, *Tnfrsf12a* **C**, *Has1*. Graphs show mean +/- S.D; Two-way ANOVA (tabulated results, **p<0.01, ***p<0.001, ****p>0.0001) with Tukey post hoc test, ^^p<0.01, ^^^p>0.001, ^^^^p>0.0001, compared to “0 h”. n=3 biological replicates.

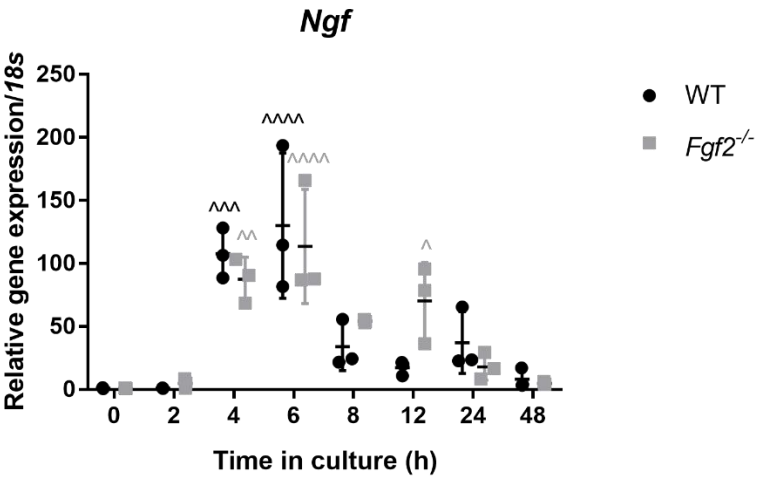

Source of Variation	% of total variation	P value	P value summary
Interaction	5.903	0.1275	ns
Time in culture	78.82	<0.0001	****
Geneotype	0.05535	0.7353	ns

Figure 3.28: Induction of *Ngf* upon murine hip explantation is not FGF2 dependent
Hips were explanted from WT or *Fgf2*$^{-/-}$ mice aged 5-6 weeks, snap frozen in liquid nitrogen (0 h) or cultured in serum-free media for 2-48 h at 37 °C, 5 % CO_2. 4 hips were pooled per point, RNA was extracted, reverse transcribed and gene expression of *Ngf* assessed by qPCR on predesigned microfluidic cards. All samples were normalised to *18s* and expressed relative to 0 h samples. Graphs show mean +/- S.D; Two-way ANOVA (tabulated results ns=non-significant, ****p>0.0001) with Tukey post hoc test ^p>0.05, ^^p>0.01, ^^^p>0.001 ^^^^p>0.0001, compared to "0 h". n=3 biological replicates.

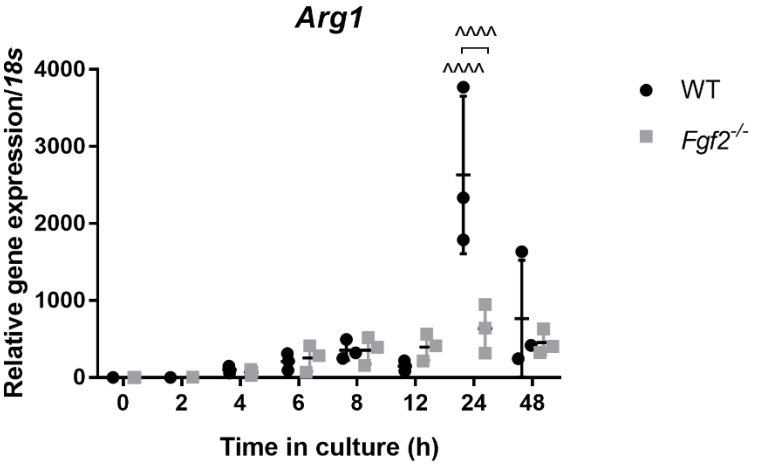

Source of Variation	% of total variation	P value	P value summary
Interaction	24.66	0.0002	***
Time in culture	53.48	<0.0001	****
Geneotype	3.17	0.0255	*

Figure 3.29: Late regulation of *Arg1* upon murine hip explantation is FGF2 dependent
Hips were explanted from WT or *Fgf2*$^{-/-}$ mice aged 5-6 weeks, snap frozen in liquid nitrogen (0 h) or cultured in serum-free media for 2-48 h at 37 °C, 5 % CO_2. 4 hips were pooled per point, RNA was extracted, reverse transcribed and gene expression of *Arg1* assessed by qPCR on predesigned microfluidic cards. All samples were normalised to *18s* and expressed relative to 0 h samples. Graphs show mean +/- S.D; Two-way ANOVA (tabulated results *p<0.05, ***p>0.001, ****p>0.0001) with Tukey post hoc test ^^^^p>0.0001, compared to "0 h". n=3 biological replicates.

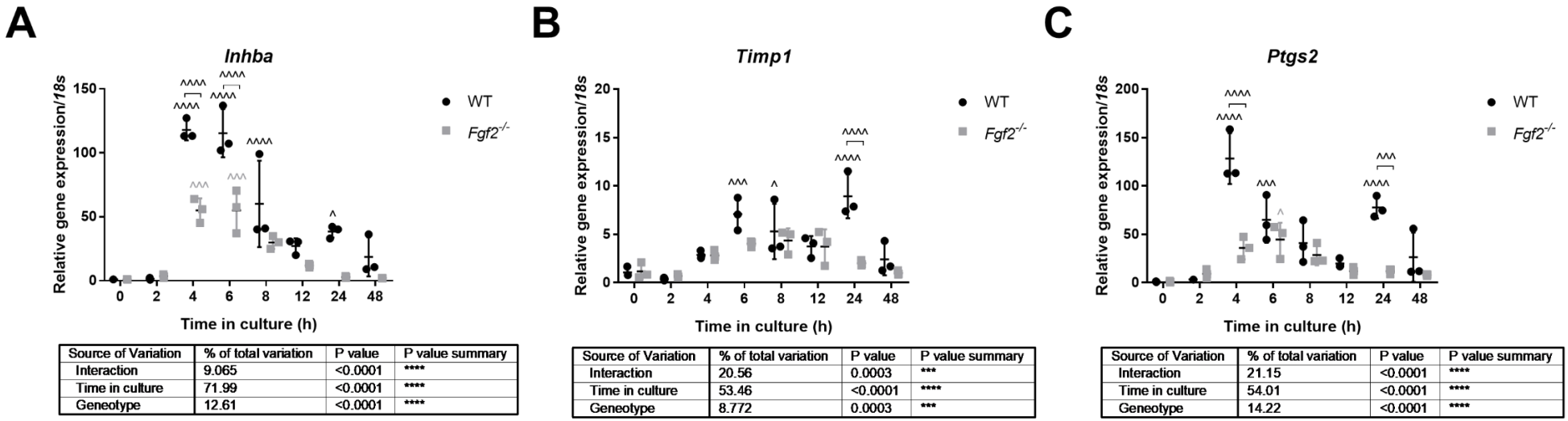

Source of Variation	% of total variation	P value	P value summary
Interaction	9.065	<0.0001	****
Time in culture	71.99	<0.0001	****
Geneotype	12.61	<0.0001	****

Source of Variation	% of total variation	P value	P value summary
Interaction	20.56	0.0003	***
Time in culture	53.46	<0.0001	****
Geneotype	8.772	0.0003	***

Source of Variation	% of total variation	P value	P value summary
Interaction	21.15	<0.0001	****
Time in culture	54.01	<0.0001	****
Geneotype	14.22	<0.0001	****

Figure 3.30: The bi-phasic induction of genes upon murine hip explantation is FGF2-dependent

Hips were explanted from WT or *Fgf2*$^{-/-}$ mice aged 5-6 weeks, snap frozen in liquid nitrogen (0 h) or cultured in serum-free media for 2-48 h at 37 °C, 5 % CO_2. 4 hips were pooled per point, RNA was extracted, reverse transcribed and expression of FGF-dependant genes assessed by qPCR on predesigned microfluidic cards. All samples were normalised to *18s* and expressed relative to 0 h samples. **A**, *Inhba* **B**, *Timp1* **C**, *Ptgs2*. Graphs show mean +/- S.D; Two-way ANOVA (tabulated results ***p<0.001, ****p>0.0001) with Tukey post hoc test ^p<0.05, ^^^p>0.001, ^^^^p>0.0001, compared to “0 h”. n=3 biological replicates.

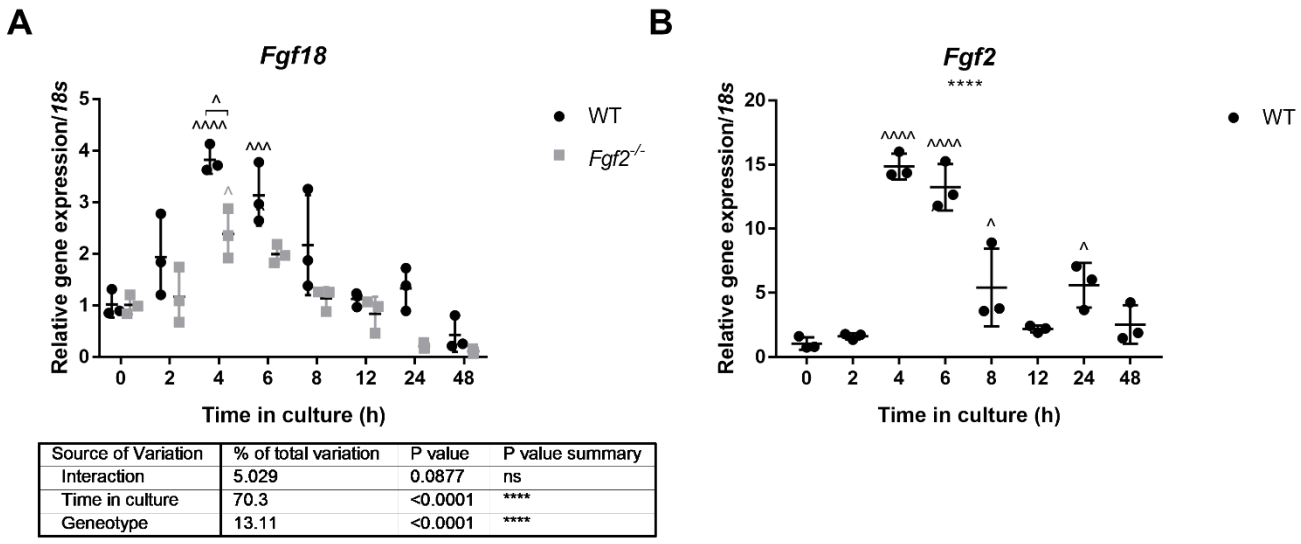

Source of Variation	% of total variation	P value	P value summary
Interaction	5.029	0.0877	ns
Time in culture	70.3	<0.0001	****
Geneotype	13.11	<0.0001	****

Figure 3.31: Regulation of *Fgf* expression upon murine hip explantation

Hips were explanted from WT or Fgf2$^{-/-}$ mice aged 5-6 weeks, snap frozen in liquid nitrogen (0 h) or cultured in serum-free media for 2-48 h at 37 °C, 5 % CO_2. 4 hips were pooled per point, RNA was extracted, reverse transcribed and gene expression of *Fgf*s assessed by qPCR on predesigned microfluidic cards. All samples were normalised to *18s* and expressed relative to 0 h samples. **A**, *Fgf18*. **B**, *Fgf2*. Graphs show mean +/- S.D; *Fgf2* graph shows one way ANOVA results ****p>0.0001, *Fgf18* graph shows Two-way ANOVA (tabulated results ns=non-significant, *p<0.05, ****p>0.0001) both graphs show Tukey post hoc test ^p<0.05, ^^p<0.01, ^^^p>0.001, ^^^^p>0.0001, compared to "0 h". n=3 biological replicates.

3.11 Discussion

Injury has been shown to predispose to osteoarthritis. One response of cartilage injury is release of FGF2 (along with other growth factors). Currently there is controversy among the scientific community as to the role of FGF2 in articular cartilage. When studied *in vitro*, it has been shown to mediate both anabolic and catabolic effects, though the *in vivo* data suggest a chondroprotective role. One theory for these differences is that the effect depends on which receptor FGF2 acts through; with FGFR1 activation thought to enhance catabolic responses and FGFR3 activation thought to enhance anabolic responses. I therefore investigated how the expression of *FGFR*s changed at an mRNA level in response to injury to better understand the role of FGF2. Explantation models were used to mimic injury in porcine and murine tissues. The effect of FGF2 was assessed by inhibition of FGFRs in porcine tissue or deletion of *Fgf2* in murine tissue.

Explantation of porcine tissue revealed the expression of *FGFR1* and *FGFR3* decreases after injury, however the rate and amount of decrease is different between the receptors. The decrease in *FGFR3* occurred within 4 to 6 hours of explantation, whereas decrease in *FGFR1* only occurred 24 hours after explantation. This decrease in *FGFR3* but not *FGFR1*, proved to be mediated by the activation of an FGFR as the decrease in *FGFR3* was mitigated by the pre-injection of the FGFRi, thus suggesting but not proving its dependence on FGF2 released during injury. The change in *FGFR1* expression was variable across the 4 different experiments (Figure 3.1, Figure ***3.2***, Figure ***3.4*** and Figure ***3.10***). A reason for this variability could have been that the receptor ratios were initially different. In experiments where *FGFR1*:*FGFR3* ratios were very similar (close to 1) *FGFR1* expression only decreased at 48 hours, whereas in experiments where there was initially more *FGFR1* present than *FGFR3*,

decrease in *FGFR1* was seen earlier at 24 hours. A reason for the initial variability in *FGFR1:FGFR3* may have been because the trotters were from pigs of variable ages (3-6 months). Totters from older pigs may be more prone to injury as they are bigger and heavier so may already be prone to OA. Indeed, the quality of cartilage was variable from trotters, with some having pristine, thick cartilage while others had thinner cartilage and some even showed signs of defects. Additionally, some trotters exhibited subdermal growths on their joints. As aberrant FGF signalling is involved in cancer progression (Turner and Grose, 2010), a growth near the vicinity of a joint could potentially effect joint homeostasis. Although care was taken to avoid trotters that had visible growths and cartilage defects, it cannot be ruled out that trotters with early stage growths/smaller defects may have been used.

Explantation of murine tissue revealed expression of *Fgfr1* and *Fgfr3* increased after injury; the opposite trend to that seen in porcine tissue. Nonetheless, the change of *FGFR3* was shown to be FGF-dependent in both species.

When *FGFR* ratios were analysed, it was found that explantation/injury caused a shift (from equal levels of expression) to favour the expression of *FGFR1* in both porcine and murine tissue and this was FGF2-dependent. This therefore suggests the abundance of the FGFRs compared with each other may be more important for determining the overall response of the tissue to injury than the individual changes in the *FGFR*s.

The expression of *Fgfr*2 was significantly downregulated upon explantation of the murine tissue in an FGF2-dependent manner but did not change upon explantation of porcine tissue. However, stimulation of isolated porcine chondrocytes with exogenous FGF2 did down-regulate *FGFR2*. At this time, we are unable to determine what effect this

downregulation would have on articular chondrocytes as FGFR2 is not well studied in adult articular cartilage of the knee.

I also looked at how the expression of known FGF2-dependent genes changed over time after explantation to see whether the pattern of gene regulation could be related to the changes in *FGFR* expression, or if the response was downstream of a particular FGFR by stimulation with the selective FGF-ligands. The porcine explantation data showed FGF2-dependent genes had different patterns of regulation after explantation with peak expression occurring either early (4-6 hours) or late (24 hours). Similar responses were also seen in the mouse hip explantation model and all genes tested were only partially FGF2-dependent, therefore suggesting the effects seen are not dependent on the ratio of *FGFR*s. These results also suggest that FGF2 is acting in combination with other factors that change during injury.

Isolating cells from porcine tissue disrupted the *FGFR* ratios. Upon plating down, the *FGFR1:FGFR3* ratios partly recovered, because *FGFR1* levels decreased while *FGFR3* levels remained constant. When cells adhere to tissue culture plastics, there are a number of factors that change; rearrangement of membrane proteins as cells change their polarisation; rearrangement of the cytoskeleton and formation of focal adhesion complexes. It has been known for some time that FGFRs have cell adhesion molecule (CAM) homology domains (CHD) so have the potential to bind CAMs in order to initiate down-stream effects (reviewed by Doherty and Walsh (1996). More recently, Zou *et al* (2012) demonstrated activation of FGFR1 by fibronectin with differential down-stream signalling in response to FGF2 in the context of cell migration in liver endothelial cells. Mohanan *et al* (2013) also showed FGFR1 was involved in increased migration via interaction with CAMs. Therefore, the

downregulation in *FGFR1* may be partly linked to the changes that occur during cell adhesion.

To mimic the expression in intact articular cartilage, roughly equal levels of FGFR1 and FGFR3 were needed before cells could be stimulated with FGF ligands. As receptor ratios partly recovered upon plating, cells were further cultured to see if they would equalize with time. Lafont *et al* (2008) had shown hypoxia induced *FGFR3* expression, therefore cells were also cultured in hypoxic conditions to see if it would help restore receptor ratios at a quicker rate. From these experiments, a time between 24 and 48 hours in the normoxic state was identified as an ideal adherence time. However, before cells could be stimulated with FGF ligands they first needed to be serum starved to synchronise cells in the cell cycle and reset any endogenous signalling events. Therefore, the effect of serum starvation on *FGFR* expression was assessed in cells in both normoxic and hypoxic conditions over 2 days. The results showed some variability between repeats, however after 24 hours of culture, *FGFR1:FGFR3* ratios plateaued. Therefore, it was concluded that prior to stimulation with FGF ligands, cells should be plated in the presence of FBS for 24 hours, then serum starved for 24 hours. These cells were also thought of as "optimal" because the ΔCt values were very similar to those of intact cartilage (Figure 3.3 and Figure 3.15) and so it can be inferred that *FGFR* ratios were restored back to basal levels (as the same amount of cDNA was used for the qPCR reactions).

To show a direct regulation of FGF2 on the *FGFR*s, primary articular chondrocytes (with optimal *FGFR* ratios) were stimulated with FGF2, with and without the presence of FGFRi. To attempt to find out which receptor FGF2 was acting through to mediate its effects, cells were also stimulated with FGF18; a pan receptor ligand with a higher selectivity for FGFR3

and mutant ligands that activate only one receptor (FGF2-V2 activating FGFR1 and FGF18-V1 activating FGFR3).

If one looks at the overall changes of *FGFR* expression, it appears that FGF18 stimulation causes very similar responses as FGF2 stimulation; FGF2-V2 stimulation also seems to cause similar responses as FGF2 stimulation but at a dampened level; and FGF18-V1 stimulation does not cause any change in *FGFR* expression. So from these results, one might infer that all the responses seen were mediated through activation of FGFR1. This would concur with work by Yan *et al* (2011), where it was demonstrated that FGF2 added exogenously to human articular chondrocytes in monolayer decreased *FGFR3* gene expression. Yet in the presence of *FGFR1* siRNA (but not *FGFR3* siRNA) decreased expression was completely abolished; suggesting that FGF2 acts through FGFR1 to downregulate *FGFR3* in isolated human chondrocytes.

A heterodimerisation theory could also account for the results seen in the FGF-ligand stimulation experiments. FGF2 and FGF18 may have similar responses as they can bind both receptors, so perhaps there is also some heterodimerisation occurring. The FGF2-V2 and FGF18-V1 can only bind to one receptor, so perhaps here we would only be able to see homodimerization effects. Moreover, it has been shown that the signal elicited by a receptor heterodimer may not simply be the sum of the signalling properties of the individual receptors. This was demonstrated by Olayioye *et al* (1999); where cells over-expressing heterodimers of the RTKs ErbB2:ErbB4 activated Stat5 when stimulated with NRG, while homodimers of either receptor failed to do so. This may explain the dampened responses seen by stimulation of FGF2-V2 and the non-responsiveness of FGF18-V1. There is some biochemical evidence to suggest FGFRs are capable of forming heterodimers (Bellot *et*

al., 1991, Del Piccolo *et al*., 2017), though these experiments were conducted using overexpression systems in cultured cells, so the existence of FGFR heterodimers *in vivo* at endogenous expression levels remains to be demonstrated. With hindsight, therefore it would have been wise to have stimulated isolated primary articular chondrocytes with both mutant ligands, to see if the added response might be the same as the FGF2 stimulation alone.

The mutant ligands used for these experiments were made available to us through our collaborators at ProCore (Israel). These ligands were deemed as "selective" (i.e. bind more readily to a particular FGF receptor than the other FGF receptors) as the Kd (disassociation constant; the concentration of ligand required to occupy 50 % of the binding sites on the receptors) was at least 10-fold different between the FGFRs according to the manufacturer. It is important to note that the ligand selectivity was validated in a bioassay in cell lines that overexpress only one isoform of the receptor. Therefore, it is unknown how these ligands behave in the presence of more than one receptor i.e. if the ligand binds to a receptor (but does not mediate an effect), its ability to activate another receptor may be reduced. This may be another explanation as to why in our hands the FGF2-V2 mediated responses are dampened. Also, FGF2-V2 had to be reactivated with DTT (discussed in 4.44.4 below) before cell stimulation in these experiments. (FGF18-V1 also had DTT added for comparison, though it did not change the activity/ERK phosphorylation). Therefore, the potency of the ligands could have been affected in this process (I did not have a reference for fully functional mutant ligands as a comparable reference).

Furthermore, we do not know what the functional levels of FGFRs are like on our cells, therefore the FGF18-V1 ligands may not be mediating an effect because there is not enough

FGFR3 available on the cells for it to bind to. An attempt was made to find out the protein levels of FGFRs in isolated cells via Western blotting; however, the antibodies provided showed multiple bands, which were faint, so we were unable to decipher which band correlated to the total protein. Consequently, I tried to look at the activated (phosphorylated) receptor expression, to decipher what band we should be focusing on, however there was barely any detectable protein. Therefore to concentrate the amount of protein in my samples, I tried acetone precipitation of the cell lysates, though these results were also inconclusive. In order to determine protein levels, an immuno-precipitation/pull-down assay would have been required, or ELISAs could have been performed on protein lysates, both of which would have required a lot of optimisation/resources. It was instead decided to focus attention on whether differences in the downstream signalling of the receptors could be detected.

4 Investigating differential signalling through FGFRs

4.1 Introduction

When FGF ligands bind to their receptors, receptor dimerization occurs and leads to transphosphorylation on 7 tyrosine residues to induce the 4 main signalling pathways; Phospho-lipase C (PLC), Janus kinase/signal transducer and activator of transcription (JAK/STAT), mitogen-activated protein kinase (MAPK) and phosphatidylinositol-3-kinase/ Protein kinase B (PI3K/AKT) (Ellman *et al*., 2013, Carter *et al*., 2015). Activation of these pathways leads to regulation of target genes and changes in cellular behaviour to mediate cellular processes.

In the context of articular cartilage, activation of ERK1/2 by FGF2 is most thoroughly documented. Yan *et al* (2012) showed in human articular chondrocytes, when FGF2 binds to its receptor, receptor phosphorylation activates Raf and Protein kinase C delta (PKCδ). These pathways then converge onto the Raf-MEK1/2-ERK1/2 cascade which goes on to regulate gene expression. What is not known however, is which receptor FGF2 acts through to mediate these effects. The FGFRi (SU5402) used for these experiments is a pan receptor inhibitor, thus is unable to help address this question.

In vitro, FGF18 has been shown to mediate cell proliferation specifically through FGFR3, however at higher doses, it has also been shown to mediate these effects through FGFR1 and FGFR2 (Ellsworth *et al*., 2002). Zhang *et al* (2006) also showed mitogenic effects of FGF18 specifically through FGFR3 in BaF3 cells. In human articular chondrocytes and mouse studies, FGF18 signals selectively through FGFR3, however the subsequent signalling cascade is not well understood. These results have been corroborated by demonstrating a

similar phenotype when *Fgf18* or *Fgfr3* is deleted in mice (Ohbayashi *et al*., 2002, Liu *et al*., 2002, Deng *et al*., 1996, Colvin *et al*., 1996).

In this chapter, I therefore investigate the cellular signalling of primary articular porcine chondrocytes when stimulated with FGF2 or FGF18. To see if there is a difference between FGFR1 and FGFR3 intracellular signalling, mutant ligands that purportedly act selectively through FGFR1 or FGFR3 were also tested.

4.2 Activation of AKT by FGF2

As previously mentioned, FGF2 is already known to strongly induce ERK activation in primary porcine chondrocytes. However, the activation of AKT had not been previously tested by our group. Therefore, I first looked at phosphorylation of AKT in response to FGF2 via Western blotting.

Primary porcine articular chondrocytes were isolated and cultured for 24 hours in serum-containing media, (to obtain cells with approximately equal levels of *FGFR1* and *FGFR3* as described in Chapter 3), then serum starved for 24 hours to set signalling cascades back to basal levels. Cells were stimulated for 1 hour with; Phorbol 12-myristate 13-acetate (PMA), Insulin-like growth factor (IGF), or 10 % FBS as positive controls for AKT phosphorylation to determine which was the best for further experiments; or FGF2 at increasing doses (5-100 ng/ml) to determine the minimal and optimal dose required for a distinct activation of the pathway. Cells were left untreated (serum-free) to determine basal levels of phosphorylation.

Cell lysates were resolved by SDS-PAGE (with reduction) and immunoblotted for p-AKT (Ser473), p-AKT substrates (peptides and proteins containing phospho-serine/threonine preceded by arginine at the -3 position) and total ERK (ERK1 and 2) as a loading control.

A moderate p-AKT activation was seen with 10 % FBS and IGF stimulation only (Figure 4.1). A more prominent phosphorylation of the substrates of p-AKT was visible compared with control (serum-free). There was no activation of p-AKT substrates with PMA; moderate activation with 10 % FBS and IGF, although the banding pattern was slightly different with 10 % FBS. There was a modest activation of p-AKT substrates from 10 ng/ml FGF2; but this appeared to plateau at higher concentrations of FGF2 (10, 20 and 50 ng/ml). From these results, it was decided that 10 % FBS was a good positive control to use for further experiments and 10 ng/ml FGF2 was sufficient to see p-AKT substrate activation.

I next wanted to see how quickly FGF2 activated p-AKT and its downstream substrates. Therefore, a time-course of FGF2 (10 ng/ml) stimulated porcine chondrocytes was run from 5 minutes to 1 hour. A 10 % FBS time-course was run in parallel as a positive control. Figure 4.2 shows phosphorylation of AKT was detectable from 5 minutes and increased with time plateauing at around 30 minutes for 10 % FBS stimulated cells. This was also true for the phosphorylation of the AKT substrates. With FGF2 stimulation, the p-AKT activation was not reliably detected. However, the AKT-substrates were detectable from 10 minutes with optimal activation occurring at 30 minutes.

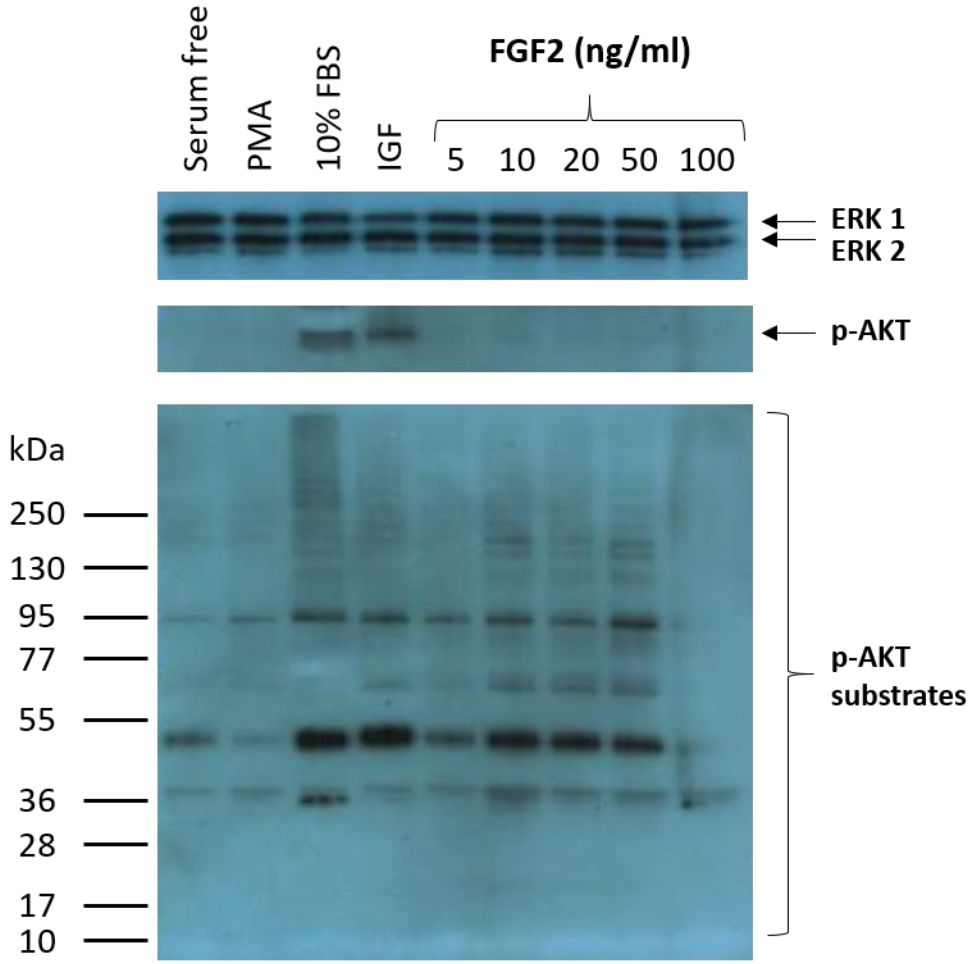

Figure 4.1: 10 ng/ml FGF2 is sufficient to activate p-AKT signalling in porcine chondrocytes

Porcine articular chondrocytes were plated at $1x10^6$ cells/well in 10 % serum-containing media and cultured for 24 h at 37 °C, 5 % CO_2 prior to a 24 h serum starvation. Cells were stimulated with either 10 mM PMA, 10 % FBS or 50 ng/ml IGF (as a positive control); or with 5-100 ng/ml FGF2; or left unstimulated (serum-free) for 1 h. Cells were lysed in RIPA buffer, protein lysates separated by SDS-PAGE and transferred onto PVDF membranes before immunoblotting for p-AKT (Ser473), p-AKT substrates and ERK (1&2) as a loading control. Immunoblotting was visualised using ECL detection reagent and X-ray film. n=1

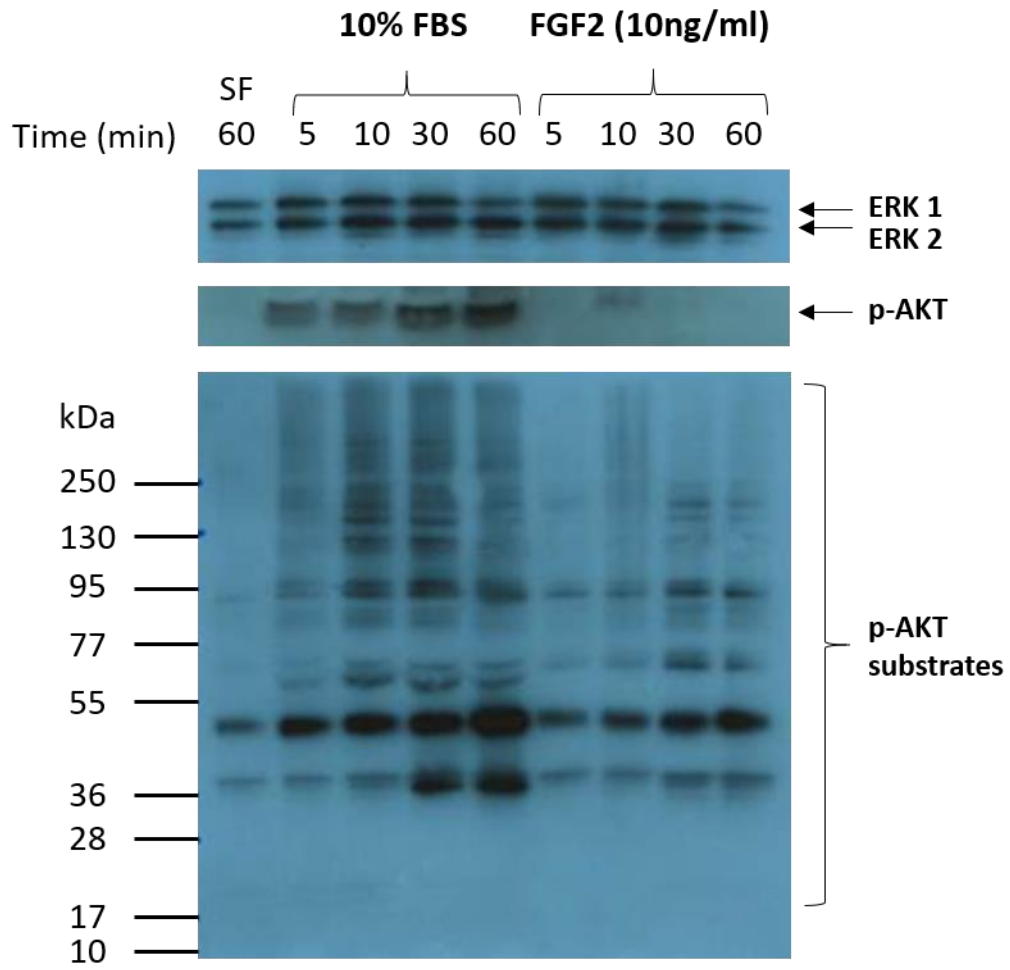

Figure 4.2: Optimal AKT signalling occurs between 10 and 30 minutes of FGF2 stimulation in porcine chondrocytes

Porcine articular chondrocytes were plated at $1x10^6$ cells/well in 10 % serum-containing media and cultured for 24 h at 37 °C, 5 % CO_2 prior to a 24 h serum starvation. Cells were stimulated with either 10 % FBS (as a positive control); or with 10 ng/ml FGF2; or left unstimulated (serum-free) for various times up to 1 hour. Cells were lysed in RIPA buffer, protein lysates separated by SDS-PAGE and transferred onto PVDF membranes before immunoblotting for p-AKT (Ser473), p-AKT substrates and ERK (1&2) as a loading control. Immunoblotting was visualised using ECL detection reagent and X-ray film. n=1

4.3 FGF2 and FGF18 show similar ERK and AKT signalling in porcine chondrocytes

FGF2 is known to bind to all mesenchymal FGFRs (Ornitz *et al*., 1996) whereas FGF18 is thought to act selectively through FGFR3 (Zhang *et al*., 2006). To investigate if there was any difference in the downstream signalling of these molecules, primary porcine chondrocytes were stimulated with either 20 ng/ml FGF2 (as this showed adequate p-AKT substrate activation in Figure 4.1), or 100 ng/ml FGF18 (as this concentration was shown to induce ERK previously by another member of the lab). Protein lysates were analysed via Western blotting and immunoblotted for p-ERK, p-AKT or p-AKT substrates with total ERK used as a loading control.

Figure 4.3 shows the loading was inconsistent as the density of the ERK1/2 bands is variable. Consequently, the relative density of the proteins were calculated using Image J software and normalised against the ERK1/2 bands before normalisation to the serum-free stimulated bands, to allow better interpretation of the results. The results show that p-ERK was induced 4-fold at 10 minutes post stimulation then slightly decreased over the 60-minute time-course for FGF2. Stimulation with FGF18, showed a 3-fold induction of p-ERK1/2 at 10 minutes which increased slightly to 4-fold induction by 60 minutes. Induction of p-AKT was 3-fold by 10 minutes for FGF2, and slightly reduced to 2-fold induced over the 60-minute time-course (similarly to ERK1/2 activation). FGF18 induced a 3-fold induction of p-AKT by 10 minutes, which peaked at 30 minutes to 4-fold and then decreased again to 3-fold by 60 minutes.

p-AKT substrates were only weakly induced (by a maximal 0.5-fold by both FGF2 and FGF18), however the results may be skewed as the blot seems to be out of the linear range for the band at around 45 kDa.

As the fold changes are quite small across the time course for both ligands (1-fold difference of basal levels), the differences in the maximal peaks of induction between FGF2 and FGF18 may not hold true if more repeats were carried out. These results therefore show no striking difference between the downstream signalling of FGF2 and FGF18. However, Ellsworth *et al* (2002) have shown that at higher concentrations, FGF18 can signal through FGFR1 and FGFR2 as well as FGFR3. Therefore, FGF2 and FGF18 may both be activating the same receptors at this higher concentration.

To address this issue, the same concentration (20 ng/ml) of FGF2 and FGF18 was used to stimulate cells and the induction of p-ERK analysed over a more extensive time-course with α-tubulin used as a loading control. Figure 4.4 shows FGF2 strongly stimulates phosphorylation of ERK within 5 minutes of stimulation, this was sustained for 20 minutes before reducing to almost basal levels at 60 minutes post stimulation. Within 5 minutes FGF18 caused a weak phosphorylation of ERK compared with control (0 minutes) and was sustained at this level over the rest of the time course. This suggests one of three possibilities; firstly, that FGF18 at low concentrations is still able to stimulate FGFR1, 2 and 3 in a weak manner; secondly, that there may be low functional levels of FGFR3 on chondrocytes; and finally that FGF18/FGFR3 signalling is different from FGF18/FGFR1/2 and does not drive strong ERK activation.

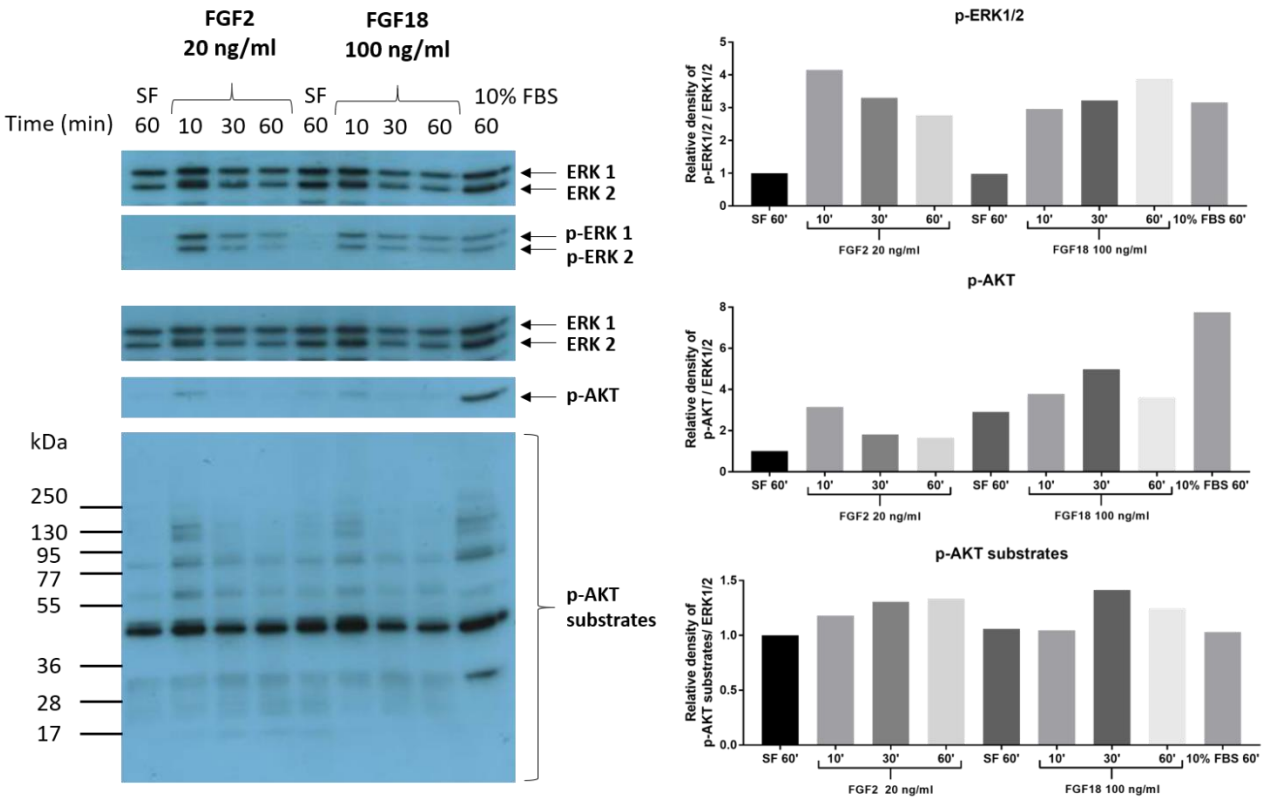

Figure 4.3: Both FGFs show similar ERK and AKT signalling in porcine chondrocytes

Porcine articular chondrocytes were plated at 1x10^6 cells/well in 10 % serum-containing media and cultured for 24 h at 37 °C, 5 % CO_2 prior to a 24 h serum starvation. Cells were stimulated with either 10 % FBS (as a positive control); 20 ng/ml FGF2; 100 ng/ml FGF18 or left unstimulated (SF) for various times up to 1 h. Cells were lysed in RIPA buffer, protein lysates separated by SDS-PAGE on two separate gels and transferred onto PVDF membranes. One membrane was immunoblotted for p-AKT (Ser473), p-AKT substrates and the other for p-ERK (1&2). Total ERK (1&2) was used as a loading control. Immunoblotting was visualised using ECL detection reagent and X-ray film. Relative density was quantified using Image J software, normalised against corresponding ERK1/2 bands and then normalised to the 1st lane "SF 60". n=1

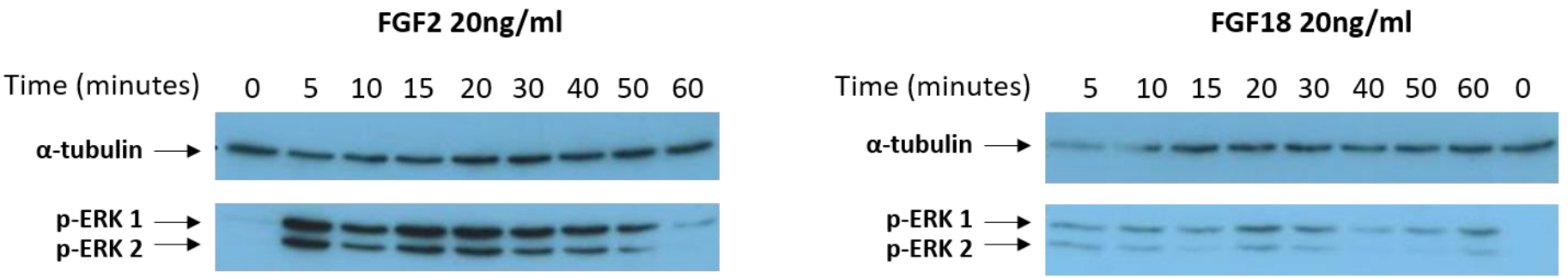

Figure 4.4: ERK phosphorylation is optimal 20 minutes post stimulation with FGF ligands in porcine chondrocytes

Porcine articular chondrocytes were plated at $1x10^6$ cells/well in 10 % serum-containing media and cultured for 24 h at 37 °C, 5 % CO_2 prior to a 24 h serum starvation. Cells were stimulated with either FGF2 or FGF18 (20 ng/ml) for various times up to 1 h. Cells were lysed in RIPA buffer, protein lysates separated by SDS-PAGE, transferred onto PVDF membranes and immunoblotted for p-ERK (1&2). α-tubulin was used as a loading control. Immunoblotting was visualised using ECL detection reagent and X-ray film. n=1

4.4 DTT alone restores FGF2-V2 phosphorylation of ERK in porcine chondrocytes

In order to test if there was a difference in the downstream signalling of FGFR1 or FGFR3 more directly, I planned to stimulate cells with the more selective FGFR mutant ligands (FGF2-V2; selective for FGFR1 and FGF18-V1; selective for FGFR3). Initially the FGF2-V2 ligand was shown to induce the phosphorylation of ERK and FGF18-V1 showed a very weak ERK phosphorylation (data not shown), however with subsequent use, FGF2-V2 ERK activation failed to occur while FGF18-V1 weak ERK phosphorylation could still be detected. On discussion with our collaborators at ProCore (the designers and manufacturers of the ligand), it was suggested that the ligands may have formed disulfide links with each other, forming larger complexes and thus preventing binding to the FGFRs.

Therefore I tested whether the reducing agent Dithiothreitol (DTT) could re-activate the FGF2-V2 ligand. DTT (50 mM) and FGF2-V2 (10 µg/ml) were combined in an Eppendorf tube and left at 4 °C overnight for the reduction reaction to occur. As heparan sulfate is a known co-factor of the FGFRs, we also tested the effect of pre-treating the cells with 20 ng/ml heparan sulfate for 30 minutes to see if this would aid in inducing the phosphorylation of ERK. As the FGF2-V2 was reconstituted in PBS, PBS was also tested as a control and FGF2 used as a positive control.

In a duplicate experiment (1 and 2), the addition of DTT to FGF2-V2 restored the ability of the ligand to induce the phosphorylation of ERK (Figure 4.5, lanes 6), compared with FGF2-V2 alone (Figure 4.5, lanes 2). The addition of heparan sulfate did not further enhance the phosphorylation of ERK (Figure 4.5 lanes 8). This was probably due to the fact that primary porcine chondrocytes cultured in monolayer start to lay down an ECM and therefore are

likely to produce their own heparan sulfate to act as a co-factor and so the system may already be saturated. DTT alone (Figure 4.5, lanes 5) did not induce the phosphorylation of ERK above that of the control sample (Figure 4.5, lanes 1). The reactivation of FGF18-V1 with DTT was also tested, however it showed no increase in the phosphorylation of ERK. (data not shown). Therefore all further experiments were conducted with the DTT treated FGF2-V2 and FGF18-V1.

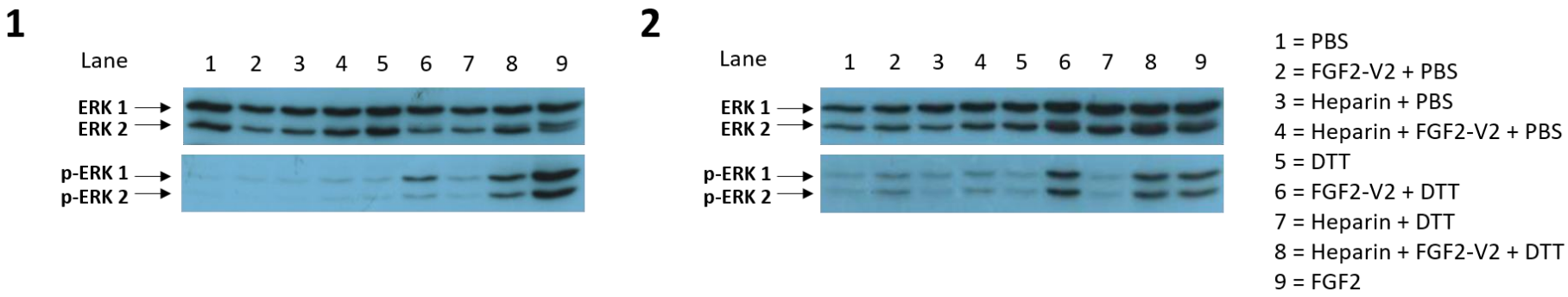

Figure 4.5: DTT alone restored FGF2-V2 phosphorylation of ERK in porcine chondrocytes

Porcine articular chondrocytes were plated at $1x10^6$ cells/well in 10 % serum-containing media and cultured for 24 h at 37 °C, 5 % CO_2 prior to a 24 h serum starvation. FGF2-V2 (10 µg/ml) was incubated with DTT (50 mM) overnight at 4 °C to reactivate it. Some wells were preincubated with 20 ng/ml heparan sulfate (to act as a co-factor of FGFRs) for 30 min. Cells were then stimulated for 15 min with either; 20 ng/ml FGF2 (as a positive control); the combination of DTT and FGF2-V2 (20 ng/ml and 0.1 mM respectively), or PBS (as a vehicle control for the DTT). DTT alone (0.1 mM) was also tested to make sure it had no stimulatory effects. Cells were lysed in RIPA buffer, protein lysates separated by SDS-PAGE, transferred onto PVDF membranes and immunoblotted for p-ERK (1&2), and total ERK (1&2) as a loading control. Immunoblotting was visualised using ECL detection reagent and X-ray film. n=2 biological replicates.

4.5 Comparing signalling responses to different FGF ligands in porcine chondrocytes

To test if the difference in phosphorylation of ERK between FGF2 and FGF18 was due to the differential activation of FGFRs, mutant ligands with higher selectivity for either receptor (FGF2-V2; an FGFR1-selective ligand and FGF18-V1; an FGFR3-selective ligand) were also used to stimulate primary porcine articular chondrocytes for 20 minutes. A concentration of 20 ng/ml was used for each ligand. The phosphorylation of ERK, AKT and the downstream phosphorylated substrates of AKT were analysed by Western blotting.

Figure 4.6 shows a duplicate experiment (1 and 2) in which there is a strong induction of p-ERK by FGF2, a weaker induction by FGF2-V2 and a further reduced induction by FGF18 and FGF18-V1. The phosphorylation of AKT (at Ser473) was extremely weak, with no difference in intensity between the ligands. However, the induction of the AKT substrates showed a similar pattern of induction across the ligands in proportion to the strength of the p-ERK activation.

Therefore, at this stage, the signalling differences appeared to be largely due to issues over ligand potency rather than selectivity, although it was not possible to exclude the possibility that FGFR3 activation was driving other signalling pathways instead of ERK and AKT.

Nonetheless, these experiments also indicated that FGF2 and FGF18 (at 20 ng/ml) behave similarly to FGF2-V2 and FGF18-V1 respectively.

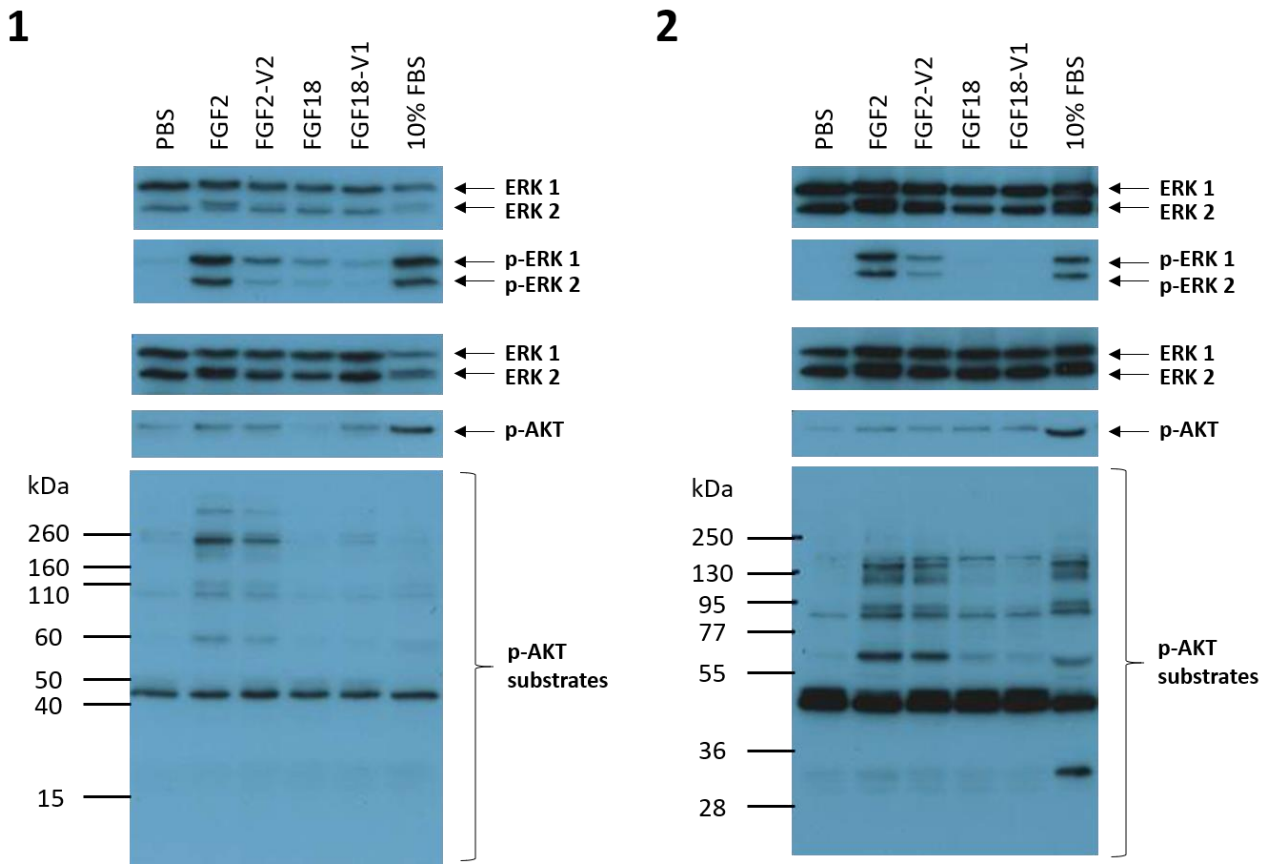

Figure 4.6: Comparing signalling responses to different FGF ligands in porcine chondrocytes

Porcine articular chondrocytes were plated at 1x10^6 cells/well in 10 % serum-containing media and cultured for 24 h at 37 °C, 5 % CO_2 prior to a 24 h serum starvation. Cells were stimulated for 20 min with either 10 % FBS (as a positive control); 20 ng/ml FGF ligands; or PBS (as vehicle control). Cells were lysed in RIPA buffer, protein lysates separated by SDS-PAGE on two separate gels and transferred onto PVDF membranes. One membrane was immunoblotted for p-AKT (Ser473), p-AKT substrates and the other for p-ERK (1&2). Total ERK (1&2) was used as a loading control. Immunoblotting was visualised using ECL detection reagent and X-ray film. n=2 biological replicates.

4.6 Phospho-kinase array of isolated porcine chondrocytes stimulated with FGF2 or FGF18

As it was still unclear whether there were differences in the downstream signalling of FGFR1 and FGFR3, a phospho-kinase array was carried out to investigate a wider range of signalling pathways after stimulation with FGF2 and FGF18.

Protein lysates of primary chondrocytes stimulated with either FGF2 or FGF18 for 0 or 20 minutes were analysed on a commercial phospho-kinase array (where antibodies for phosphorylated proteins were blotted onto a membrane). Immunoblots were visualised using ECL detection reagent and X-ray film. Relative density was calculated for differences between 0 and 20-minute stimulations using Image J and plotted as a heatmap; where green indicates up-regulated phosphorylated protein (relative density >1) and red indicates down-regulated phosphorylated protein (relative density between 0 and <1).

The most highly upregulated phosphorylated proteins for both ligands were ERK1/2 and cAMP response element-binding protein (CREB) (Figure 4.7). However, FGF18 seemed to be inducing a more potent response than that of FGF2. P-70 S6 kinase (T389) was highly upregulated but only by FGF18 stimulation. There were some phosphorylated proteins that were considerably down-regulated upon stimulation with the FGF ligands, most notably p53 (S392), Signal transducer and activator of transcription 3 (STAT3) (Y705) and PLC-γ1 (Y783). A few phosphorylated proteins were down-regulated by FGF2 but not FGF18. They were AKT1/2/3 (T308), p53 (S46), p70 S6 kinase (T421/S424) and endothelial nitric oxide synthase (eNOS) (S1177). (Figure 4.7). Although this experiment was a single snapshot in time and the temporal change in phosphorylation may be different between ligands, it nonetheless provided me with some other candidate pathways to investigate in detail. Consequently, a

validation of selective phospho-kinases was carried out over a more extensive time course (0-60 minutes) and analysed by Western blotting. Immunoblotting was carried out for the most upregulated phosphorylated proteins ERK1/2, P70 S6 kinase (T389) and CREB; a phosphorylated AKT (T308) epitope not previously measured; and a protein that was un-regulated MTOR (S2448).

Figure 4.8 shows some variability in the induction of phosphorylated proteins between repeats (1, 2 and 3), however the time at which maximal phosphorylation occurred was consistent. For p-ERK, this was 10 minutes post stimulation; for p-P70 S6 kinase, this was 40 minutes post stimulation. The phosphorylation of CREB was only seen for 1 repeat, with maximal activation occurring at 30 minutes. The time at which maximal activation occurred was the same for FGF2 and FGF18. p-AKT at Thr308 showed inconsistent expression and did not seem to be differentially regulated by stimulation with the different FGF ligands.

The relative density of each phospho-band was calculated relative to the corresponding β-actin band as shown in Figure 4.9 which highlights the variability between repeats of the time-course.

Figure 4.10 focuses in on the 20-minute time points from the validation time-course, to compare with the original phospho-array data. The graphs show considerable variation between repeats as seen by the large spread of the data. Also due to the spread of the data, there does not seem to be a noticeable difference between FGF2 and FGF18 stimulation unlike that seen in the original phospho-array.

Protein	Relative change in density	
	FGF2	FGF18
Akt 1/2/3 (S473)	0.886	0.903
Akt 1/2/3 (T308)	0.512	1.094
AMPKα1 (T183)	1.082	0.996
AMPKα2 (T172)	0.945	0.810
Chk-2 (T68)	1.041	1.013
c-Jun (S63)	0.540	0.665
CREB (S133)	2.101	4.229
EGF R (Y1068)	1.200	1.425
eNOS (S1177)	0.611	1.000
ERK1/2 (T202/Y204, T185/Y187)	4.458	7.305
FAK (Y397)	0.859	0.972
Fgr (Y412)	1.105	1.472
Fyn (Y420)	1.130	0.919
GSK-3α/β (S21/S9)	1.002	0.965
Hck (Y411)	0.893	0.678
HSP27 (S78/S82)	1.247	1.550
HSP60	0.855	1.046
JNK1/2/3 (T183/Y185, T221/Y223)	1.173	1.247
Lck (Y394)	1.329	1.267
Lyn (Y397)	1.283	1.490
MSK1/2 (S376/S360)	1.102	1.299
p27 (T198)	0.551	0.549
p-38α (T180/Y182)	1.402	1.502
p-53 (S15)	0.452	0.605
p53 (S392)	0.600	0.214
p53 (S46)	0.570	0.983
p70S6 Kinase (T389)	1.224	9.827
p-70 S6 Kinase (T421/S424)	0.593	1.149
PBS (-ve)	1.000	1.000
PBS (-ve)	1.000	1.000
PDGF Rβ (Y751)	0.885	0.896
PLC-γ1 (Y783)	0.535	0.333
PRAS40 (T246)	1.092	0.843
PYK2 (Y402)	0.434	0.422
ref (+ve)	1.062	1.042
ref (+ve)	1.003	1.037
ref (+ve)	1.007	1.022
RSK1/2/3 (S380)	0.659	0.815
Src (Y419)	0.999	0.984
STAT2 (Y689)	0.960	0.877
STAT3 (Y705)	0.365	0.710
STAT3 (Y705)	0.315	0.568
STAT5a (Y699)	0.873	0.849
STAT5a/b (Y699)	0.897	0.815
STAT5b (Y699)	0.974	0.960
STAT6 (Y641)	0.897	0.872
TOR (S2448)	0.895	1.259
WNK1 (T60)	0.510	0.540
Yes (Y426)	0.980	1.166
β-Catenin	0.816	1.137

Figure 4.7: Phospho-kinase array of isolated porcine chondrocytes stimulated with FGF2 or FGF18
Porcine articular chondrocytes were plated at $1x10^6$ cells/well in 10 % serum-containing media and cultured for 24 h at 37 °C, 5 % CO_2 prior to a 24 h serum starvation. Cells were stimulated for 20 min with 20 ng/ml FGF2 or FGF18. Cell lysates were run on a commercial phospho-kinase array. Immunoblots were visualised using ECL detection reagent and X-ray film. Relative density was calculated for differences between 0 and 20-minute stimulation using Image J and plotted as a heatmap; where green indicated up-regulated phosphorylated protein (>1) and red indicates down-regulated phosphorylated protein (0<1). n=1

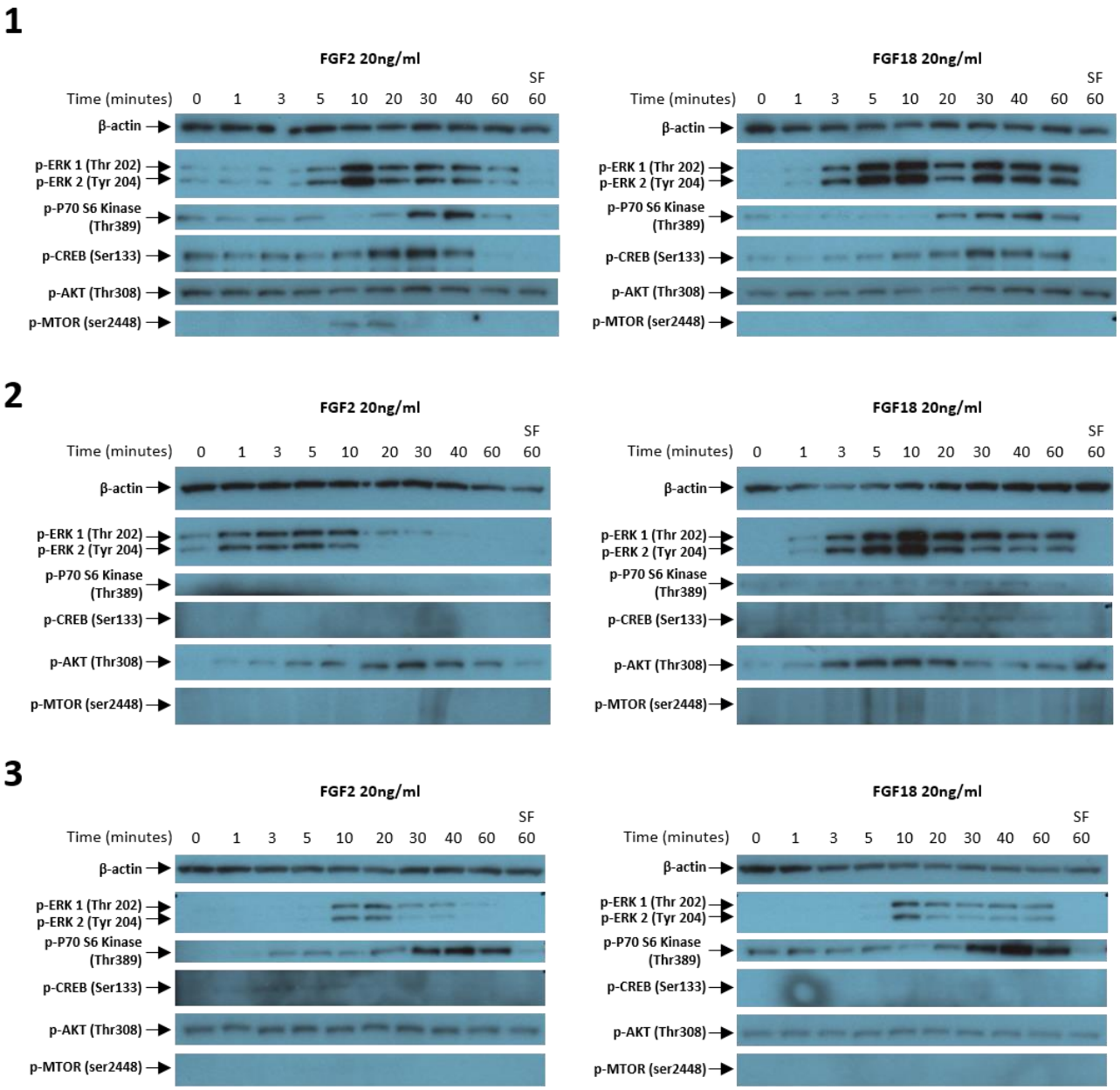

Figure 4.8: Phospho-kinase array validation

Porcine articular chondrocytes were plated at $1x10^6$ cells/well in 10 % serum-containing media and cultured for 24 h at 37 °C, 5 % CO_2 prior to a 24 h serum starvation. Cells were stimulated for various times up to 60 min with either 20 ng/ml FGF2 or FGF18. Cells were lysed in RIPA buffer, protein lysates separated by SDS-PAGE on two separate gels and transferred onto PVDF membranes. One membrane was immunoblotted for p-ERK 1&2 (Thr202 & Try204), p-MTOR (Ser2448), p-70 S6 Kinase (Thr389) and the other p-AKT (Thr308). B-actin was used as a loading control. Immunoblotting was visualised using ECL detection reagent and X-ray film. n=3 biological replicates.

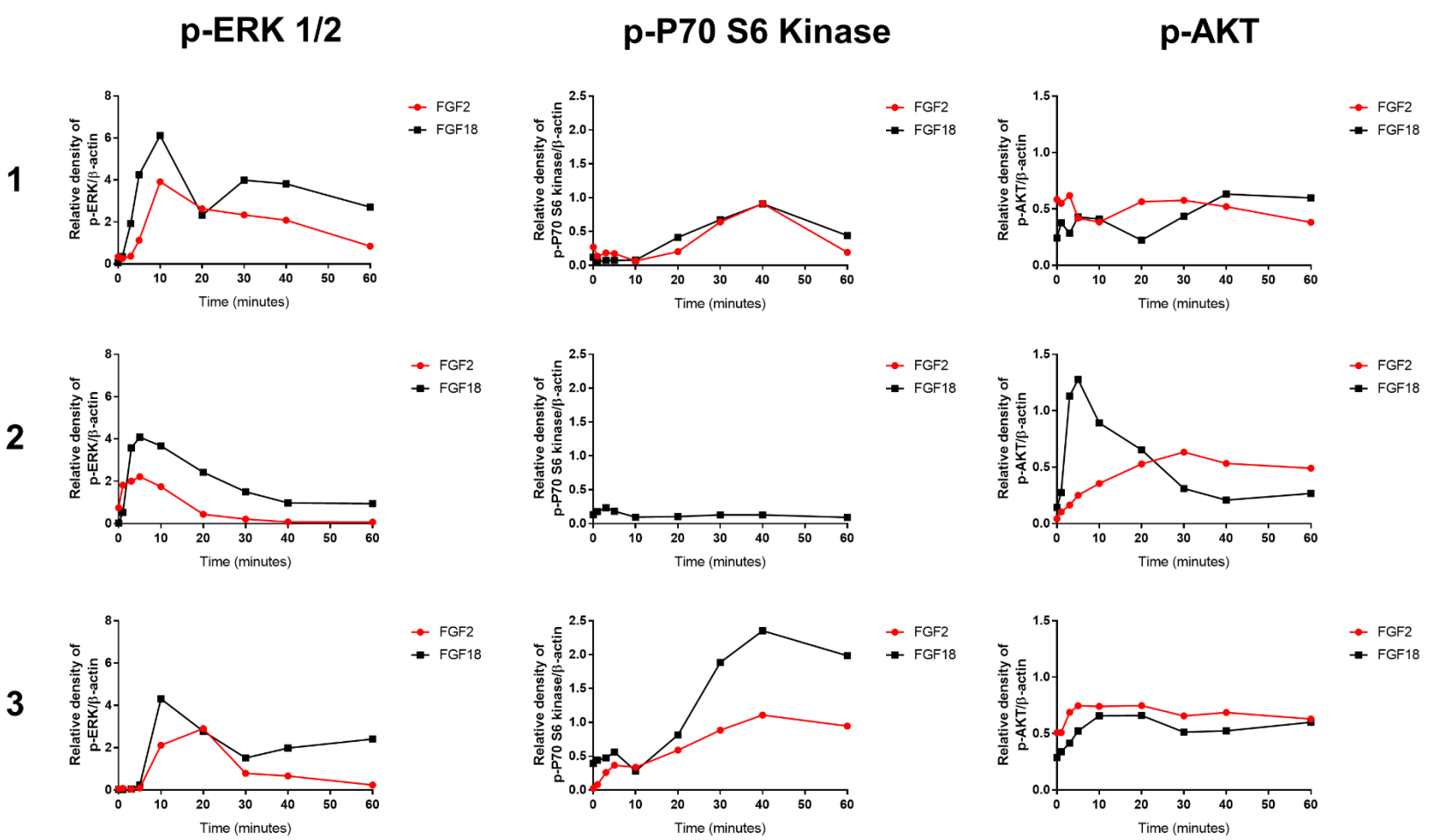

Figure 4.9: Plots of relative density of phospho-kinase array validation

Relative density of bands was quantified from the phospho-array validation immunoblots of p-ERK, p-P70 S6 kinase, p-AKT and β-actin using Image J software. The relative density of the bands at each time-point were normalized to those of β-actin to account for the differences in loading and plotted as shown. n=3 biological replicates.

Protein	Relative change in density	
	FGF2	FGF18
Akt 1/2/3 (T308)	0.512	1.094
ERK1/2 (T202/Y204, T185/Y187)	4.458	7.305
p70 S6 Kinase (T389)	1.224	9.827

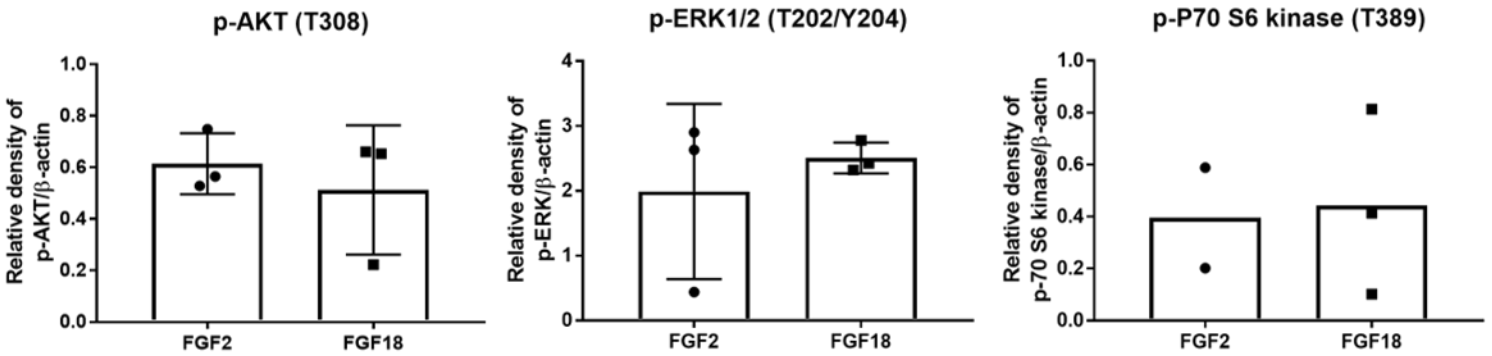

Figure 4.10: Validation of phospho-array: 20-minute relative density blots.
Relative density of bands was quantified from the phospho-array validation immunoblots of p-ERK, p-P70 S6 kinase, p-AKT and β-actin using Image J software. The relative density of the bands were normalized to those of β-actin to account for the differences in loading and plotted as shown for the 20-minute time points only to compare with those from the phospho-array (cropped table). Graphs show mean (boxes) +/-S.D. (bars) with individual points for each immunoblot.

4.7 Discussion

FGFR1 and FGFR3 expression do not overlap during joint development (Ornitz and Marie, 2015) and the conditional KO models in post-natal articular cartilage show opposing phenotypes in relation to cartilage homeostasis (Valverde-Franco *et al*., 2006, Weng *et al*., 2012). This suggests the receptors have unique functions in cartilage. There are many factors that can affect the cellular outcome of FGF signalling; ligand availability to the receptor, the type of HS present in the ECM, FGFR expression levels in the tissue of interest, differential signalling pathways, different activation of accessory molecules, sustained or temporal signalling etc (Ornitz and Itoh, 2015). Here I have focused on investigating if there are differential signalling pathways activated by these FGFRs in porcine articular chondrocytes by stimulation with FGF ligands that purportedly have differing selectivity for the receptors. No conclusive differences were observed due to a number of limitations to this study which have made data interpretation difficult.

There was variable potency of the ligands across experiments; in 3 out of 4 experiments, FGF18 was less potent than FGF2 at inducing ERK phosphorylation but in the last experiment the opposite was true. This may have been due to a new aliquot of FGF18 having been used for the final experiment; suggesting the ligand may have been sensitive to repeated freeze-thawing.

Interpretation of the data, with regards to stimulation with mutant ligands was also clouded for a number of reasons. Firstly, the mutant ligands needed to be “reactivated” using DTT in order to detect phosphorylated ERK. The manufacturer recommended 50 mM DTT to break the disulfide bonds that were presumed to have formed between ligands. DTT itself is cytotoxic to cells at this concentration. Therefore the experiment was designed such that,

when the ligand was added to cells, the final concentration of DTT in the cell media was 0.1 mM, a concentration that was thought to be negligible to cell function. When chondrocytes undergo stress, they tend to float and change their morphology. When the morphology of the chondrocytes was checked, no difference could be seen between those treated with DTT and those that were not. Plus, DTT did not activate ERK above basal levels, nor were there drastically more dead cells visible when stained with trypan blue (data not shown). Therefore the DTT concertation was deemed safe for the cells. However, it would have been beneficial to have performed a more conclusive and quantitative cell toxicity assays such as colorimetric lactate dehydrogenase (LDH) assays or luciferase assays. Therefore it cannot be ruled out that the DTT may have been partly responsible for the lack of activation in mutant ligand treated cells.

Interpretation of the mutant ligands data may also have been hindered by the fact that the total ERK1/2 loading control seemed to be out of the linear range for repeat 2 (as the immunoblots seemed over-exposed). This is important because there may appear to be more protein than is actually present on the blot. To rectify this, I should have calculated the relative density from the blots, with varying exposures to see if the pattern of induction was still the same across the different stimulations.

FGF2 and FGF18 may activate the same pathways because it cannot be excluded that FGF18 could potentially signal through FGFR1 and FGFR2 in addition to FGFR3 in chondrocytes, and so the selectivity of the ligands remains an issue. There is also a lack of information regarding the mutant ligands in terms of confirming the selectivity and purity (i.e. the presence of bacterial products). Furthermore, although we assume the *FGFR1:FGFR3* ratio is equal in accordance with the previous chapter, we still do not know the level of functional

protein of the FGFRs on the cell surface. With regards to the phospho-array, it is reassuring that the most strongly regulated pathway was ERK1/2 and P70 S6 kinase, though curiously the array data suggested that FGF18 was a stronger inducer of the pathway than FGF2. It was possible to validate some of the array data but other pathways like CREB activation were inconsistent (phosphorylation was only seen in 1 of the 3 repeats). The phospho-array data may also be questionable as the relative density of the blots were calculated using only one exposure time. Although care was taken to avoid over exposure, the blot used may not have had an ideal exposure for all of the proteins as the linear range may not have been the same for all proteins. Therefore, a range of exposures should have been taken and relative densities of all dots calculated for each exposure and compared against each other to see if the changes in the densities were the same.

Though there were no detectable difference in the proteins phosphorylated by FGF2 and FGF18, the validation of the phospho-array did give some information on the temporal signalling events, with ERK1/2 phosphorylation occurring first (at 5-10 minutes), followed by phosphorylation of CREB and then P70 S6 kinase (occurring at 20 and 40 minutes respectively). As the 20-minute validations of the phospho-array were extremely variable, it suggests that perhaps a 20-minute stimulation was not an optimal time to detect multiple phosphorylated proteins. Proteins that are phosphorylated early in the signalling response may have been missed. Therefore it would have been ideal to have used a phospho-array on multiple time points to capture the signalling events as they occur. However this would be an expensive experiment.

Other pathways activated by FGF have been described. These include PLCγ and JAK/STAT, but they were not up-regulated in my phospho-array. I did not investigate these further as it

is known that FGFs can exhibit different cellular responses in different cell types. Iwata *et al* (2000) showed signalling through FGFR3 can inhibit but also promote chondrocyte proliferation depending on the stage of development. In immature committed chondrocytes FGF18 signalling through FGFR3 enhances chondrocyte proliferation; though in the growth plate, where mature proliferating chondrocytes reside, signalling of FGF18-FGFR3 inhibits chondrocyte proliferation (Ellsworth *et al*., 2002, Liu *et al*., 2002). A difference that could account for the variability in signalling could be the type of HS incorporated in these different tissues. Delehedde *et al* (2000) showed that in chlorate-treated cells, FGF2 can transiently induce the phosphorylation of ERK1/2, but in the presence of HS there is a sustained ERK1/2 phosphorylation. Only sustained phosphorylation led to DNA synthesis/cell proliferation. The authors went on to show that anything longer than a tetrasaccharide was able to induce sustained phosphorylation of ERK1/2 and cell proliferation, and that longer oligosaccharides were more potent (Delehedde *et al*., 2002). Furthermore, in these chlorate-treated cells, FGF2 failed to stimulate the phosphorylation of the adaptor FGFR substrate 2α (FRS2α), providing evidence that different receptor-proximal mechanisms control whether transient or sustained ERK1/2 phosphorylation occurs with FGF2 stimulation (Zhu *et al*., 2010). In my experiments ERK activation appeared sustained, presumably due to cell surface and pericellular heparan sulfates.

Furthermore, the phospho-array used was designed for use with human cell lysates (not porcine). Although pig proteins are deemed to highly similar to human proteins, their posttranslational modifications (i.e. glycosylations) may be very different. Therefore, proteins which were not detected by the phospho-array may be falsely negative as the epitope present for pigs could be significantly different to prevent the antibody from

recognising it. Moreover, the phosphorylation sites may also be different. This further limits the conclusions made from the phospho-array.

As there were no conclusive differences in signalling responses between FGF ligands, this may not have been the best approach to study differences in FGFR signalling. A more direct approach would have been to knockdown specific FGFRs in chondrocytes, then stimulate with FGF2 and look at the downstream signalling pathways. However, it is extremely difficult to knockdown proteins in primary porcine chondrocytes as it is thought that they produce a lot of ECM, which prevents the siRNA/vector from penetrating the cells. Human chondrocytes are easier to transfect, though truly "normal" chondrocytes are hard to come by; they are usually from joint replacement surgery where the adjacent cartilage is already damaged, or from amputees were a tumour was present in the tissue. They also rapidly de-differentiate *in vitro*.

The literature is divided on whether there is different intracellular signalling of FGFR1 and FGFR3. Naski *et al* (1996) showed that in BaF3 cell lines, which were made to express FGFRs, FGF1 stimulation led to proliferation in FGFR1-expressing cells but not in FGFR3-expressing cells. When the intracellular domain of FGFR3 was replaced with that of FGFR1, the proliferative activity was restored; therefore demonstrating that FGFR1 and FGFR3 have different intracellular signalling. However, Wang *et al* (2001) showed that a transgenic mouse which expressed a chimeric FGFR (that contained the extracellular region of FGFR3 with the achondroplastic transmembrane domain mutation G380R, and the intracellular region of FGFR1) still developed achondroplasia. This suggested that the intracellular signalling of FGFR1 and FGFR3 is the same. This then begs the question; if there is no difference in signalling, then why do the KO mouse models have different phenotypes?

Perhaps it depends on which cells are most affected. Articular chondrocytes intrinsically have equal levels of FGFRs, so maybe it does not matter which FGFR they activate, but other cell types may be different. Moreover, different tissues of the joint have different FGFR expression, different FGF expression, along with differences in ECM components (i.e. type of HSPG), which may combine to elicit different effects that could influence the cartilage indirectly. So far we have only looked at chondrocyte responses, and in OA there is a tendency to be very chondrocentric, but perhaps we should be looking at other parts of the joint e.g. synovium (where there is a differential expression of the *FGFR*s as demonstrated in the previous chapter) and in cells outside the joint that could nonetheless contribute to joint health, e.g. mesenchymal stem cells (MCSs). Therefore, in the next chapter, I examine the *in vivo* response to cartilage damage, focusing on FGF2's role in cartilage repair. I then perform a series of experiments to consider the role of FGF2 on MSCs.

5 FGF2 in cartilage repair

5.1 Introduction

For a long time, it was thought that once damaged, articular cartilage could not repair itself perhaps due to its lack of blood supply. However, with the advancement of new technologies, evidence of cartilage repair has been seen by MRI (Intema *et al.*, 2011, Wiegant *et al*., 2013) and arthroscopically (Nakamura *et al.*, 2008); although the mechanisms by which it repairs still need to be elucidated. One of these mechanisms of repair may be mediated through FGF2.

FGF2 has been known to have mitogenic effects on chondrocytes and mesenchymal stem cells (MSCs) *in vitro*. Kato and Gospodarowicz were among the first to demonstrate the mitogenic effect of FGF2 in a dose-dependent manner on rabbit costal chondrocytes. They also showed it to maintain chondrocyte phenotype (i.e. prevent them from de-differentiating upon culturing); though these effects did depend on the confluency of cells (Kato and Gospodarowicz, 1984, Kato and Gospodarowicz, 1985). Tsutsumi *et al* (2001) showed FGF2 to be a potent mitogen of human and rabbit bone marrow-derived MSCs. It was also shown to maintain MSC "stemness" (multi-lineage differentiation potential) over different passages. FGF2 has been shown to enhance cartilage repair of full-thickness cartilage defects in rabbits when administered intraarticularly (Otsuka *et al*., 1997, Chuma *et al.*, 2004). However, the mechanisms by which FGF2 aids in repair have not yet been shown. Our group has shown that when articular cartilage is injured, FGF2 is released from its pericellular pool and acts in a chondroprotective manner (as *Fgf2*$^{-/-}$ mice have accelerated OA with joint destabilisation, which can be prevented with FGF2 injection) (Vincent *et al*.,

2002, Vincent *et al*., 2007, Chia *et al*., 2009). Which cell type FGF2 is affecting, whether intrinsic to the cartilage or extrinsic, is unknown.

In 2009 Francesco Dell'Accio created a novel joint surface regeneration model in which a focal cartilage defect is made in the patella groove of mice. As this system is amenable to genetic manipulation, it is possible to test molecular pathways in the process of cartilage regeneration *in vivo*. Eltawil *et al* (2009) showed that this cartilage regeneration model was strain-dependent. C57BL/6 mice do not regenerate cartilage but do attempt to repair the defect, whereas DBA/1 mice do regenerate hyaline cartilage. To our knowledge no molecular drivers have been identified in this process in this model.

5.2 FGF2 promotes cartilage regeneration *in vivo*

In order to test whether FGF2 was important in cartilage regeneration, constitutive *Fgf2*$^{-/-}$ mice that were on a C57BL/6 background, were first backcrossed onto the repairing DBA/1 strain for 10 generations before focal cartilage injury was carried out.

10-week-old male mice underwent the surgical procedure, which involved an incision medially and proximally to the insertion of the patellar tendon and extension proximally to the attachment of the quadriceps muscle.

Figure ***5.1***A shows how the patella was dislocated laterally and the joint fully flexed to expose the patellar groove. A longitudinal full-thickness cartilage defect was made in the patellar groove using a needle. The patellar dislocation was then reduced, the patellar tendon sutured back into place and the skin sutured before mice were allowed to recover and to resume normal activity. Mice were culled 8 weeks post-surgery and the right knees

processed for histology and serially sectioned at 5 µm intervals. 3 histological sections were taken from defined anatomical locations as shown in

Figure ***5.1***B and C, with section 1 taken from where the growth plate (GP) is just visible as 4 distinct points; section 3 taken from where the points of the growth plate begin to touch and section 2 being the middle section between 1 and 3. This ensures anatomical precision for scoring. The three sections were stained with haematoxylin and eosin and safranin-O fast green and imaged under a brightfield microscope.

Figure ***5.1***C also shows the depth and width of the original defect from a cadaveric sample.

The surgery was performed on 12 male wild-type (WT) DBA/1 mice and 12 male *Fgf2*$^{-/-}$ mice. The repair tissue of each section was scored by two independent assessors that were blinded to the genotype of the mice using a modified Pineda score (Pineda *et al*., 1992). In the modified Pineda score, a score of 1 equates to poor repair and 14 equates to complete repair (this is inverted in the original Pineda score) (see **Error! Reference source not found.** for details of each score). First, the mean of the summed score for each section was calculated for the assessors. Then the median of the 3 sections was used as the final repair score for each mouse.

Figure 5.2 shows the final repair score of the WT and *Fgf2*$^{-/-}$ mice. The WT mice repaired well, with a mean repair score of 12. The *Fgf2*$^{-/-}$ mice had a significantly lower repair score with a mean of 8. Representative histology (Figure 5.3) of the WT joints shows a range of repair responses from fully filled defects with tissue that had good proteoglycan staining (red, even and very similar to the surrounding cartilage) and the cells were highly chondrocytic in nature (Figure 5.3, (1)) to moderate repair with filling of the defect but

reduced matrix staining (Figure 5.3, (2,3 and 4)). The image from WT mouse 1 shows complete regeneration of the cartilage (100 % filling of the defect, reconstitution of the osteochondral junction, with staining and cell morphology completely indistinguishable from the surrounding tissue). Conversely, the *Fgf2*$^{-/-}$ mice joints had incomplete filling, patchy proteoglycan staining and were less cellular, suggesting a more fibrotic repair tissue. Also, the surrounding tissue showed signs of OA with reduced cartilage thickness and loss of proteoglycan staining elsewhere in the joint (Figure 5.3, *Fgf2*$^{-/-}$ mice 1, 2 &4).

These results indicate that FGF2 promotes intrinsic cartilage regeneration *in vivo*. However, the mechanism by which it does so is unclear. Eltawil *et al* (2009) showed that when the defect first begins to repair, spindle-shaped cells line the defect. It is thought that these cells are mesenchymal stem cells (MSCs) that come into the injured site and undergo differentiation into chondrocytes to regenerate the cartilage. Therefore, we next investigated the effect of FGF2 on MSCs *in vitro* to see whether FGF2 stimulates migration of the MSCs to the injured site, promotes adhesion of MSCs, or promotes the differentiation of MSCs into chondrocytes.

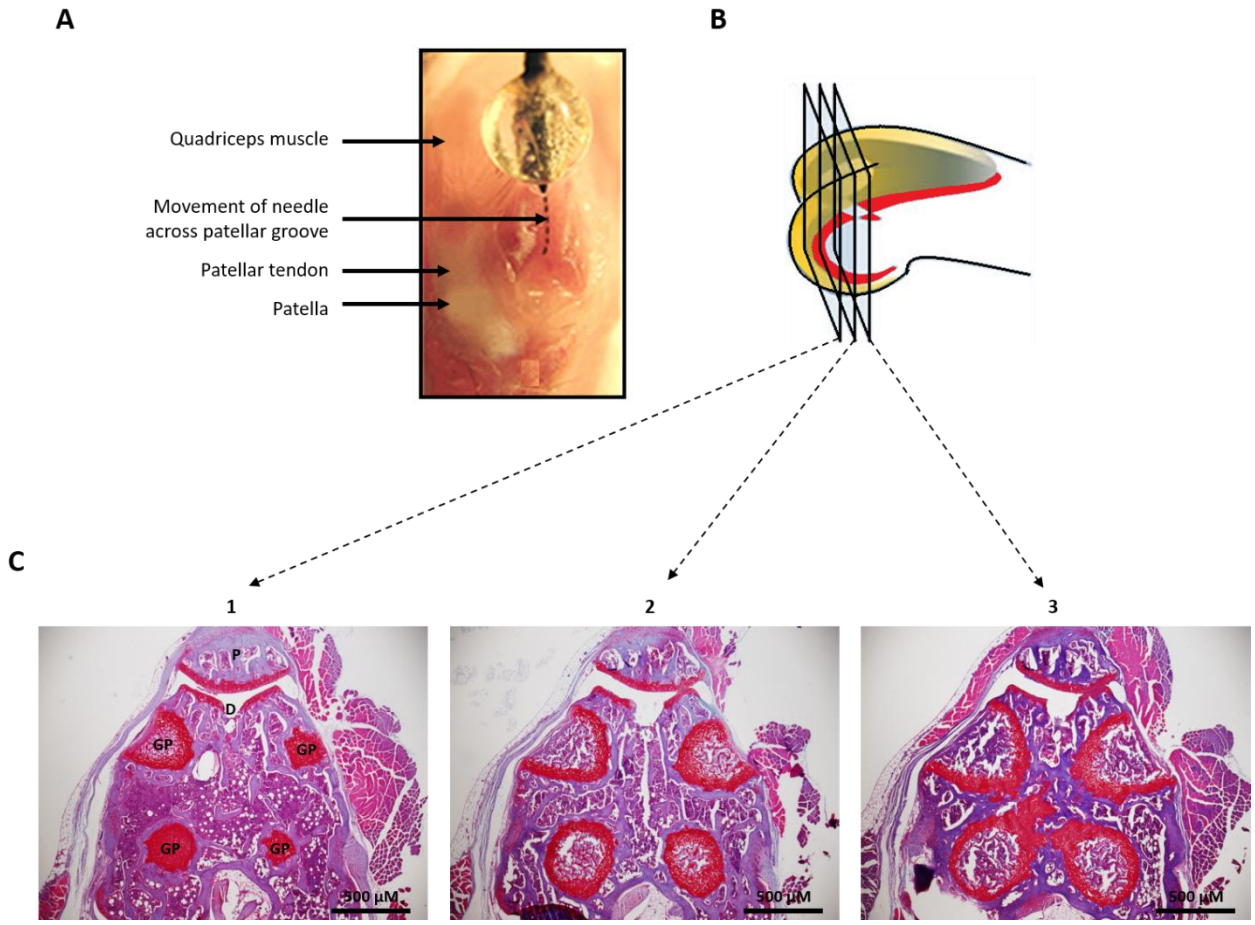

Figure 5.1: *in vivo* murine cartilage repair model

(A) Cadaveric preparation of the right knee joint of a 10-week-old male mouse to show the generation of a full-thickness defect in the patellar groove. An incision was made medially and proximally to the insertion of the patellar tendon and extended proximally to the attachment of the quadriceps muscle. The patella was dislocated laterally and the joint fully flexed to expose the patellar groove. A 25 G needle was placed with its tip just anteriorly to the intercondylar notch in the centre of the groove (lower end of dotted line) and dragged proximally across the entire length of the patellar groove (dotted line) repeatedly to create a longitudinal full-thickness cartilage defect. **(B)** Schematic representation of a mouse knee joint; articular cartilage in yellow and the growth plate in red. The knees were dissected, fixed, decalcified, paraffin embedded and serially sectioned at 5 µm intervals. 3 sections (1,2,3) were taken from defined anatomical locations; (1) where the growth plate (GP) is just visible as 4 distinct points, (3) where the points of the growth plate begin to touch and (2) the middle section between this region. **(C)** The three sections were stained with haematoxylin and eosin and safranin-O fast green and imaged under a brightfield microscope with a 4X objective. P= patella, D= cartilage defect. Parts A and B were sourced and modified from Eltawil *et al* (2009).

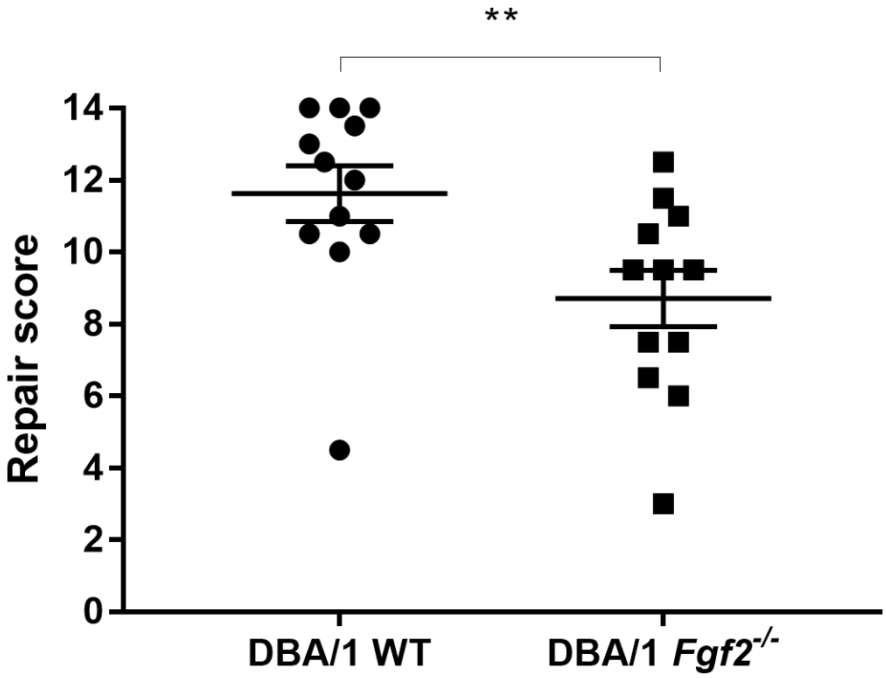

Figure 5.2: FGF2 promotes cartilage repair *in vivo*

Full thickness cartilage defects were created along the patellar groove of the right leg of 10-week-old male mice under sedation. Mice were allowed to recover and to resume normal activity. Mice were culled 8 weeks post-surgery, the knees dissected, fixed, decalcified, paraffin embedded and serially sectioned at 5 µm intervals. 3 sections were taken from defined anatomical locations throughout the joint and stained with haematoxylin and eosin and safranin-O fast green. The stained sections were imaged and repair of the cartilage defect scored by two blinded scorers using a modified Pineda score; where full repair= a score of 14 (as described in materials and methods 2.14). First, the mean of the summed score for each section was calculated for the assessors. Then the median of the 3 sections was used as the final repair score for each mouse. Graphs show mean +/- S.E.M.; Mann-Whitney test; **p>0.01 n=12 biological replicates.

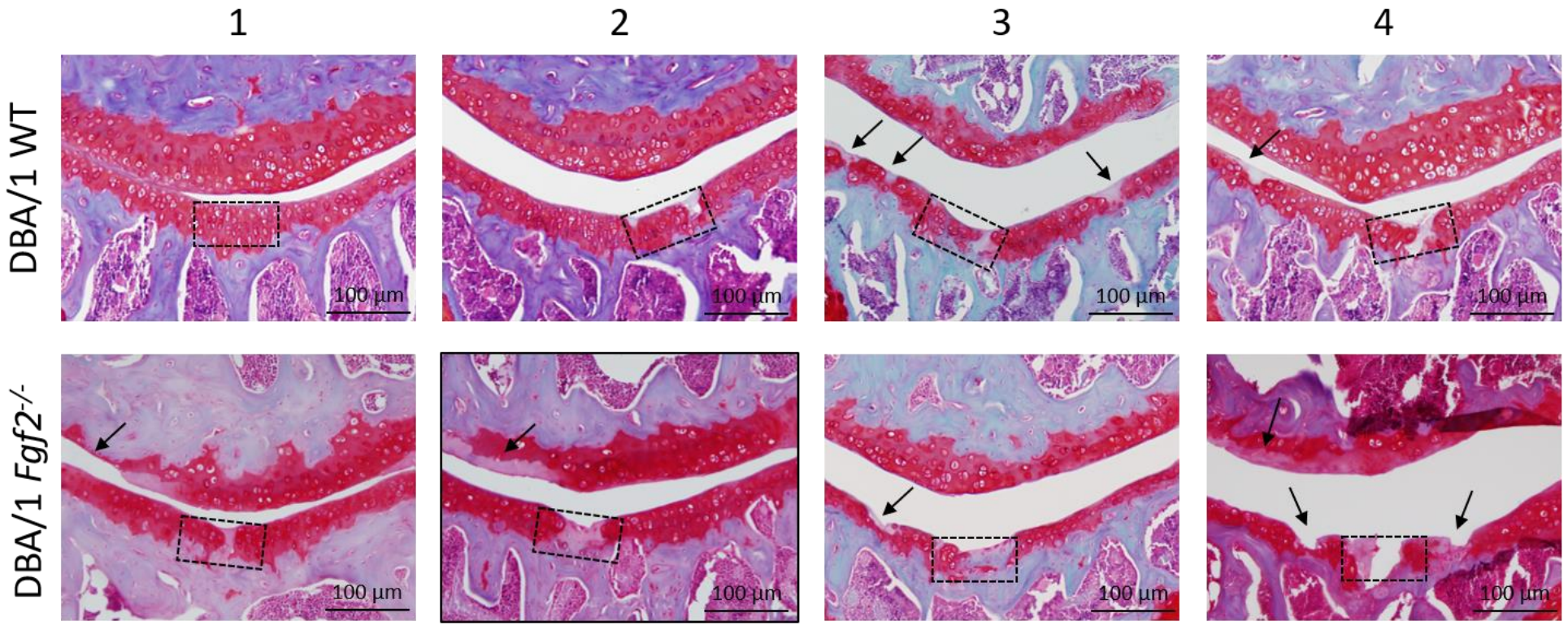

Figure 5.3: Histology of murine *in vivo* scarification

Full thickness cartilage defects were created along the patella groove of the right leg of 10-week-old male mice under sedation. Mice were allowed to recover and to resume normal activity. Mice were culled 8 weeks post-surgery, the knees dissected, fixed, decalcified, paraffin embedded and serially sectioned at 5 µm intervals. 3 sections were taken from defined anatomical locations throughout the joints and stained with haematoxylin and eosin and safranin-O fast green. Images show one of the 3 sections for 4 different mice per genotype and are magnified to the defect site.

All the following MSC experiments were initially carried out as proof-of-concept experiments to build on for future work to aid in the understanding of FGF2's intrinsic repair capabilities. This work ventured on new territory as our group had no previous experience with working with MSCs. However, our newly employed postdoctoral researcher; Dr Hayat Muhammad, had been working on MSCs for a number of years. Therefore, he has helped with setting up the techniques used in this chapter and validating them for our laboratory. The assays used are commonplace in the field and include migration assessment by scratch assays and chondrogenic disc assays for chondrogenesis.

All MSCs used in this chapter were either purchased from Lonza (human) or isolated in-house from the epididymal fat pad of 4 to 6-week-old male WT, *Fgf2*$^{-/-}$ or green fluorescent protein (GFP)-labelled mice by differential adhesion to plastic, by myself and Dr Muhammad. MSC markers were confirmed by FACS analysis and cells were tested for their ability to undergo tri-lineage differentiation (adipogenesis, osteogenesis and chondrogenesis) by Dr Muhammad. MSCs were propagated in standard media until desired quantities for experiments.

5.3 FGF2 promotes migration of human and murine MSCs by enhancing their motility

Dr Muhammad and I carried out the experimental procedures and took images for all migration experiments. I carried out all analyses myself.

To test the role of FGF2 on MSC motility, murine GFP MSCs (passage 11) were cultured in monolayer until they reached 70-80 % confluency. Cells were serum starved for 4 hours to remove the effects of any growth factors present in the FBS-containing growth medium. A

10 µl pipette tip was used to create a scratch in the middle of each well. The medium was aspirated to remove any floating cells and replaced with fresh serum-free medium (control) or that containing 250 nM FGFRi in triplicate wells. Cells were immediately imaged (0 h) and placed in an incubator at 37 °C, 5 % CO_2 for 36 hours, then imaged again. Closure of the gap was assessed across 3 wells using Image J software and plotted as a percentage of the gap filled.

Figure 5.4 shows control cells completely closed the gap in the 36-hour time period, whereas FGFRi-treated cells showed a significant reduction in gap closure to approximately 50 %. A similar pattern was seen for human MSCs that had undergone the same experimental procedure with control cells exhibiting 90 % closure but FGFRi-treated cells only closed the gap by 20 % (

Figure ***5.5***). These results therefore indicate that FGF2 is important for scratch closure.

To examine if exogenous FGF2 would enhance the gap closure, the experiment was repeated for GFP murine MSCs with a control group and that containing 20 ng/ml FGF2. Figure 5.6 shows FGF2 modestly enhanced gap closure to 90 % closure compared to 80 % in control cells, though this remained statistically insignificant.

These experiments only captured one time-point, therefore any early effects on gap closure could not be assessed. Hence the experiment was repeated, and time-lapse images taken every 20 minutes for 24 hours using a JuLi stage microscope (videos available on enclosed USB stick, in PowerPoint presentation, slide 2). Image J was used to calculate the gap closure of hourly images across 3 different points in one well for each condition. Figure 5.7 shows the rate of gap closure was similar for FGF2-treated and control cells for the first 12

hours post-scratch (as indicated by the slope of the line). After this time-point, the lines begin to diverge with a steeper line for FGF2-treated cells, indicating a faster closure rate compared to control cells. The FGFRi-treated cells had a lower rate of gap closure than control cells from 4 hours post-scratch. 6-hourly images are also shown for one representative sample for the three different conditions (

Figure ***5.8***). The incomplete and slow closure in this experiment may have been due to the fact that these cells had been passaged 11 times.

To assess the migratory capabilities of MSCs from *Fgf2*$^{-/-}$ mice, the time-lapse experiment was repeated with MSCs from WT mice and those from *Fgf2*$^{-/-}$ mice (videos available on enclosed USB stick, in PowerPoint presentation, slides 3 and 4 respectively). In these experiments cells were passage 4. In WT cells the rate of gap closure was very similar for the first 6 hours post-scratch between all treatment groups (FGF2 20 ng/ml, FGFRi 250 nM or control). After this time-point, FGF2-treated cells had a slightly higher rate of gap closure than control cells, with complete gap closure occurring at 16 and 17 hours respectively. FGFRi gap closure rate diverged from that of control cells at 8 hours post-scratch, with complete closure occurring at 21 hours. (Figure 5.9A).

For the *Fgf2*$^{-/-}$ control cells, the rate of gap closure was lower than that of WT cells and complete gap closure did not occur until 22 hours post-scratch (Figure 5.9B). As expected the time taken for complete gap closure was not increased by FGFRi. Addition of exogenous FGF2 did not seem to affect the rate of gap closure until 15 hours post-scratch where it increased and therefore full gap closure was seen by 18 hours. Although this was a single experiment, it nonetheless showed similar trends towards FGF2 enhancing gap closure and evidence that WT cells are making their own FGF2.

One advantage of using time-lapse video is the ability to observe real-time cell division. I counted cell division over the 24-hour period in each of the treatment groups. When control cells were considered, little difference in division rate was observed between WT and *Fgf2*$^{-/-}$ cells (Figure 5.12). However the *Fgf2*$^{-/-}$ cells, but not WT cells, showed an increase in the number of dividing cells with exogenous FGF2 treatment. This was partly reduced in the presence of the FGFRi. The apparent responsiveness of the *Fgf2*$^{-/-}$ MSCs could be because these cells are hypersensitive to FGF2 having not seen it before.

Time-lapse video also allows one to examine the morphology of the cells with different treatments over time. In the first hour after scratch injury, cells had a more rounded appearance and appeared to clump together. Between 4 and 8 hours, cells had begun to spread out, elongate their processes and move into the gap. Beyond 8 hours, cell retraction; where processes became less prominent, occurred. They took on a rounded morphology but mostly did not divide. These cells remained rounded for the rest of the time-course. This was true of all treatment groups, however the number of rounded cells (at the end of the 24-hour period) in the FGF2-treated groups were much lower (Figure 5.12, B). A smaller proportion of the rounded cells underwent division, but this was not predictable from their morphology.

In order to track the velocity and course of individual cells, the assay was repeated with GFP murine MSCs (passage 11) on a holographic phase microscope that focused on one side of the scratch front. Time-lapse images were taken every 20 minutes for 36 hours (videos available on enclosed USB stick, in PowerPoint presentation, slide 5). 10 (randomly chosen) cells were tracked for each treatment group over this time period. Hstudio 2.7 software was used to calculate the velocity of each cell. Figure 5.13A, B and C show the speed of 10

tracked cells for untreated (control) cells, 20 ng/ml FGF2 treated cells and 250 nM FGFRi treated cells respectively. The mean speed of 10 tracked cells for each treatment group (Figure 5.13D) shows that the speed of control cells varied across the time period from 20-80 µm/h, whereas FGF2-treated cells maintained a more constant speed of 20-30 µm/h. FGFRi-treated cells had reduced speed at around 10 µm/h. Interestingly we also observed an apparent 4-hourly periodicity in the control cells that was lost with FGF2 treatment. In this small sample size, the significance of this is unclear. Control cells also showed a peak in speed at around 13-17 hours post-scratch.

The migration of the tracked cells was also calculated for each treatment group. There was considerable variability in the migration of individual control and FGF2-treated cells (Figure 5.14A and B) whereas, FGFRi-treated cells had very low levels of migration (Figure 5.14C). The mean migration of the 10 cells (Figure 5.14D) shows that FGF2-treated cells migrated continually across the time period, plateauing at around 21 hours whereas control cells showed 2 phases of migration, with an initial surge for the first hour and 30 minutes and then again at about 13 hours post-scratch (this correlates with the peak increases in speed).

To assess the directionality of the cells, trajectories of the 10 tracked cells were plotted on an axis with the starting position of the cell as coordinates 0,0 (x,y). Figure 5.15 shows that the cell movement does not appear to have a particular direction as individual cells move in all directions. With FGFRi treatment the movement of the cells is almost completely prevented. Taken together these results suggest that FGF2 enhances gap closure of MSCs by keeping cells in a more motile state.

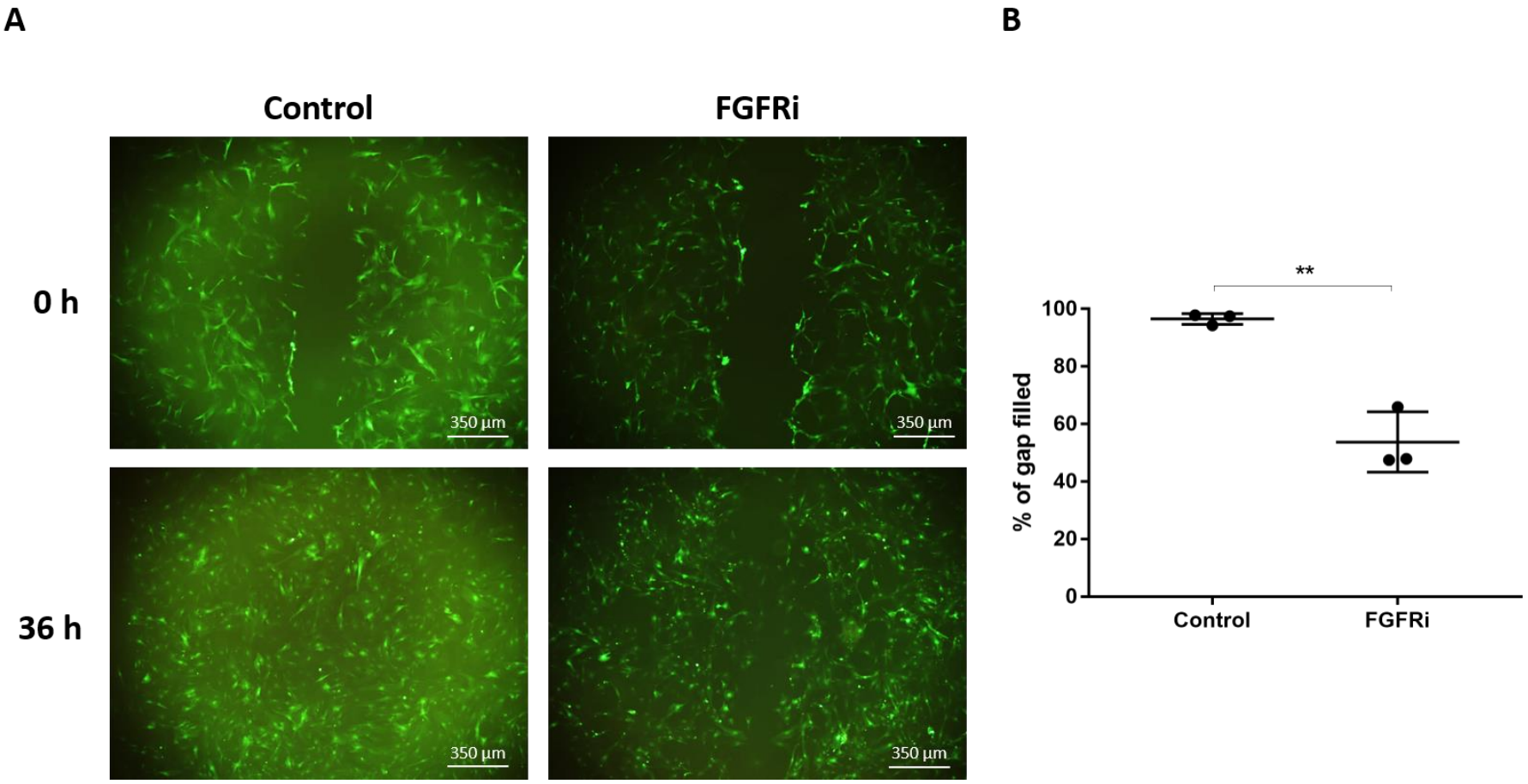

Figure 5.4: FGFRi reduces gap closure of GFP murine MSCs in a scratch assay

Passage 11 murine GFP MSCs were cultured in monolayer. Cells were serum starved for 4 h. A 10 µl pipette tip was used to create a scratch in the middle of each well. Medium was aspirated to remove any floating cells and replaced with fresh serum-free medium (control) or that containing 250 nM FGFRi. Cells were immediately imaged (0 h) and placed in an incubator at 37 °C, 5 % CO_2 for 36 h, then imaged again **(A).** Closure of the gap was assessed across 3 wells using Image J software and plotted as a percentage of the gap filled **(B)**. Graph shows mean +/- S.D.; unpaired t-test; **p<0.01. n=3 technical replicates.

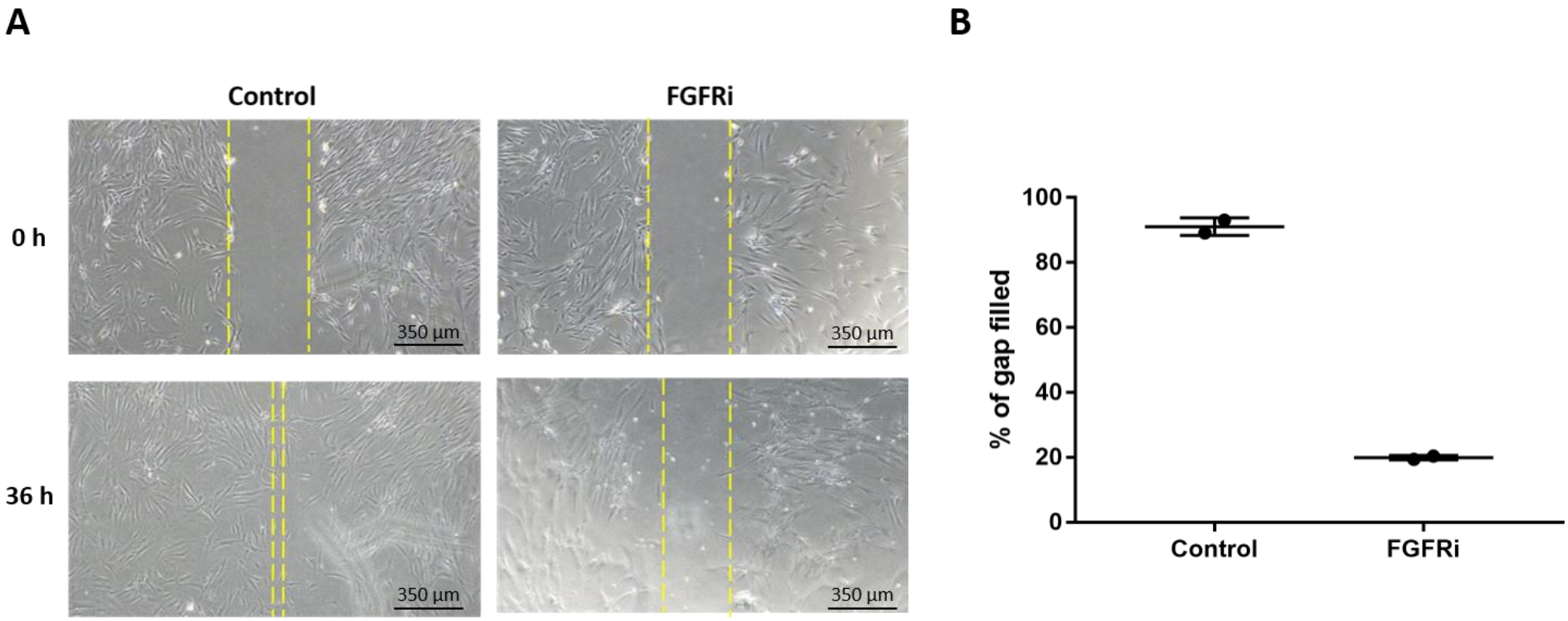

Figure 5.5: FGFRi reduces gap closure of human MSCs in a scratch assay

Passage 11 human MSCs were cultured in monolayer. Cells were serum starved for 4 h. A 10 µl pipette tip was used to create a scratch in the middle of each well. Medium was aspirated to remove any floating cells and replaced with fresh serum-free medium (control) or that containing 250 nM FGFRi. Cells were immediately imaged (0 h) and placed in an incubator at 37 °C, 5 % CO_2 for 36 h, then imaged again. Yellow dotted lines mark the region of the gap **(A)**. Closure of the gap was assessed using Image J software and plotted as a percentage of the gap filled **(B)**. Graph shows mean +/- S.D. n=2 technical replicates.

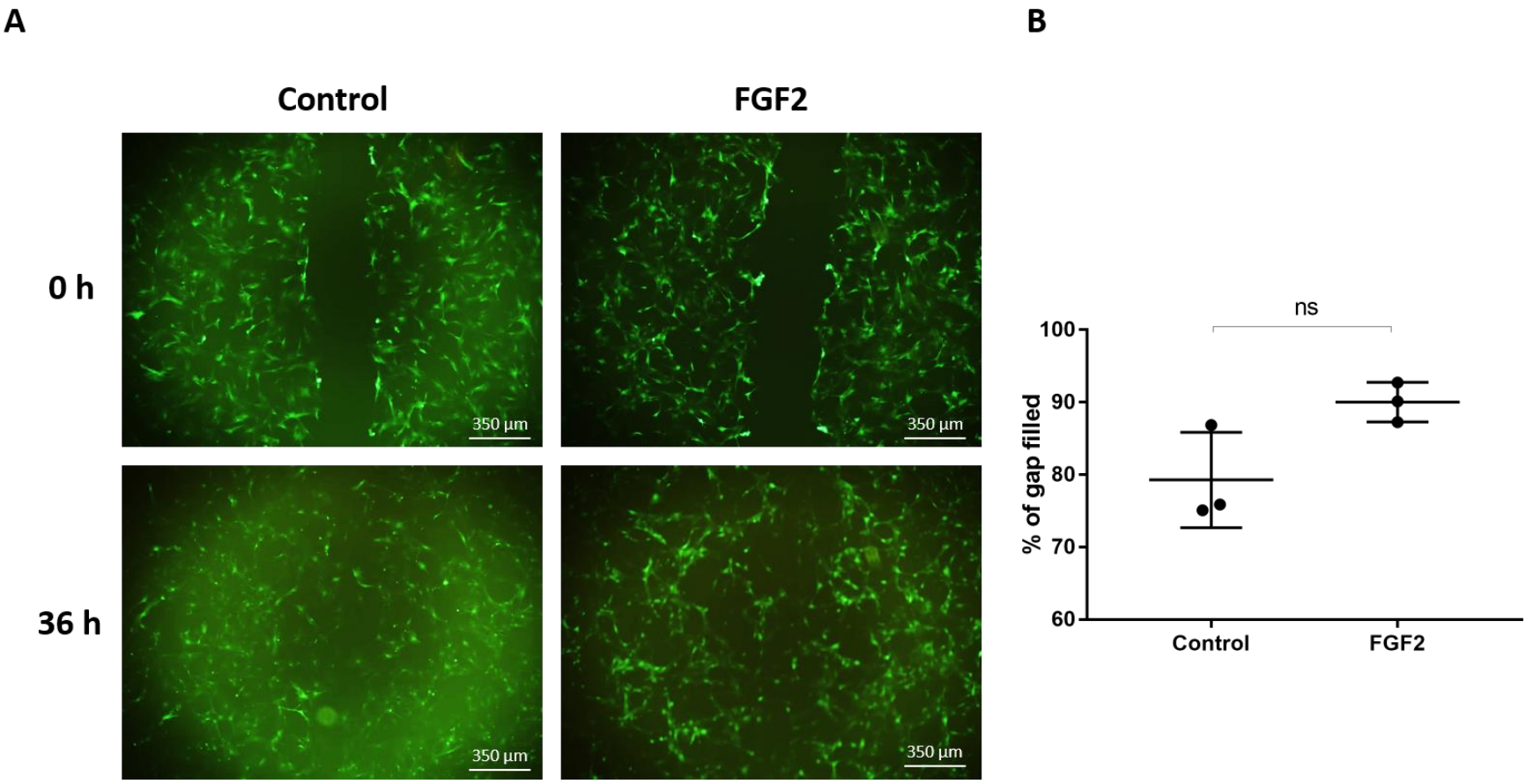

Figure 5.6: Exogenous FGF2 modestly enhances gap closure of murine MSCs in a scratch assay

Passage 11 murine GFP MSCs were cultured in monolayer. Cells were serum starved for 4 h. A 10 µl pipette tip was used to create a scratch in the middle of each well. Medium was aspirated to remove any floating cells and replaced with fresh serum-free medium (control) or that containing 20 ng/ml FGF2. Cells were immediately imaged (0 h) and placed in an incubator at 37 °C, 5 % CO_2 for 36 h, then imaged again **(A)**. Closure of the gap was assessed across 3 wells using Image J software and plotted as a percentage of the gap filled **(B)**. Graph shows mean +/- S.D.; unpaired t-test; ns=non-significant. n=3 technical replicates.

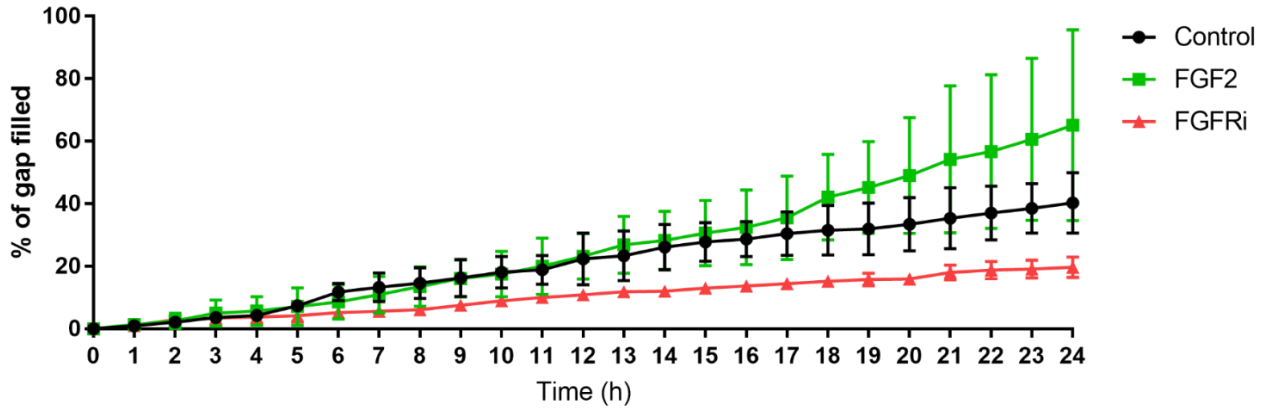

Figure 5.7: Gap closure of murine MSCs in elapsed time scratch assay

Passage 11 murine GFP MSCs were cultured in monolayer. Cells were serum starved for 4 h. A 10 µl pipette tip was used to create a scratch in the middle of each well. Medium was aspirated to remove any floating cells and replaced with fresh serum-free medium (control) or that containing 20 ng/ml FGF2 or 250 nM FGFRi. The plate was placed in a JuLi Stage microscope in an incubator at 37 °C, 5 % CO_2. The microscope was set up to take brightfield images of the scratch at 3 defined points, every 20 min for 24 h. Closure of the gap was assessed for each point using Image J software and plotted as a percentage of the gap filled. Graph shows mean +/- S.D. n=3 technical replicates.

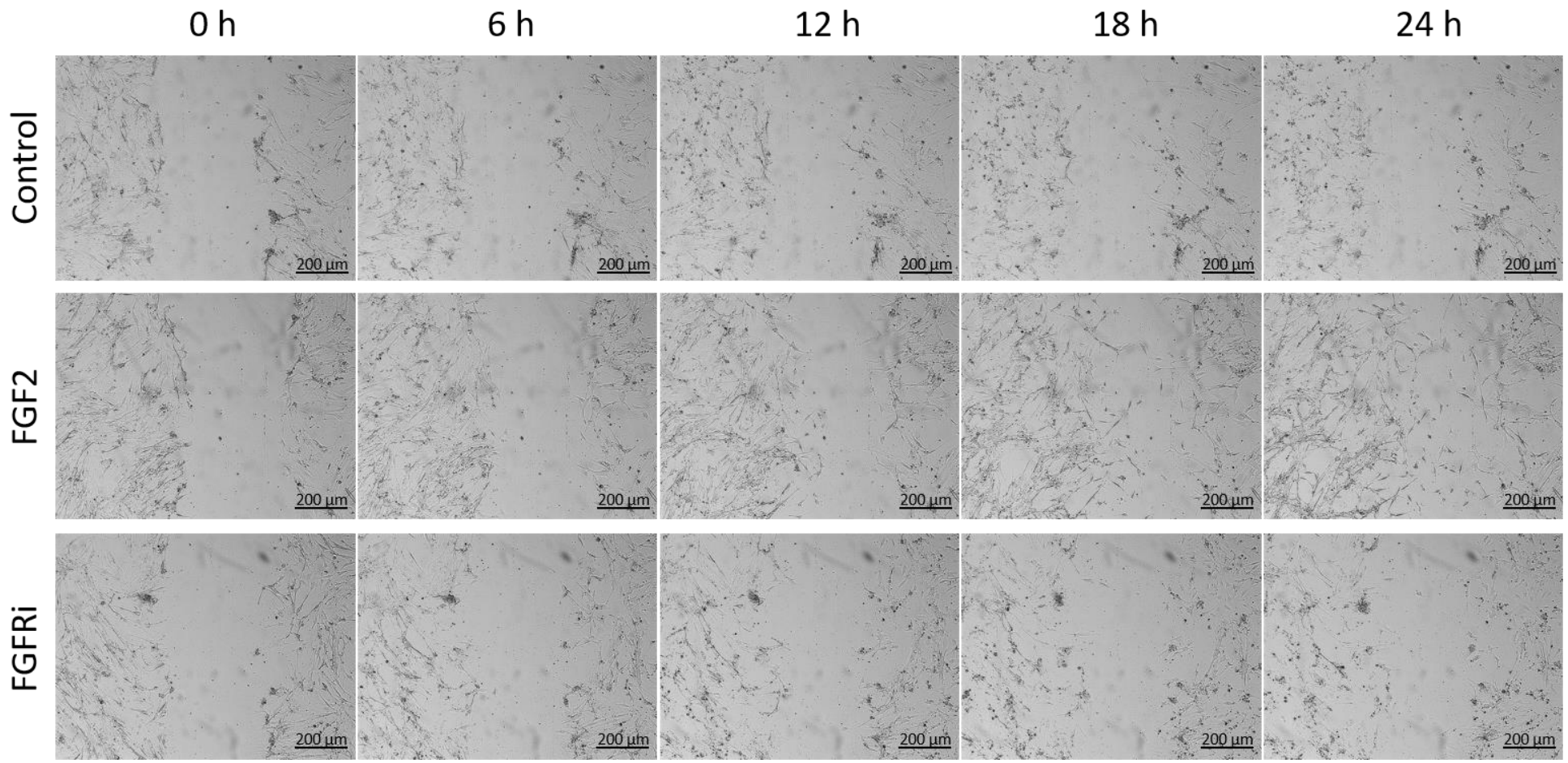

Figure 5.8: Time-lapsed images of GFP murine MSC scratch assay

Passage 11 murine GFP MSCs were cultured in monolayer. Cells were serum starved for 4 h. A 10 µl pipette tip was used to create a scratch in the middle of each well. Medium was aspirated to remove any floating cells and replaced with fresh serum-free medium (control) or that containing 20 ng/ml FGF2 or 250 nM FGFRi. The plate was placed in a JuLi Stage microscope in an incubator at 37 °C, 5 % CO_2. The microscope was set up to take brightfield images of the scratch at 3 defined points, every 20 min for 24 h. 6 hourly images are shown. n=3 technical replicates.

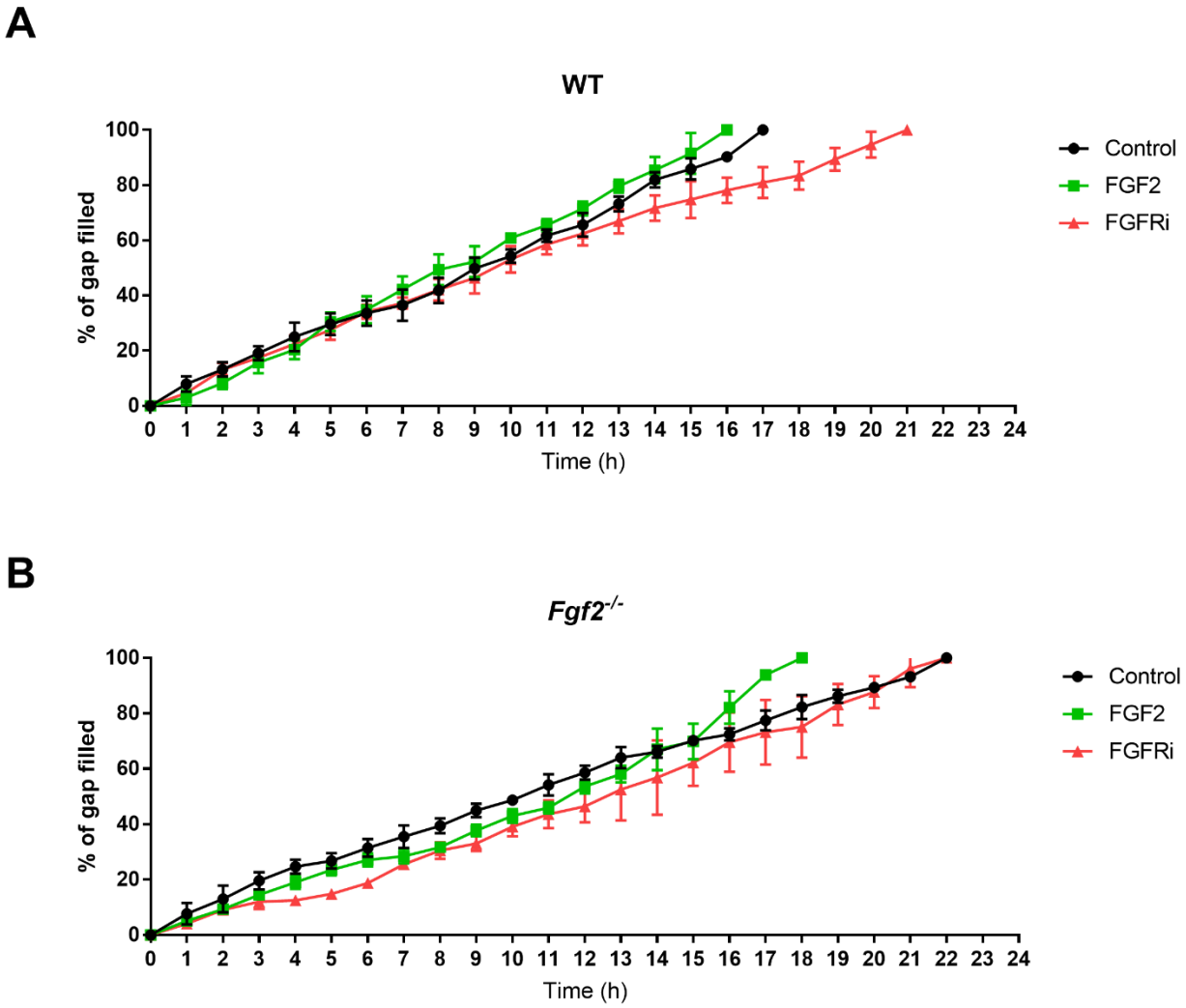

Figure 5.9: Gap closure of murine WT and *Fgf2*$^{-/-}$ MSCs in elapsed time scratch assay

Passage 4 murine MSCs from WT **(A)** or *Fgf2*$^{-/-}$ **(B)** mice were cultured in monolayer. Cells were serum starved for 4 h. A 10 µl pipette tip was used to create a scratch in the middle of each well. Medium was aspirated to remove any floating cells and replaced with fresh serum-free medium (control) or that containing 20 ng/ml FGF2 or 250 nM FGFRi. The plate was placed in a JuLi Stage microscope in an incubator at 37 °C, 5 % CO_2. The microscope was set up to take brightfield images of the scratch at 3 defined points, every 20 min for 24 h. Closure of the gap was assessed for each point using Image J software and plotted as a percentage of the gap filled. Graph shows mean +/- S.D. n=3 technical replicates.

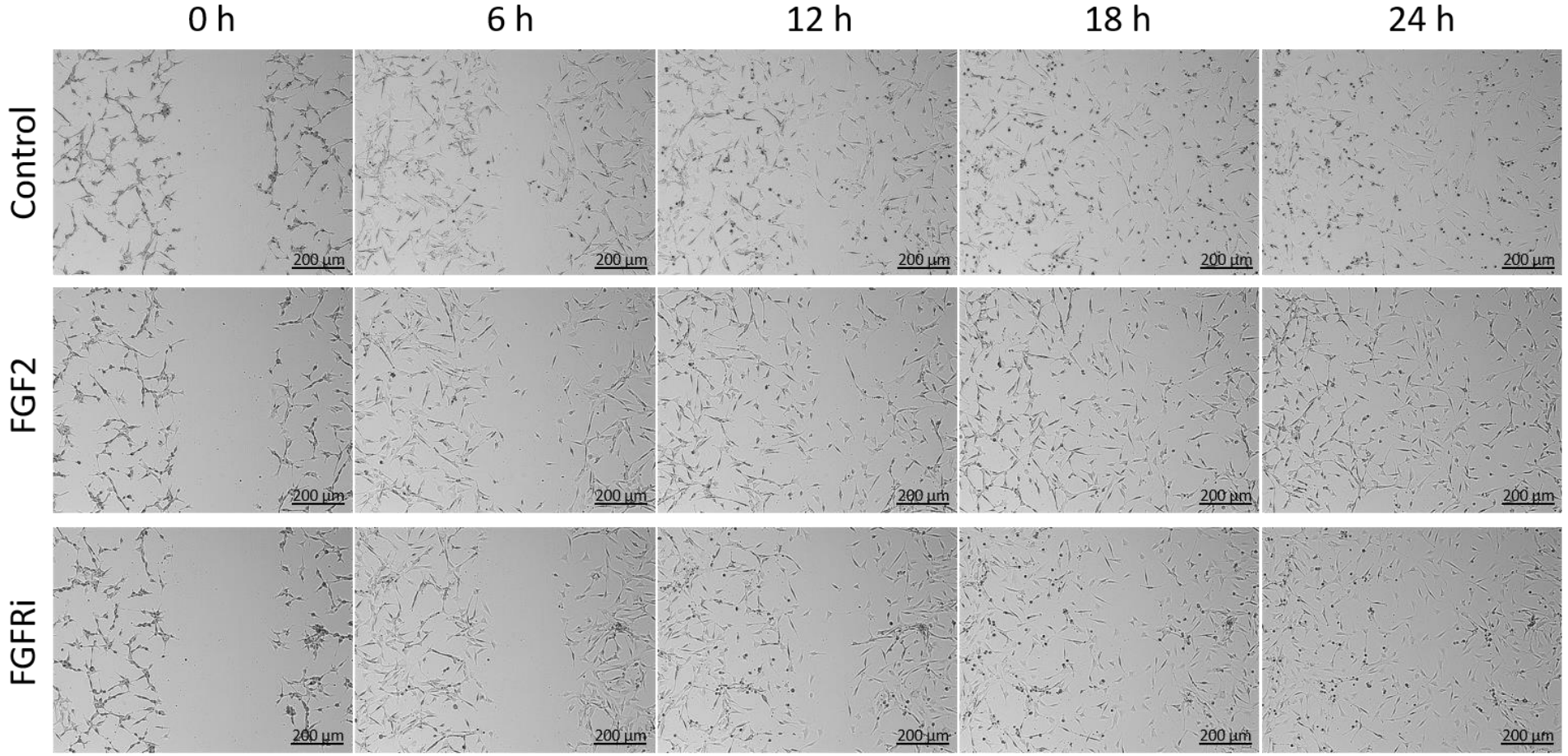

Figure 5.10: Time-lapse images of murine WT MSC scratch assay

Passage 4 murine WT MSCs were cultured in monolayer. Cells were serum starved for 4 h. A 10 µl pipette tip was used to create a scratch in the middle of each well. Medium was aspirated to remove any floating cells and replaced with fresh serum-free medium (control) or that containing 20 ng/ml FGF2 or 250 nM FGFRi. The plate was placed in a JuLi Stage microscope in an incubator at 37 °C, 5 % CO_2. The microscope was set up to take brightfield images of the scratch at 3 defined points, every 20 min for 24 h. 6 hourly images are shown. n=3 technical replicates

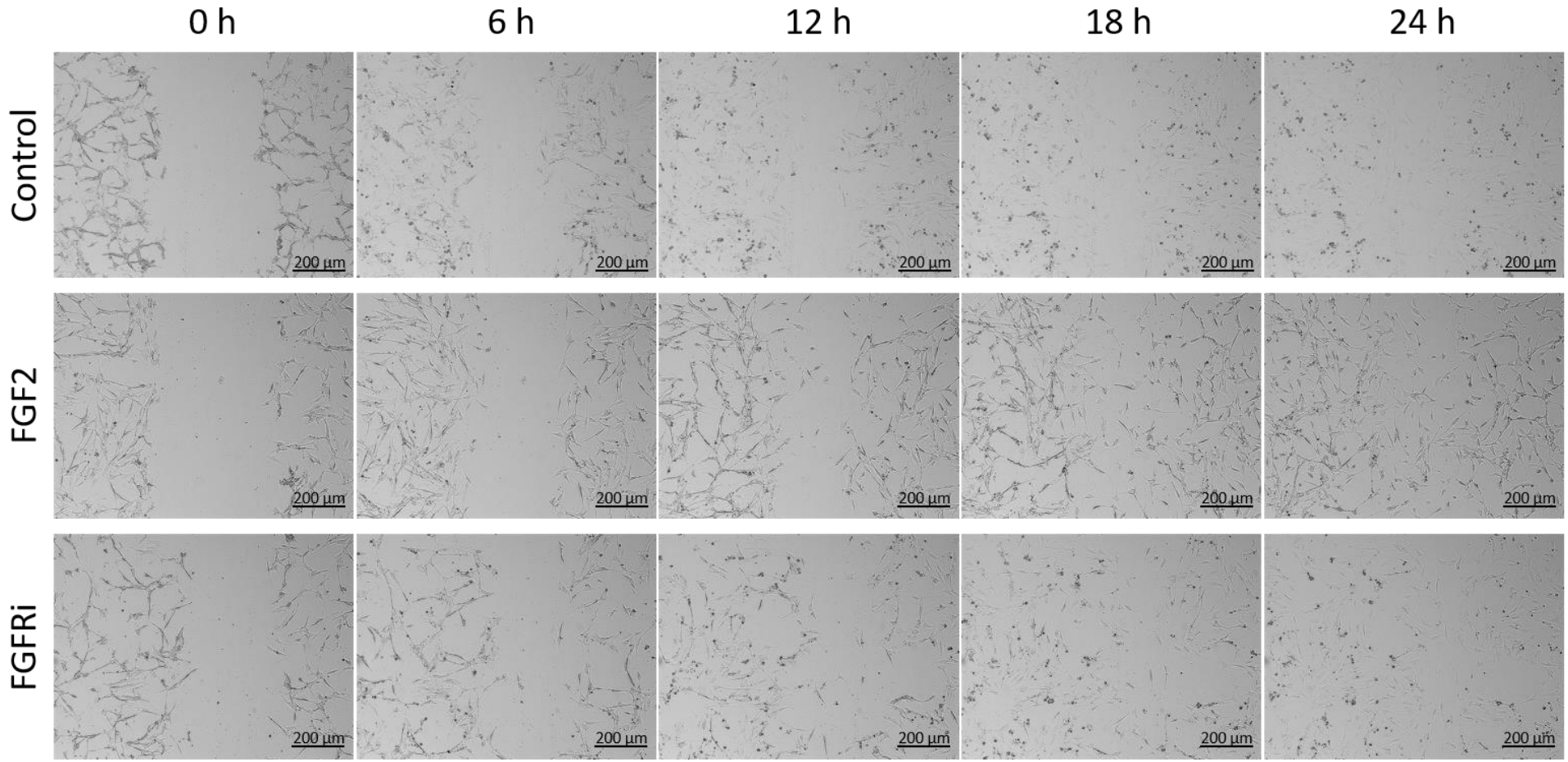

Figure 5.11: Time-lapse images of murine *Fgf2*$^{-/-}$ MSC scratch assay
Passage 4 murine *Fgf2*$^{-/-}$ MSCs were cultured in monolayer. Cells were serum starved for 4 h. A 10 µl pipette tip was used to create a scratch in the middle of each well. Medium was aspirated to remove any floating cells and replaced with fresh serum-free medium (control) or that containing 20 ng/ml FGF2 or 250 nM FGFRi. The plate was placed in a JuLi Stage microscope in an incubator at 37 °C, 5 % CO_2. The microscope was set up to take brightfield images of the scratch at 3 defined points, every 20 min for 24 h. 6 hourly images are shown. n=3 technical replicates.

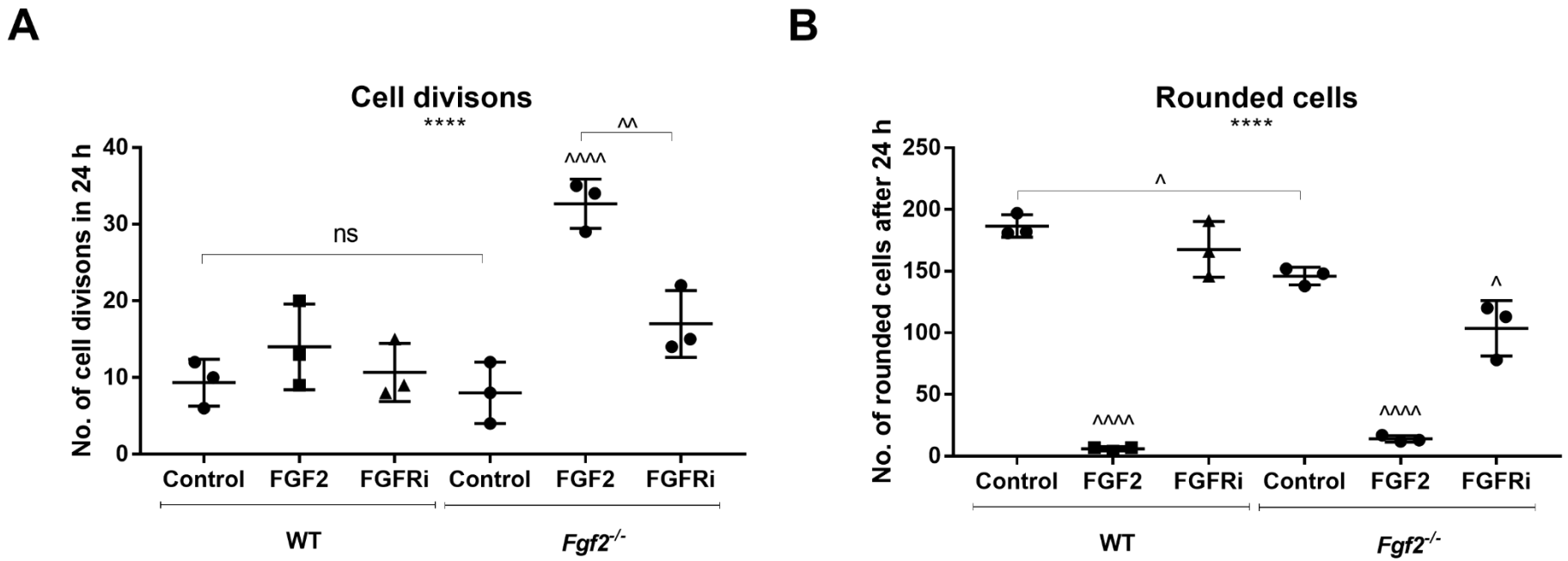

Figure 5.12: Cell proliferation and morphology of murine MSCs from time-lapsed videos

Passage 4 murine WT and *Fgf2*$^{-/-}$ MSCs were cultured in monolayer. Cells were serum starved for 4 h. A 10 µl pipette tip was used to create a scratch in the middle of each well. Medium was aspirated to remove any floating cells and replaced with fresh serum-free medium (control) or that containing 20 ng/ml FGF2 or 250 nM FGFRi. The plate was placed in a JuLi Stage microscope in an incubator at 37 °C, 5 % CO_2. The microscope was set up to take brightfield images of the scratch at 3 defined points, every 20 min for 24 h. Images were analysed frame by frame and the number of cell divisions (defined by 1 cell rounding up, dividing and splitting into 2 cells) counted by eye **(A)**. The number of cells that had a completely rounded morphology in the last frame of the video were counted by eye **(B)**. Graphs show mean +/- S.D; one-way ANOVA ****p<0.0001; with Tukey post hoc test, ns=non-significant, ^p<0.05, ^^p<0.01, ^^^^p<0.0001 compared against respective control or as shown. n=3 technical replicates.

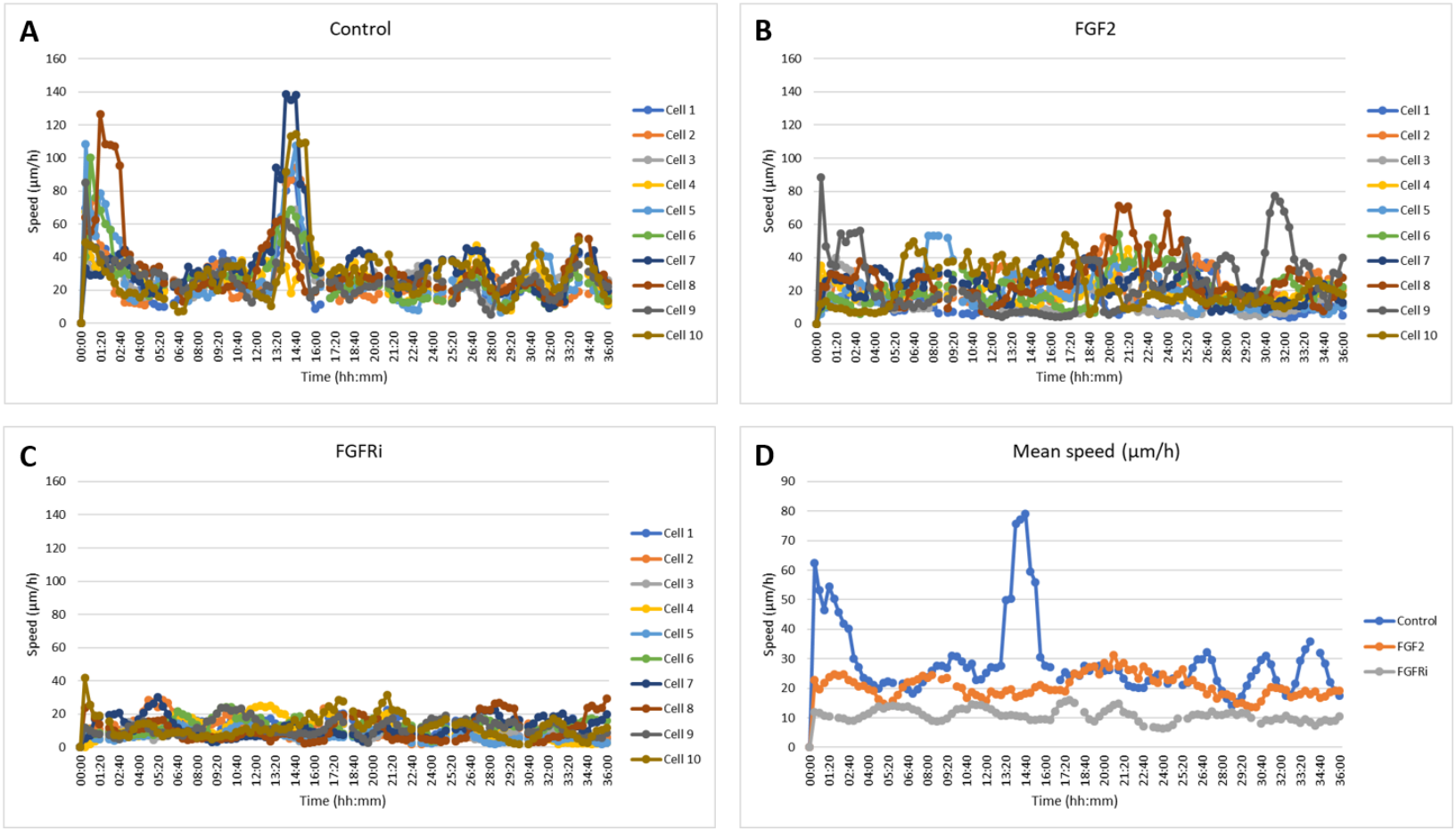

Figure 5.13: Speed of tracked murine GFP MSCs post-scratch

Passage 11 murine GFP MSCs were cultured in monolayer. Cells were serum starved for 4 h. A 10 µl pipette tip was used to create a scratch in the middle of each well. Medium was aspirated to remove any floating cells and replaced with fresh serum-free medium "control" **(A)** or that containing 20 ng/ml FGF2 **(B)** or 250 nM FGFRi **(C)**. The plate was placed in a holographic phase microscope in an incubator at 37 °C, 5 % CO_2. The microscope was set up to image one side of the scratch and take images every 20 min for 36 h. Hstudio 2.7 software was used to track 10 cells per group and calculate their speed. The average speed of the 10 tracked cells was calculated for each time-point and plotted as a graph **(D)**. n=1.

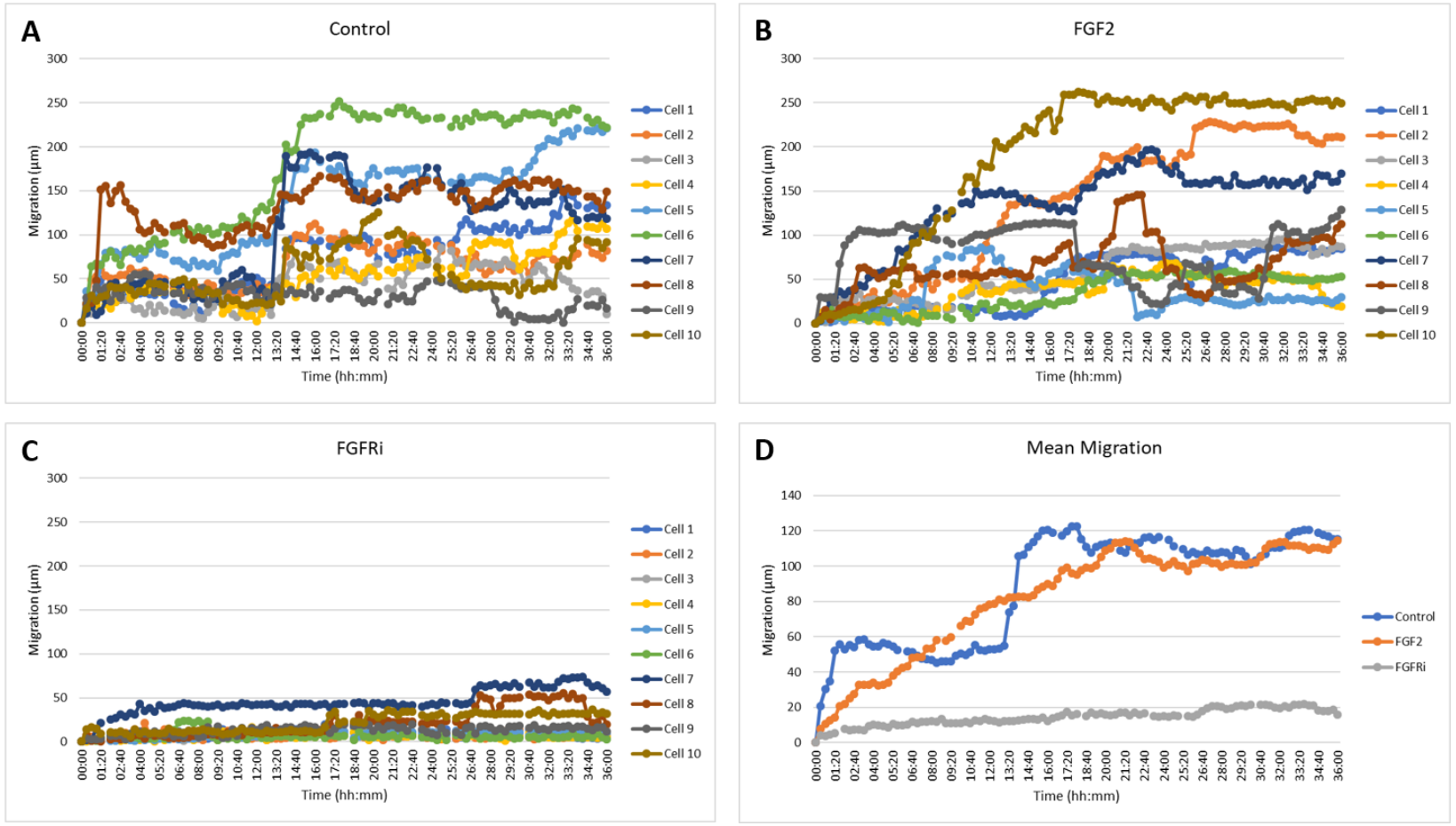

Figure 5.14: Migration of tracked murine GFP MSCs post-scratch

Passage 11 murine GFP MSCs were cultured in monolayer. Cells were serum starved for 4 h. A 10 µl pipette tip was used to create a scratch in the middle of each well. Medium was aspirated to remove any floating cells and replaced with fresh serum-free medium "control" **(A)** or that containing 20 ng/ml FGF2 **(B)** or 250 nM FGFRi **(C)**. The plate was placed in a holographic phase microscope in an incubator at 37 °C, 5 % CO_2. The microscope was set up to image one side of the scratch and take images every 20 min for 36 h. Hstudio 2.7 software was used to track 10 cells per group and calculate the migration of the cells. The average migration of the 10 tracked cells was calculated for each time-point and plotted as a graph **(D)**. n=1.

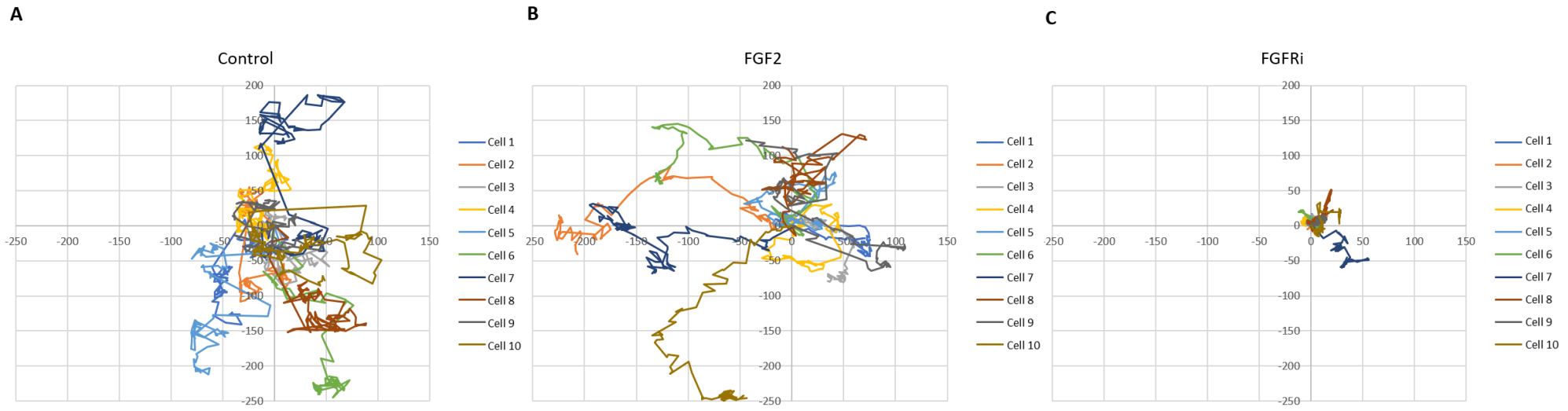

Figure 5.15: Trajectory map of individual murine GFP MSCs post-scratch

Passage 11 murine GFP MSCs were cultured in monolayer. Cells were serum starved for 4 h. A 10 µl pipette tip was used to create a scratch in the middle of each well. Medium was aspirated to remove any floating cells and replaced with fresh serum-free medium "control" **(A)** or that containing 20 ng/ml FGF2 **(B)** or 250 nM FGFRi **(C)**. The plate was placed in a holographic phase microscope in an incubator at 37 °C, 5 % CO_2. The microscope was set up to image one side of the scratch and take images every 20 min for 36 h. Hstudio 2.7 software was used to track the relative position of 10 cells per group and their trajectories plotted as an axis from initial coordinates 0,0 (x,y). n=1.

There is a possibility that FGF2 released from damaged cartilage either directly or indirectly (e.g. by enhancing cell adhesion factors) promotes the adhesion of MSCs to the injured part of the tissue. I set up a novel assay to test whether MSCs were more likely to adhere to the damaged surface. This response would be indicative of either an effect of the MSC binding to exposed tissue epitopes/molecules or could be related to FGF2 release.

5.4 MSCs do not bind preferentially to damaged cartilage

To investigate if MSCs adhere better to injured cartilage than intact cartilage, 4 mm cartilage explants were taken from the distal part of porcine MCP joints, washed in PBS and placed in a well containing media just below the surface of the explant, with either the cut (injured) or articular (uninjured) surface facing up as depicted in Figure 5.16. Murine GFP MSCs were resuspended to $2x10^5$ cells/ml; 10 µl of cell suspension was added to the top of each explant (as this concentration of cells would achieve a 70-80 % coverage of the area of the explants once cells settled). Explants were then cultured in an incubator at 37 °C, 5 % CO_2, for various times up to 24 hours. Explants were washed in PBS to remove non-adhered cells, fixed for 24 hours in formalin and washed in PBS before imaging under a fluorescent microscope. Explants without cells added (no cells) were used as a negative control, to assess autofluorescence.

Figure **5.17** shows that although cells adhered to the explant 1-hour post-application, they still exhibited a more rounded morphology. Due to the fluorescence of the cells, this made counting individual cells difficult. As time post-application increased, the number of cells attached appeared to remain the same, but the morphology became more fibroblastic and therefore easier to count individual cells. Hence, the number of cells adhered for only the

24-hour samples were quantified by eye for 4 different experiments (each with 3 replicates) as shown by the graph. No significant difference was seen in the number of attached cells between the uninjured or cut surface.

To investigate if adding exogenous FGF2 would increase the adherence of MSCs, a similar assay was carried out applying cells that had been resuspended in different concentrations of FGF2 (0-40 ng/ml) for 24 hours. Cells were only applied to the articular (uninjured) surface as it was easier to count the cells on this surface. No significant difference was seen in the number of adhered cells between the different concentrations of FGF2 (Figure 5.18), however there was a lot of variability between the 3 replicates for each concentration. These results therefore suggest that FGF2 does not increase the ability of MSCs to adhere to articular cartilage.

This assay did not appear to show enhanced binding of MSCs to damaged cartilage over the intact surface. However, the assay was variable and not as robust as I would have liked. Therefore, we did not further investigate the dependence of the binding such as it was on FGF2 i.e. by replicating the experiment in the presence of FGFRi. Better still, I could have explored this by using *Fgf2*$^{-/-}$ mouse cartilage as my substrate. If I had more time I would have pursued this further.

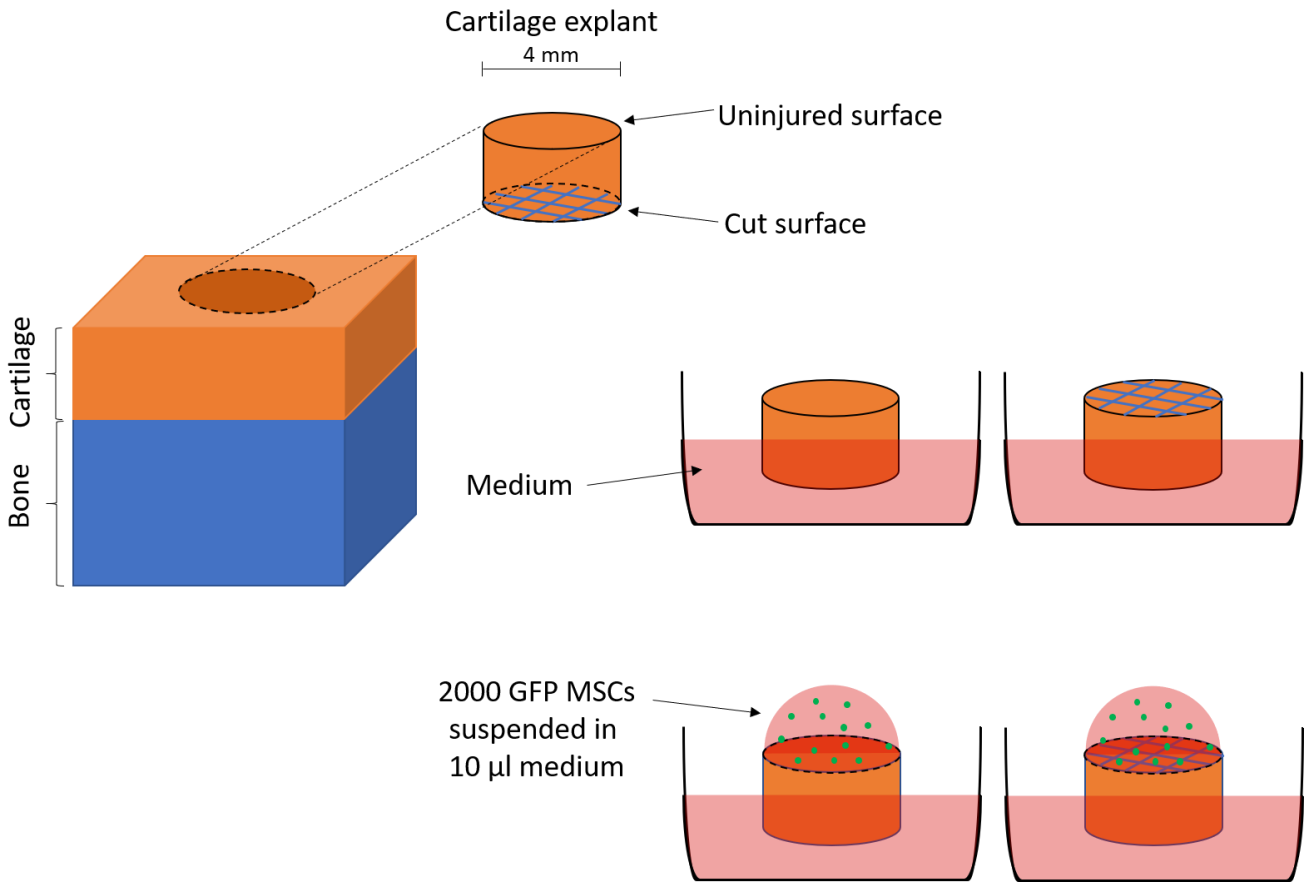

Figure 5.16: Diagram of adhesion assay

4 mm cartilage explants were taken from the distal part of porcine MCP joints using a biopsy punch, washed in PBS and placed in a well of a 24 well plate containing 100 µl serum-free α-MEM with either the cut (blue hatched surface) or uninjured (orange surface) facing up. Murine GFP MSCs were trypsinised, counted and resuspended to $2x10^5$ cells/ml; 10 µl of cell suspension was added to the top of each explant and cultured in an incubator at 37 °C, 5 % CO_2.

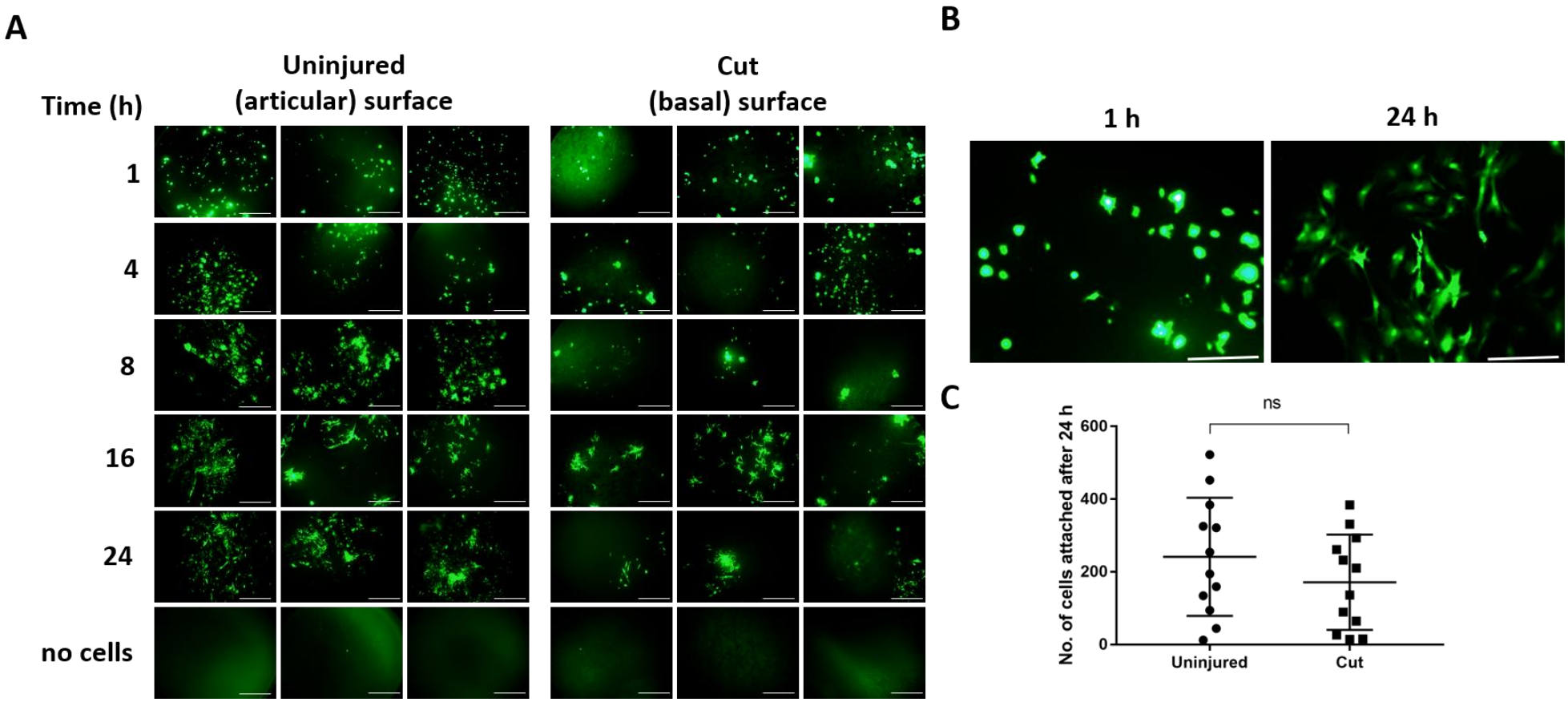

Figure 5.17: Murine MSC adhesion is similar on articular or cut surfaces of porcine cartilage explants

(A) 4 mm cartilage explants were taken from the distal part of porcine MCP joints, washed in PBS and placed in a well containing media just below the surface of the explant with either the cut or articular surface facing up. Passage 11 murine GFP MSCs were resuspended to $2x10^5$ cells/ml; 10 µl of cell suspension was added to the top of each explant and cultured in an incubator at 37 °C, 5 % CO_2, for various times up to 24 h. Explants were washed in PBS to remove non-adhered cells, fixed for 24 h in formalin and washed in PBS before imaging. Explants without cells added (no cells) were used as a negative control, to assess autofluorescence. Scale bar= 1000 µm **(B)** Magnified images of cells adhered to the uninjured surface 1 and 24 h post-application. Scale bar= 250 µm **(C)** The number of cells adhered for the 24 h samples were quantified by eye for 4 different experiments as shown by the graph; mean+/- S.D; unpaired t-test; ns=non-significant. n=3 technical replicates of 3 biological replicates.

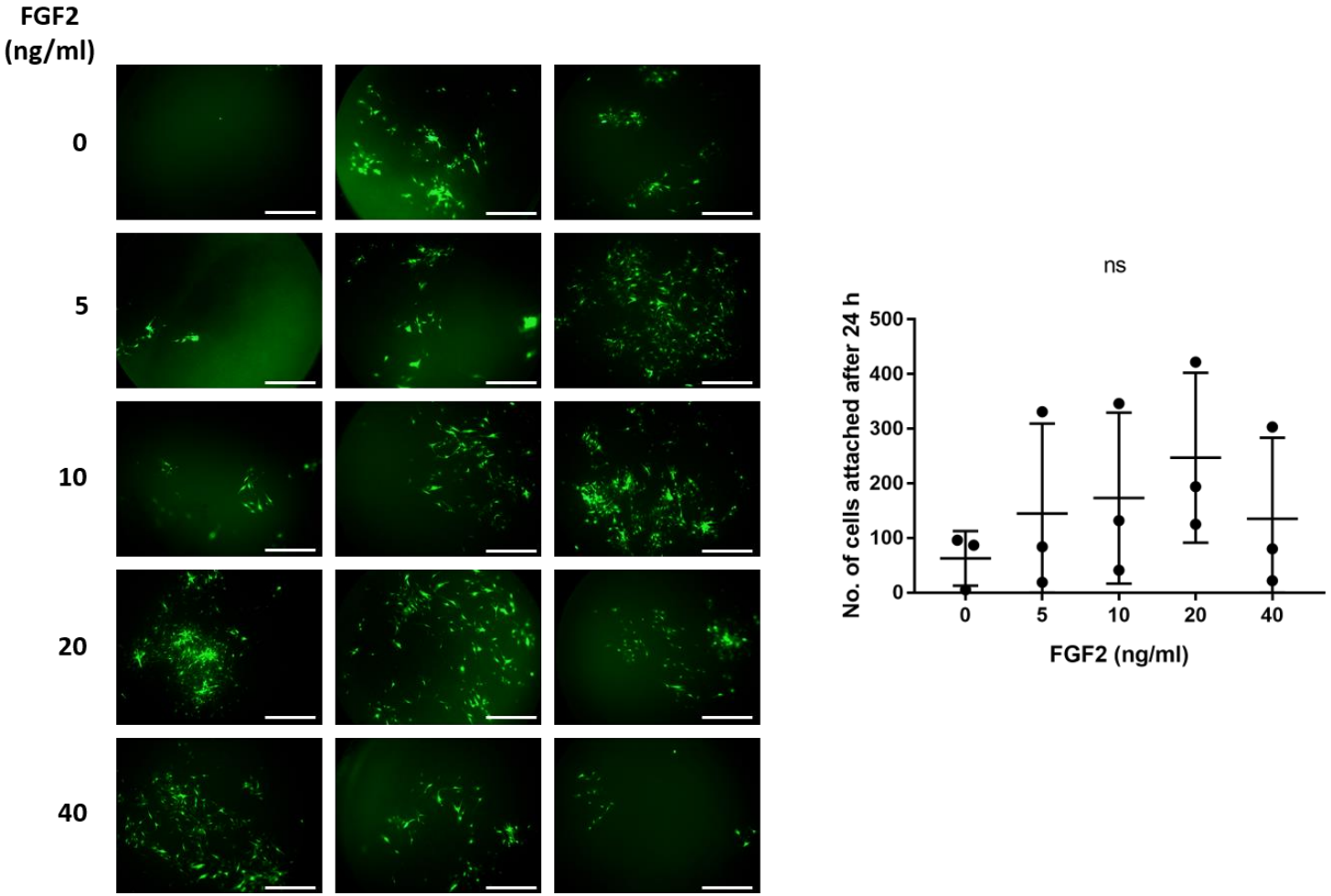

Figure 5.18: FGF2 does not increase the adhesion of murine MSCs to the articular surface of porcine cartilage explants

4 mm cartilage explants were taken from the distal part of 3 porcine MCP joints, washed in PBS and placed in a well containing medium (with various concentrations of FGF2) just below the surface of the explant with the articular surface facing up. Passage 11 murine GFP MSCs were resuspended to $2x10^5$ cells/ml in medium containing various concentrations of FGF2; 10 µl of cell suspension was added to the top of each explant and cultured in an incubator at 37 °C 5 % CO_2, for 24 h. Explants were washed in PBS to remove non-adhered cells, fixed for 24 h in formalin and washed in PBS before imaging. Scale bar= 1000 µm. The number of cells attached were counted by eye. Graph shows mean+/- S.D; one-way ANOVA with Tukey post hoc test; ns=non-significant. n=3 biological replicates.

FGF2 is known to be a potent mitogen of MSCs and is thought to maintain their stemness (Tsutsumi *et al*., 2001). Solchaga *et al* (2005) showed the mitogenic effect to be dose-dependent but found variability among donors. The authors also showed that when MSCs were expanded in 10 ng/ml FGF2 (during expansion) prior to inducing chondrogenic differentiation (in a pellet assay); 21 day pellets exhibited enhanced GAG content, but not enhance DNA content. This suggested FGF2 does not enhance proliferation of MSCs once they begin to differentiate. Moreover, FGF2 primes the MSC so that subsequent chondrogenesis is more successful (Solchaga *et al*., 2005). Hellingman *et al* (2010) demonstrated that the events of *in vitro* chondrogenesis in a pellet assay was extremely similar to *in vivo* endochondral ossification in terms of collagen production, as well as FGFR expression. They also showed that when FGF2 was added throughout the chondrogenesis period, it inhibited chondrogenesis in that the GAG content of FGF2 treated pellets were reduced after 35 days of culture compared to controls. However, they did use a high concentration of FGF2 (5 nM/ 100 ng/ml). As our group has previously shown that latent TGFβ is released along with FGF2 upon cartilage injury (Tang *et al*., 2018), we investigated the effect of combining ligands on the differentiation of MSCs into chondrocytes, to try to recapitulate what happens after cartilage injury.

5.5 FGF2 inhibits chondrogenesis

Human MSCs were cultured in a trans-well chondrogenic disc assay for 21 days with either standard chondrogenic medium (that containing 1X ITS, 100 µg/ml sodium pyruvate, 25 µg/ml ascorbate-2-phosphate, 40 µg/m L-proline, 1X L-glutamine 100 nM dexamethasone and 10 ng/ml TGFβ3), as a positive control; or standard chondrogenic medium that did not contain TGFβ3 as a negative control; or standard chondrogenic medium supplemented with

20 ng/ml FGF2. The medium was replaced every other day during the assay. The chondrogenic nature of the discs was assessed by histology and qPCR analysis of gene expression. All cell culturing, RNA extraction and reverse transcription were carried out equally by myself and Dr Muhammad. Dr Muhammad carried out the qPCR; I did all the analysis myself.

Safranin-O staining was used to assess proteoglycan deposition. Sirius red, which stains collagen fibres red, was used to assess how fibrous the discs were (an indication of collagen deposition). Under polarised light microscopy this stain also distinguishes between thick and thin fibres; with yellow-orange birefringence indicative of thick fibres and green birefringence indicative of thin fibres.

The discs treated with chondrogenic media alone appeared highly cartilaginous in nature, with strong proteoglycan staining and cells that appeared morphologically like chondrocytes. There was also some fibrous staining (presumably due to type II collagen fibrils). In contrast, the discs treated without the main chondrogenic driver TGFβ3 showed no proteoglycan staining, more fibrous (Sirius red) staining and a loss of integrity of the shape of the disc; representing cells that had not undergone chondrogenesis. The FGF2-treated discs seemed to be very similar to the negative control discs in that there was little proteoglycan staining, however they exhibited a more fibrous staining. (Figure 5.19).

When gene expression was analysed, the chondrocytic gene markers transcription factor *SOX9*, *aggrecan* (*ACAN*), *collagen type II* (*COL2*) and *cartilage oligomeric matrix protein* (*COMP*) were all significantly down-regulated for negative control discs and those treated with FGF2 (Figure 5.20).

The *FGFR* gene expression was also analysed in these discs. *FGFR1* expression was not affected by the different stimulating media (Figure 5.21A). *FGFR2* and *FGFR3* on the other hand, were significantly down-regulated in the absence of TGFβ3 or in the presence of FGF2 (Figure 5.21B and C).

These results confirm what others have reported previously; that FGF2 inhibits chondrogenesis *in vitro* when present for the duration of chondrogenesis.

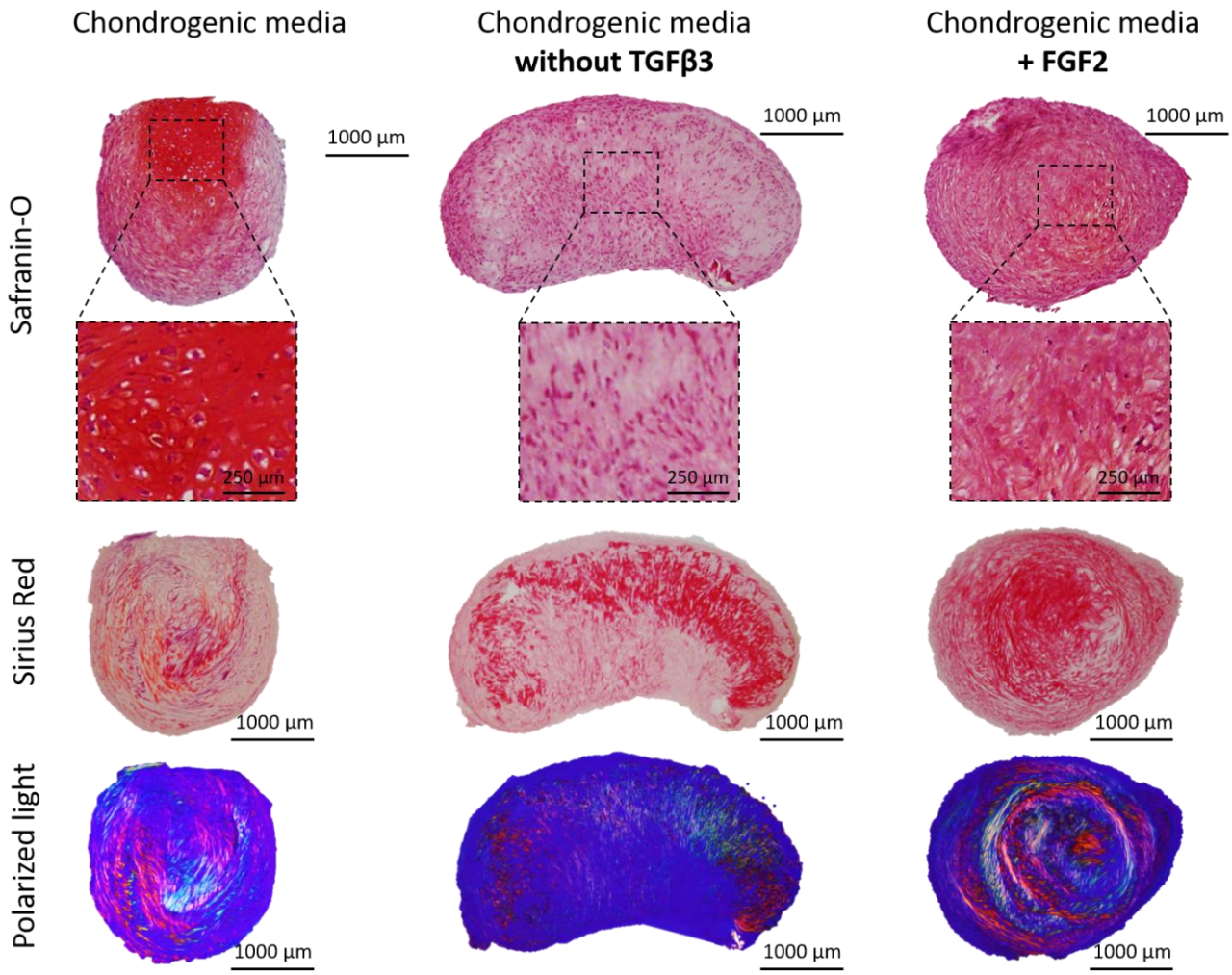

Figure 5.19: FGF2 inhibits *in vitro* chondrogenesis, reducing proteoglycan deposition and increasing fibrosis

Passage 3 human MSCs were cultured in a trans-well chondrogenic disc assay for 21 days with standard chondrogenic medium as a positive control, or standard chondrogenic medium that did not contain TGFβ3 as a negative control, or standard chondrogenic medium that contained 20 ng/ml FGF2. The discs were processed, paraffin embedded and sectioned at 5 µm intervals. Sections were stained with Safranin-O, which stain proteoglycans red; or Sirius red, which stains collagen fibres red. Sections were imaged under light microscopy and Sirius red samples also under polarized light, where yellow-orange birefringence indicates thick fibres and green birefringence indicates thin fibres. n=1

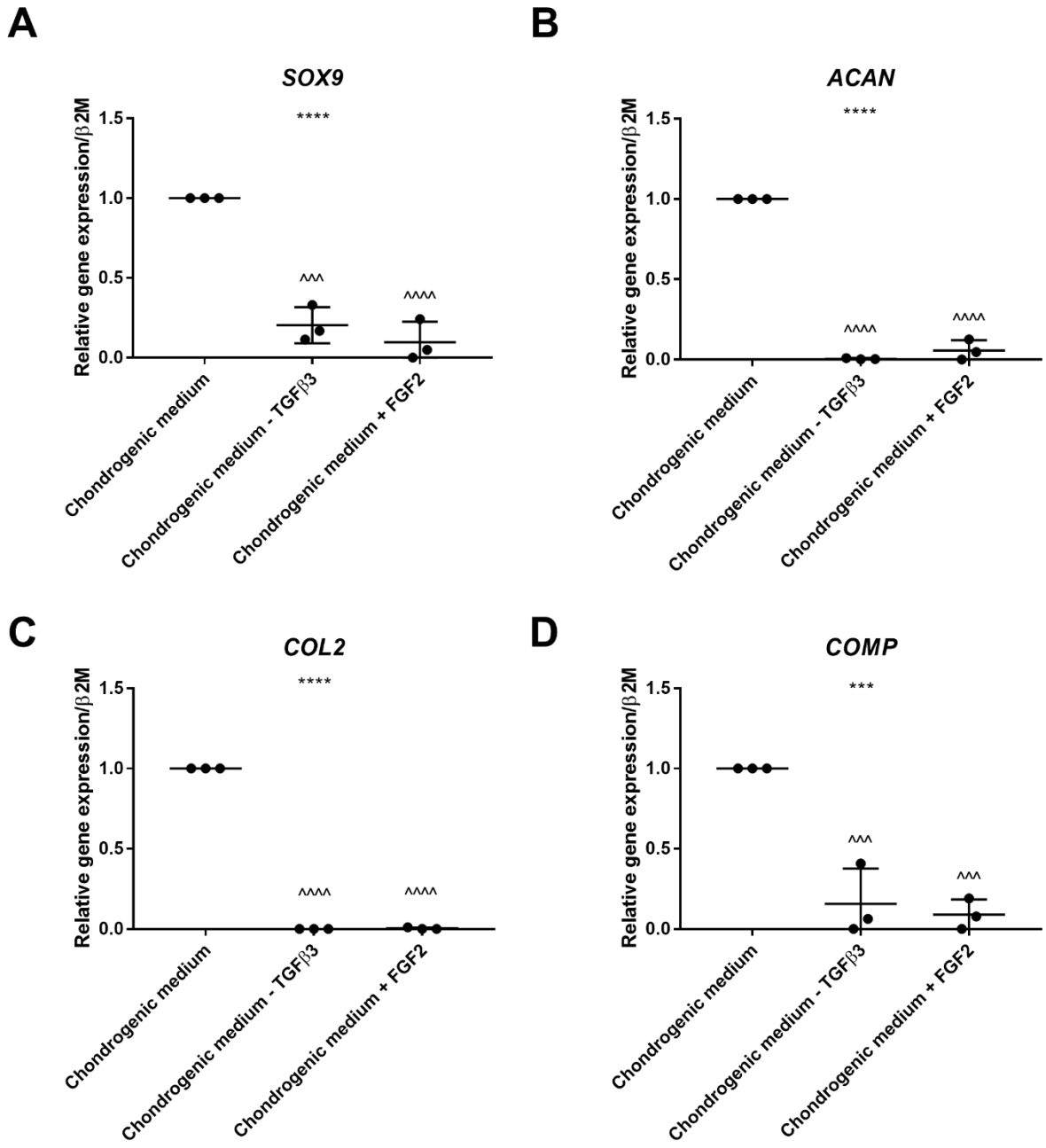

Figure 5.20: FGF2 reduces chondrogenic gene expression

Passage 3 human MSCs were cultured in a trans-well chondrogenic disc assay for 21 days with standard chondrogenic medium as a positive control, or with standard chondrogenic medium that did not contain TGFβ3 as a negative control, or with standard chondrogenic medium that contained 20 ng/ml FGF2. Discs were lysed in TRIzol, RNA extracted, reverse transcribed and gene expression for *SOX9* **(A)**, *ACAN* **(B)**, *COL2* **(C),** and *COMP* **(D)** assessed by qPCR using TaqMan probes. All samples were normalised to *β2M* and expressed relative to positive control discs. Samples that had undetectable levels of genes were given a relative expression of 0 to allow statistical analysis. Graphs show mean +/- S.D; one-way ANOVA ***p<0.001 ****p<0.0001; with Tukey post hoc test ^^^p<0.001, ^^^^p<0.0001 compared against positive control discs. n=3 technical replicates.

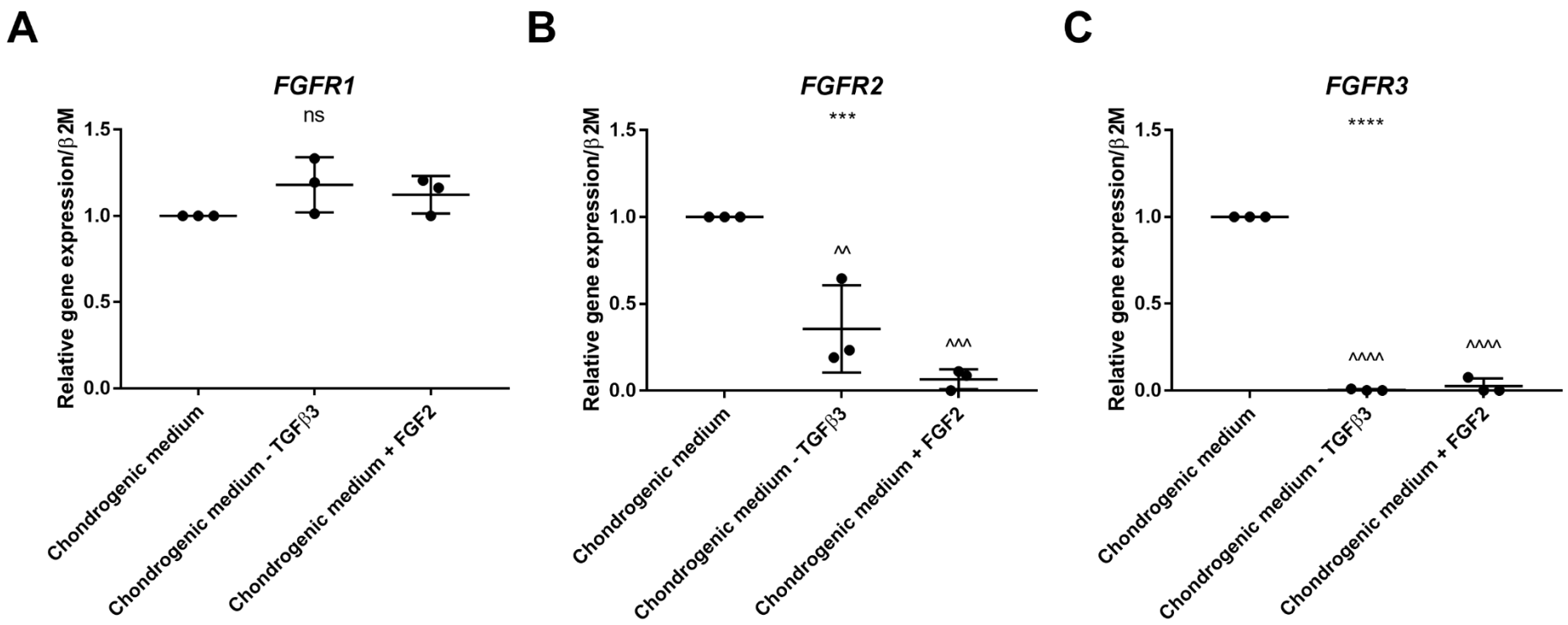

Figure 5.21: *FGFR* expression in chondrogenic disc assay

Passage 3 human MSCs were cultured in a trans-well chondrogenic disc assay for 21 days with standard chondrogenic medium as a positive control, or with standard chondrogenic medium that did not contain TGFβ3 as a negative control, or with standard chondrogenic medium that contained 20 ng/ml FGF2. Discs were lysed in TRIzol, RNA extracted, reverse transcribed and gene expression for *FGFR1* **(A)**, *FGFR2* **(B),** and *FGFR3* **(C)**, assessed by qPCR with TaqMan probes. All samples were normalised to *β2M* and expressed relative to positive control discs. Samples that had undetectable levels of genes were given a relative expression of 0 to allow statistical analysis. Graphs show mean +/- S.D; one-way ANOVA ns=non-significant, ***p<0.001, ****p<0.0001; with Tukey post hoc test ^^p<0.01, ^^^p<0.001, ^^^^p<0.0001 compared against positive control discs. n=3 technical replicates.

5.6 Discussion

Due to time and cost restraints, there are a number of limitations to this part of the study. Firstly, time was a constraint as there were many issues with getting the *in vivo* model up and running. This is because initially backcrossing the mice took longer than expected. There were some issues regarding sectioning, partly due to the smaller size of mice; which meant that the scoreable part of the section was lost. Consequently, I had to serial section further batches of knees in order to make sure the correct sections were obtained. This was especially laborious as the bones of *Fgf2*$^{-/-}$ mice are more brittle. Montero *et al* (2000) have shown that *Fgf2*$^{-/-}$ mice develop low bone density later in life, with changes first seen at 18 weeks of age. Therefore, this could account for their brittleness. Another issue with this model was that after surgery, some mice are prone to patella dislocations, especially if the mice fight a lot. Additionally, the dislocation is very hard to visualise by the naked eye on a live animal. The dislocation also leads to destabilisation of the joint and uneven loading, so osteophytes form and the repair tissue becomes confounded. Therefore, the mice in which this happened also had to be disregarded. Moreover, some of the *Fgf2*$^{-/-}$ mice had joints which were fused at an approximately 90 ° angle which were not detectable until the knee was shaved, and so surgeries could not be performed on these mice. A few mice also had very thin cartilage (visualised upon opening the joint) and when I attempted to make the defect the bone collapsed under the needle (which was again suggestive of low bone density). These defects were more noticeable in mice that seemed to be more aggressive (animal husbandry technicians noted them fighting more and I noted them having tail wounds and noticeably scarred skin on their hind region when I culled them). It is possible that their injuries are more apparent because they have delayed skin healing responses also (Ortega *et al*., 1998).

Some of my MSC experiments were only carried out once. This is because of time constraints and the fact that the number of MSCs that can be isolated is very small, and so it takes a few weeks to propagate cells before experiments can be carried out. Moreover, the time-lapse microscopes were on loan to us, and this limited how many experiments I could do. Initially we had propagated enough cells to carry out 3 repeats of the experiments within the time limit, but various issues prevented completing this. For instance, when it came to do the experiment, cells were plated at confluency and left to adhere to the culture dish as suggested by the manufacturer; however, this led to all of the cells adhering to each other and they formed a clump in the corner of the well. Therefore, I had to plate the cells at sub-confluency and wait for them to reach 70-80 % confluency before the scratch could be made. But at this point, the cells also proliferated at a slower rate than usual, which could have been due to a number of factors including the fact that the more cells are passaged, the less stem cell-like they become (Tsutsumi *et al*., 2001). Consequently, I was only able to perform the experiment once before the machine had to be returned.

FGF2 is important for intrinsic repair of articular cartilage. The work presented here is the first demonstration of a genetically modified mouse that has a delayed cartilage repair phenotype. This may account for the chondroprotective role of FGF2 *in vivo* after induction of OA (Chia *et al*., 2009) and if so, it also provides insight into OA pathogenesis; suggesting that the disease course *in vivo* is not just dictated by control of degradative pathways, but also by counteracting repair processes.

The mechanism by which FGF2 promotes repair could either affect cells local to the injury (chondrocytes, local progenitor cells) or those elsewhere in the joint or extra-articular e.g. MSCs or inflammatory cells. I explored whether FGF2 affected the activity of MSCs. The data

clearly show that FGF2 affects motility of MSCs and scratch closure but not adhesion to cartilage. Nor does it affect chemotaxis as previously published (Mishima and Lotz, 2008) and personal communication (De Bari). Growth factors such as platelet-derived growth factor (PDGF) have described chemotactic effects (Mishima and Lotz, 2008), but whether PDGF is released upon cartilage injury is unknown. It could possibly come from the blood clot formed when the osteochondral junction is breached (as clot formation requires platelets).

I confirmed, as other groups have published, that FGF2 does not promote chondrogenesis (Hellingman *et al*., 2010, Weiss *et al*., 2010). Rather it prevents differentiation of the MSCs. However, it may prime the cells to become better differentiated chondrocytes eventually as shown by Solchaga *et al* (2005) and Correa *et al* (2015). Correa *et al* (2015) also showed that *FGFR1* and *FGFR3* mRNA expression changes during *in vitro* chondrogenesis and is modulated by FGF2 treatment during the expansion phase. The authors also showed that addition of FGFs (9 and 18) at different stages of chondrogenesis impacted the differentiation program. When added at earlier stages, they inhibit chondrogenesis but at later stages they enhance chondrogenesis by delaying hypertrophy (through effects mediated by FGFR3). Kato and Iwamoto (1990) also demonstrated that FGF2 inhibits terminal differentiation of chondrocytes, only when added at in the transition period between matrix maturation and hypertrophy. So the point at which FGF2 acts, and the expression of the FGFRs is important to take into account when considering the effects on intrinsic cartilage repair.

I therefore propose the following schematic for intrinsic repair of cartilage:

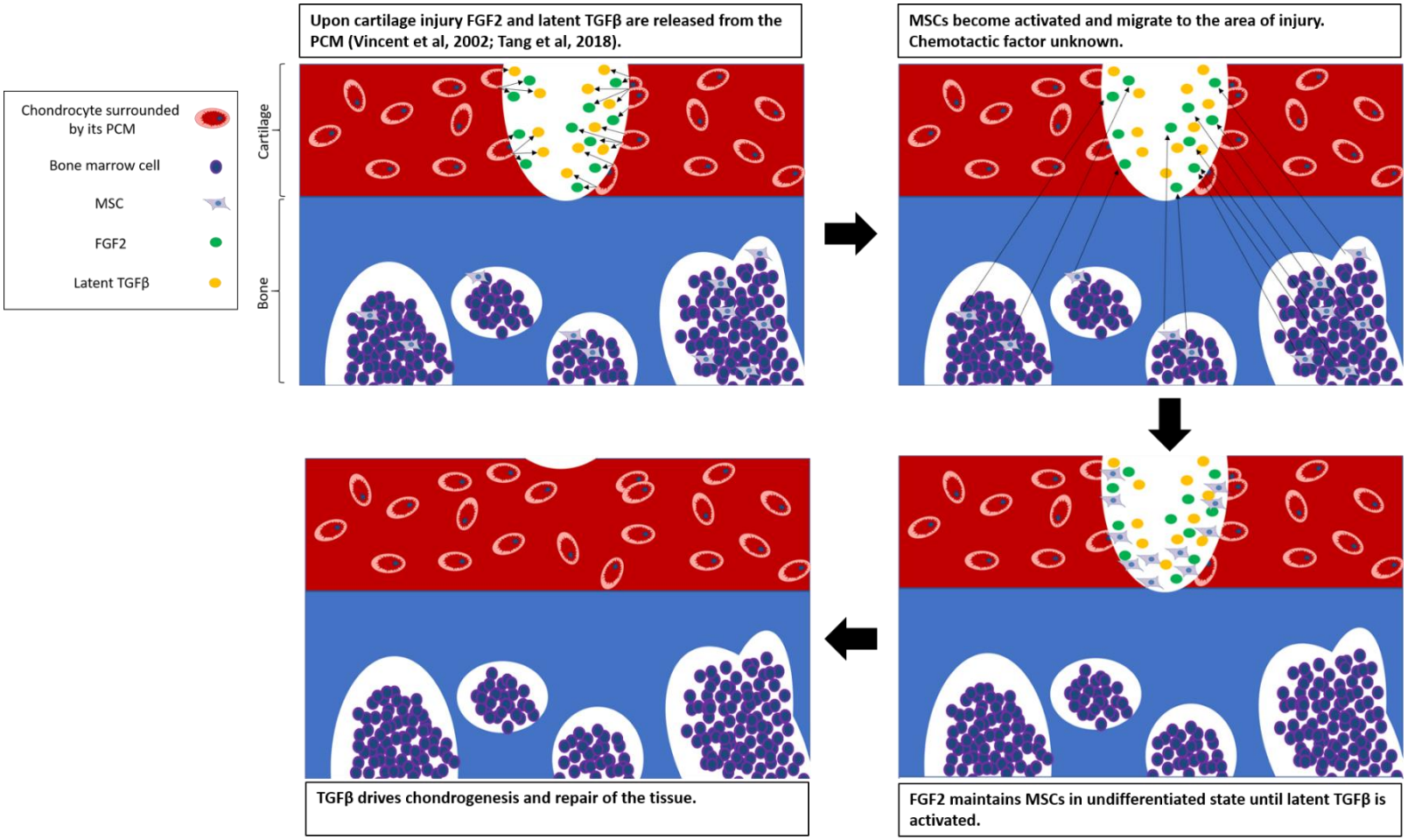

Figure 5.22: Schematic for intrinsic repair of cartilage

When articular cartilage (in red) is injured, FGF2 (green ovals) is released from the pericellular pool, along with other molecules such as latent TGFβ (yellow ovals). Then MSCs migrate to the damaged area in response to an unknown chemotactic factor. It is thought that they migrate up from the underlining bone marrow when the osteochondral junction is breached, although there is some evidence that MSCs may also originate from the synovium. Once MSCs reach the site of damage, it is thought that FGF2 maintains them in their undifferentiated state and primes them to undergo chondrogenesis. Once latent TGFβ is activated it is thought to drive chondrogenesis of the MSCs in order to repair the damaged area.

There are a few questions left unanswered:

What is the significance of the drop in *FGFR3* in cartilage upon injury and does it eventually go back to original expression levels? Does this response occur *in vivo*? Perhaps it is necessary for promoting FGFR1-driven catabolic responses. There may be some benefit in initially degrading part of the injured cartilage, i.e. to allow for better integration of the MSCs. It has been noted in the rabbit reparative tissue, that the cartilage at the periphery of the defect loses its proteoglycan staining, this occurs alongside cell death in this region, in the early stages of cartilage repair (Shapiro *et al*., 1993). Cell death around the defect was also noted in the Eltawil *et al* (2009) paper and aggrecanase activity was also found.

Where do the MSCs that repair the tissue come from, and how are they directed there? Roelofs *et al* (2017) have used *in vivo* lineage-tracing experiments where *Gdf5*-Cre mice were crossed with tdTomato fluorescent reporter mice to trace cells from the embryonic joint interzone. They show that postnatally, GDF5-lineage cells persist as MSCs in adult synovium and proliferate after cartilage injury. GDF5-lineage cells also give rise to chondrocytes in the reparative tissue, however not all of the cells express the fluorescent reporter, indicating that they are derived from another source of cells.

Could the response of the MSCs be mediated through FGFRs and is that why we see a difference in the *Fgfr* KO phenotypes when OA is induced? Dombrowski *et al* (2013) have shown that FGF2 enhanced proliferation of MSCs is FGFR1-dependent. They used siRNA or neutralising antibodies for FGFR1 and showed a decrease in the proliferation rate of MSCs. Furthermore, *FGFR1* and *FGFR3* are expressed by human MSCs at equal mRNA expression levels (Correa *et al*., 2015). When the MSCs are primed by FGF2, they increase chondrogenic

lineage-specific transcription factors; SOX9 and PPARγ2 (Handorf and Li, 2011, Correa *et al*., 2015) but which receptor this is mediated through is unknown.

I did not have time to do the next step of the experiment which would have been to use CRISPR/CAS9 to knockdown FGFR1 or FGFR3 in MSCs and then use them for the chondrogenic disc assay to see which receptor is important for driving chondrogenesis. I suspect they are both important but at different stages of chondrogenesis as exhibited by their differential expression during endochondral ossification (Ornitz and Marie, 2015). Also, to find out which receptor is important for cartilage repair, it would be useful to use a mouse which has a conditional KO of FGFR1 or FGFR3 in adult articular cartilage, to perform the repair model on.

6 Final discussion

The question of whether cartilage repairs after mechanical injury is one that has divided the OA community for many years. Many of the textbooks define cartilage as one of the few tissues that does not regenerate after injury. This has been attributed to lack of blood supply and very slow turnover of the principle collagen (type II), which has a purported half-life of >100 years. This was initially shown in *in vitro* and animal models, and more recently in human tissue by making use of the atomic bomb pulse method (Heinemeier *et al*., 2016). In this study Heinemeier *et al* (2016) looked at the levels of ^{14}C in the cartilage of people born around the time of the atomic bomb testing around the 1950s and 1960s (where atmospheric levels of ^{14}C were a lot higher) to assess turnover. Tissues that have a high turnover and are constantly renewed will contain amounts of ^{14}C close to the current atmospheric levels of ^{14}C, whereas tissues with very slow turnover will retain ^{14}C from the years close to the formation of the tissue. The ^{14}C levels observed in cartilage collagen showed that no replacement of collagen occurred after skeletal maturity and was not affected by the induction of OA (Heinemeier *et al*., 2016).

Evidence that human cartilage can repair comes from many sources. Spontaneous repair has been seen following focal cartilage lesions in young individuals following sporting injuries (Dell'Accio and Vincent, 2010). It is established that during autologous chondrocyte implantation, the non-loaded site from which cartilage is removed to obtain autologous chondrocytes, always repairs spontaneously. Moreover, surgical procedures that off-load the joint such as high tibial osteotomy (where a wedge of bone is removed to realign the joint) leads to clinical improvement and apparent cartilage regrowth. A similar observation has been made by surgical joint distraction, whereby an external fixator is attached to the

opposing bones of the joint and is used to separate them by a few millimetres, which off-loads the joint. When applied for just 2 months to the knee joints of young patients (<65 years) with severe knee OA, there is long-lasting clinical and structural improvement as seen by increased joint space width on MRI and reduced pain scores (Intema *et al*., 2011, Wiegant *et al*., 2013, van der Woude *et al*., 2017, Jansen *et al*., 2018).

Interestingly work from our laboratory in which synovial fluid was analysed from 20 patients whose joint was undergoing distraction for severe knee OA, showed that increasing levels of FGF2 and TGFβ over the distraction period (6 weeks) was associated with a significantly higher chance of clinical success (reduction in pain and better function). (Vincent, in preparation).

Taken together, the human studies argue that cartilage regeneration is feasible and can be enhanced by improving the mechanical environment of the joint. The question remains whether it might be possible to harness the pro-regeneration effects of a growth factor such as FGF2 to drive repair. Indeed, intraarticular injection of a truncated recombinant FGF18 (named Sprifermin) has already been used in a phase II clinical study to induce the repair of osteoarthritic tissue. (Merck Serono, www.merckgroup.com/en/news/acr-full-data-release-04-11-2017.html). The report confirms statistical significance between Sprifermin-treated and placebo groups in the increase of cartilage thickness (as observed by increased joint space on MRI analysis). Injection of FGF2 however is not a feasible treatment for OA/cartilage regeneration in humans as it can bind to and activate all FGFR isoforms and has been shown to have varying roles within the joint tissue. Also, the controversy around FGF2's opposing effects in cartilage biology make it an unattractive candidate to pharmaceutical companies. If one can understand the signalling responses of FGF2 with

each FGFR in cartilage, then perhaps a downstream molecule could be exposed as a potential drug target.

During this thesis I was unable to determine if there was a difference in the downstream signalling of the FGFRs in response to injury and release of FGF2. There were a number of limitations across this study. The porcine data exhibited some variability, for example the time at which *FGFR1* expression decreased was either at 24 h or 48 h post explantation; receptor ratios were variable from 2.5-fold higher *FGFR1* than *FGFR3* to equal levels; porcine chondrocytes had variable responses to stimulation with FGF ligands. Therefore, although easily obtainable, porcine articular cartilage may not have been the best tissue to study FGF-signalling as the regulations for trotters are not as tight as those for mice. For example, there was variability in the age of the trotters; the annotations of the genome are incomplete; and antibodies for proteins may not be as specific due to differing glycosylation/other posttranslational modifications. As not many people work in porcine tissue this information is hard to come by and so these unknowns influence the conclusions made.

The experiments presented here were also carried out in different species and tissues types. mRNA expression changes to injury were carried out in porcine metacarpophalangeal joints or murine hip explants; protein signalling experiments were in porcine metacarpophalangeal isolated primary chondrocytes; repair experiments were in murine knees and MSCs were derived from murine epididymal fat pad or human bone marrow. Therefore, trying to piece together the injury and signalling events in these experiments may not be the best approach to understanding FGF2 signalling in cartilage injury and repair. We do not know how comparable hand cartilage is to that of a knee or a hip. Indeed,

the incidence of OA is different in the different tissue types and different joints have different loads exerted through them. As FGF2 has already been shown to be mechanically sensitive (Vincent *et al*., 2007), the signalling is likely to be different in these tissue types. Moreover, the idea that there may be a species difference in the signalling of FGF2 has already been suggested by Li *et al* (2012). This could be why some of the porcine and murine data do not correlate (i.e. down-regulation of FGFRs in porcine tissue but increase in expression in murine tissue in response to injury). Another reason for the difference in FGF signalling across tissue types and species could be that the FGFR/FGF ligands/HS components are different. Therefore, it would be beneficial to collect data on the different types of HS/FGFR/FGF ligands present in different cartilage types perhaps via a proteomics approach, in order to gauge any differences that could affect signalling.

Another limitation throughout the study was the validity of the mutant ligands. With hindsight it was naïve to assume that these ligands would work in primary porcine articular chondrocytes as they did in the cell line they were tested on. As FGF18-V1 did not show any response in regulating any of the genes tested, or strong phosphorylation of the proteins tested, we cannot be sure that the ligand was present. As the potency of FGF2-V2 was dampened both in the phosphorylation of proteins tested and regulation of the genes tested, the concentration of both mutant ligands is questionable. To address this issue dot blots should have been carried out with a protein standard to determine protein concentrations. Also, a sliver stain would be ideal for smaller concentrations as it is more sensitive. (This was not possible as there was not enough protein left over from the aliquots made available to us). Moreover, DTT had to be added to the ligands in order to detect ERK phosphorylation by FGF2-V2, but addition to FGF18-V1 did not affect its ERK

phosphorylation, which further questions the concentration of the ligand. However a range of DTT concentrations were not tested, so perhaps the bonds between FGF18-V1 monomers were stronger than those of FGF2-V2. Without information on how the ligands were mutated/ information on their structure, it is difficult to assess this. Furthermore, the selective nature of FGFs for specific FGFRs that is frequently quoted in the literature, have only been measured in cell lines expressing only one type of receptor and using rate of proliferation as a biological readout of activity (Ornitz *et al*., 1996, Zhang *et al*., 2006). It is well known that FGF signalling through FGFRs does not always promote proliferation in all types of cells. Therefore, the FGF/FGFR selectivity may not hold true for all cell types. Consequently, ligand-receptor selectivity should be assessed for the particular cell-type one is working on; though gauging what the biological readout should be is another challenge. This is particularly challenging for FGF-signalling in adult chondrocytes, as we do not yet know the precise function of FGF/FGFRs (most of the functions studied to date are in the developmental processes).

Although injury responses in these experiments showed changes in the expression of mRNA, this does not necessarily mean that the protein levels on the cell surface were affected in the same way. The dynamics of receptor internalisation could be further explored using cells with fluorescently labelled FGFRs, stimulating with FGF2 and examining internalisation with live-cell confocal microscopy. This would also allow comparison of the half-life of different FGFRs on the cell surface in response to FGF2.

The MSC data was mainly limited by its preliminary nature. However, the data correlate with that already in the literature; that FGF2 enhances the migratory capability of MSCs and inhibits chondrogenesis when added in long term culture. Although I have demonstrated

that FGF2 is important for cartilage repair through the *in vivo* model, understanding how this effect occurs needs further study within the *in vivo* system rather than an *in vitro* system. This is because we do not know if the cells used in an *in vitro* system are the same as those in an *in vivo* system and new subsets of MSCs are constantly emerging. Therefore, it is hard to determine if an MSC from the bone marrow is the same as that from fat tissue or synovium (or any other source). Further studies using KO mice in which the FGFRs are conditionally knocked out in either adult articular cartilage or MSCs would be beneficial in determining which FGFR is important for repair and in which cell type. Another type of repair model is also in the process of being validated, in which the joint is not required to be opened to create the cartilage defect. This bypasses the post-surgical problems of patella dislocations and wound openings and reduces recovery time (communication with Dell'Accio).

Considering the limitations of the experiments in presented here, I propose the following schematic of the possible interactions regarding the role of FGF2 in cartilage related repair. When articular cartilage is damaged, there is a release of certain molecules from extracellular pools including FGF2 and latent TGFβ but also HDGF (Tang *et al*., 2018, Vincent *et al*., 2002, Vincent *et al*., 2007) (Figure 6.1, 1). FGF2 binds to an FGFR on the surface of chondrocytes, which is likely to be FGFR1 as demonstrated by Yan *et al* (2011). This leads to autophosphorylation of the FGFRs to mediate an intracellular signalling response, most notably the phosphorylation of ERK1/2 but also phosphorylation of AKT (and its substrates) and P70 S6 kinase as demonstrated in chapter 4. The signalling leads to changes in transcription, which alters the expression of FGFRs so that there is greater expression of *FGFR1* than *FGFR3* (demonstrated in chapter 3). This may lead to changes in the protein

expression of these receptors on the cell surface. Higher levels of FGFR1 on the cell surface are likely to mediate catabolic responses (suggested by the fact that *Fgfr1* KO leads to protection against cartilage degradation (Weng *et al*., 2012)). This response may be responsible for the loss of cellular content and proteoglycan staining observed early in repair near the defect site (Shapiro *et al*., 1993, Eltawil *et al.*, 2009) (Figure 6.1, 2). FGF2 released upon injury may diffuse to MSCs in the vicinity such as those in bone marrow (Shapiro *et al*., 1993) or synovium (Roelofs *et al*., 2017) and bind to FGFRs on the cell surface. This leads to cellular responses (unknown) that can increase the motility of MSCs (as demonstrated in chapter 5) and may prime them for chondrogenesis (Tsutsumi *et al*., 2001, Solchaga *et al*., 2005) (Figure 6.1, 3). When MSCs reach the injured site, latent TGFβ is activated and binds to TGFβ receptors on the surface of MSCs. This triggers the cells to differentiate into chondrocytes by upregulating *SOX9* and *COL2* expression (Figure 6.1, 4). As these cells differentiate they produce an ECM to regenerate cartilage in the defect (Figure 6.1, 5).

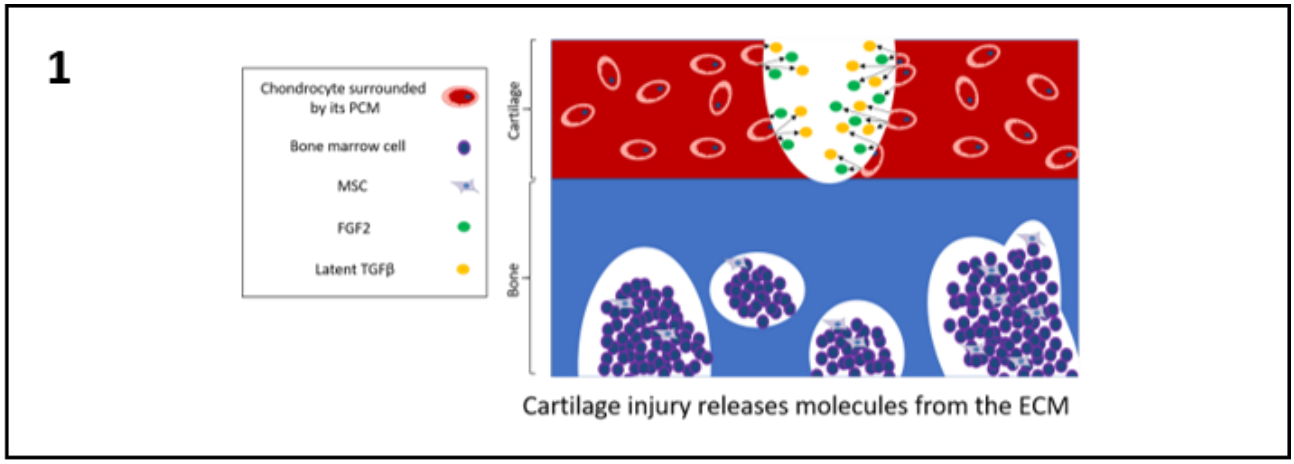
1
Chondrocyte surrounded by its PCM
Bone marrow cell
MSC
FGF2
Latent TGFβ
Cartilage
Bone
Cartilage injury releases molecules from the ECM

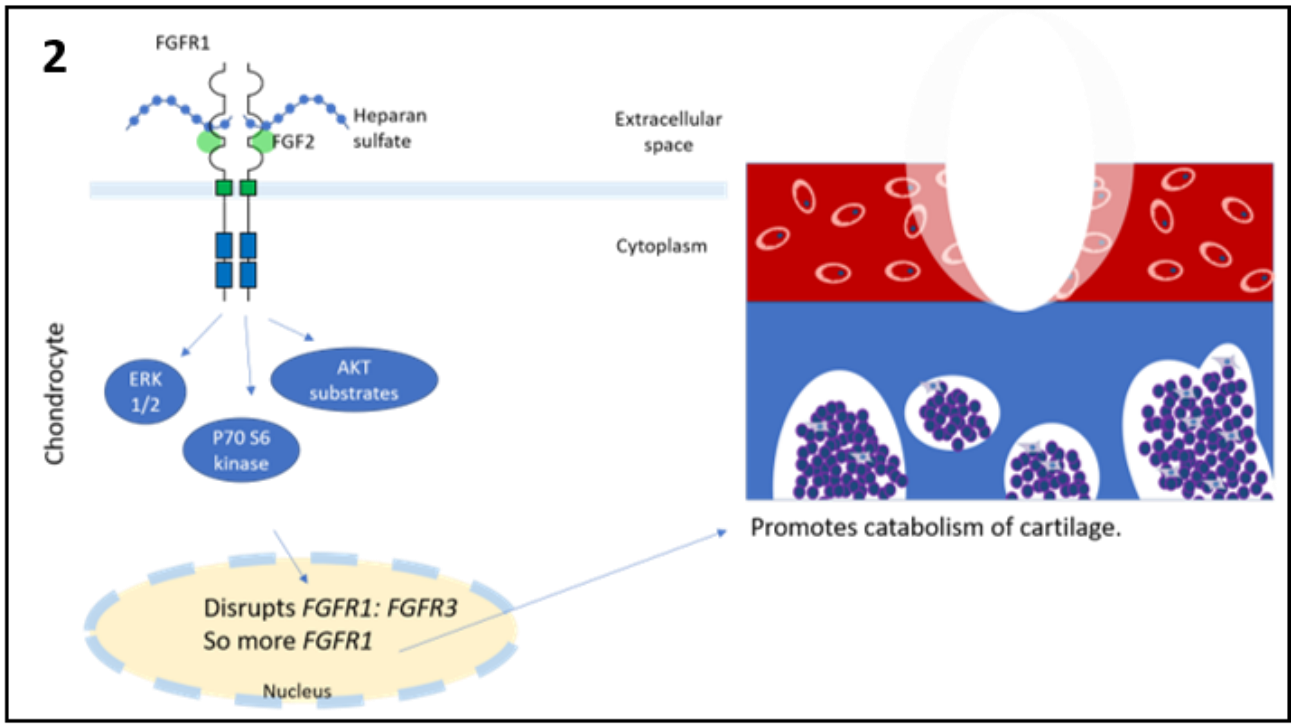
2
FGFR1
Heparan sulfate
FGF2
Extracellular space
Cytoplasm
Chondrocyte
ERK 1/2
AKT substrates
P70 S6 kinase
Disrupts FGFR1: FGFR3
So more FGFR1
Nucleus
Promotes catabolism of cartilage.

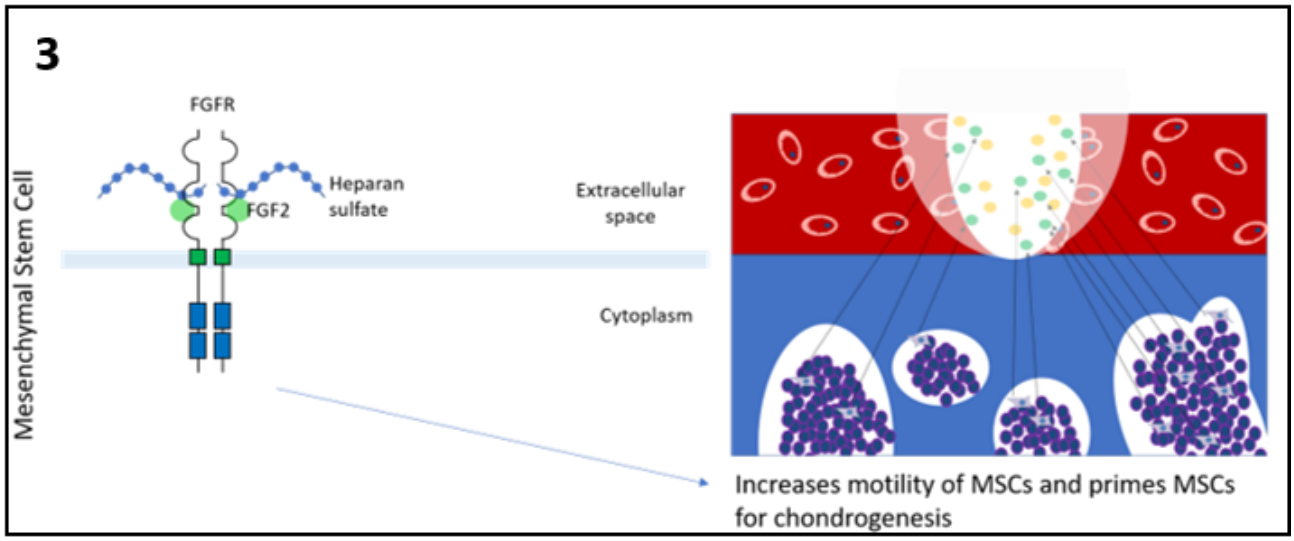
3
FGFR
Heparan sulfate
FGF2
Extracellular space
Cytoplasm
Mesenchymal Stem Cell
Increases motility of MSCs and primes MSCs for chondrogenesis

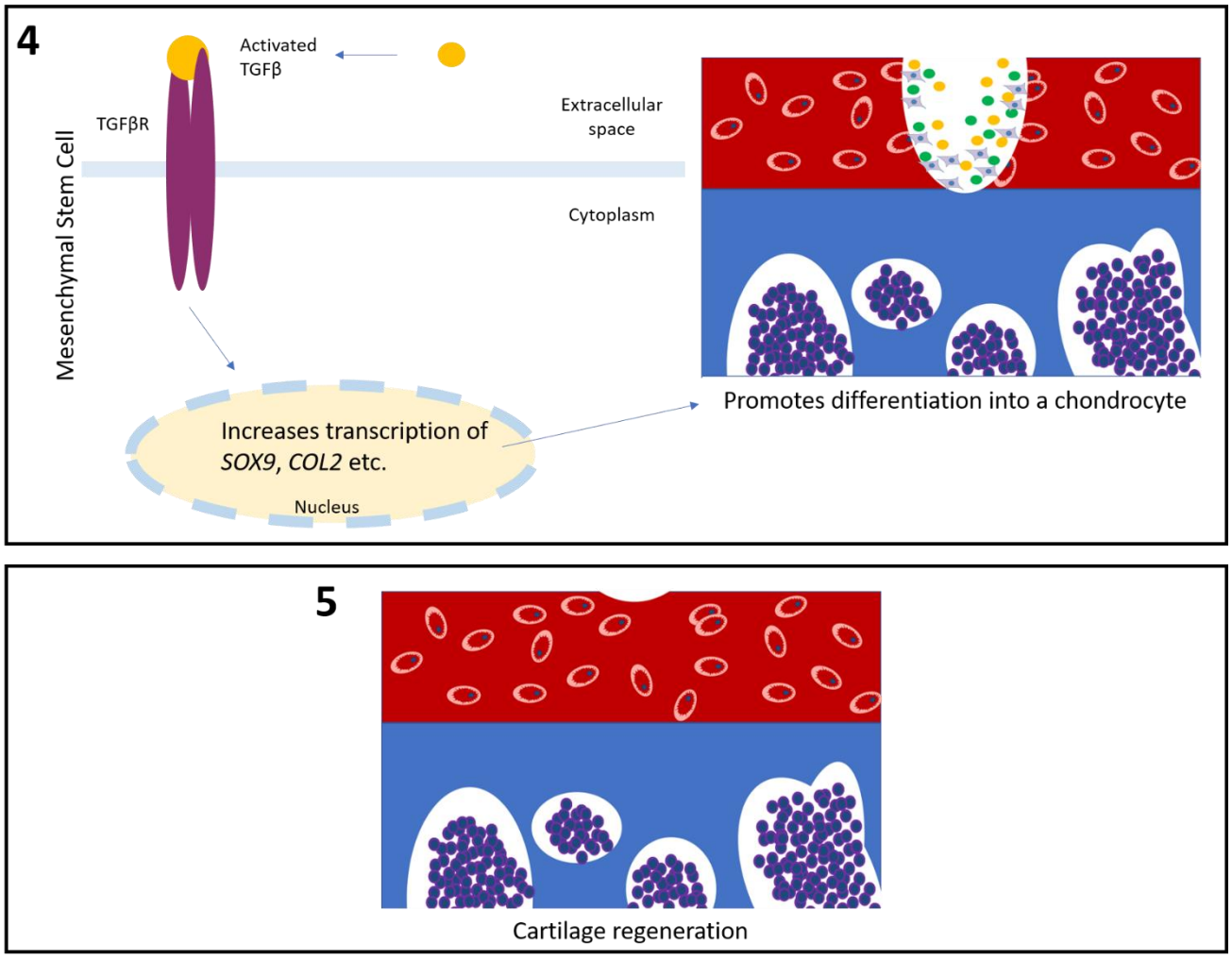

Figure 6.1: Schematic of FGF2 in OA-related repair
(1) When articular cartilage is damaged, molecules including FGF2 and latent TGFβ are released from the extracellular matrix. (2) FGF2 binds to an FGFR on the surface of chondrocytes, which is most likely FGFR1. This leads to autophosphorylation of the FGFRs to mediate an intracellular signalling response, most notably the phosphorylation of ERK1/2 but also phosphorylation of AKT (and its substrates) and P70 S6 kinase. The signalling leads to changes in transcription, which alters the expression of FGFRs so that there is greater expression of *FGFR1* than *FGFR3*, which may lead to changes in the protein expression of these receptors on the cell surface. Higher levels of FGFR1 on the cell surface are likely to mediate catabolic responses which may be responsible for the loss of cellular content and proteoglycan staining observed early in repair near the defect site. (3) FGF2 released upon injury may diffuse to MSCs in the vicinity such as those in bone marrow and bind to FGFRs on the cell surface. This leads to cellular responses (unknown) that can increase the motility of MSCs and may prime them for chondrogenesis. (4) When MSCs reach the injured site, latent TGFβ is activated and binds to TGFβ receptors on the surface of MSC. This triggers the cells to differentiate into chondrocytes by upregulating *SOX9* and *COL2* expression. (5) As MSCs differentiate they produce an ECM to regenerate the cartilage in the defect.

FGF signalling has been shown to be important for regeneration of many different types of tissues, with the regeneration process akin to developmental processes. Most of the reparative functions of FGFs have been shown to be mediated by paracrine-acting FGFs, (those that do not diffuse far from their site of origin) and their roles have been reviewed expertly by Maddaluno *et al* (2017). *Fgf2*$^{-/-}$ and over expression models have been used extensively to study the role of FGF2 in repair and have demonstrated that FGF2 is of particular importance in the repair of nerves (Jungnickel *et al*., 2006, Goldshmit *et al*., 2014, Seitz *et al*., 2011), cardiac tissue (Virag *et al*., 2007, House *et al*., 2015), bones (Hurley *et al.*, 2016) and skin wound healing (Ortega *et al*., 1998). Some of the common key findings included, affecting proliferation of cells within the repairing tissues and signalling through FGFR1 or FGFR2 (Maddaluno *et al*., 2017*)*. In mouse digit regeneration, *Fgf2* expression is correlated with that of *Fgfr1* and ERK1/2 (Takeo *et al*., 2013). Enhanced *Fgf2* expression is abrogated after denervation and the tissue does not regenerate; reflecting the importance of FGF2 mechanosensitive properties in the role of digit regeneration. FGF2 affects wound angiogenesis through effects on FGFR1 and FGFR2 as deletion of these receptors in endothelial cells and hematopoietic cells affects neo-vascularisation and thus delays repair (Maddaluno *et al*., 2017). Also antagonising FGF signalling, through deletions of SRPY proteins has also been shown to aid repair in brain injury models in a similar way to overexpressing FGF signals (Goldshmit e*t al*., 2014, Goldshmit *et al*., 2015). Therefore in order to better understand repair of articular cartilage, future experiments should also focus on signalling dynamics not tested in this thesis such as the expression of inhibitory proteins such as SEF, SPRY and DUSP6, as well as endocytosis pathways and receptor translocations.

7 Chapter 7: References

ABBASZADE, I., LIU, R. Q., YANG, F., ROSENFELD, S. A., ROSS, O. H., LINK, J. R., ELLIS, D. M., TORTORELLA, M. D., PRATTA, M. A., HOLLIS, J. M., WYNN, R., DUKE, J. L., GEORGE, H. J., HILLMAN, M. C., MURPHY, K., WISWALL, B. H., COPELAND, R. A., DECICCO, C. P., BRUCKNER, R., NAGASE, H., ITOH, Y., NEWTON, R. C., MAGOLDA, R. L., TRZASKOS, J. M. & BURN, T. C. 1999. Cloning and characterization of ADAMTS11, an aggrecanase from the ADAMTS family. *J Biol Chem,* 274**,** 23443-50.

ANDERSON, J., BURNS, H. D., ENRIQUEZ-HARRIS, P., WILKIE, A. O. & HEATH, J. K. 1998. Apert syndrome mutations in fibroblast growth factor receptor 2 exhibit increased affinity for FGF ligand. *Hum Mol Genet,* 7**,** 1475-83.

ANRAKU, Y., MIZUTA, H., SEI, A., KUDO, S., NAKAMURA, E., SENBA, K. & HIRAKI, Y. 2009. Analyses of early events during chondrogenic repair in rat full-thickness articular cartilage defects. *J Bone Miner Metab,* 27**,** 272-86.

ANTONSSON, P., HEINEGÅRD, D. & OLDBERG, A. 1991. Posttranslational modifications of fibromodulin. *J Biol Chem,* 266**,** 16859-61.

ARMELIN, H. A. 1973. Pituitary extracts and steroid hormones in the control of 3T3 cell growth. *Proc Natl Acad Sci U S A,* 70**,** 2702-6.

ARNAUD, E., TOURIOL, C., BOUTONNET, C., GENSAC, M. C., VAGNER, S., PRATS, H. & PRATS, A. C. 1999. A new 34-kilodalton isoform of human fibroblast growth factor 2 is cap dependently synthesized by using a non-AUG start codon and behaves as a survival factor. *Mol Cell Biol,* 19**,** 505-14.

BATTAGLIA, C., MAYER, U., AUMAILLEY, M. & TIMPL, R. 1992. Basement-membrane heparan sulfate proteoglycan binds to laminin by its heparan sulfate chains and to nidogen by sites in the protein core. *Eur J Biochem,* 208**,** 359-66.

BEAUVAIS, D. M. & RAPRAEGER, A. C. 2004. Syndecans in tumor cell adhesion and signaling. *Reprod Biol Endocrinol,* 2**,** 3.

BELLOT, F., CRUMLEY, G., KAPLOW, J. M., SCHLESSINGER, J., JAYE, M. & DIONNE, C. A. 1991. Ligand-induced transphosphorylation between different FGF receptors. *EMBO J,* 10**,** 2849-54.

BENGTSSON, E., MÖRGELIN, M., SASAKI, T., TIMPL, R., HEINEGÅRD, D. & ASPBERG, A. 2002. The leucine-rich repeat protein PRELP binds perlecan and collagens and may function as a basement membrane anchor. *J Biol Chem,* 277**,** 15061-8.

BI, W., DENG, J. M., ZHANG, Z., BEHRINGER, R. R. & DE CROMBRUGGHE, B. 1999. Sox9 is required for cartilage formation. *Nat Genet,* 22**,** 85-9.

BIANCO, P., FISHER, L. W., YOUNG, M. F., TERMINE, J. D. & ROBEY, P. G. 1990. Expression and localization of the two small proteoglycans biglycan and decorin in developing human skeletal and non-skeletal tissues. *J Histochem Cytochem,* 38**,** 1549-63.

BIGG, H. F., SHI, Y. E., LIU, Y. E., STEFFENSEN, B. & OVERALL, C. M. 1997. Specific, high affinity binding of tissue inhibitor of metalloproteinases-4 (TIMP-4) to the COOH-terminal hemopexin-like domain of human gelatinase A. TIMP-4 binds progelatinase A and the COOH-terminal domain in a similar manner to TIMP-2. *J Biol Chem,* 272**,** 15496-500.

BLAIN, E. J., GILBERT, S. J., WARDALE, R. J., CAPPER, S. J., MASON, D. J. & DUANCE, V. C. 2001. Up-regulation of matrix metalloproteinase expression and activation following

cyclical compressive loading of articular cartilage in vitro. *Arch Biochem Biophys,* 396**,** 49-55.

BRENT, A. E. & TABIN, C. J. 2004. FGF acts directly on the somitic tendon progenitors through the Ets transcription factors Pea3 and Erm to regulate scleraxis expression. *Development,* 131**,** 3885-96.

BREW, K., DINAKARPANDIAN, D. & NAGASE, H. 2000. Tissue inhibitors of metalloproteinases: evolution, structure and function. *Biochim Biophys Acta,* 1477**,** 267-83.

BRUNET, L. J., MCMAHON, J. A., MCMAHON, A. P. & HARLAND, R. M. 1998. Noggin, cartilage morphogenesis, and joint formation in the mammalian skeleton. *Science,* 280**,** 1455-7.

BUGLER, B., AMALRIC, F. & PRATS, H. 1991. Alternative initiation of translation determines cytoplasmic or nuclear localization of basic fibroblast growth factor. *Mol Cell Biol,* 11**,** 573-7.

BURLEIGH, A., CHANALARIS, A., GARDINER, M. D., DRISCOLL, C., BORUC, O., SAKLATVALA, J. & VINCENT, T. L. 2012. Joint immobilization prevents murine osteoarthritis and reveals the highly mechanosensitive nature of protease expression in vivo. *Arthritis Rheum,* 64**,** 2278-88.

BURTON-WURSTER, N., LUST, G. & MACLEOD, J. N. 1997. Cartilage fibronectin isoforms: in search of functions for a special population of matrix glycoproteins. *Matrix Biol,* 15**,** 441-54.

BUTLER, G. S., WILL, H., ATKINSON, S. J. & MURPHY, G. 1997. Membrane-type-2 matrix metalloproteinase can initiate the processing of progelatinase A and is regulated by the tissue inhibitors of metalloproteinases. *Eur J Biochem,* 244**,** 653-7.

CAMPER, L., HEINEGÂRD, D. & LUNDGREN-AKERLUND, E. 1997. Integrin alpha2beta1 is a receptor for the cartilage matrix protein chondroadherin. *J Cell Biol,* 138**,** 1159-67.

CARTER, E. P., FEARON, A. E. & GROSE, R. P. 2015. Careless talk costs lives: fibroblast growth factor receptor signalling and the consequences of pathway malfunction. *Trends Cell Biol,* 25**,** 221-33.

CHIA, S. L., SAWAJI, Y., BURLEIGH, A., MCLEAN, C., INGLIS, J., SAKLATVALA, J. & VINCENT, T. 2009. Fibroblast growth factor 2 is an intrinsic chondroprotective agent that suppresses ADAMTS-5 and delays cartilage degradation in murine osteoarthritis. *Arthritis Rheum,* 60**,** 2019-27.

CHONG, K. W., CHANALARIS, A., BURLEIGH, A., JIN, H., WATT, F. E., SAKLATVALA, J. & VINCENT, T. L. 2013. Fibroblast growth factor 2 drives changes in gene expression following injury to murine cartilage in vitro and in vivo. *Arthritis Rheum,* 65**,** 2346-55.

CHUMA, H., MIZUTA, H., KUDO, S., TAKAGI, K. & HIRAKI, Y. 2004. One day exposure to FGF-2 was sufficient for the regenerative repair of full-thickness defects of articular cartilage in rabbits. *Osteoarthritis Cartilage,* 12**,** 834-42.

COLE, A. G. 2011. A review of diversity in the evolution and development of cartilage: the search for the origin of the chondrocyte. *Eur Cell Mater,* 21**,** 122-9.

COLVIN, J. S., BOHNE, B. A., HARDING, G. W., MCEWEN, D. G. & ORNITZ, D. M. 1996. Skeletal overgrowth and deafness in mice lacking fibroblast growth factor receptor 3. *Nat Genet,* 12**,** 390-7.

CORREA, D., SOMOZA, R. A., LIN, P., GREENBERG, S., ROM, E., DUESLER, L., WELTER, J. F., YAYON, A. & CAPLAN, A. I. 2015. Sequential exposure to fibroblast growth factors

(FGF) 2, 9 and 18 enhances hMSC chondrogenic differentiation. *Osteoarthritis Cartilage,* 23**,** 443-53.
CRAIG, F. M., BAYLISS, M. T., BENTLEY, G. & ARCHER, C. W. 1990. A role for hyaluronan in joint development. *J Anat,* 171**,** 17-23.
DAVIS, M. G., ZHOU, M., ALI, S., COFFIN, J. D., DOETSCHMAN, T. & DORN, G. W. 1997. Intracrine and autocrine effects of basic fibroblast growth factor in vascular smooth muscle cells. *J Mol Cell Cardiol,* 29**,** 1061-72.
DE POLLACK, C., RENIER, D., HOTT, M. & MARIE, P. J. 1996. Increased bone formation and osteoblastic cell phenotype in premature cranial suture ossification (craniosynostosis). *J Bone Miner Res,* 11**,** 401-7.
DEL PICCOLO, N., SARABIPOUR, S. & HRISTOVA, K. 2017. A New Method to Study Heterodimerization of Membrane Proteins and Its Application to Fibroblast Growth Factor Receptors. *J Biol Chem,* 292**,** 1288-1301.
DELEHEDDE, M., LYON, M., GALLAGHER, J. T., RUDLAND, P. S. & FERNIG, D. G. 2002. Fibroblast growth factor-2 binds to small heparin-derived oligosaccharides and stimulates a sustained phosphorylation of p42/44 mitogen-activated protein kinase and proliferation of rat mammary fibroblasts. *Biochem J,* 366**,** 235-44.
DELEHEDDE, M., SEVE, M., SERGEANT, N., WARTELLE, I., LYON, M., RUDLAND, P. S. & FERNIG, D. G. 2000. Fibroblast growth factor-2 stimulation of p42/44MAPK phosphorylation and IkappaB degradation is regulated by heparan sulfate/heparin in rat mammary fibroblasts. *J Biol Chem,* 275**,** 33905-10.
DELEZOIDE, A. L., BENOIST-LASSELIN, C., LEGEAI-MALLET, L., LE MERRER, M., MUNNICH, A., VEKEMANS, M. & BONAVENTURE, J. 1998. Spatio-temporal expression of FGFR 1, 2 and 3 genes during human embryo-fetal ossification. *Mech Dev,* 77**,** 19-30.
DELISE, A. M., FISCHER, L. & TUAN, R. S. 2000. Cellular interactions and signaling in cartilage development. *Osteoarthritis Cartilage,* 8**,** 309-34.
DELL'ACCIO, F. & VINCENT, T. L. 2010. Joint surface defects: clinical course and cellular response in spontaneous and experimental lesions. *Eur Cell Mater,* 20**,** 210-7.
DENG, C., WYNSHAW-BORIS, A., ZHOU, F., KUO, A. & LEDER, P. 1996. Fibroblast growth factor receptor 3 is a negative regulator of bone growth. *Cell,* 84**,** 911-21.
DENG, C. X., WYNSHAW-BORIS, A., SHEN, M. M., DAUGHERTY, C., ORNITZ, D. M. & LEDER, P. 1994. Murine FGFR-1 is required for early postimplantation growth and axial organization. *Genes Dev,* 8**,** 3045-57.
DOHERTY, P. & WALSH, F. S. 1996. CAM-FGF receptor interactions: a model for axonal growth. *Mol Cell Neurosci,* 8**,** 99-111.
DOMBROWSKI, C., HELLEDIE, T., LING, L., GRÜNERT, M., CANNING, C. A., JONES, C. M., HUI, J. H., NURCOMBE, V., VAN WIJNEN, A. J. & COOL, S. M. 2013. FGFR1 signaling stimulates proliferation of human mesenchymal stem cells by inhibiting the cyclin-dependent kinase inhibitors p21(Waf1) and p27(Kip1). *Stem Cells,* 31**,** 2724-36.
DOWTHWAITE, G. P., EDWARDS, J. C. & PITSILLIDES, A. A. 1998. An essential role for the interaction between hyaluronan and hyaluronan binding proteins during joint development. *J Histochem Cytochem,* 46**,** 641-51.
DRISCOLL, C., CHANALARIS, A., KNIGHTS, C., ISMAIL, H., SACITHARAN, P. K., GENTRY, C., BEVAN, S. & VINCENT, T. L. 2016. Nociceptive Sensitizers Are Regulated in Damaged Joint Tissues, Including Articular Cartilage, When Osteoarthritic Mice Display Pain Behavior. *Arthritis Rheumatol,* 68**,** 857-67.

DÜRR, J., LAMMI, P., GOODMAN, S. L., AIGNER, T. & VON DER MARK, K. 1996. Identification and immunolocalization of laminin in cartilage. *Exp Cell Res,* 222**,** 225-33.

EKEROT, M., STAVRIDIS, M. P., DELAVAINE, L., MITCHELL, M. P., STAPLES, C., OWENS, D. M., KEENAN, I. D., DICKINSON, R. J., STOREY, K. G. & KEYSE, S. M. 2008. Negative-feedback regulation of FGF signalling by DUSP6/MKP-3 is driven by ERK1/2 and mediated by Ets factor binding to a conserved site within the DUSP6/MKP-3 gene promoter. *Biochem J,* 412**,** 287-98.

ELLMAN, M. B., YAN, D., AHMADINIA, K., CHEN, D., AN, H. S. & IM, H. J. 2013. Fibroblast growth factor control of cartilage homeostasis. *J Cell Biochem,* 114**,** 735-42.

ELLSWORTH, J. L., BERRY, J., BUKOWSKI, T., CLAUS, J., FELDHAUS, A., HOLDERMAN, S., HOLDREN, M. S., LUM, K. D., MOORE, E. E., RAYMOND, F., REN, H., SHEA, P., SPRECHER, C., STOREY, H., THOMPSON, D. L., WAGGIE, K., YAO, L., FERNANDES, R. J., EYRE, D. R. & HUGHES, S. D. 2002. Fibroblast growth factor-18 is a trophic factor for mature chondrocytes and their progenitors. *Osteoarthritis Cartilage,* 10**,** 308-20.

ELTAWIL, N. M., DE BARI, C., ACHAN, P., PITZALIS, C. & DELL'ACCIO, F. 2009. A novel in vivo murine model of cartilage regeneration. Age and strain-dependent outcome after joint surface injury. *Osteoarthritis Cartilage,* 17**,** 695-704.

FISHER, L. W., TERMINE, J. D. & YOUNG, M. F. 1989. Deduced protein sequence of bone small proteoglycan I (biglycan) shows homology with proteoglycan II (decorin) and several nonconnective tissue proteins in a variety of species. *J Biol Chem,* 264**,** 4571-6.

FLORKIEWICZ, R. Z., SHIBATA, F., BARANKIEWICZ, T., BAIRD, A., GONZALEZ, A. M., FLORKIEWICZ, E. & SHAH, N. 1991. Basic fibroblast growth factor gene expression. *Ann N Y Acad Sci,* 638**,** 109-26.

FRANCIS-WEST, P. H., PARISH, J., LEE, K. & ARCHER, C. W. 1999. BMP/GDF-signalling interactions during synovial joint development. *Cell Tissue Res,* 296**,** 111-9.

GALVIN, B. D., HART, K. C., MEYER, A. N., WEBSTER, M. K. & DONOGHUE, D. J. 1996. Constitutive receptor activation by Crouzon syndrome mutations in fibroblast growth factor receptor (FGFR)2 and FGFR2/Neu chimeras. *Proc Natl Acad Sci U S A,* 93**,** 7894-9.

GLASSON, S. S., ASKEW, R., SHEPPARD, B., CARITO, B., BLANCHET, T., MA, H. L., FLANNERY, C. R., PELUSO, D., KANKI, K., YANG, Z., MAJUMDAR, M. K. & MORRIS, E. A. 2005. Deletion of active ADAMTS5 prevents cartilage degradation in a murine model of osteoarthritis. *Nature,* 434**,** 644-8.

GLASSON, S. S., ASKEW, R., SHEPPARD, B., CARITO, B. A., BLANCHET, T., MA, H. L., FLANNERY, C. R., KANKI, K., WANG, E., PELUSO, D., YANG, Z., MAJUMDAR, M. K. & MORRIS, E. A. 2004. Characterization of and osteoarthritis susceptibility in ADAMTS-4-knockout mice. *Arthritis Rheum,* 50**,** 2547-58.

GOETZ, R., BEENKEN, A., IBRAHIMI, O. A., KALININA, J., OLSEN, S. K., ELISEENKOVA, A. V., XU, C., NEUBERT, T. A., ZHANG, F., LINHARDT, R. J., YU, X., WHITE, K. E., INAGAKI, T., KLIEWER, S. A., YAMAMOTO, M., KUROSU, H., OGAWA, Y., KURO-O, M., LANSKE, B., RAZZAQUE, M. S. & MOHAMMADI, M. 2007. Molecular insights into the klotho-dependent, endocrine mode of action of fibroblast growth factor 19 subfamily members. *Mol Cell Biol,* 27**,** 3417-28.

GOLDFARB, M. 2005. Fibroblast growth factor homologous factors: evolution, structure, and function. *Cytokine Growth Factor Rev,* 16**,** 215-20.

GOLDSHMIT, Y., FRISCA, F., KASLIN, J., PINTO, A. R., TANG, J. K., PÉBAY, A., PINKAS-KRAMARSKI, R. & CURRIE, P. D. 2015. Decreased anti-regenerative effects after spinal cord injury in spry4-/- mice. *Neuroscience,* 287**,** 104-12.

GOLDSHMIT, Y., FRISCA, F., PINTO, A. R., PÉBAY, A., TANG, J. K., SIEGEL, A. L., KASLIN, J. & CURRIE, P. D. 2014. Fgf2 improves functional recovery-decreasing gliosis and increasing radial glia and neural progenitor cells after spinal cord injury. *Brain Behav,* 4**,** 187-200.

GOSPODAROWICZ, D. 1975. Purification of a fibroblast growth factor from bovine pituitary. *J Biol Chem,* 250**,** 2515-20.

GRUBER, J., VINCENT, T. L., HERMANSSON, M., BOLTON, M., WAIT, R. & SAKLATVALA, J. 2004. Induction of interleukin-1 in articular cartilage by explantation and cutting. *Arthritis Rheum,* 50**,** 2539-46.

GUILAK, F., MEYER, B. C., RATCLIFFE, A. & MOW, V. C. 1994. The effects of matrix compression on proteoglycan metabolism in articular cartilage explants. *Osteoarthritis Cartilage,* 2**,** 91-101.

GUO, X., DAY, T. F., JIANG, X., GARRETT-BEAL, L., TOPOL, L. & YANG, Y. 2004. Wnt/beta-catenin signaling is sufficient and necessary for synovial joint formation. *Genes Dev,* 18**,** 2404-17.

HAJIHOSSEINI, M. K. & HEATH, J. K. 2002. Expression patterns of fibroblast growth factors-18 and -20 in mouse embryos is suggestive of novel roles in calvarial and limb development. *Mech Dev,* 113**,** 79-83.

HAJIHOSSEINI, M. K., WILSON, S., DE MOERLOOZE, L. & DICKSON, C. 2001. A splicing switch and gain-of-function mutation in FgfR2-IIIc hemizygotes causes Apert/Pfeiffer-syndrome-like phenotypes. *Proc Natl Acad Sci U S A,* 98**,** 3855-60.

HANDORF, A. M. & LI, W. J. 2011. Fibroblast growth factor-2 primes human mesenchymal stem cells for enhanced chondrogenesis. *PLoS One,* 6**,** e22887.

HART, K. C., ROBERTSON, S. C., KANEMITSU, M. Y., MEYER, A. N., TYNAN, J. A. & DONOGHUE, D. J. 2000. Transformation and Stat activation by derivatives of FGFR1, FGFR3, and FGFR4. *Oncogene,* 19**,** 3309-20.

HARTMANN, C. & TABIN, C. J. 2001. Wnt-14 plays a pivotal role in inducing synovial joint formation in the developing appendicular skeleton. *Cell,* 104**,** 341-51.

HEINEGÅRD, D. 2009. Fell-Muir Lecture: Proteoglycans and more--from molecules to biology. *Int J Exp Pathol,* 90**,** 575-86.

HEINEGÅRD, D., LARSSON, T., SOMMARIN, Y., FRANZÉN, A., PAULSSON, M. & HEDBOM, E. 1986. Two novel matrix proteins isolated from articular cartilage show wide distributions among connective tissues. *J Biol Chem,* 261**,** 13866-72.

HEINEMEIER, K. M., SCHJERLING, P., HEINEMEIER, J., MØLLER, M. B., KROGSGAARD, M. R., GRUM-SCHWENSEN, T., PETERSEN, M. M. & KJAER, M. 2016. Radiocarbon dating reveals minimal collagen turnover in both healthy and osteoarthritic human cartilage. *Sci Transl Med,* 8**,** 346ra90.

HELLINGMAN, C. A., KOEVOET, W., KOPS, N., FARRELL, E., JAHR, H., LIU, W., BAATENBURG DE JONG, R. J., FRENZ, D. A. & VAN OSCH, G. J. 2010. Fibroblast growth factor receptors in in vitro and in vivo chondrogenesis: relating tissue engineering using adult mesenchymal stem cells to embryonic development. *Tissue Eng Part A,* 16**,** 545-56.

HOLDER, N. 1977. An experimental investigation into the early development of the chick elbow joint. *J Embryol Exp Morphol,* 39**,** 115-27.

HOMER-BOUTHIETTE, C., DOETSCHMAN, T., XIAO, L. & HURLEY, M. M. 2014. Knockout of nuclear high molecular weight FGF2 isoforms in mice modulates bone and phosphate homeostasis. *J Biol Chem,* 289**,** 36303-14.

HOPF, M., GÖHRING, W., KOHFELDT, E., YAMADA, Y. & TIMPL, R. 1999. Recombinant domain IV of perlecan binds to nidogens, laminin-nidogen complex, fibronectin, fibulin-2 and heparin. *Eur J Biochem,* 259**,** 917-25.

HOUSE, S. L., WANG, J., CASTRO, A. M., WEINHEIMER, C., KOVACS, A. & ORNITZ, D. M. 2015. Fibroblast growth factor 2 is an essential cardioprotective factor in a closed-chest model of cardiac ischemia-reperfusion injury. *Physiol Rep,* 3.

HUGHES, C. E., LITTLE, C. B., BÜTTNER, F. H., BARTNIK, E. & CATERSON, B. 1998. Differential expression of aggrecanase and matrix metalloproteinase activity in chondrocytes isolated from bovine and porcine articular cartilage. *J Biol Chem,* 273**,** 30576-82.

HUNG, I. H., YU, K., LAVINE, K. J. & ORNITZ, D. M. 2007. FGF9 regulates early hypertrophic chondrocyte differentiation and skeletal vascularization in the developing stylopod. *Dev Biol,* 307**,** 300-13.

HURLEY, M. M., ADAMS, D. J., WANG, L., JIANG, X., BURT, P. M., DU, E. & XIAO, L. 2016. Accelerated fracture healing in transgenic mice overexpressing an anabolic isoform of fibroblast growth factor 2. *J Cell Biochem,* 117**,** 599-611.

HÉBERT, J. M., BASILICO, C., GOLDFARB, M., HAUB, O. & MARTIN, G. R. 1990. Isolation of cDNAs encoding four mouse FGF family members and characterization of their expression patterns during embryogenesis. *Dev Biol,* 138**,** 454-63.

IBRAHIMI, O. A., ELISEENKOVA, A. V., PLOTNIKOV, A. N., YU, K., ORNITZ, D. M. & MOHAMMADI, M. 2001. Structural basis for fibroblast growth factor receptor 2 activation in Apert syndrome. *Proc Natl Acad Sci U S A,* 98**,** 7182-7.

IM, H. J., MUDDASANI, P., NATARAJAN, V., SCHMID, T. M., BLOCK, J. A., DAVIS, F., VAN WIJNEN, A. J. & LOESER, R. F. 2007. Basic fibroblast growth factor stimulates matrix metalloproteinase-13 via the molecular cross-talk between the mitogen-activated protein kinases and protein kinase Cdelta pathways in human adult articular chondrocytes. *J Biol Chem,* 282**,** 11110-21.

INTEMA, F., VAN ROERMUND, P. M., MARIJNISSEN, A. C., COTOFANA, S., ECKSTEIN, F., CASTELEIN, R. M., BIJLSMA, J. W., MASTBERGEN, S. C. & LAFEBER, F. P. 2011. Tissue structure modification in knee osteoarthritis by use of joint distraction: an open 1-year pilot study. *Ann Rheum Dis,* 70**,** 1441-6.

ISMAIL, H. M., DIDANGELOS, A., VINCENT, T. L. & SAKLATVALA, J. 2017. Rapid Activation of Transforming Growth Factor β-Activated Kinase 1 in Chondrocytes by Phosphorylation and K. *Arthritis Rheumatol,* 69**,** 565-575.

ISMAIL, H. M., MIOTLA-ZAREBSKA, J., TROEBERG, L., TANG, X., STOTT, B., YAMAMOTO, K., NAGASE, H., FOSANG, A. J., VINCENT, T. L. & SAKLATVALA, J. 2016. Brief Report: JNK-2 Controls Aggrecan Degradation in Murine Articular Cartilage and the Development of Experimental Osteoarthritis. *Arthritis Rheumatol,* 68**,** 1165-71.

ITO, M. M. & KIDA, M. Y. 2000. Morphological and biochemical re-evaluation of the process of cavitation in the rat knee joint: cellular and cell strata alterations in the interzone. *J Anat,* 197 Pt 4**,** 659-79.

IWATA, T., CHEN, L., LI, C., OVCHINNIKOV, D. A., BEHRINGER, R. R., FRANCOMANO, C. A. & DENG, C. X. 2000. A neonatal lethal mutation in FGFR3 uncouples proliferation and differentiation of growth plate chondrocytes in embryos. *Hum Mol Genet,* 9**,** 1603-13.

JACOB, A. L., SMITH, C., PARTANEN, J. & ORNITZ, D. M. 2006. Fibroblast growth factor receptor 1 signaling in the osteo-chondrogenic cell lineage regulates sequential steps of osteoblast maturation. *Dev Biol,* 296**,** 315-28.

JANSEN, M. P., VAN DER WEIDEN, G. S., VAN ROERMUND, P. M., CUSTERS, R. J. H., MASTBERGEN, S. C. & LAFEBER, F. P. J. G. 2018. Initial tissue repair predicts long-term clinical success of knee joint distraction as treatment for knee osteoarthritis. *Osteoarthritis Cartilage,* 26**,** 1604-1608.

JAZRAWI, L. M., ALAIA, M. J., CHANG, G., FITZGERALD, E. F. & RECHT, M. P. 2011. Advances in magnetic resonance imaging of articular cartilage. *J Am Acad Orthop Surg,* 19**,** 420-9.

JUNGNICKEL, J., HAASE, K., KONITZER, J., TIMMER, M. & GROTHE, C. 2006. Faster nerve regeneration after sciatic nerve injury in mice over-expressing basic fibroblast growth factor. *J Neurobiol,* 66**,** 940-8.

KASHIWAGI, M., TORTORELLA, M., NAGASE, H. & BREW, K. 2001. TIMP-3 is a potent inhibitor of aggrecanase 1 (ADAM-TS4) and aggrecanase 2 (ADAM-TS5). *J Biol Chem,* 276**,** 12501-4.

KATO, Y. & GOSPODAROWICZ, D. 1984. Growth requirements of low-density rabbit costal chondrocyte cultures maintained in serum-free medium. *J Cell Physiol,* 120**,** 354-63.

KATO, Y. & GOSPODAROWICZ, D. 1985. Sulfated proteoglycan synthesis by confluent cultures of rabbit costal chondrocytes grown in the presence of fibroblast growth factor. *J Cell Biol,* 100**,** 477-85.

KATO, Y. & IWAMOTO, M. 1990. Fibroblast growth factor is an inhibitor of chondrocyte terminal differentiation. *J Biol Chem,* 265**,** 5903-9.

KAVANAGH, E. & ASHHURST, D. E. 1999. Development and aging of the articular cartilage of the rabbit knee joint: Distribution of biglycan, decorin, and matrilin-1. *J Histochem Cytochem,* 47**,** 1603-16.

KAVANAGH, E., CHURCH, V. L., OSBORNE, A. C., LAMB, K. J., ARCHER, C. W., FRANCIS-WEST, P. H. & PITSILLIDES, A. A. 2006. Differential regulation of GDF-5 and FGF-2/4 by immobilisation in ovo exposes distinct roles in joint formation. *Dev Dyn,* 235**,** 826-34.

KEENE, D. R., JORDAN, C. D., REINHARDT, D. P., RIDGWAY, C. C., ONO, R. N., CORSON, G. M., FAIRHURST, M., SUSSMAN, M. D., MEMOLI, V. A. & SAKAI, L. Y. 1997. Fibrillin-1 in human cartilage: developmental expression and formation of special banded fibers. *J Histochem Cytochem,* 45**,** 1069-82.

KIM, H. J., RICE, D. P., KETTUNEN, P. J. & THESLEFF, I. 1998. FGF-, BMP- and Shh-mediated signalling pathways in the regulation of cranial suture morphogenesis and calvarial bone development. *Development,* 125**,** 1241-51.

KORVER, T. H., VAN DE STADT, R. J., KILJAN, E., VAN KAMPEN, G. P. & VAN DER KORST, J. K. 1992. Effects of loading on the synthesis of proteoglycans in different layers of anatomically intact articular cartilage in vitro. *J Rheumatol,* 19**,** 905-12.

KOUHARA, H., HADARI, Y. R., SPIVAK-KROIZMAN, T., SCHILLING, J., BAR-SAGI, D., LAX, I. & SCHLESSINGER, J. 1997. A lipid-anchored Grb2-binding protein that links FGF-receptor activation to the Ras/MAPK signaling pathway. *Cell,* 89**,** 693-702.

KOVALENKO, D., YANG, X., CHEN, P. Y., NADEAU, R. J., ZUBANOVA, O., PIGEON, K. & FRIESEL, R. 2006. A role for extracellular and transmembrane domains of Sef in Sef-mediated inhibition of FGF signaling. *Cell Signal,* 18**,** 1958-66.

KRUSIUS, T. & RUOSLAHTI, E. 1986. Primary structure of an extracellular matrix proteoglycan core protein deduced from cloned cDNA. *Proc Natl Acad Sci U S A,* 83**,** 7683-7.

KUNO, K., OKADA, Y., KAWASHIMA, H., NAKAMURA, H., MIYASAKA, M., OHNO, H. & MATSUSHIMA, K. 2000. ADAMTS-1 cleaves a cartilage proteoglycan, aggrecan. *FEBS Lett,* 478**,** 241-5.

LAFONT, J. E., TALMA, S., HOPFGARTEN, C. & MURPHY, C. L. 2008. Hypoxia promotes the differentiated human articular chondrocyte phenotype through SOX9-dependent and -independent pathways. *J Biol Chem,* 283**,** 4778-86.

LAMB, K. J., LEWTHWAITE, J. C., BASTOW, E. R. & PITSILLIDES, A. A. 2003. Defining boundaries during joint cavity formation: going out on a limb. *Int J Exp Pathol,* 84**,** 55-67.

LAMOTHE, B., YAMADA, M., SCHAEPER, U., BIRCHMEIER, W., LAX, I. & SCHLESSINGER, J. 2004. The docking protein Gab1 is an essential component of an indirect mechanism for fibroblast growth factor stimulation of the phosphatidylinositol 3-kinase/Akt antiapoptotic pathway. *Mol Cell Biol,* 24**,** 5657-66.

LAO, D. H., CHANDRAMOULI, S., YUSOFF, P., FONG, C. W., SAW, T. Y., TAI, L. P., YU, C. Y., LEONG, H. F. & GUY, G. R. 2006. A Src homology 3-binding sequence on the C terminus of Sprouty2 is necessary for inhibition of the Ras/ERK pathway downstream of fibroblast growth factor receptor stimulation. *J Biol Chem,* 281**,** 29993-30000.

LEE, W., LEDDY, H. A., CHEN, Y., LEE, S. H., ZELENSKI, N. A., MCNULTY, A. L., WU, J., BEICKER, K. N., COLES, J., ZAUSCHER, S., GRANDL, J., SACHS, F., GUILAK, F. & LIEDTKE, W. B. 2014. Synergy between Piezo1 and Piezo2 channels confers high-strain mechanosensitivity to articular cartilage. *Proc Natl Acad Sci U S A,* 111**,** E5114-22.

LEGEAI-MALLET, L., BENOIST-LASSELIN, C., DELEZOIDE, A. L., MUNNICH, A. & BONAVENTURE, J. 1998. Fibroblast growth factor receptor 3 mutations promote apoptosis but do not alter chondrocyte proliferation in thanatophoric dysplasia. *J Biol Chem,* 273**,** 13007-14.

LEGEAI-MALLET, L., BENOIST-LASSELIN, C., MUNNICH, A. & BONAVENTURE, J. 2004. Overexpression of FGFR3, Stat1, Stat5 and p21Cip1 correlates with phenotypic severity and defective chondrocyte differentiation in FGFR3-related chondrodysplasias. *Bone,* 34**,** 26-36.

LEMMON, S. K. & BRADSHAW, R. A. 1983. Purification and partial characterization of bovine pituitary fibroblast growth factor. *J Cell Biochem,* 21**,** 195-208.

LEWANDOSKI, M., SUN, X. & MARTIN, G. R. 2000. Fgf8 signalling from the AER is essential for normal limb development. *Nat Genet,* 26**,** 460-3.

LI, X., ELLMAN, M. B., KROIN, J. S., CHEN, D., YAN, D., MIKECZ, K., RANJAN, K. C., XIAO, G., STEIN, G. S., KIM, S. G., COLE, B., VAN WIJNEN, A. J. & IM, H. J. 2012. Species-specific biological effects of FGF-2 in articular cartilage: implication for distinct roles within the FGF receptor family. *J Cell Biochem,* 113**,** 2532-42.

LITTLE, C. B., BARAI, A., BURKHARDT, D., SMITH, S. M., FOSANG, A. J., WERB, Z., SHAH, M. & THOMPSON, E. W. 2009. Matrix metalloproteinase 13-deficient mice are resistant to osteoarthritic cartilage erosion but not chondrocyte hypertrophy or osteophyte development. *Arthritis Rheum,* 60**,** 3723-33.

LIU, Z., LAVINE, K. J., HUNG, I. H. & ORNITZ, D. M. 2007. FGF18 is required for early chondrocyte proliferation, hypertrophy and vascular invasion of the growth plate. *Dev Biol,* 302**,** 80-91.

LIU, Z., XU, J., COLVIN, J. S. & ORNITZ, D. M. 2002. Coordination of chondrogenesis and osteogenesis by fibroblast growth factor 18. *Genes Dev,* 16**,** 859-69.

LIZARRAGA, G., LICHTLER, A., UPHOLT, W. B. & KOSHER, R. A. 2002. Studies on the role of Cux1 in regulation of the onset of joint formation in the developing limb. *Dev Biol,* 243**,** 44-54.

LOESER, R. F., CHUBINSKAYA, S., PACIONE, C. & IM, H. J. 2005. Basic fibroblast growth factor inhibits the anabolic activity of insulin-like growth factor 1 and osteogenic protein 1 in adult human articular chondrocytes. *Arthritis Rheum,* 52**,** 3910-7.

LOMRI, A., LEMONNIER, J., HOTT, M., DE PARSEVAL, N., LAJEUNIE, E., MUNNICH, A., RENIER, D. & MARIE, P. J. 1998. Increased calvaria cell differentiation and bone matrix formation induced by fibroblast growth factor receptor 2 mutations in Apert syndrome. *J Clin Invest,* 101**,** 1310-7.

MADDALUNO, L., URWYLER, C. & WERNER, S. 2017. Fibroblast growth factors: key players in regeneration and tissue repair. *Development,* 144**,** 4047-4060.

MANNING, B. D. & CANTLEY, L. C. 2007. AKT/PKB signaling: navigating downstream. *Cell,* 129**,** 1261-74.

MATRISIAN, L. M. 1990. Metalloproteinases and their inhibitors in matrix remodeling. *Trends Genet,* 6**,** 121-5.

MEHRARA, B. J., MACKOOL, R. J., MCCARTHY, J. G., GITTES, G. K. & LONGAKER, M. T. 1998. Immunolocalization of basic fibroblast growth factor and fibroblast growth factor receptor-1 and receptor-2 in rat cranial sutures. *Plast Reconstr Surg,* 102**,** 1805-17; discussion 1818-20.

MELROSE, J., ROUGHLEY, P., KNOX, S., SMITH, S., LORD, M. & WHITELOCK, J. 2006. The structure, location, and function of perlecan, a prominent pericellular proteoglycan of fetal, postnatal, and mature hyaline cartilages. *J Biol Chem,* 281**,** 36905-14.

MIN, H., DANILENKO, D. M., SCULLY, S. A., BOLON, B., RING, B. D., TARPLEY, J. E., DEROSE, M. & SIMONET, W. S. 1998. Fgf-10 is required for both limb and lung development and exhibits striking functional similarity to Drosophila branchless. *Genes Dev,* 12**,** 3156-61.

MISHIMA, Y. & LOTZ, M. 2008. Chemotaxis of human articular chondrocytes and mesenchymal stem cells. *J Orthop Res,* 26**,** 1407-12.

MOBASHERI, A., LEWIS, R., MAXWELL, J. E., HILL, C., WOMACK, M. & BARRETT-JOLLEY, R. 2010. Characterization of a stretch-activated potassium channel in chondrocytes. *J Cell Physiol,* 223**,** 511-8.

MOHANAN, V., TEMBURNI, M. K., KAPPES, J. C. & GALILEO, D. S. 2013. L1CAM stimulates glioma cell motility and proliferation through the fibroblast growth factor receptor. *Clin Exp Metastasis,* 30**,** 507-20.

MONTERO, A., OKADA, Y., TOMITA, M., ITO, M., TSURUKAMI, H., NAKAMURA, T., DOETSCHMAN, T., COFFIN, J. D. & HURLEY, M. M. 2000. Disruption of the fibroblast growth factor-2 gene results in decreased bone mass and bone formation. *J Clin Invest,* 105**,** 1085-93.

MOON, A. M. & CAPECCHI, M. R. 2000. Fgf8 is required for outgrowth and patterning of the limbs. *Nat Genet,* 26**,** 455-9.

NAGASE, H. & KASHIWAGI, M. 2003. Aggrecanases and cartilage matrix degradation. *Arthritis Res Ther,* 5**,** 94-103.

NAGASE, H., VISSE, R. & MURPHY, G. 2006. Structure and function of matrix metalloproteinases and TIMPs. *Cardiovasc Res,* 69**,** 562-73.

NAKAMURA, N., HORIBE, S., TORITSUKA, Y., MITSUOKA, T., NATSU-UME, T., YONEDA, K., HAMADA, M., TANAKA, Y., BOORMAN, R. S., YOSHIKAWA, H. & SHINO, K. 2008. The

location-specific healing response of damaged articular cartilage after ACL reconstruction: short-term follow-up. *Knee Surg Sports Traumatol Arthrosc,* 16**,** 843-8.

NASKI, M. C., COLVIN, J. S., COFFIN, J. D. & ORNITZ, D. M. 1998. Repression of hedgehog signaling and BMP4 expression in growth plate cartilage by fibroblast growth factor receptor 3. *Development,* 125**,** 4977-88.

NASKI, M. C. & ORNITZ, D. M. 1998. FGF signaling in skeletal development. *Front Biosci,* 3**,** d781-94.

NASKI, M. C., WANG, Q., XU, J. & ORNITZ, D. M. 1996. Graded activation of fibroblast growth factor receptor 3 by mutations causing achondroplasia and thanatophoric dysplasia. *Nat Genet,* 13**,** 233-7.

NEAME, P. J., SOMMARIN, Y., BOYNTON, R. E. & HEINEGÅRD, D. 1994. The structure of a 38-kDa leucine-rich protein (chondroadherin) isolated from bovine cartilage. *J Biol Chem,* 269**,** 21547-54.

NEILSON, K. M. & FRIESEL, R. E. 1995. Constitutive activation of fibroblast growth factor receptor-2 by a point mutation associated with Crouzon syndrome. *J Biol Chem,* 270**,** 26037-40.

NEUHOLD, L. A., KILLAR, L., ZHAO, W., SUNG, M. L., WARNER, L., KULIK, J., TURNER, J., WU, W., BILLINGHURST, C., MEIJERS, T., POOLE, A. R., BABIJ, P. & DEGENNARO, L. J. 2001. Postnatal expression in hyaline cartilage of constitutively active human collagenase-3 (MMP-13) induces osteoarthritis in mice. *J Clin Invest,* 107**,** 35-44.

NISHIDA, T., KUBOTA, S., FUKUNAGA, T., KONDO, S., YOSIMICHI, G., NAKANISHI, T., TAKANO-YAMAMOTO, T. & TAKIGAWA, M. 2003. CTGF/Hcs24, hypertrophic chondrocyte-specific gene product, interacts with perlecan in regulating the proliferation and differentiation of chondrocytes. *J Cell Physiol,* 196**,** 265-75.

O'CONOR, C. J., LEDDY, H. A., BENEFIELD, H. C., LIEDTKE, W. B. & GUILAK, F. 2014. TRPV4-mediated mechanotransduction regulates the metabolic response of chondrocytes to dynamic loading. *Proc Natl Acad Sci U S A,* 111**,** 1316-21.

OBERLENDER, S. A. & TUAN, R. S. 1994. Expression and functional involvement of N-cadherin in embryonic limb chondrogenesis. *Development,* 120**,** 177-87.

OHBAYASHI, N., SHIBAYAMA, M., KUROTAKI, Y., IMANISHI, M., FUJIMORI, T., ITOH, N. & TAKADA, S. 2002. FGF18 is required for normal cell proliferation and differentiation during osteogenesis and chondrogenesis. *Genes Dev,* 16**,** 870-9.

OLAYIOYE, M. A., BEUVINK, I., HORSCH, K., DALY, J. M. & HYNES, N. E. 1999. ErbB receptor-induced activation of stat transcription factors is mediated by Src tyrosine kinases. *J Biol Chem,* 274**,** 17209-18.

ORNITZ, D. M. & ITOH, N. 2015. The Fibroblast Growth Factor signaling pathway. *Wiley Interdiscip Rev Dev Biol,* 4**,** 215-66.

ORNITZ, D. M. & LEDER, P. 1992. Ligand specificity and heparin dependence of fibroblast growth factor receptors 1 and 3. *J Biol Chem,* 267**,** 16305-11.

ORNITZ, D. M. & MARIE, P. J. 2002. FGF signaling pathways in endochondral and intramembranous bone development and human genetic disease. *Genes Dev,* 16**,** 1446-65.

ORNITZ, D. M. & MARIE, P. J. 2015. Fibroblast growth factor signaling in skeletal development and disease. *Genes Dev,* 29**,** 1463-86.

ORNITZ, D. M., XU, J., COLVIN, J. S., MCEWEN, D. G., MACARTHUR, C. A., COULIER, F., GAO, G. & GOLDFARB, M. 1996. Receptor specificity of the fibroblast growth factor family. *J Biol Chem,* 271**,** 15292-7.

ORNITZ, D. M., YAYON, A., FLANAGAN, J. G., SVAHN, C. M., LEVI, E. & LEDER, P. 1992. Heparin is required for cell-free binding of basic fibroblast growth factor to a soluble receptor and for mitogenesis in whole cells. *Mol Cell Biol,* 12**,** 240-7.

ORR-URTREGER, A., GIVOL, D., YAYON, A., YARDEN, Y. & LONAI, P. 1991. Developmental expression of two murine fibroblast growth factor receptors, flg and bek. *Development,* 113**,** 1419-34.

ORTEGA, S., ITTMANN, M., TSANG, S. H., EHRLICH, M. & BASILICO, C. 1998. Neuronal defects and delayed wound healing in mice lacking fibroblast growth factor 2. *Proc Natl Acad Sci U S A,* 95**,** 5672-7.

OTSUKA, Y., MIZUTA, H., TAKAGI, K., IYAMA, K., YOSHITAKE, Y., NISHIKAWA, K., SUZUKI, F. & HIRAKI, Y. 1997. Requirement of fibroblast growth factor signaling for regeneration of epiphyseal morphology in rabbit full-thickness defects of articular cartilage. *Dev Growth Differ,* 39**,** 143-56.

PACIFICI, M., KOYAMA, E. & IWAMOTO, M. 2005. Mechanisms of synovial joint and articular cartilage formation: recent advances, but many lingering mysteries. *Birth Defects Res C Embryo Today,* 75**,** 237-48.

PALMOSKI, M., PERRICONE, E. & BRANDT, K. D. 1979. Development and reversal of a proteoglycan aggregation defect in normal canine knee cartilage after immobilization. *Arthritis Rheum,* 22**,** 508-17.

PAVLOFF, N., STASKUS, P. W., KISHNANI, N. S. & HAWKES, S. P. 1992. A new inhibitor of metalloproteinases from chicken: ChIMP-3. A third member of the TIMP family. *J Biol Chem,* 267**,** 17321-6.

PELLEGRINI, L., BURKE, D. F., VON DELFT, F., MULLOY, B. & BLUNDELL, T. L. 2000. Crystal structure of fibroblast growth factor receptor ectodomain bound to ligand and heparin. *Nature,* 407**,** 1029-34.

PETERS, K., ORNITZ, D., WERNER, S. & WILLIAMS, L. 1993. Unique expression pattern of the FGF receptor 3 gene during mouse organogenesis. *Dev Biol,* 155**,** 423-30.

PETERS, K. G., WERNER, S., CHEN, G. & WILLIAMS, L. T. 1992. Two FGF receptor genes are differentially expressed in epithelial and mesenchymal tissues during limb formation and organogenesis in the mouse. *Development,* 114**,** 233-43.

PINEDA, S., POLLACK, A., STEVENSON, S., GOLDBERG, V. & CAPLAN, A. 1992. A semiquantitative scale for histologic grading of articular cartilage repair. *Acta Anat (Basel),* 143**,** 335-40.

PITSILLIDES, A. A., ARCHER, C. W., PREHM, P., BAYLISS, M. T. & EDWARDS, J. C. 1995. Alterations in hyaluronan synthesis during developing joint cavitation. *J Histochem Cytochem,* 43**,** 263-73.

PITSILLIDES, A. A. & ASHHURST, D. E. 2008. A critical evaluation of specific aspects of joint development. *Dev Dyn,* 237**,** 2284-94.

PLOTNIKOV, A. N., HUBBARD, S. R., SCHLESSINGER, J. & MOHAMMADI, M. 2000. Crystal structures of two FGF-FGFR complexes reveal the determinants of ligand-receptor specificity. *Cell,* 101**,** 413-24.

PLOTNIKOV, A. N., SCHLESSINGER, J., HUBBARD, S. R. & MOHAMMADI, M. 1999. Structural basis for FGF receptor dimerization and activation. *Cell,* 98**,** 641-50.

POOLE, C. A., AYAD, S. & SCHOFIELD, J. R. 1988. Chondrons from articular cartilage: I. Immunolocalization of type VI collagen in the pericellular capsule of isolated canine tibial chondrons. *J Cell Sci,* 90 (Pt 4)**,** 635-43.

POOLE, C. A., GLANT, T. T. & SCHOFIELD, J. R. 1991. Chondrons from articular cartilage. (IV). Immunolocalization of proteoglycan epitopes in isolated canine tibial chondrons. *J Histochem Cytochem,* 39**,** 1175-87.

POTTHOFF, M. J., KLIEWER, S. A. & MANGELSDORF, D. J. 2012. Endocrine fibroblast growth factors 15/19 and 21: from feast to famine. *Genes Dev,* 26**,** 312-24.

RAGAN, P. M., BADGER, A. M., COOK, M., CHIN, V. I., GOWEN, M., GRODZINSKY, A. J. & LARK, M. W. 1999. Down-regulation of chondrocyte aggrecan and type-II collagen gene expression correlates with increases in static compression magnitude and duration. *J Orthop Res,* 17**,** 836-42.

RAPRAEGER, A. C., KRUFKA, A. & OLWIN, B. B. 1991. Requirement of heparan sulfate for bFGF-mediated fibroblast growth and myoblast differentiation. *Science,* 252**,** 1705-8.

REBOUL, P., PELLETIER, J. P., TARDIF, G., CLOUTIER, J. M. & MARTEL-PELLETIER, J. 1996. The new collagenase, collagenase-3, is expressed and synthesized by human chondrocytes but not by synoviocytes. A role in osteoarthritis. *J Clin Invest,* 97**,** 2011-9.

RICE, D. P., ABERG, T., CHAN, Y., TANG, Z., KETTUNEN, P. J., PAKARINEN, L., MAXSON, R. E. & THESLEFF, I. 2000. Integration of FGF and TWIST in calvarial bone and suture development. *Development,* 127**,** 1845-55.

ROBERTSON, S. C., MEYER, A. N., HART, K. C., GALVIN, B. D., WEBSTER, M. K. & DONOGHUE, D. J. 1998. Activating mutations in the extracellular domain of the fibroblast growth factor receptor 2 function by disruption of the disulfide bond in the third immunoglobulin-like domain. *Proc Natl Acad Sci U S A,* 95**,** 4567-72.

ROELOFS, A. J., ZUPAN, J., RIEMEN, A. H. K., KANIA, K., ANSBORO, S., WHITE, N., CLARK, S. M. & DE BARI, C. 2017. Joint morphogenetic cells in the adult mammalian synovium. *Nat Commun,* 8**,** 15040.

ROSS, T. D., COON, B. G., YUN, S., BAEYENS, N., TANAKA, K., OUYANG, M. & SCHWARTZ, M. A. 2013. Integrins in mechanotransduction. *Curr Opin Cell Biol,* 25**,** 613-8.

ROUGHLEY, P. J. & LEE, E. R. 1994. Cartilage proteoglycans: structure and potential functions. *Microsc Res Tech,* 28**,** 385-97.

SANDY, J. D., FLANNERY, C. R., NEAME, P. J. & LOHMANDER, L. S. 1992. The structure of aggrecan fragments in human synovial fluid. Evidence for the involvement in osteoarthritis of a novel proteinase which cleaves the Glu 373-Ala 374 bond of the interglobular domain. *J Clin Invest,* 89**,** 1512-6.

SANDY, J. D., NEAME, P. J., BOYNTON, R. E. & FLANNERY, C. R. 1991. Catabolism of aggrecan in cartilage explants. Identification of a major cleavage site within the interglobular domain. *J Biol Chem,* 266**,** 8683-5.

SAUERLAND, K., RAISS, R. X. & STEINMEYER, J. 2003. Proteoglycan metabolism and viability of articular cartilage explants as modulated by the frequency of intermittent loading. *Osteoarthritis Cartilage,* 11**,** 343-50.

SAWAJI, Y., HYNES, J., VINCENT, T. & SAKLATVALA, J. 2008. Fibroblast growth factor 2 inhibits induction of aggrecanase activity in human articular cartilage. *Arthritis Rheum,* 58**,** 3498-509.

SCHLESSINGER, J., PLOTNIKOV, A. N., IBRAHIMI, O. A., ELISEENKOVA, A. V., YEH, B. K., YAYON, A., LINHARDT, R. J. & MOHAMMADI, M. 2000. Crystal structure of a ternary

FGF-FGFR-heparin complex reveals a dual role for heparin in FGFR binding and dimerization. *Mol Cell,* 6**,** 743-50.

SEITZ, M., GROSHEVA, M., SKOURAS, E., ANGELOVA, S. K., ANKERNE, J., JUNGNICKEL, J., GROTHE, C., KLIMASCHEWSKI, L., HÜBBERS, C. U., DUNLOP, S. A. & ANGELOV, D. N. 2011. Poor functional recovery and muscle polyinnervation after facial nerve injury in fibroblast growth factor-2-/- mice can be improved by manual stimulation of denervated vibrissal muscles. *Neuroscience,* 182**,** 241-7.

SEKINE, K., OHUCHI, H., FUJIWARA, M., YAMASAKI, M., YOSHIZAWA, T., SATO, T., YAGISHITA, N., MATSUI, D., KOGA, Y., ITOH, N. & KATO, S. 1999. Fgf10 is essential for limb and lung formation. *Nat Genet,* 21**,** 138-41.

SETTLE, S. H., ROUNTREE, R. B., SINHA, A., THACKER, A., HIGGINS, K. & KINGSLEY, D. M. 2003. Multiple joint and skeletal patterning defects caused by single and double mutations in the mouse Gdf6 and Gdf5 genes. *Dev Biol,* 254**,** 116-30.

SHAPIRO, F., KOIDE, S. & GLIMCHER, M. J. 1993. Cell origin and differentiation in the repair of full-thickness defects of articular cartilage. *J Bone Joint Surg Am,* 75**,** 532-53.

SHEEBA, C. J., ANDRADE, R. P., DUPREZ, D. & PALMEIRIM, I. 2010. Comprehensive analysis of fibroblast growth factor receptor expression patterns during chick forelimb development. *Int J Dev Biol,* 54**,** 1517-26.

SHIANG, R., THOMPSON, L. M., ZHU, Y. Z., CHURCH, D. M., FIELDER, T. J., BOCIAN, M., WINOKUR, S. T. & WASMUTH, J. J. 1994. Mutations in the transmembrane domain of FGFR3 cause the most common genetic form of dwarfism, achondroplasia. *Cell,* 78**,** 335-42.

SOLCHAGA, L. A., PENICK, K., PORTER, J. D., GOLDBERG, V. M., CAPLAN, A. I. & WELTER, J. F. 2005. FGF-2 enhances the mitotic and chondrogenic potentials of human adult bone marrow-derived mesenchymal stem cells. *J Cell Physiol,* 203**,** 398-409.

SONG, R. H., TORTORELLA, M. D., MALFAIT, A. M., ALSTON, J. T., YANG, Z., ARNER, E. C. & GRIGGS, D. W. 2007. Aggrecan degradation in human articular cartilage explants is mediated by both ADAMTS-4 and ADAMTS-5. *Arthritis Rheum,* 56**,** 575-85.

STANTON, H., ROGERSON, F. M., EAST, C. J., GOLUB, S. B., LAWLOR, K. E., MEEKER, C. T., LITTLE, C. B., LAST, K., FARMER, P. J., CAMPBELL, I. K., FOURIE, A. M. & FOSANG, A. J. 2005. ADAMTS5 is the major aggrecanase in mouse cartilage in vivo and in vitro. *Nature,* 434**,** 648-52.

STORM, E. E. & KINGSLEY, D. M. 1996. Joint patterning defects caused by single and double mutations in members of the bone morphogenetic protein (BMP) family. *Development,* 122**,** 3969-79.

SU, W. C., KITAGAWA, M., XUE, N., XIE, B., GAROFALO, S., CHO, J., DENG, C., HORTON, W. A. & FU, X. Y. 1997. Activation of Stat1 by mutant fibroblast growth-factor receptor in thanatophoric dysplasia type II dwarfism. *Nature,* 386**,** 288-92.

SURI, S. & WALSH, D. A. 2012. Osteochondral alterations in osteoarthritis. *Bone,* 51**,** 204-11.

TAKEO, M., CHOU, W. C., SUN, Q., LEE, W., RABBANI, P., LOOMIS, C., TAKETO, M. M. & ITO, M. 2013. Wnt activation in nail epithelium couples nail growth to digit regeneration. *Nature,* 499**,** 228-32.

TANG, J., SU, N., ZHOU, S., XIE, Y., HUANG, J., WEN, X., WANG, Z., WANG, Q., XU, W., DU, X., CHEN, H. & CHEN, L. 2016. Fibroblast Growth Factor Receptor 3 Inhibits Osteoarthritis Progression in the Knee Joints of Adult Mice. *Arthritis Rheumatol,* 68**,** 2432-43.

TANG, X., MUHAMMAD, H., MCLEAN, C., MIOTLA-ZAREBSKA, J., FLEMING, J., DIDANGELOS, A., ÖNNERFJORD, P., LEASK, A., SAKLATVALA, J. & VINCENT, T. L. 2018. Connective tissue growth factor contributes to joint homeostasis and osteoarthritis severity by controlling the matrix sequestration and activation of latent TGFβ. *Ann Rheum Dis,* 77**,** 1372-1380.

TORII, S., KUSAKABE, M., YAMAMOTO, T., MAEKAWA, M. & NISHIDA, E. 2004. Sef is a spatial regulator for Ras/MAP kinase signaling. *Dev Cell,* 7**,** 33-44.

TORTORELLA, M. D., BURN, T. C., PRATTA, M. A., ABBASZADE, I., HOLLIS, J. M., LIU, R., ROSENFELD, S. A., COPELAND, R. A., DECICCO, C. P., WYNN, R., ROCKWELL, A., YANG, F., DUKE, J. L., SOLOMON, K., GEORGE, H., BRUCKNER, R., NAGASE, H., ITOH, Y., ELLIS, D. M., ROSS, H., WISWALL, B. H., MURPHY, K., HILLMAN, M. C., HOLLIS, G. F., NEWTON, R. C., MAGOLDA, R. L., TRZASKOS, J. M. & ARNER, E. C. 1999. Purification and cloning of aggrecanase-1: a member of the ADAMTS family of proteins. *Science,* 284**,** 1664-6.

TROEBERG, L. & NAGASE, H. 2012. Proteases involved in cartilage matrix degradation in osteoarthritis. *Biochim Biophys Acta,* 1824**,** 133-45.

TRUEB, B. 2011. Biology of FGFRL1, the fifth fibroblast growth factor receptor. *Cell Mol Life Sci,* 68**,** 951-64.

TSUTSUMI, S., SHIMAZU, A., MIYAZAKI, K., PAN, H., KOIKE, C., YOSHIDA, E., TAKAGISHI, K. & KATO, Y. 2001. Retention of multilineage differentiation potential of mesenchymal cells during proliferation in response to FGF. *Biochem Biophys Res Commun,* 288**,** 413-9.

TURNER, N. & GROSE, R. 2010. Fibroblast growth factor signalling: from development to cancer. *Nat Rev Cancer,* 10**,** 116-29.

VALVERDE-FRANCO, G., BINETTE, J. S., LI, W., WANG, H., CHAI, S., LAFLAMME, F., TRAN-KHANH, N., QUENNEVILLE, E., MEIJERS, T., POOLE, A. R., MORT, J. S., BUSCHMANN, M. D. & HENDERSON, J. E. 2006. Defects in articular cartilage metabolism and early arthritis in fibroblast growth factor receptor 3 deficient mice. *Hum Mol Genet,* 15**,** 1783-92.

VALVERDE-FRANCO, G., LIU, H., DAVIDSON, D., CHAI, S., VALDERRAMA-CARVAJAL, H., GOLTZMAN, D., ORNITZ, D. M. & HENDERSON, J. E. 2004. Defective bone mineralization and osteopenia in young adult FGFR3-/- mice. *Hum Mol Genet,* 13**,** 271-84.

VAN DER WOUDE, J. A. D., WIEGANT, K., VAN ROERMUND, P. M., INTEMA, F., CUSTERS, R. J. H., ECKSTEIN, F., VAN LAAR, J. M., MASTBERGEN, S. C. & LAFEBER, F. P. J. G. 2017. Five-Year Follow-up of Knee Joint Distraction: Clinical Benefit and Cartilaginous Tissue Repair in an Open Uncontrolled Prospective Study. *Cartilage,* 8**,** 263-271.

VAN WART, H. E. & BIRKEDAL-HANSEN, H. 1990. The cysteine switch: a principle of regulation of metalloproteinase activity with potential applicability to the entire matrix metalloproteinase gene family. *Proc Natl Acad Sci U S A,* 87**,** 5578-82.

VANWANSEELE, B., ECKSTEIN, F., KNECHT, H., SPAEPEN, A. & STÜSSI, E. 2003. Longitudinal analysis of cartilage atrophy in the knees of patients with spinal cord injury. *Arthritis Rheum,* 48**,** 3377-81.

VINCENT, T., HERMANSSON, M., BOLTON, M., WAIT, R. & SAKLATVALA, J. 2002. Basic FGF mediates an immediate response of articular cartilage to mechanical injury. *Proc Natl Acad Sci U S A,* 99**,** 8259-64.

VINCENT, T. L., HERMANSSON, M. A., HANSEN, U. N., AMIS, A. A. & SAKLATVALA, J. 2004. Basic fibroblast growth factor mediates transduction of mechanical signals when articular cartilage is loaded. *Arthritis Rheum,* 50**,** 526-33.

VINCENT, T. L., MCLEAN, C. J., FULL, L. E., PESTON, D. & SAKLATVALA, J. 2007. FGF-2 is bound to perlecan in the pericellular matrix of articular cartilage, where it acts as a chondrocyte mechanotransducer. *Osteoarthritis Cartilage,* 15**,** 752-63.

VINCENT, T. L. & WANN, A. K. T. 2018. Mechanoadaptation: articular cartilage through thick and thin. *J Physiol*.

VIRAG, J. A., ROLLE, M. L., REECE, J., HARDOUIN, S., FEIGL, E. O. & MURRY, C. E. 2007. Fibroblast growth factor-2 regulates myocardial infarct repair: effects on cell proliferation, scar contraction, and ventricular function. *Am J Pathol,* 171**,** 1431-40.

VOGEL, K. G. & TROTTER, J. A. 1987. The effect of proteoglycans on the morphology of collagen fibrils formed in vitro. *Coll Relat Res,* 7**,** 105-14.

VORTKAMP, A., LEE, K., LANSKE, B., SEGRE, G. V., KRONENBERG, H. M. & TABIN, C. J. 1996. Regulation of rate of cartilage differentiation by Indian hedgehog and PTH-related protein. *Science,* 273**,** 613-22.

WALSH, D. A., MCWILLIAMS, D. F., TURLEY, M. J., DIXON, M. R., FRANSÈS, R. E., MAPP, P. I. & WILSON, D. 2010. Angiogenesis and nerve growth factor at the osteochondral junction in rheumatoid arthritis and osteoarthritis. *Rheumatology (Oxford),* 49**,** 1852-61.

WANG, Q., GREEN, R. P., ZHAO, G. & ORNITZ, D. M. 2001. Differential regulation of endochondral bone growth and joint development by FGFR1 and FGFR3 tyrosine kinase domains. *Development,* 128**,** 3867-76.

WANN, A. K., ZUO, N., HAYCRAFT, C. J., JENSEN, C. G., POOLE, C. A., MCGLASHAN, S. R. & KNIGHT, M. M. 2012. Primary cilia mediate mechanotransduction through control of ATP-induced Ca2+ signaling in compressed chondrocytes. *FASEB J,* 26**,** 1663-71.

WATT, F. E., ISMAIL, H. M., DIDANGELOS, A., PEIRCE, M., VINCENT, T. L., WAIT, R. & SAKLATVALA, J. 2013. Src and fibroblast growth factor 2 independently regulate signaling and gene expression induced by experimental injury to intact articular cartilage. *Arthritis Rheum,* 65**,** 397-407.

WEISS, S., HENNIG, T., BOCK, R., STECK, E. & RICHTER, W. 2010. Impact of growth factors and PTHrP on early and late chondrogenic differentiation of human mesenchymal stem cells. *J Cell Physiol,* 223**,** 84-93.

WENG, T., YI, L., HUANG, J., LUO, F., WEN, X., DU, X., CHEN, Q., DENG, C., CHEN, D. & CHEN, L. 2012. Genetic inhibition of fibroblast growth factor receptor 1 in knee cartilage attenuates the degeneration of articular cartilage in adult mice. *Arthritis Rheum,* 64**,** 3982-92.

WHITELOCK, J. M., MURDOCH, A. D., IOZZO, R. V. & UNDERWOOD, P. A. 1996. The degradation of human endothelial cell-derived perlecan and release of bound basic fibroblast growth factor by stromelysin, collagenase, plasmin, and heparanases. *J Biol Chem,* 271**,** 10079-86.

WIDELITZ, R. B., JIANG, T. X., MURRAY, B. A. & CHUONG, C. M. 1993. Adhesion molecules in skeletogenesis: II. Neural cell adhesion molecules mediate precartilaginous mesenchymal condensations and enhance chondrogenesis. *J Cell Physiol,* 156**,** 399-411.

WIEDEMANN, M. & TRUEB, B. 2000. Characterization of a novel protein (FGFRL1) from human cartilage related to FGF receptors. *Genomics,* 69**,** 275-9.

WIEGANT, K., VAN ROERMUND, P. M., INTEMA, F., COTOFANA, S., ECKSTEIN, F., MASTBERGEN, S. C. & LAFEBER, F. P. 2013. Sustained clinical and structural benefit after joint distraction in the treatment of severe knee osteoarthritis. *Osteoarthritis Cartilage,* 21**,** 1660-7.

WONG, A., LAMOTHE, B., LEE, A., SCHLESSINGER, J., LAX, I. & LI, A. 2002. FRS2 alpha attenuates FGF receptor signaling by Grb2-mediated recruitment of the ubiquitin ligase Cbl. *Proc Natl Acad Sci U S A,* 99**,** 6684-9.

XU, X., WEINSTEIN, M., LI, C., NASKI, M., COHEN, R. I., ORNITZ, D. M., LEDER, P. & DENG, C. 1998. Fibroblast growth factor receptor 2 (FGFR2)-mediated reciprocal regulation loop between FGF8 and FGF10 is essential for limb induction. *Development,* 125**,** 753-65.

YAN, D., CHEN, D., COOL, S. M., VAN WIJNEN, A. J., MIKECZ, K., MURPHY, G. & IM, H. J. 2011. Fibroblast growth factor receptor 1 is principally responsible for fibroblast growth factor 2-induced catabolic activities in human articular chondrocytes. *Arthritis Res Ther,* 13**,** R130.

YAN, D., CHEN, D. & IM, H. J. 2012. Fibroblast growth factor-2 promotes catabolism via FGFR1-Ras-Raf-MEK1/2-ERK1/2 axis that coordinates with the PKCδ pathway in human articular chondrocytes. *J Cell Biochem,* 113**,** 2856-65.

YAYON, A., KLAGSBRUN, M., ESKO, J. D., LEDER, P. & ORNITZ, D. M. 1991. Cell surface, heparin-like molecules are required for binding of basic fibroblast growth factor to its high affinity receptor. *Cell,* 64**,** 841-8.

YU, K., HERR, A. B., WAKSMAN, G. & ORNITZ, D. M. 2000. Loss of fibroblast growth factor receptor 2 ligand-binding specificity in Apert syndrome. *Proc Natl Acad Sci U S A,* 97**,** 14536-41.

YU, K., XU, J., LIU, Z., SOSIC, D., SHAO, J., OLSON, E. N., TOWLER, D. A. & ORNITZ, D. M. 2003. Conditional inactivation of FGF receptor 2 reveals an essential role for FGF signaling in the regulation of osteoblast function and bone growth. *Development,* 130**,** 3063-74.

ZHANG, X., IBRAHIMI, O. A., OLSEN, S. K., UMEMORI, H., MOHAMMADI, M. & ORNITZ, D. M. 2006. Receptor specificity of the fibroblast growth factor family. The complete mammalian FGF family. *J Biol Chem,* 281**,** 15694-700.

ZHOU, M., SUTLIFF, R. L., PAUL, R. J., LORENZ, J. N., HOYING, J. B., HAUDENSCHILD, C. C., YIN, M., COFFIN, J. D., KONG, L., KRANIAS, E. G., LUO, W., BOIVIN, G. P., DUFFY, J. J., PAWLOWSKI, S. A. & DOETSCHMAN, T. 1998. Fibroblast growth factor 2 control of vascular tone. *Nat Med,* 4**,** 201-7.

ZHU, H., DUCHESNE, L., RUDLAND, P. S. & FERNIG, D. G. 2010. The heparan sulfate co-receptor and the concentration of fibroblast growth factor-2 independently elicit different signalling patterns from the fibroblast growth factor receptor. *Cell Commun Signal,* 8**,** 14.

ZOU, L., CAO, S., KANG, N., HUEBERT, R. C. & SHAH, V. H. 2012. Fibronectin induces endothelial cell migration through beta1 integrin and Src-dependent phosphorylation of fibroblast growth factor receptor-1 at tyrosines 653/654 and 766. *J Biol Chem,* 287**,** 7190-202.

8 Appendices

Conferences attended:

BSMB: The matrix and microenvironment; March 2015; Oxford -Abstract submitted- Poster presentation.

Cutting Edge OA: June 2015; Oxford – 3-minute presentation and poster

OARSI world congress: March 2016; Amsterdam – Abstract submitted- Poster

Fusion: FGFs in development and repair: March 2017; Cancun – Abstract submitted - Poster

Cutting edge OA: June 2017; Oxford – Poster presented.

OARSI world congress: March 2018; Liverpool – Abstract submitted- 10-minute presentation.

Awards:

Best poster presentation at Cutting edge OA: June 2017; Oxford.